The Hydroclimate Variability of Central Africa: seasonal cycle, mechanisms, teleconnections and impacts on neighbouring regions

Georges-Noel Tiersmondo Longandjo

Thesis presented for the degree of
Doctor of Philosophy
Department of Oceanography
Faculty of Science

November 2017

à Hattie Marie-Johanna

The real voyage of discovery consists not in seeking new landscapes but in having new eyes

Marcel Proust, 1871-1922

Finally, the seventh time, his servant told him, "I saw a little cloud about the size of a man's hand rising from the sea." ... And soon the sky was black with clouds. A heavy wind brought a terrific rainstorm, and Ahab left quickly for Jezreel.

Bible, 1 Kings 18:44; 45

For thus saith the LORD, "Ye shall not see wind, neither shall ye see rain; yet that valley shall be filled with water, that ye may drink, both ye, and your cattle, and your beasts".

Bible, 2 Kings 3:17

Acknowledgments

I am particularly indebted to my supervisor A/Prof Mathieu Rouault for his continuing generous help, guidance, patience and support during all phases of this dissertation. It has been a wonderful journey since the first day we met, particularly when for the first time my registration failed due to the equivalence of my Master of Science Degree. Despite that you were always there to encourage me and help me to sort out this big issue with the Faculty of Science. You gave me the opportunity to be involved in one of the big European Project, namely PREFACE, where I met eminent and thoughtful scientists. With your positive, confident and optimistic attitude towards scientific research, I gained skills and independence that will benefit me not only today, but also tomorrow and beyond my research scientist career. Mostly, your unfailing encouragement to follow my own research interests did allow me the scientific freedom needed to pursue this PhD research. Originating from a non-English speaking country, it was actually for me, a big challenge to write this dissertation. Thank God this was not an English language PhD! Although fraught will many spelling mistakes and grammatical faux pas, you did try to fix some of them. Looking forward for next steps. Pour tout ca, un seul mot, **merci!** Et que mon Dieu vous benisse.

I would also like to thank Noel Keenlyside and Stephanie Gleixner for helpful discussion and for sharing with me the ECHAM5.3 model. I am also indebted to Nicolas Vigaud and Thomas Toniasso for helpful suggestions and advice to my research.

This dissertation would not have been possible without the support provides by ACCESS and Nansen–Tutu Center for Environmental Marine Research and I am grateful of them. My research was supported by the PREFACE project (EU FP7/2007-2013 under grant agreement no. 603521), National Research Foundation SARChI Chair in Ocean–Atmosphere–Land modelling, Water Research Commission and AfDB-ACMAD-SADC_CSC/ ISACIP Project.

Finally, as a believer, I would like to thank my God, my Lord Jesus Christ for not only the gift of life, but also for the spoken Words He provided for me in this last time of a changing world, the humankind is experiencing.

Table of Contents

Abstract

Central Africa is, climatologically speaking, a poorly studied region (Clivar, 2000; Dezfuli and Nicholson, 2012; Nicholson and Dezfuli, 2012; Todd and Washington, 2004). It is considered as a knowledge gap in the understanding of the tropical climate system (Todd and Washington, 2004). Drivers of Central Africa rainfall are not well documented and deserve more attention. The aims of thesis are to enhance our fundamental understanding of Central Africa rainfall and the mechanisms involved in its seasonal and interannual variability as well as to assess how an atmospheric general circulation model forced by observed sea surface temperature (SST), the ECHAM5.3 model, does represent the main features of Central Africa hydroclimate variability.

The seasonal cycle of Central Africa rainfall is primarily driven by change in the atmospheric low-pressure system of Central Africa landmass, water vapor and latent heat release rather than change of local temperature. From October to April, over Central Africa and its neighbouring regions, we highlight the existence in the mid-lower troposphere, between 1000 and 500 hPa of a dominant cyclonic and quasi-permanent circulation pattern that drives the atmospheric large-scale circulation and its associated water vapor transports, namely the Central Africa Low. The Central Africa Low, with its variation strongly modulated by El Niño Southern Oscillations (ENSO), is characterized by strong convective activity due to an unstable atmosphere over central Africa, leading to high rainfall with less variance. Nevertheless, when the Central Africa Low prevails, Central Africa is a sink of water vapor, with the Indian Ocean as the main supplier. The weakening of the Central Africa Low, in May to September, is associated with the reversal of the water vapor transport at the northern boundary channel, leading Central Africa to become a source of moisture. During this season, both surrounding oceans are suppliers of moisture, with some additional contribution from the Congo basin rainforest.

Central Africa rainfall variability is controlled by large-scale circulation variation, rather than variation in tropospheric water vapor. Year-round, the large-scale circulation is characterized by dominant easterly jets at middle (African easterly jets, AEJs) and upper (tropical easterly jets, TEJ) levels, owed by the Central Africa Low. At low-levels, there is a shallow zonal overturning circulation thermally direct, namely the Congo Basin Cell, driven by near-surface land-ocean thermal contrast between the warm central Africa landmass and the relatively cold Atlantic Ocean. The Congo Basin Cell, characterizes by eastward flow, persists year-round, with a maximum strength (-196.92±32.89 Sv) and width (30^{o} degree) in August/September and minimum strength (-24.80± 17.83 Sv) and width (~6^{o} degree) in May. The Congo Basin Cell does not play any crucial role in modulating Central Africa rainfall but it does regulate the rainfall distribution, through the seasonal position of the ITCZ. At midlevel, the atmospheric convective instability over Central Africa is controlled by the southward import of high moist static energy from the warmer Sahel associated with the AEJ over Central Africa. The saturation of the rising moist air at midlevel determines the location of high rainfall over central Africa year-round. Nevertheless, the absence of significant trend (-0.013 mm per decade) of the Central Africa rainfall is associated with the weakening of the Central Africa Low in recent decades (1979 to 2015), consistent with Lau and Wu (2006). Further investigations on

physical mechanisms affecting the Central Africa hydroclimate reveals that the Central Africa Low and land-ocean thermal contrasts are the main drivers of Central Africa rainfall variability at seasonal and interannual time scale, through the control of AEJs and the Congo Basin Cell strength and width. The analysis of ECHAM5.3 experiments provide a support to these mechanisms.

Finally, to unravel what are the physical mechanisms shaping the rainfall anomalies patterns associated with the interannual variability of Central Africa rainfall, we found out that the Central Africa does reflect the regional-scale response of the atmosphere to the variation of the interbasin SST anomalies gradient (ΔSST) between tropical Atlantic and Indian Oceans. Likely, the zonal contrast of central Africa rainfall is owed by the Central Africa Low, which separates central Africa in two distinct regions of opposite polarity by regulating the strength of the low-level westerly and mid-upper easterly jets and their associated water vapor transports. This east-west dipole-like pattern of Central Africa rainfall is similar to the second leading mode obtained by empirical orthogonal functions (EOF) analysis of rainfall anomalies during the long rainy season. Thus, during the positive phase of ΔSST, the Central Africa Low area change induces an anomalous clockwise zonal overturning cell over Central Africa, with ascending branch over Atlantic, indicative of deep convection leading to rainfall surplus, and sinking branch over Indian Ocean, indicative of subsistence, which suppress convection and lead to rainfall deficit, consistent with the mechanism proposed by Dezfuli et al. (2015). However, the impact of ΔSST on Central Africa rainfall variability is asymmetrical during positive and negative phases of ΔSST

Chap. 1

Introduction

1.1. Motivation and objectives

"*Oza na mvula boni*?" from Lingala, the most popular language in Central Africa, means "how old are you?" and could be translated as "how many rainy seasons did you experience?" In the hierarchical societies based on the right of primogeniture, one could understand through this mere question how rainfall is the most vital and determinant factor for each person's life in this part of Africa. Indeed, more than 100 million people rely their lives mostly on rain fed agriculture and others natural resources (forests, river, lakes…) for their daily food subsistence and on economic activities related to hydroelectricity production. Hence, any change in the rainfall variability will make those people more vulnerable and most of them are unlikely to survive rainfall extremes as they will not be able to cope such occurrences such as a drought followed by food insecurity. Meanwhile severe flood favours the recurrence of waterborne diseases such as malaria, cholera, dysentery, and typhoid fever and lead to humanitarian crisis. Understanding the underlying physical mechanisms leading to such climate extreme conditions is the basis sound forecasting and real time monitoring and could help either government, the United Nations (UN) Office for the Coordination of Humanitarian Affairs (OCHA) or any infrastructure project officers to be better prepared to manage efficiently such climate conditions in this part of Africa. As reported by many local and international newspapers each year and particularly during 20014/2015 (Fig. 1.1), the Democratic Republic of Congo and its neighbouring regions experienced once more a severe drier than normal year, which occurred since June-July-August season (JJA) of 2013 (Fig. 1.1), and culminate later in 2015 when El Niño Southern Oscillation

(ENSO) started to prevail over the central equatorial Pacific and impacted global climate and weather. This situation leads to about 1 million affected people (www.bbc.com 2014; 2015; www.reuters.com 2014; 2015; www.radiookapi.org 2014; 2015; etc…) that resulted from bad coordination and management by both local and national government and OCHA.

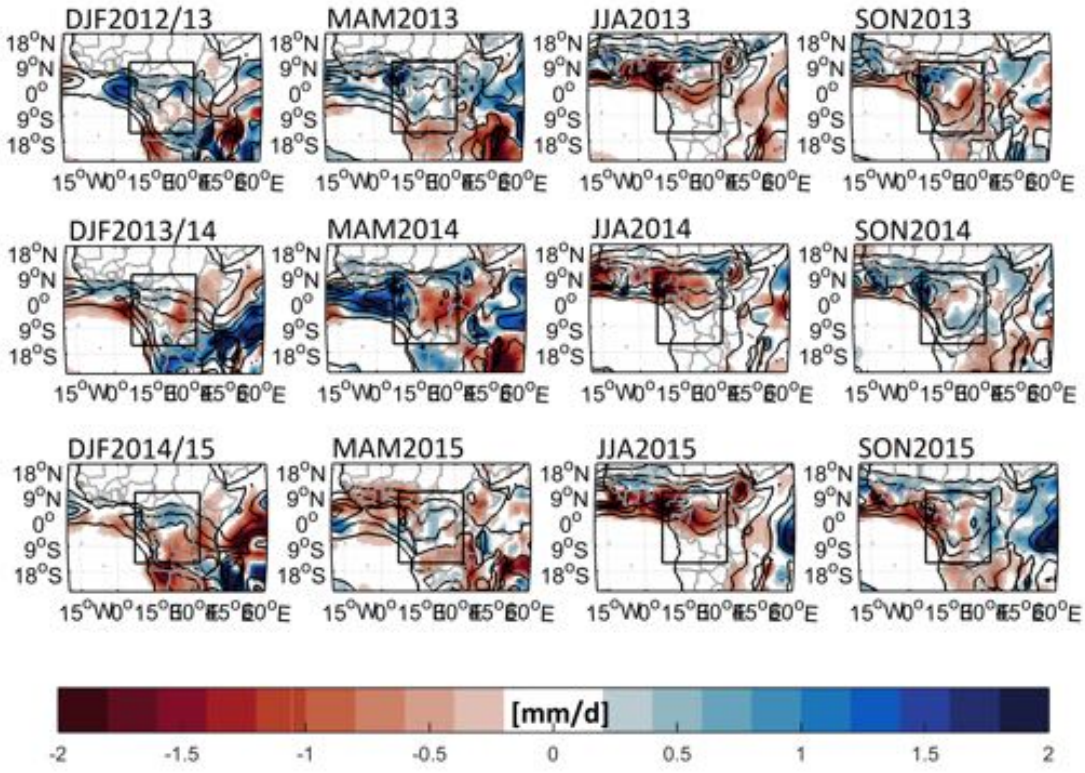

Fig. 1.1. Evolution of 3-months rainfall anomalies (shading, mm/day) over central Africa and its neighbouring regions from December 2012 to November 2015. Black box and lines in each panel represents Central Africa region and the seasonal mean rainfall, with contour interval of 2mm/d. The first contour is 1mm/d. Rainfall are from both GPCP (Huffman et al. 2009) and CMAP datasets (Xie and Arkin 1997).

Such climate extremes over central Africa impacted also one of the greatest hydropower dam project in the world, the "Grand Inga", on Congo River with a mean flow of 40,000 m^3/s at its mouth, in Democratic Republic of Congo. This planned megaproject will cost around 3 billion US Dollar and will generate about 42,000MW at its completion (www.internationalrivers.org/campaigns/grand-inga-dam-dr-congo 2015). For the Inga third phase (Inga 3) which will generate about 4,800MW by 2022, South Africa has projected to invest almost 1 billion US Dollar to secure around 2,500MW for its economy (www.sanews.gov.za, 2013). But hitherto, drivers of Central Africa rainfall are not well documented and should warrant more investigation. Thus, the main objectives of this dissertation are to provide answer to the following questions:

(i) What are fundamental processes that determine key features of the seasonal evolution of Central Africa rainfall?

(ii) What mechanisms do control the large-scale atmospheric dynamics of the central Africa rainfall system;

(iii) What are physical processes involved in the relationships between Central Africa rainfall variability and its adjoining tropical Oceans?

In the literature, Sahel is defined as the region of Africa north of 10°N (Chappell and Agnew, 2004; Martin and Thorncroft, 2014), while Southern Africa is the region of Africa south of 15°S (Richard et al. 2000, Cretat et al. 2012). Hence, Central Africa (Fig. 1.2) spans from the Eastern Atlantic Ocean border (7°E) to African Highlands known as the Rift valley highlands (33°E), while East Africa is confined between the Rift valley highlands and the Western Indian Ocean. Cameroon highlands and the Angolan plateau lies in its north-western and south-western boundaries respectively. Central Africa covers about ten states, including Angola, Burundi, Cameroun, Congo, Democratic Republic of Congo (DRC), Equatorial Guinea, Gabon, Rwanda, South Sudan and Zambia and encompasses one of the biggest rainforests in the world – the Congo basin rainforest. Central Africa is a vast bio-diverse region containing approximately 90% of Africa's remaining tropical forest and experiences the highest frequency of lightning strikes than anywhere else in the world (Nicholson and Grist, 2003; Balas et al, 2007; Jackson et al. 2009). Central African orography and vegetation characteristics (Fig. 1.2) do highly influence rainfall (Balas et al, 2007). Central Africa area could be estimated around 4,000,000 square km.

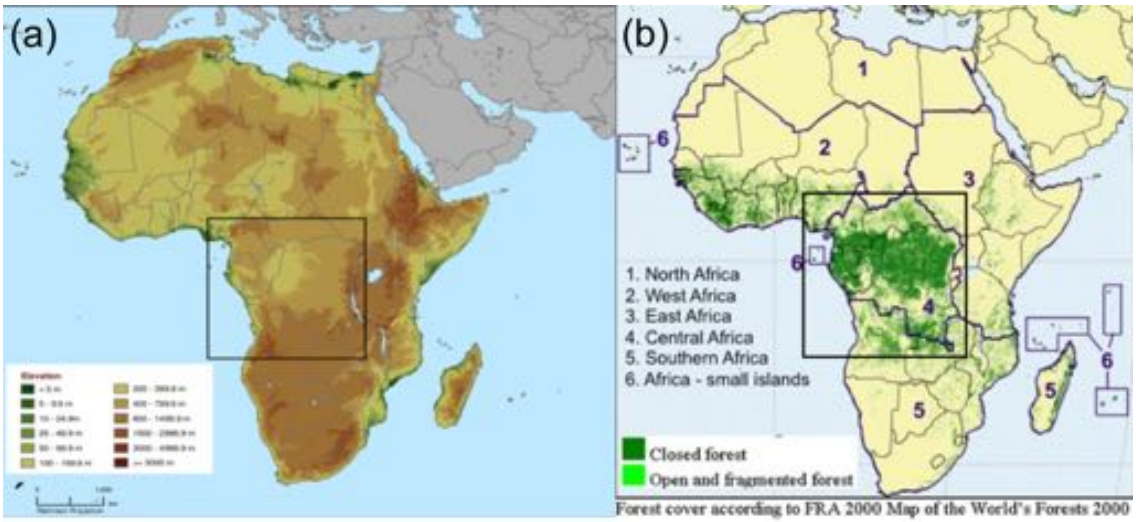

Fig. 1.2. African (a) topography and (b) rainforest. The black box delineates Central Africa (07°-33°E; 10°N-15°S). Those figures are adapted from http://sedac.ciesin.columbia.edu/data/collection/nagdc/maps/ and from http://www.fao.org/docrep/004/Y1997E/y1997e0g.htm#bm16.1

1.2. Literature review/Background

It is important to highlight that Central Africa is, climatologically speaking, a relatively poor studied region (Clivar, 2000; Dezfuli and Nicholson, 2012; Nicholson and Dezfuli, 2012; Todd and Washington, 2004), mostly due to political instability and turmoil not conducive for science. This situation had led to sporadic and sparse ground based datasets – spatially and temporally (Todd and Washington 2004; Balas et al. 2007; Nicholson and Dezfuli. 2012; Washington et al. 2013). In 2013, for instance, only three stations in Democratic Republic of Congo reported to global telecommunications system (Washington et al. 2013). To investigate the inter-annual variability of rainfall over Central Africa, many studies (Balas et al. 2007; Nicholson and Grist, 2003; Todd and Washington, 2004) used various rainfall datasets. But, few studies tried to evaluate rain rate in observations, reanalysis and climate models over Central Africa. McCollum et al. (1999) found that for long-term mean, Global Precipitation Climatology Project (GPCP) dataset is in better agreement with rain-gauged data; however, because of the scarcity of meteorological stations, gauged observations did not provide accurate spatial rainfall estimates for comparison. In addition, they showed that peculiarity of Central Africa precipitation processes might lead to substantial errors in satellite based rainfall estimates. Asadullah et al. (2008) assessed five satellite products (TRMM 3B42, CMORPH, TAMSAT, RFE 2.0 and PERSIANN) over Uganda and showed that seasonal patterns of rainfall are well reproduced and he recommended the use of more than one product for any applications. Washington et al (2013) examined, over Central Africa, rainfall biases and spatial distribution within observations (CMAP, CRU, GPCP, TRMM, TAMSAT, CMORPH), reanalysis (ERA Interim, ERA-40, NCEP) and climate model of the Coupled Model Intercomparison Project Phase 3 (CMIP3) and Phase 5 (CMIP5). They showed that rainfall is distributed zonally in March to May (MAM), essentially in observational datasets with high rainfall amount either over the Guinea Gulf (CMAP, ERA-40, ERA-Interim, TRMM) or in the east of central Africa (TAMSAT, NCEP, CMORPH). They also showed that, over Central Africa, satellite data and coupled models used in CMIP3/5 failed to capture the spatial distribution and amount of annual precipitation, with some satellite rainfall products overestimating rain rate by a factor of 2 or 3 (Nicholson and Grist, 2003; Washington et al. 2013). They also showed that all observational datasets can reproduce the bimodal annual cycle of rainfall over central Africa (Fig. 1.3). While assessing the hydrological cycle over Congo Basin, Siam et al. (2014) showed that among the reanalysis climate datasets (ERA-Interim, ERA-40, NCEP), ERA-Interim dataset does accurately represent the annual cycle of rainfall, but almost all general circulation models (GCMs) in CMIP3/5 were deficient by overestimating rainfall and runoffs (Siam et al. 2014). Those positive biases in CMIP4/5 climate models depend deeply on their respective spatial resolution (Siam et al. 2014). The above results underscore the non-consistency of rainfall distribution pattern in climate models, reanalysis and observations products. And thus, depending on the precipitation products used, rainfall studies over central Africa is likely to produce distinct results (Washington et al. 2013; Siam et al. 2014), which imply different variation, frequency and intensity at different time

scale. Moreover, using available observational datasets, Balas et al. (2007) and Desfuli and Nicholson (2013) portrayed substantial heterogeneity of rain rate within Central Africa.

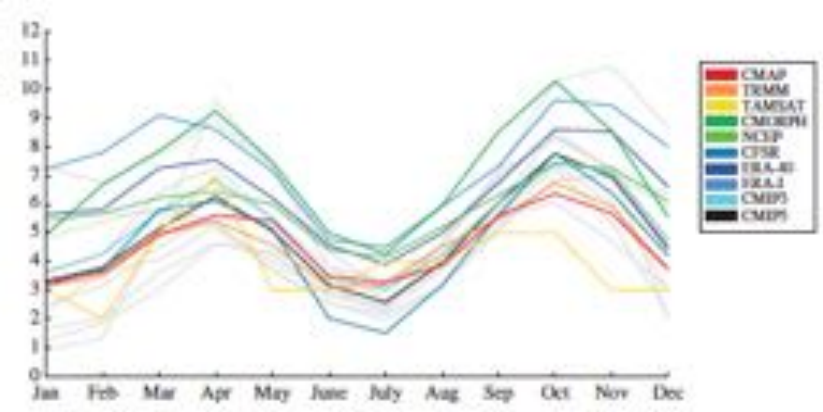

Fig. 1.3. Annual cycle of central Africa rainfall area-averaged over 5oN-5oS; 12.5o-30oE for CMAP.TRMM TAMSAT, CMORPH, NCEP, CSFR, ERA-40, ERA-Interim, ensemble mean of CMIP3 and CMIP5. Figure from (Washington et al. 2013)

Central Africa climate variability is due to interactions of numerous mechanisms suggesting that the physical process of formation of rainfall over central Africa could be different to that of other tropical/equatorial regions (McCoullum et al., 1999; Balas et al., 2007). Central Africa rainfall is modulated by Indian Ocean (Black et al. 2003; Washington and Preston, 2006; Seidel et al. 2008; Ummenhofer et al. 2009), Atlantic Ocean (Hirst and Hastenrath, 1983; Hastenrath, 1984; Philander, 1986; Nicholson and Entekhabi, 1987, Camberlin et al. 2001; Vizy and Cook, 2001; Todd and Washington, 2004; Balas, et al., 2007; Kucharski et al., 2007, 2008; Vigaud et al. 2008; Losada et al., 2010; Pokam et al. 2012; Nicholson and Dezfuli, 2013; Dezfuli and Nicholson, 2013; Lutz et al, 2015), land surface conditions (McGuffie, et al. 1995; Eltahir, 1996; Zhang, et al. 2001; Paeth, et al. 2009; James et al., 2013), African easterly jet (AEJ, Nicholson and Grist, 2002), mesoscale convective systems (MCS, Jackson et al., 2009; Nicholson, 2009), as well as by remote ocean basins such as the Pacific Ocean through El Nino Southern Oscillation (ENSO, Nicholson and Kim, 1997; Camberlin et al., 2001; Balas et al., 2007; Dezfuli and Nicholson, 2013; Nicholson and Dezfuli, 2013).

Figure 1.4 shows the seasonal march of rainfall over central Africa and its neighbouring regions using the mean of GPCP (Huffman et al. 2009) and CMAP (Xie and Arkin 1997) datasets. Both CMAP and GPCP data are retrieved from merged satellite precipitation data and are bias-corrected over land through continental rain-gauge observations (Bolvin et al. 2009). Therefore, CMAP and GPCP data reproduce quite well the mean state features of Central Africa rainfall (McCollum et al. 1999; Siam et al., 2014), with the mean of both datasets likely to reduce errors (Asadullah et al. 2008). The seasonal south-north march of deep convection over central Africa is largely driven by insolation (Biasutti et al. 2003). During June-July-August season (JJA), the east-west elongated rain-belt feature of Central

Africa rainfall is at its northernmost position, with high rain occurring extensively in north central Africa (~ 0°-10°N), with a maximum around Guinea Gulf (Fig. 1.4a). In September-October-November (SON), the rain-belt move southward to reach its southernmost position in December-January-February (DJF), when it rains mostly over the southern edge of central Africa (~ 5°S-15°S) (Figs. 1.4b-c). In March-April-May (MAM), high rainfall start to move northward (Fig. 1.4d). Notably, from September to April, high rainfall (> 4mm/day) falls over the entire Central Africa (Figs 1.4b-d).

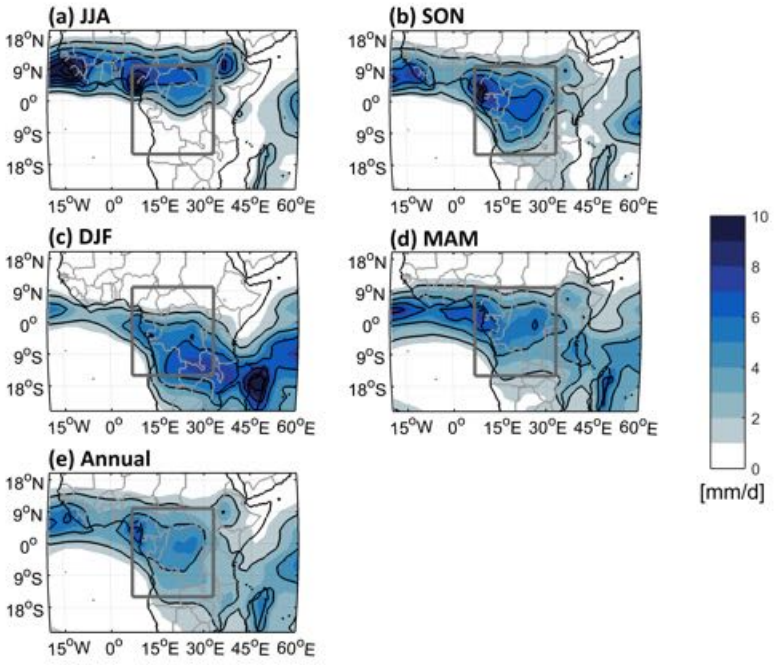

Fig. 1.4. Long term mean rainfall (mm/day, shaded) from 1979 to 2015 of the mean of both GPCP (Huffman et al. 2009) and CMAP datasets (Xie and Arkin 1997). From top to bottom: (a) JJA; (b) SON; (c) DJF; (d) MAM; (e) annual mean. In each panel, the gray box delineates Central Africa, while black lines represent the mean-rainfall at 2 mm/day interval.

The displacement of the large rainfall over Central Africa is not only meridional, with Central Africa seeming to be a transitional region between northern and southern edges of Africa, but rainfall varies zonally, with more rainfall over Central Africa and less in East Africa and Western Atlantic (Fig. 1.4). Annually, it appears that high rainfall occurs in two regions over central Africa: Guinea Gulf and East central Africa (15°-30°E) along the equator (Fig. 1.4e). However, the position of high rainfall does not always lead to areas of intense rainfall (Nicholson, 2009). Overall, the annual cycle of central Africa rainfall has a bimodal distribution with two maxima occurring in austral fall (MAM) and austral spring (SON) separated by two minima during austral winter (JJA) and austral summer (DJF) respectively (Fig. 1.3) so that Central Africa rainfall shows strong seasonality (Figs. 1.3-4). This above march of rainfall over Central Africa outlines the fact that the direct and dominant mode of rainfall variability over Central Africa is the intertropical convergence zone (ITCZ, Fansworth et al. 2011; Preston-Whyte

and Tyson 1988; Schott et al. 2003). It is characterized by low pressure system, maximum surface temperature, high rainfall, trade wind convergence and confluence and cloud clusters associated with tropical waves disturbances (McGregor and Nieuwolt, 1998; Nicholson, 2009). The clouds clusters associated with the ITCZ are defined as mesoscale convective systems (MCS). Mesoscale convective systems occur where transport of energy and moisture are vented vertically up to allow strong convection to occur. Central Africa experiences some of the world most severe thunderstorms and deep convection (Jackson et al. 2009). As an ascending branch of the Hadley cell, the central Africa ITCZ and its associated mesoscale convective systems are influenced by the trade winds and by the middle and upper levels jets known as African easterly jets (AEJ) and tropical easterly jets (TEJ) (Nicholson and Grist, 2003), respectively. The strengthening of AEJ enhances convection through African easterly waves, which lead to increased rainfall, while the weakening of African easterly jet suppresses convection and then, lead to decrease rainfall (Nicholson and Grist, 2003). Atmospheric convective instability leading to mesoscale convective systems is more related to vertical wind shear (Jackson et al. 2009). Formation of mesoscale convective systems is also related to land surface – atmosphere interactions (Jackson et al. 2009). More, wind plays crucial role in redistributing the energy and moisture, which in turn, influence temperature and precipitation patterns worldwide. But little is known about the large-scale circulation over central Africa. McCollum et al. (2000) reported that the westerly low-level jet over Atlantic supplied moisture into central Africa landmass and Vigaud et al. (2007) outlined the importance role of this low-level westerly jet for deep convection occurring during summer. Nicholson and Grist (2003) found the existence of AEJ and tropical easterly jet (TEJ) in mid- (i.e. ~600- hPa) and upper (200- hPa) troposphere over Central Africa respectively. Pokam et al. (2012) argued that the recycle of Central Africa precipitation is regulated by both low-level moisture flux direction and strength at seasonal time scale. All these findings point out to the key role of low-level circulation on Central Africa rainfall system. Another point of view is to consider this low-level transport of moisture as the lower branch of the Walker–type cell over central Africa. Some papers (Flohn, 1971; Webster, 1983; Yu and Zwiers, 2010; Yu et al. 2012; Thorsten and Richter, 2014) suggested the existence of a Walker–type cell over central Africa. Flohn (1971, cfr his Fig. 12) depicted a dominant asymmetric overturning circulation over Central Africa, with low-level westerlies suppling water vapour fluxes from eastern Atlantic as lower branch. Over the Rift Valley highlands, warm air uplifts (rising branch), while at upper levels, dominant easterlies form the returning branch. Finally, over the eastern Atlantic, the air subsides, constituting the closing branch. This Walker-like cell over Central Africa was confirmed by Yu and Zwiers (2010) and Yu et al. (2012) while they approximated the tropical planetary scale circulation to a thermally driven divergent component of the atmospheric flow. Whereas Webster (1983) and recently Thorsten and Richter (2014, cfr their Fig. 13) found a symmetrical overturning cells, with convergent branches, at low-levels, flowing moist air from surrounding Oceans into central Africa. Ascending branch of warm air is located over Central Africa landmass. At upper levels, the upward motion diverges and is considered as the return branches, before sinking over eastern Atlantic and western Indian Oceans respectively, closing the

circulation. With respect to the seasons, the ascending branch is situated either over eastern Africa or over the eastern Atlantic Ocean. And hitherto, no consensus has been made on the Walker–type circulation over central Africa. In addition, Pokam et al. (2014) found at low-level troposphere, a Walker–type overturning circulation driven by divergent circulation over equatorial central Africa (15^{o} – 45^{o}E of longitude and equator – 10^{o}N of latitude), with strong westerlies between 10–15^{o}E. Also, they added that this overturning circulation over Central Africa is due to the differential adiabatic heating between Central Africa and eastern Atlantic Ocean, which is stronger during rainy seasons in September to November (SON) and March to May (MAM) (Pokam et al. 2014). More recently, Kerry and Vizy (2015) and Neupane (2016) outlined an overturning zonal circulation over Congo basin (15–25^{o}E of longitude and 3^{o}S – 3^{o}N of latitude) centered at ~700- hPa, from June to October. This zonal overturning over Central Africa forms when the Atlantic cold tongue matures to set up favourable atmospheric conditions for its development. However, this zonal overturning circulation over Central Africa is timing out of phase with central Africa rainfall, but it does play crucial role in regulating precipitation over Sahel and western Africa (Kerry and Vizy, 2015; Neupane, 2016). To the best of our knowledge, the large–scale atmospheric dynamics over Central Africa rainfall system has been studies little and is not consistent yet.

On inter-annual timescales, sea surface temperatures (SSTs) of tropical Oceans – particularly Atlantic and Indian – may impact climate in their surrounding continents such as central Africa (Wang et al, 2009; Balas et al, 2007; Fisher et al, 2005). However, the tropical Indian and Atlantic Oceans are home to intense convection and subject of strong thermal and dynamical ocean-atmosphere interactions (Xie and Carton, 2004; Ruiz-Barradas et al. 2003, Keenlyside et al, 2007; Weller et al. 2014; Cai et al., 2014). The Indian Ocean is influenced by both ENSO and Indian Ocean dipole (IOD) climate modes (Yamagata et al., 2004; Luo et al., 2010; Cai et al., 2012). Moreover, the remote forcing occurring over tropical Pacific (ENSO) might influence the Indian and Atlantic Ocean variability, and then, modulates the location and intensity of major zonal atmospheric cells (Alexander et al. 2002; Dezfuli and Nicholson 2013; Giannini et al. 2008; Nicholson and Dezfuli 2013). Thus, this atmospheric condition is likely to affect the rainfall over Central Africa. Balas et al. (2007) have presented the most comprehensive investigation of SSTs relationships with central Africa rainfall. They argued that the Atlantic Ocean, especially the coastal region, influence the north-south excursion of the ITCZ. Positive SSTs anomalies over Atlantic Ocean increase rainfall directly near the Atlantic coast (Balas et al. 2007; Lutz et al. 2015). Furthermore, indirectly, Atlantic SSTs anomalies could have both a positive and negative impact on rainfall through modification of moisture advection (Balas et al., 2007; Vigaud et al. 2008; Lutz et al, 2015). Washington and Preston (2006) studied the Africa climate response to Indian SST anomalies using NCEP reanalysis and HadAM3 models. Their results show that Indian SSTs anomalies might play an important role in modulating rainfall over Central Africa by supplying moisture from Indian ocean. Balas et al. (2007) argued that the role of SSTs anomalies over the Indian Ocean was potentially important for inter-annual rainfall variability over Central Africa. During austral

spring (SON), Central Africa rainfall is positively correlated with SST anomalies over the Indian Ocean and negatively correlated with Atlantic coastal regions (Congo, Gabon) (Balas et al. 2007). For Central Africa, the main sources of moisture are tropical Atlantic (Vigaud et al., 2008) and tropical Indian, for the southern and eastern part of Central Africa. Kucharski et al. (2009) – using atmospheric general circulation model (AGCM) – found for austral winter a teleconnection between the tropical Atlantic and Indian SSTs that could impact Central Africa rainfall. They suggested that this teleconnection between tropical Atlantic and Indian Oceans is due to the Gill-Matsuno effect with the atmospheric Kelvin and Rossby waves transporting the signal across central Africa to the east towards Indian Ocean and further to the west of Pacific Ocean. Indeed, the Gill-Matsuno mechanism is a response of the atmosphere to the heating anomaly in the equatorial Atlantic and Indian Ocean regions, with the equatorial Kelvin waves transport the signal from to the east, whereas equatorial Rossby waves are responsible for the westward propagation. However, the relationship between central Africa rainfall and SSTs over Atlantic and Indian Oceans remains complex and seasonally dependent (Balas et al., 2007), with the main drivers of the inter-annual variability still unknown and undocumented.

Some studies (Balas et al. 2007; Camberlin et al. 2001; Nicholson and Kim 1997) have reported potential impacts of remote mechanisms on central Africa rainfall such as ENSO. Nicholson and Kim (1997) have shown negative correlation between central Africa rainfall and ENSO (Niño 3 SST anomalies) during austral late summer (January – March) and spring (August – November), with Walker circulation playing a major role (Hua et al. 2016). In fact, Hua et al. (2016) showed that El Nino-like variation in the tropical Pacific may weaken the ascent motion over Central Africa that is associated with the reduced low-level moisture transport and so, lead to drought particularly in April-May-June (AMJ) season. Meanwhile ENSO tends to extend dry season during austral winter and to increase rainfall during late austral spring (October – December) over south east of central Africa (Nicholson and Kim 1997). But the impacts of ENSO over central Africa rainfall are limited (Camberlin et al. 2001 and Malhi and Wright, 2004). Furthermore, Todd and Washington (2004) reported that there is a strong teleconnection between large-scale circulation over tropical North Atlantic and Central Africa rainfall as well as with the Congo river discharge. Rainfall surplus over Central Africa is associated with anomalous westerly mid-tropospheric zonal winds over the coastal (Central Africa/Atlantic) region. These anomalies appear to be a coherent structure of zonal wind anomalies extending to the polar regions of the North Atlantic, similar to that associated with the NAO pattern at multi-annual timescales, while at inter-annual timescales they may be relatively independent of tropical North Atlantic.

Finally, the Congo basin rainforests, like any forests, regulates central Africa rainfall by interacting with atmosphere via exchange of huge amounts of water through evaporation, evapotranspiration and recycled moisture (Zeng and Neelin, 1999). Deforestation may diminish the development of mesoscale convective systems through reduced moist static energy (Clark and Arrit, 1995).

1.3. Outline

In this dissertation, we largely focus on the seasonal cycle of the large-scale dynamics of central Africa rainfall system. Each chapter could be read separately since it is motivated by a specific question and all of them are in preparation for publication in peer review journals. However, the mutual thread connecting these questions is an understanding of the physical mechanisms involved in the hydroclimate variability of central Africa. In chapter 2, we use available reanalysis, observations and satellite estimate to unfold the key features of the seasonal cycle of central Africa rainfall in term of spatial distribution and intensity. In addition, the ECHAM5.3 atmospheric climate model over Central Africa is assessed to represent the main features of the annual cycle of Central Africa rainfall. While dealing with this question, Chapter 3 provides an insight of the formation, seasonal evolution, strength, structure and trends of the Walker-like circulation over central Africa and its associated moisture and energy transports. The chapter 4 investigates how to identify and characterize the mid-lower tropospheric pressure system over central Africa and its influence on regional climate. This allow us to unravel how do AEJs affect the Central Africa water budget and what do control the Central Africa rainfall variability in chapters 5 and 6. Finally, in chapter 7, the dominant modes of central Africa rainfall inter-annual variability are revisited, and we try to shed more light on the physical mechanisms involved in the relationship between central Africa rainfall and its surrounding tropical Oceans focusing particularly on the impact of the inter-basin SST gradient on central Africa rainfall variability. Finally, in chapter 8, we conclude, by presenting the main results of the physical mechanisms driving Central Africa rainfall system and its adjacent Oceans and propose some future works.

Chap. 2

Representation of Central Africa rainfall annual cycle in observations, reanalysis and ECHAM climate model

2.1. Introduction

In addition to accurately assess the abundance of water resources over central Africa, understanding of spatial and temporal variability of rainfall is important to estimate rainfall availability. Studies on central Africa climate suffer from the dearth of available data related to a lack of sustained meteorological network – with for instance only three stations in Democratic Republic of Congo reporting to global telecommunications system in 2013 (Washington et al. 2013). As a warmer climate is expected to change precipitation patterns over Africa through its distribution, frequency and intensity (IPCC, 2007, 2012), there is a strong demand of future impacts studies of global warming on water resources in Central Africa. Unfortunately, access to quality controlled long term in-situ data is lacking. In this situation, the use of alternative sources of rainfall data such as satellite estimate of rainfall or numerical weather prediction (NWP) may be profitable and useful. To investigate the inter-annual variability of rainfall over central Africa, many studies (Balas et al. 2007; Nicholson and Grist, 2003; Todd and Washington, 2004; Washington et al. 2013; Pokam et al. 2014; Dezfuli and Nicholson, 2013.) used various rainfall datasets. But, few studies tried to evaluate rainfall in observations, reanalysis and climate models over central Africa. McCollum et al. (1999) found that for long-term mean, Global Precipitation Climatology Project

(GPCP) dataset is in better agreement with rain-gauged data; however, because of scarcity of meteorological stations, gauged observations did not provide accurate spatial rainfall estimates for comparison. In addition, they showed that peculiarity of central Africa precipitation processes might lead to substantial errors in satellite based rainfall estimates. To minimize those errors, the use of more than one product is recommended (Asadullah et al. 2008). While Siam et al. (2014) showed that ERA-Interim dataset does accurately represent the annual cycle of central Africa rainfall. The above results underscore the non-consistency of rainfall distribution pattern in climate models, reanalysis and observations products. Depending on the precipitation products used, rainfall studies over Central Africa is likely to produce distinct results (Washington et al. 2013; Siam et al. 2014), which imply different variation, frequency and intensity at different time scale.

Many studies focused on inter-annual variability of rainfall and less on understanding the annual cycle. To unfold the key features of the annual cycle of rainfall over central Africa, it is better to understand the spatial distribution of rainfall and its intensity in association with thermodynamic, moisture and circulation balance in each season. Because, there is almost no study evaluating the performance of atmospheric general climate models (AGCM) over Central Africa, we will try to evaluate the capability of ECHAM5.3 to represent the Central Africa rainfall. These are our main objectives for this chapter. Nevertheless, according to Pokam et al. (2012), the season window is classified as follow in this chapter: March-April-May (MAM), June-July_August (JJA), September-October-November (SON) and December-January-February (DJF). Many papers (e.g. Suzuki, 2011; Nicholson, 2009) have reported on meridional displacement of the annual cycle of rainfall over Central Africa linked to ITCZ. In this chapter, the zonal displacement of Central Africa rainfall annual cycle is also investigated.

2.2. Datasets

In this chapter, a variety of rainfall data sources (observed, reanalysis and climate model) are used to ascertain the zonal migration of Central Africa rainfall annual cycle. Nevertheless, observed rainfall datasets have been classified in two classes: ground-based only and merged satellite and rain-gauges datasets so that they can be used as such or in combination. In addition, many studies (Gleixner et al. 2014; Mohino et al. 2011; Sperber et al. 2013) pointed out the good performance of ECHAM version 5 to document the tropical climate variability and predictability. So, in this chapter, we try to extend their studies over central Africa to investigate not only how does well ECHAM version 5.3 capture the zonal propagation of central Africa rainfall, but also to figure out what are the physical mechanisms driving its seasonal cycle.

2.2.1. Ground-based data

Rain gauge datasets are in situ measurements. They used to be considered at first sight as "ground-based truth". In this chapter, I chose only two gridded-gauge only data, which are used in numerous studies: Climatic Research Unit, CRU TS3.10 (referred as CRU, Harris et al. 2013) and

Global Precipitation Climatology Centre dataset (hereafter GPCC, Schneider et al. 2013; Becker et al. 2013). GPCC and CRU are based on interpolation of in situ rain measurements and they cover land areas at monthly temporal resolution from 1901 to present. GPCC is available gridded at 2.5×2.5-degree longitude/latitude whereas the CRU dataset is available at 0.5×0.5 degree respectively. It is clear that many grid point do not use any rain gauges and are just interpolated or built using statistical techniques, particularly over central Africa.

2.2.2. Merged satellites and rain-gauges data

We used essentially the Climate Prediction Center Merged Analysis of Precipitation dataset (CMAP, Xie and Arkin 1997) and the Global Precipitation Climatology Project monthly precipitation dataset (GPCP, Huffman et al. 2009), available at monthly temporal resolution (1979 to present) at 2.5×2.5 degrees because of the long time span they cover. CMAP and GPCP datasets are compiled from merged satellite precipitation data and bias-corrected over land through continental rain-gauge observations (Bolvin et al. 2009). These datasets cover the whole globe, including the oceans. In addition, Asadullah et al. (2008) evaluated CMAP and GPCP datasets among many other observation data and found that these two data represent quite well the mean state features of central Africa rainfall. We added in this category the TAMSAT African Rainfall Climatology and Time-series (TARCAT) (Tarnavsky et al., 2014; Maidment et al., 2014). To the best of our knowledge, many studies did evaluate TAMSAT over the entire Africa region, but not over Central Africa yet. TAMSAT data combined satellite thermal infrared measurements with other data sources such as microwave retrievals and rain gauge measurements (Maidment et al. 2014). It is available to a regular resolution of 2.5° latitude/longitude grid and its temporal resolution spans from 1983 to present at monthly basis.

2.2.3. Reanalysis

The NCEP-DOE rainfall reanalysis (hereafter NCEP-2, Kanamitsu et al. 2002) and ERA-Interim products (Dee et al. 2011) are used in this study. NCEP uses CPC Merged Analysis of Precipitation (CMAP), described in Xie and Arkin (1997), from its pentad dataset to adjust the model precipitation that drives the land-surface scheme, to produce more realistic hydroclimatology and employs the simplified Arakawa-Schubert cumulus convection scheme (Pan and Wu, 1995; Hong and Pan, 1998). While ERA-Interim reanalysis has cumulus convection parametrized by a bulk mass flux scheme originally described by Tiedtke (1989), which considers deep, shallow and mid-level convection. The model precipitation depends on temperature and humidity derived from the assimilated observations (Dee et al., 2011). The spatial resolutions are 2.5×2.5 degrees grid and 0.75×0.75 degrees respectively. In reanalysis, rain rate is the total precipitation defined as a sum of convective precipitation and large scale precipitation, owed by the differences in thermodynamics, related to vertical air motions, and microphysical processes governing rain formation (Houze, 1993), available at 6-hours interval. To compute the moist static energy, we used atmospheric variables of ERA-Interim, which include, air temperature, geopotential height,

specific humidity, zonal and meridional wind at 13 pressure levels (1000, 925, 850, 775, 700, 750, 700, 600, 500, 400, 300, 200, 100) at monthly time steps

2.2.4. SST-forced atmospheric climate model

The European Centre Hamburg Model (ECHAM, Roeckner et al. 2003) is an atmospheric general circulation model forced by SST from the Max Planck Institute for Meteorology. It uses a spectral dynamical core with a triangular truncation of spherical harmonics and a semi-implicit leapfrog time difference scheme. This spectral model is used with T106 (approximately 1°) horizontal resolution and 31 vertical levels extending up to 10 hPa (approximately 30 km). The convection parameterization is based on the Tiedke scheme (Tiedtke, 1996). The ECHAM5.3 model runs consist on the historical simulations of a five-member ensemble driven with the ERSST monthly SSTs from 1870 to 2009 previously produced (Tseng 2012). These simulations include no time-varying external atmospheric forcing, and the ensemble members only differ in the initial 1870 SST conditions (Gleixner et al. 2016). Thus, we use mainly the ensemble mean of 5 simulations. The control run is driven by the global SST monthly climatology for the period 1870–2009 computed from the ERSSTv3b. Total precipitation is obtained as a sum of convective and large scale precipitation. We also use air temperature, geopotential, specific humidity, zonal and meridional wind components at 13 pressure levels (1000, 925, 850, 775, 700, 750, 700, 600, 500, 400, 300, 200, 100) at monthly time steps, while the spatial resolution is gridded at 1.125°×1.125. The model output spans from 1870 to 2009.

In this study, rainfall and all atmospheric variables of all these datasets are interpolated onto the same 1.125°×1.125° grids to help with comparison, which is in fact the setting up resolution for the ECHAM5.3 models.

2.3. The Central Africa rainfall annual cycle: Intercomparison

The annual cycle of rainfall averaged over Central Africa (7°-33°E) is presented in Fig. 2.1 through a Hovmoller diagram for observations, reanalysis and ECHAM5.3, with the time as X-axis and the latitude as Y-axis. It corresponds to the well-known northward displacement of the zonal-mean rainfall annual cycle. In this chapter, the ITCZ is defined as the maximum of rainfall over latitude. Central Africa rainfall is characterized by the northward displacement of rainfall from 15^{o}S to the equator year-round. However, in May/June, a sudden shift of central Africa rainfall occurs and it is characterized by a surge of high rainfall (> 5mm/d) moving rapidly northward to reach about 10^{o}N a month later. This surge of high rainfall associated with a rapid northward move of rainfall, over Sahel, is referred to as monsoon jump (Sultan and Janicot, 2003). The core of Central Africa rainfall persists until October/November, while associated with sharply southward move back to the equator. Whilst still moving southward, an abrupt termination of high rainfall over central Africa corresponds to the end of the year (Fig. 2.1). But in rain-gauge datasets (CRU, CMAP and their

related average), another core of rainfall located between 5°S and 15°S (Fig. 2.1d-f) occurred from December to February. This southward rainfall jump (as referred to Sultan and Janicot, 2003) is only reproduced in TAMSAT (Fig. 2.2j).

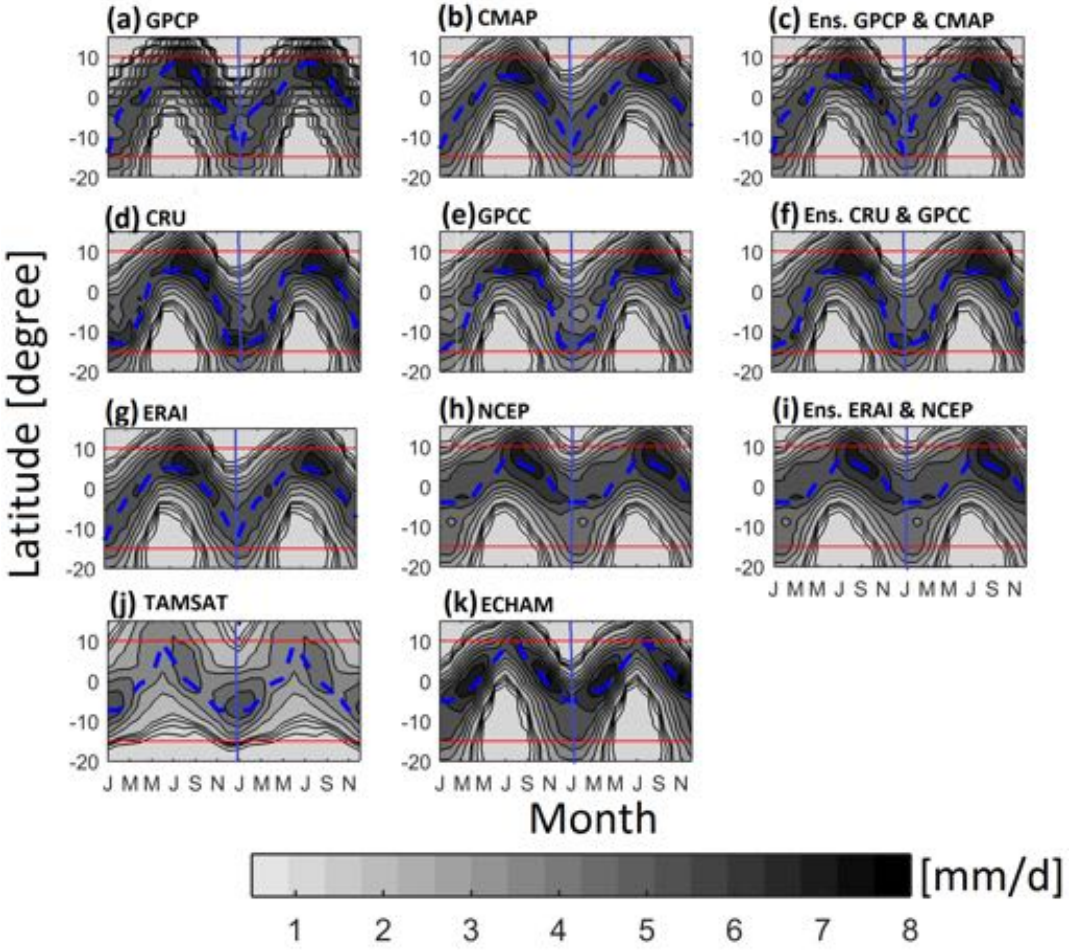

Fig. 2.1. Hovmoller (latitude-time) of annual march of rainfall (mm/day). averaged over central Africa (7°-33°E) (X-axis: all months and Y-axis: latitude): (a) GPCP; (b) CMAP; (c) Ensemble of GPCP and CMAP; (d) CRU; (e) GPCC; (f) Ensemble of CRU and GPCC; (g) ERAI; (h) NCEP-2; (i) Ensemble of ERAI and NCEP-2; (j) TAMSAT and (k) ECHAM5.3. The thin and bold blue dashed line on all panels highlights the meridional migration of ITCZ defined as rainfall maximum, and January month. The red lines delineate central Africa (10°N-15°S). The annual cycle has been represented twice. The contour interval is 0.5 mm/d.

In ECHAM5.3, the rainfall jump occurs twice per year, over equatorial region of central Africa between 5°N and 5°S, from January to May and August/September to December (Fig. 2.1k), which is also simulated in some Cordex data (UC WRF, UCAM CRCM5) (Tanguela et al. 2016). In addition, the observed high rainbelts – associated with deep convection – move as far as 10°N in June-July-August (JJA) to down 10°S in December-January-February (DJF) before moving north

again the next season (Fig. 2.1). This south-north march of deep convection over Central Africa is largely driven by insolation (Biasutti et al. 2003). The ITCZ location is principally found in the northern hemisphere in NCEP-2 and ECHAM5.3 (Fig. 2.2). In the other products, the ITCZ is equally spread between North and South hemispheres (Fig. 2.1). In TAMSAT, the ITCZ southernmost position is located near 10°S (Fig. 2.1j). Whereas for the rainfall rate, rain-gauges data (CRU, GPCC and their ensemble) have large rainfall amount. ECHAM5.3 has relatively the same rainfall amount as the average of GPCP and CMAP (Fig. 2.1c). But TAMSAT seems to underestimate the rainfall when compared to other products (Fig. 2.1j). Although all rainfall datasets have a similar representation of the meridional distribution of ITCZ and associated rainfall amount, differences are found mostly in TAMSAT. However,

After having described the meridional distribution of central Africa rainfall, it is also interesting to assess the zonal distribution of rainfall over central Africa to better understand the comprehensive seasonal evolution of rainfall in this region. The longitude vs. time Hovmoller plot of meridional-mean rainfall averaged between 10°N and 15°S is shown in Figs. 2.2. The longitude axis provides a view of the eastward/westward migration of central Africa rainfall. For CRU and GPCC (rain-gauges datasets), we should notice the missing rainfall data over Atlantic Ocean region (Harris et al. 2013, Schneider et al. 2013 and Becker et al. 2013). In January, ITCZ starts to develop at ~24°E and propagates westward toward Guinea Gulf or Atlantic offshore regions (07-15°E). In MAM, a rainfall jump occurs over Atlantic offshore regions, while decreasing a bit over east of central Africa, leading to almost uniform rainfall of ~ 2mm/d overall central Africa (Fig. 2.2). By May, rainfall weakens abruptly (< 2mm/d) over the entire central Africa, but remains high over the Atlantic offshore regions (Fig. 2.2), which is associated with the northward propagation of ITCZ over Gulf of Guinea (Thorncroft et al. 2008). In SON, rainfall increase to about 5 mm/d (Fig. 2.2). This re-intensification of rainfall is associated with a rainfall jump to east central Africa, associated with suppression of convection over Guinea Gulf (Fig. 2.2). This could be interpreted as eastward displacement of the ITCZ towards central Africa. In December, high rainfall is still confined west of ~24°E marking the return of the ITCZ to its initial position. The annual cycle of the zonal central Africa rainfall depicts a “X-ray lung” cliché”, with two rainfall maxima in SOND and JFMA separated by a rainfall minimum in MJJA (Fig. 2.2). CRU shows high rainfall bands (>8mm/d) over Atlantic offshore regions (at around ~10°E) from April to November (Fig. 2.2d). TAMSAT (Fig. 2.2j) features less rainfall than all the other observational and satellite estimate datasets, while NCEP (Fig. 2.2h) shows high rainfall over the highlands between 20° and 33°E. In NCEP-2, the ITCZ longitudinal migration is confined at ~24°E (Fig. 2.2h-i). CRU has a westward rainfall migration starting in March, while all remaining observed datasets have a westward propagation one month before. Only TAMSAT has an eastward displacement of the ITCZ, spanning from March to September before returning at its initial location in Guinea Gulf by October (Fig. 2.2j), consistent with Washington et al. (2013). The bimodal zonal characteristic of central Africa rainfall morphed in a

unique rainfall season over the Atlantic offshore regions and persists as long as the ITCZ overlays this region (Fig. 2.2).

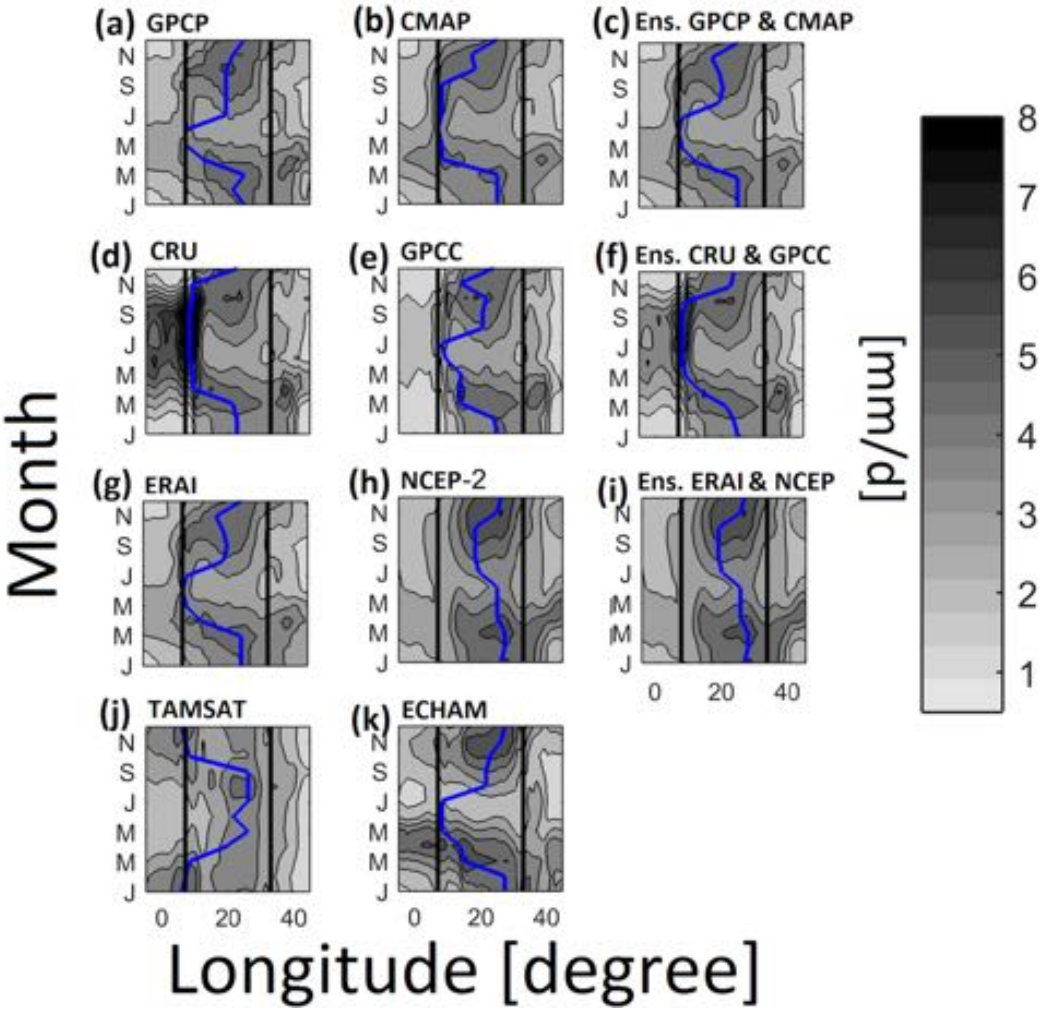

Fig. 2.2. Hovmoller (longitude-time) of observed and modelled central Africa seasonal rainfall-mean (mm/day) averaged between 10°N-15°S (X-axis: longitude and Y-axis all calendar months): (a) GPCP; (b) CMAP; (c) Ensemble of GPCP and CMAP; (d) CRU; (e) GPCC; (f) Ensemble of CRU and GPCC; (g) ERAI; (h) NCEP-2; (i) Ensemble of ERAI and NCEP-2; (j) TAMSAT and (k) ECHAM5.3. The bold blue line on each panel represent the zonal displacement of central Africa rainfall maximum (ITCZ), while the black vertical lines delineate the boundaries of central Africa (7°-33°E). The contour interval is 0.5 mm/d.

This unique rainfall season over Atlantic offshore regions ranged from two months in GPCP to eight months in CRU respectively (Fig. 2.2). ECHAM5.3 does relatively well to represent the ITCZ westward displacement over central Africa and it also displays the bimodal characteristic of zonal

central Africa rainfall annual cycle (Fig. 2.2k). It does have slightly larger amplitudes during high rainy seasons (Fig. 2.2k).

Table 2.1. Correlation between annual rainfall-mean in observations, reanalysis and ECHAM

	GPCP	CMAP	GPCP+CMAP	CRU	GPCC	CRU+GPCC	ERAI	NCEP -2	ERAI+NCEP	TAMSAT	ECHAM
GPCP	1.00										
CMAP	0.86	1.00									
GPCP+CMAP	0.96	0.96	1.00								
CRU	0.62	0.53	0.60	1.00							
GPCC	0.96	0.83	0.93	0.69	1.00						
CRU+GPCC	0.84	0.72	0.81	0.93	0.90	1.00					
ERAI	0.87	0.82	0.89	0.76	0.72	0.76	1.00				
NCEP-2	0.77	0.70	0.76	0.47	0.78	0.66	0.81	1.00			
ERAI+NCEP	0.77	0.70	0.77	0.49	0.77	0.59	0.95	0.97	1.00		
TAMSAT	0.02	0.02	0.02	-0.08	0.01	-0.04	0.15	0.08	0.08	1.00	
ECHAM	0.87	0.78	0.91	0.79	0.89	0.90	0.88	0.86	0.86	0.21	1.00

Furthermore, the inconsistency between rainfall datasets could be due either to the intrinsic technique used for estimation of rainfall rate or to the quality of the gauge observations used (McCollum et al. 2000). This becomes evident when I calculated the cross correlation between central Africa rainfall datasets (Table 2.1).

The result indicates substantial difference among the datasets. Low correlation has been scored by TAMSAT ($r < 0.1$), highest values of correlation are found for other observational datasets ranging between 0.47 for CRU and NCEP-2 and 0.96 between GPCP and GPCC. Although each rainfall product shows similar feature of the seasonal rainfall evolution, they have different spatial pattern and rainfall magnitude. For the rainfall of the average of datasets related to observations, satellite and reanalysis, correlation does not only improve (Table 2.1), but also the discrepancy seems to be reduced (Figs. 2.1-2). This suggests that the simple and effective method to reduce uncertainty between observed datasets is to combine at least two datasets (Asadullah et al. 2008). In fact, Asadullah et al. (2008) recommended the use of more than one product for any applications to reduce biases and enhance quite well the representation of seasonal patterns of rainfall over Central Africa. More, strong relation is found between ECHAM and all others datasets, ranging from 0.1 with TAMSAT to 0.91 in the ensemble of GPCP and CMAP. This method confirms the use of ECHAM5.3 to represent central Africa rainfall, consistent with the findings of Gleixner et al. (2014) and Yang et al. (2015) over tropical regions of Africa.

2.4. Seasonal intensity of Central Africa rainfall

Another helpful diagnostic of central Africa rainfall is to determine how suitable is the distribution of rainfall over Central Africa, in term of its intensity. We use the monthly rainfall to define the

intensity as a rate of rainfall over either a season (MAM, JJA, SON and DJF) according to Pokam et al. (2012) or annually (all months). Then we computed the probability density functions (PDF) related to rainfall intensity during whole the seasons and years across 37 years spanning from 1979 to 2015 and displayed them in Fig. 2.3. The annual and seasonal rainfall-mean are area-averaged over central Africa (07°N-33°E; 10°N-15°S) and binned at 0.005 mm/d. As shown in Fig. 2.3, all rainfall datasets – except TAMSAT – show positive skewed unimodal seasonal rainfall distribution ranging between 2 and 6 mm/day (Fig. 2.3a-i). In all datasets, high rainfall intensity occurs in SON and less rainfall in JJA. For CRU, less rainfall intensity is found in DJF. TAMSAT features negative skewness of mean rainfall intensity for annual and all seasons, except for MAM. Moreover, TAMSAT presents a bimodal distribution of seasonal rainfall intensity with two maxima at 2 and 4 mm/d for JJA, SON, DJF and annual-mean (Fig. 2.3j) respectively.

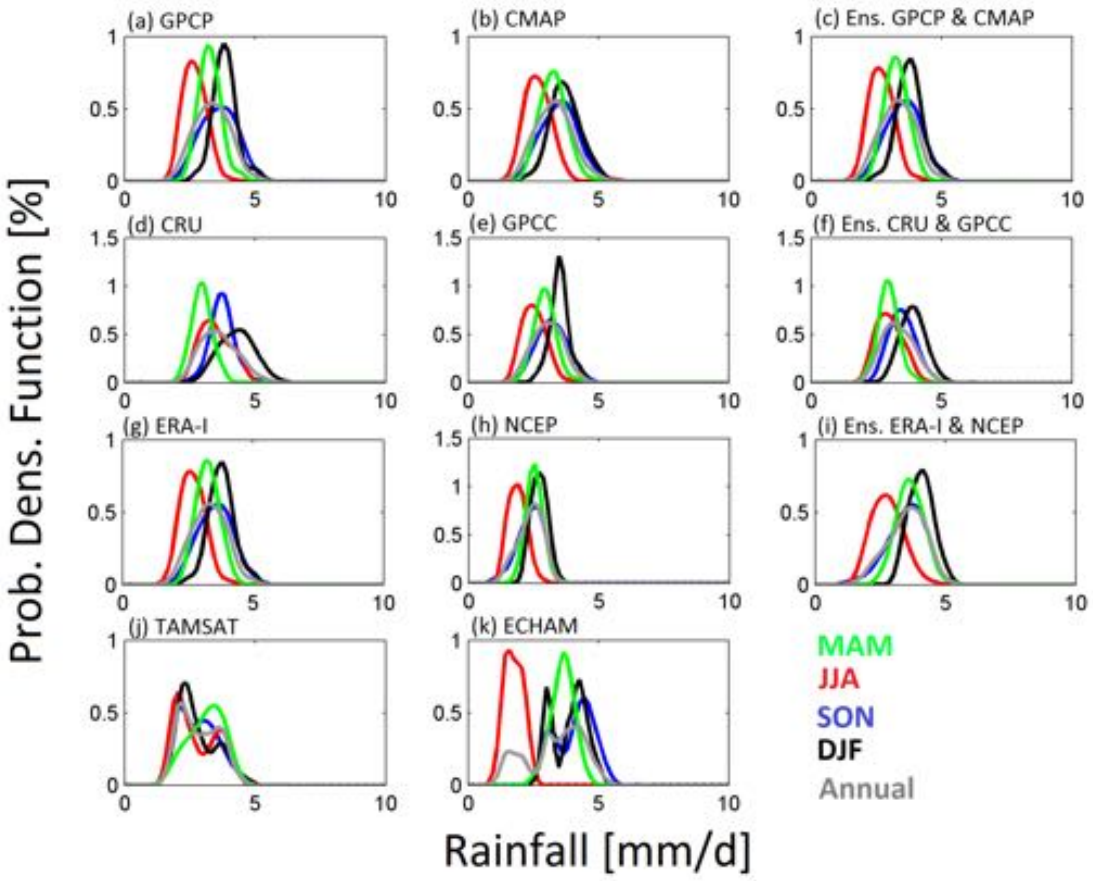

Fig. 2.3. Probability density functions (PDF, %) of the annual and seasonal rainfall (area-averaged over central Africa, 7°-33°E, 10°N-15°S). (a) GPCP; (b) CMAP; (c) Ensemble of GPCP and CMAP; (d) CRU; (e) GPCC; (f) Ensemble of CRU and GPCC; (g) ERAI; (h) NCEP-2; (i) Ensemble of ERAI and NCEP-2; (j) TAMSAT and (k) ECHAM5.3.

As for ECHAM5.3, three distinctive rainfall intensities emerge at 2, 3 and 4 mm/day for annual rainfall mean (Fig. 2.3k). This is due to the combination of seasonal characteristic of rainfall – unimodal in MAM and JJA and bimodal in DJF and SON, with less rainfall occurs in JJA and more in SON (Fig. 2.3k). As mentioned previously, large difference in rainfall distribution is found between "observations"/reanalyses data and ECHAM5.3, during JJA, when rainfall is underestimated, while it is overestimated in all remaining seasons' rainfall.

2.5. Atmospheric thermal conditions of central Africa rainfall system

Based on moist static energy (*h*, Neelin and Held, 1987), we try to understand how thermodynamics processes lead to rainfall over central Africa. Neelin et al., 2003; Chou and Neelin, 2004; Chou et al. 2009; Giannini, 2010, Seth et al. 2011; 2013 among others used moist static energy to examine the role of both energy and water budgets to understand precipitation over regions of deep convection. The vertical profile of moist static energy is a good indicator of atmospheric stability derived from the vertical distribution of moisture and temperature. The moist static energy (*h*) is defined as follow:

$$h = DSE + L_v q \qquad (2.1)$$

$$DSE = C_p T + \phi \qquad (2.2)$$

where *DSE* is dry static energy, with contribution of both internal ($C_p T$) and potential (ϕ) energies respectively; C_p is specific heat capacity of dry air at constant pressure; T is the air temperature; L_v is the latent heat of vaporization; q is the specific humidity and ϕ is the geopotential.

We normalized equations 2.1 and 2.2 by C_p so that unit of moist static energy (J/kg) and each of its components in equations (2.1 and 2.2) are expressed in K. The saturated moist static energy (h^*) is calculated in using the saturated specific humidity q^* in equation (2.1). Then, the moist static stability or instability index is defined as difference between moist static energy at near surface (1000- hPa) and saturated moist static energy at 700- hPa (Neelin and Held, 1987). The air column is unstable whether the moist static stability is positive.

The seasonal evolution of the meridional-mean of moist static energy averaged over 10°N-15°S of latitude is plotted in Fig. 2.4. At near-surface, the moist static energy shows a similar "lung-like" pattern as of the zonal march of Central Africa rainfall annual cycle, with warmer and moister air (h > 340 K) at ~24°E (over Central Africa landmass) associated with high rainbelts, and a westward extension towards tropical Atlantic from September to April (Figs. 2.4 top left; 2.2). In May to August (MJJA), strong reduction of moist static energy occurs over Atlantic Offshore region and East Africa (33°–40°E) respectively. This reduced moist static energy (h < 330 K) at near surface is associated with decreased rainfall (Figs. 2.4 top left & 2.2).

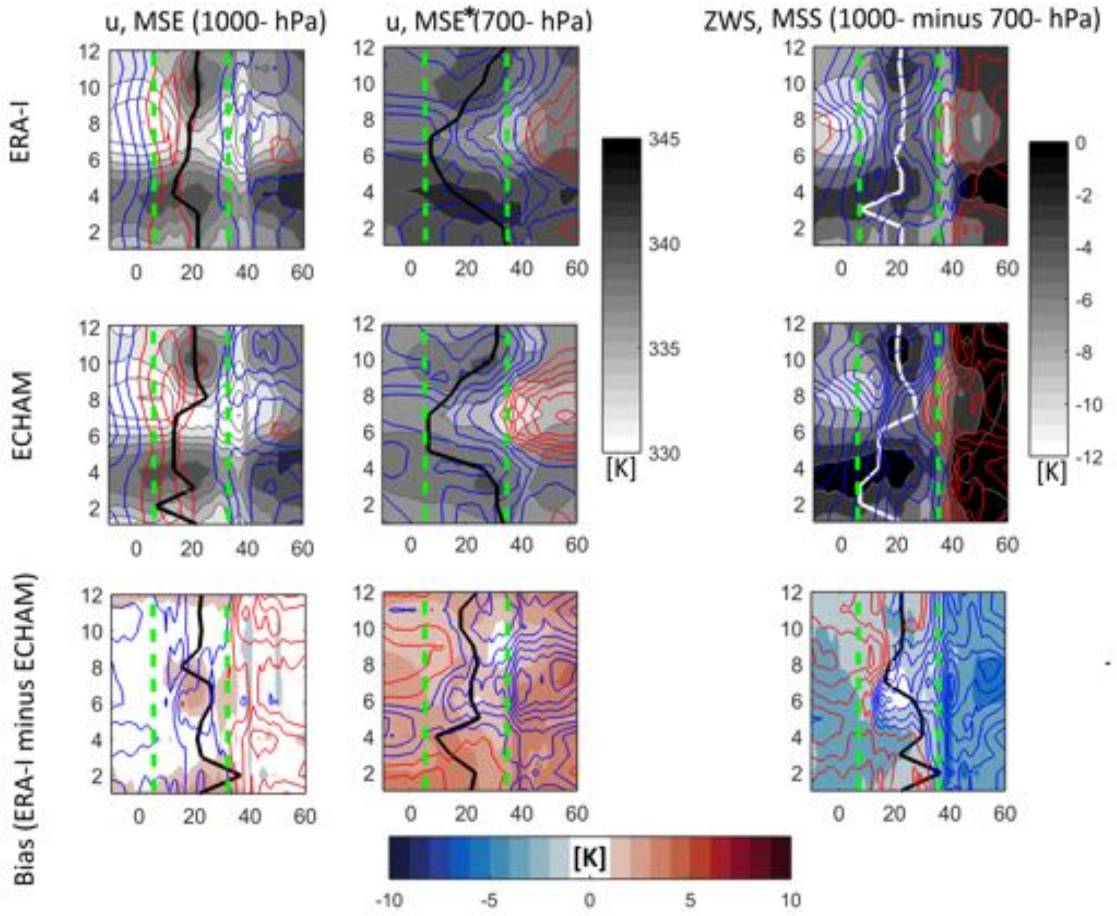

Fig. 2.4. Hovmoller (longitude-time) of ERA-Interim (top panel) and ECHAM (middle panel) and bias (ERA-Interim minus ECHAM, bottom panel) of moist static energy (MSE, K) and zonal wind component (u, m/s) at 1000- hPa (left panel), saturated moist static energy (MSE*, K) and zonal wind component (u, m/s) at 700-hPa (middle panel) and moist static stability (MSS, K) and vertical zonal wind shear (ZWS, m/s) (right panel) averaged over central Africa (10N°-15°S). The bold black line on all panels represents the zonal propagation of ITCZ over central Africa, while the bold white line indicates the moist static stability maximum over central Africa and bold green dashed line indicate the limit of central Africa. Blue and red line represent the easterly and westerly respectively, with contour interval of 1m/s and the zero line is omitted.

At 700- hPa, saturated moist static energy strengthens and produces the “lung-like” pattern of rainfall, owed likely by the midlevel easterlies wind (Fig. 2.4). Indeed, reduced saturated moist static energy is associated with decrease of midlevel easterly wind in May to August/September, while its strengthening is associated with the increasing of the midlevel easterly over central Africa. Furthermore, while comparing Figs. 2.2 and 2.4 (top right panel), it emerges that, in SOND and FMA, the intensification of rainfall over central Africa is associated with strengthened negative

vertical zonal wind shear and atmospheric instability, as moist static stability become close to zero or slightly positive (Fig. 2.4 top right panel). Whereas in MJJAS, near surface atmosphere is more stable, particularly over Atlantic Ocean, due probably to the intensification of cold tongue (Richter et al. 2012, Tokinaga and Xie, 2011). This means that in Central Africa, the rising motions of warm moist air at ~24°E is associated with atmospheric convective instability, likely triggered by strong easterly wind shear (Anber et al. 2014).

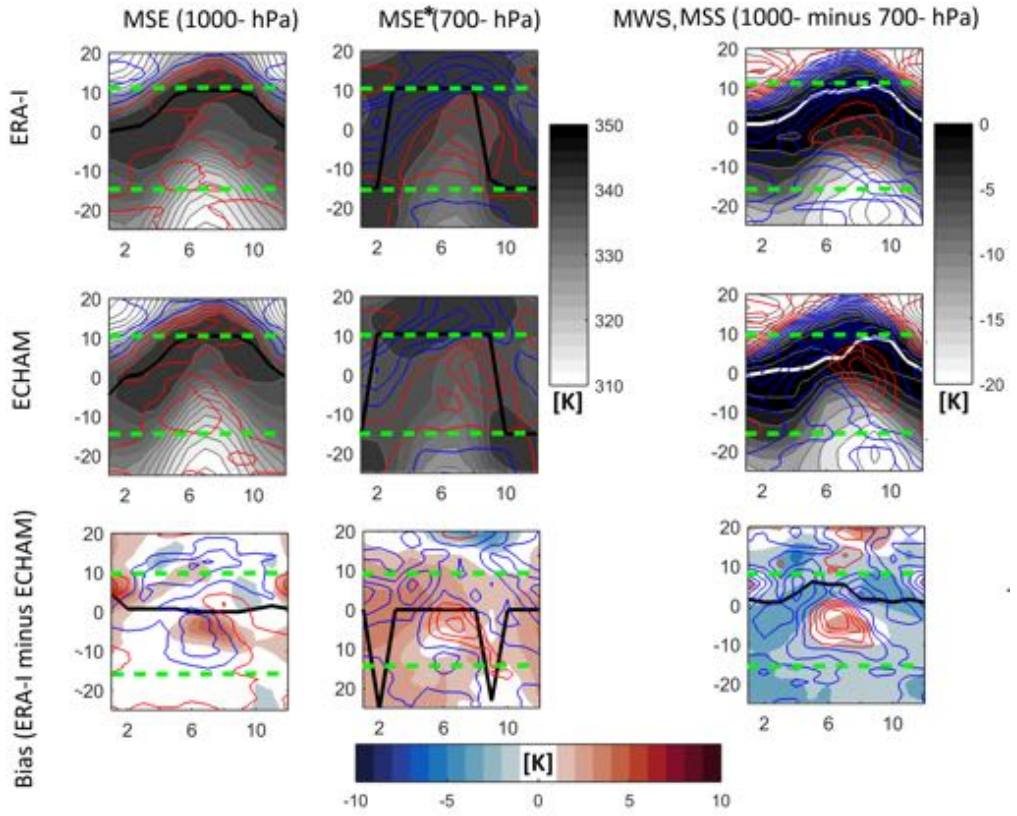

Fig. 2.5. Hovmoller (latitude-time) of ERA-Interim (top panel) and ECHAM (middle panel) and bias (ERA-Interim minus ECHAM, bottom panel) of moist static energy (MSE, K) and zonal wind component (u, m/s) at 1000- hPa (left panel), saturated moist static energy (MSE*, K) and zonal wind component (u, m/s) at 700-hPa (middle panel) and moist static stability (MSS, K) and vertical zonal wind shear (ZWS, m/s) (right panel) averaged over central Africa (7°-33°E). The bold black line on all panels represents the zonal propagation of ITCZ over central Africa, while the bold white line indicates the moist static stability maximum over central Africa and bold green dashed line indicate the limit of central Africa. Blue and red line represent the northerly and southerly respectively, with contour interval of 1m/s and zero line omitted.

In MJJAS, the atmospheric stability is associated with import of less moist static energy. This is characterized by the suppression of convection, indicative of subsidence essentially over Atlantic offshore regions. It is relevant to note the seasonal changes of surface moist static energy at near-

surface and saturated moist static energy at 700- hPa (Fig. 2.6). Notably, at near-surface, the westerly flow from Atlantic Ocean seems to be confined west of the moist static energy maximum (black line) over central Africa (Fig. 2.4, top left). While at 700- hPa, the maximum of moist static energy (black line) is strongly related with the core of the midlevel easterly over central Africa (Fig. 2.4, top middle). Conversely, strong meridional moist static stability lasts year-round over central Africa landmass, indicative of instable atmosphere (positive value), which is surrounded by regions of stable atmosphere over Sahel and southern Africa (negative value of moist static stability, Fig. 2.5 right panels). The spatial patterns of rainfall and meridional vertical wind shear suggest a strong relationship between them so that strengthening or lessening of the meridional vertical wind shear leads to more or less rainfall (Fig. 2.4, top right). Indeed, in OND and FMAM, high rainfall over central Africa is associated with strong northerly wind shear, while in JJAS, relatively low rainfall over central Africa is associated with southerly vertical wind shear (Fig. 2.5, top right). In addition, at near surface, the neutral atmospheric conditions (h < 330K) dominate over central Africa landmass, while in the other hand, the presence of warm and moist air is likely to destabilize the low-level troposphere, particularly during SOND and FMAM. The similarity of annual cycle of spatial patterns between rainfall and moist static stability over Central Africa suggests that the atmospheric instability controls the seasonal seesaw (northward–southward and east-west) march of rainfall over central Africa, with southerly and easterly wind shears contributing to destabilize further the atmosphere. Consequently, Central Africa rainfall maximum (black line in Figs. 2.1-2) is regulated by moist static stability (white line in Figs. 2.4 and 2.5), as indicated by their strong correlation (r=0.8). ECHAM5.3 reproduces quite well this mechanism. But unstable atmosphere occurs at lower moist static energy in ECHAM5.3 than in ERA-Interim, as suggested by the negative moist static stability bias, except in MJJAS between 15°-33°E and equator-10°S, where south-easterly wind shear bias dominates (Figs. 2.4 and 2.5, bottom panels). High rainfall belts in ECHAM5.3 are associated with a north-westerly bias from October to April (Figs. 2.2; 2.4 and 2.5, bottom panels). However, contrasted wind shear feature over surrounding oceans, with easterly wind shear over Atlantic and westerly wind shear over Indian (Figs. 2.4, bottom panels).

We further investigated the atmospheric thermodynamics conditions over Central Africa to determine what do lead to more longitudinal rainfall from October to May and less longitudinal rainfall in June to September season (cfr. Fig. 2.2). To do so, we first analyse the terms involved in the calculation of moist static energy (equations 2.1-2) represented in the Hovmoller diagram of moist static energy at near surface (1000- hPa) and midlevel (700-hPa) in Figs. 2.6 and 2.7 respectively. At near surface, the internal energy (T) term (Fig. 2.6, top) is larger than $L_v q/C_p$ (Fig. 2.6, middle) and ϕ/C_p terms (Fig. 2.6, bottom), and represents more than 85% of the total value of moist static energy. This means that the near-surface air temperature provides the bulk of surface moist static energy. However, warm temperature prevails from January to May, while internal

energy (T) decreases by about 3.5 K in JJA with respect to the annual mean (Fig. 2.6, top panels) due probably to the decrease of insolation over Central Africa (Biasutti et al. 2004).

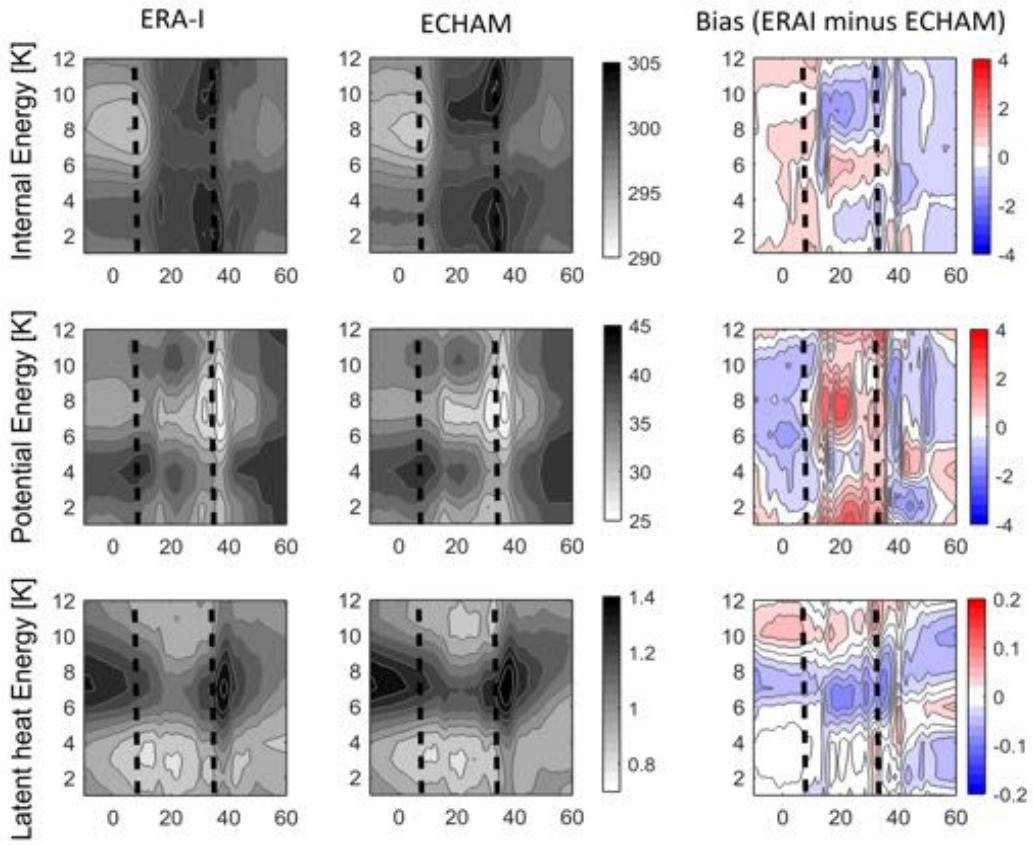

Fig. 2.6. Hoevmoller (longitude-time) of ERA-Interim (left column), ECHAM (middle column) and biases (ERA-Interim minus ECHAM, right column) of internal energy (T, K) (a-c); potential energy ($\phi/c_{p,}$ K) (d-f) and latent heat energy ($L_v q/c_p$, K) (g-i) at near surface (1000-hPa) over central Africa (10°N-15°S). The bold black line represents the limit of Central Africa.

In August/September, longitudinal-increased of the internal energy (T) occurs, with a maximum over Rift valley highlands (at ~30°E) in SOND and FMA respectively. Over Atlantic offshore regions (west of 15^{o}E), near-surface temperature is strongly dependant of tropical eastern Atlantic sea surface temperature (SST) (Biasutti et al. 2004), where the so call “cold tongue sea surface temperature” prevails in MJJAS. This indicates that land/ocean–atmosphere interactions are dominant over Atlantic offshore region so that internal energy term over Central Africa is controlled by SST. In the same season (MJJAS), East Africa and western Indian ocean experience relatively cold temperature even though with higher magnitude than its counterpart eastern Atlantic (Figs. 2.6, top panels). As result, Central Africa landmass is warmer than its surroundings oceans, except over East Africa, year-round (Fig. 2.8a). This is indicative of a zonal temperature gradient at near-surface between cold surrounding oceans and warm central Africa landmass (Fig. 2.8b). This zonal

land-ocean thermal contrast can reach a maximum of ~4^{o}C in July/August and a minimum of ~0.6^{o}C in April, particularly between Central Africa landmass (15^{o}-30^{o}E; 5^{o}S-5^{o}N) and eastern Atlantic (5^{o}W-5^{o}E; 5^{o}S-5^{o}N) (Fig 2.8b). But the land-ocean thermal contrast between central Africa landmass and Indian Ocean is two times lower than with its counterpart Atlantic Ocean (Fig. 2.8b). The near-surface warming over central Africa landmass is associated with increased latent heat ($L_v q/c_p$) and low surface pressure (ϕ/c_p) in SOND and FMA (Fig. 2.6, middle and bottom panels) respectively. In MJJAS, the near-surface cooling is associated with reduced latent heat ($L_v q/c_p$) and increased surface pressure (ϕ/c_p), essentially over East Africa (Fig. 2.6). Whereas over eastern Atlantic in SOND, there is a slight increase of latent heat ($L_v q/c_p$) despite relatively low internal energy (T). Therefore, the "lung-like" pattern of moist static energy is likely owed mainly to internal energy (T), even though the latent heat ($L_v q/c_p$) and surface pressure (ϕ/c_p) feature this spatial pattern.

ECHAM5.3 reproduces quite well the internal energy (T), latent heat ($L_v q/c_p$) and surface pressure (ϕ/c_p). But year-round in ECHAM5.3, the Atlantic Ocean is colder than the Indian Ocean, as indicated by cold bias over Atlantic and warm bias over Indian ocean (Fig. 2.6). The opposite sign of internal energy bias over surrounding Oceans is associated with positive bias of latent heat in Atlantic and negative bias in Indian oceans (Fig. 2.6). Whereas, central Africa landmass is relative warmer from September to April with maximum in SON, while it is colder in May to August in ERA-Interim than in ECHAM5.3 (Fig. 2.6 top right). However, central Africa landmass shows negative bias of latent heat year-round (Fig. 2.6 bottom right). As for potential energy (ϕ/c_p), the positive bias occurs from September to April, while in May to August, negative bias is prevailing (Fig. 2.6 middle right).

Likewise, at midlevel (~700- hPa), the internal energy in ECHAM5.3 (Fig. 2.7, top middle) produces the same "lung-like" pattern, but with overall less magnitude than that of internal energy at near-surface (Fig. 2.6, top) when compare with ERA-Interim (2.7, top left) as shown by positive biases (Fig. 2.7, top right). At this pressure level, the contribution of potential energy (ϕ/c_p, Fig. 2.7 bottom) to moist static energy (h) is as small as 12% while it is less than 6% for ERA-Interim. While at the same level, the contribution of the internal energy is still dominated in saturated moist static energy. The saturated latent heat ($L_v q^*/c_p$) mirrors the internal energy, though it accounts only ~10% of the former (Fig 2.7). Further, air temperature maxima over Central Africa occurs during the high rainy seasons (SOND and FMA). In MJJAS, the temperature minimum is located over East Africa, with its tails propagating westward (Fig. 2.7 top). This is a reversed situation from near-surface (Fig. 2.6, top), where cold air occurred over eastern Atlantic when SST cold tongue is predominant (Fig. 2.7). Hence, despite predominance of internal energy in moist static energy and saturated moist static energy at near surface and 700- hPa respectively, the moist static stability variation is likely to be more influenced by near-surface water vapour latent heat ($L_v q/c_p$) variability than by

contribution of low near-surface pressure (ϕ/c_p). This influence of near-surface latent heat ($L_v q/c_p$) is owed mostly to the seasonal cycle of atmospheric water vapour over Central Africa landmass, probably due to its vegetated surface.

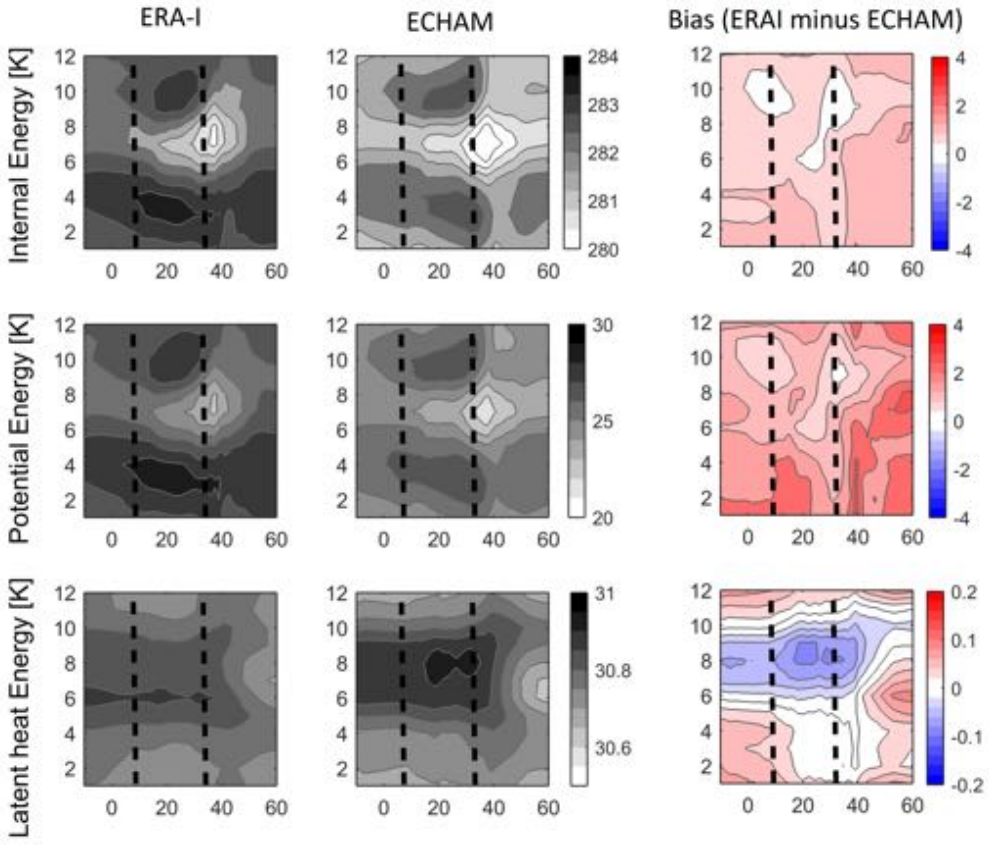

Fig. 2.7. Hoevmoller (longitude-time) of ERA-Interim (left column), ECHAM (middle column) and biases (ERA-Interim minus ECHAM, right column) of internal energy (T, K) (a-c); potential energy (ϕ/c_p, K) (d-f) and saturated latent heat energy (Lq/c_p, K) (g-i) at 700- hPa over central Africa (10°N-15°S). The bold black line represents the limit of Central Africa.

Indeed, according to Clausius-Clapeyron relation, the maximum of latent heat ($L_v q/c_p$) should occur over Rift valley highlands due to high temperature, which in turn, would lead the moist static stability maximum to shift eastward. But unlikely, the moist static stability peaks at ~20°E, with relatively high values in FMA and SOND. This confirms that the moist static stability is driven by near-surface atmospheric water vapour latent heat, with some influence of near-surface low pressure (ϕ/c_p) to balance the atmospheric thermodynamic energy budget over central Africa. At midlevel (700- hPa), the ECHAM5.3 represents quite well the internal energy (T), saturated latent heat ($L_v q^*/c_p$) and geopotential energy (ϕ/c_p), but with less magnitude as indicated by the negative biases (Fig. 2.7, right column) year-round, except for geopotential energy (ϕ/c_p) from June to October, while positive bias dominates (Fig. 2.7, bottom panels).

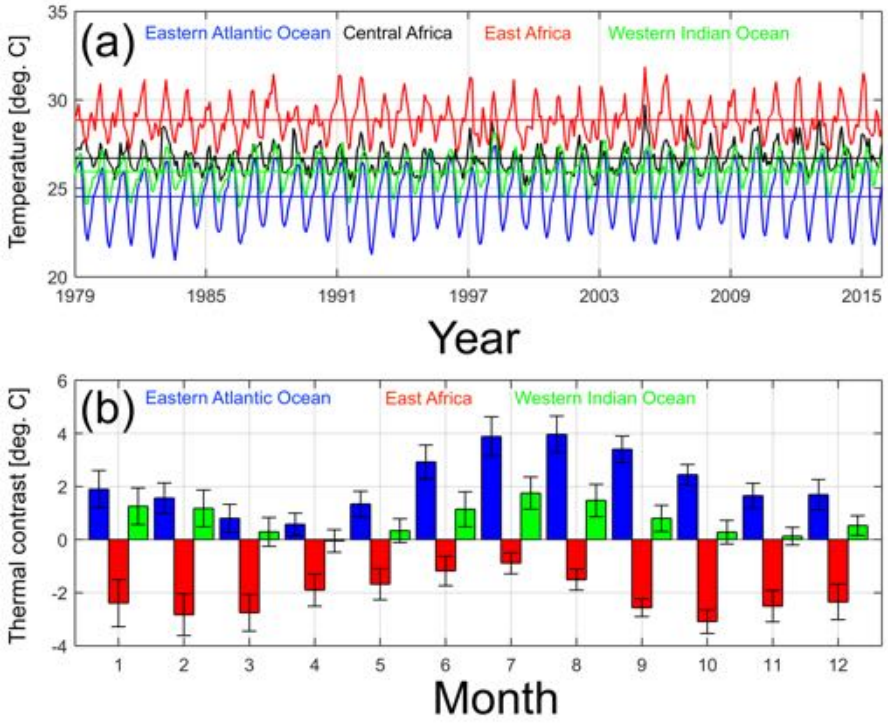

Fig. 2.8. (a) Near-surface temperature (^{o}C, at 1000- hPa) time series in ERA-Interim over Eastern Atlantic Ocean (5^{o}W-5^{o}E; 5^{o}S-5^{o}N, blue line), central Africa (15^{o}-30^{o}E; 5^{o}S-5^{o}N, black line), East Africa (33^{o}-40^{o}E; 5^{o}S-5^{o}N, red line) and western Indian Ocean (40^{o}-60^{o}E; 5^{o}S-5^{o}N, green line); (b) The annual cycle of the zonal thermal contrast (difference) in ERA-Interim between near-surface temperature over central Africa landmass and Eastern Atlantic Ocean (blue bar), East Africa (red bar) and Western Indian Ocean (green bar) respectively. The horizontal line in (a) represent the mean temperature over each region 24.53^{o}C for eastern Atlantic; 26.71^{o}C for central Africa, 28.85^{o}C for east Africa and 25.95^{o}C for western Indian Ocean. The vertical line in (b) represent the standard deviation.

Considering closely Figs. 2.2, 2.4, 2.6, 2.6 and 2.8, one can notice a pronounced land-ocean thermal contrast in the response of rainfall and moist static energy and saturated moist static energy as well as their components over Central Africa. Over surrounding Oceans, the atmospheric convection is likely a combination of near surface moist static energy build-up and induced atmospheric drying at midlevel associated with strong subsidence. This mechanism is referred as a recharge-discharge mechanism by Kemball-Cook and Weare (2001) for Madden-Julian Oscillation (MJO) activity. On the other hand, over Central Africa landmass, convective (high) rainfall is initiated by a combination of moist static energy build-up at near surface and more moistening of midlevel associated with atmospheric low pressure, year-round. Conversely, the low

rainfall over Central Africa landmass is likely due to the combination of midlevel atmospheric cooling and subsidence, associated with limited water vapour latent heat.

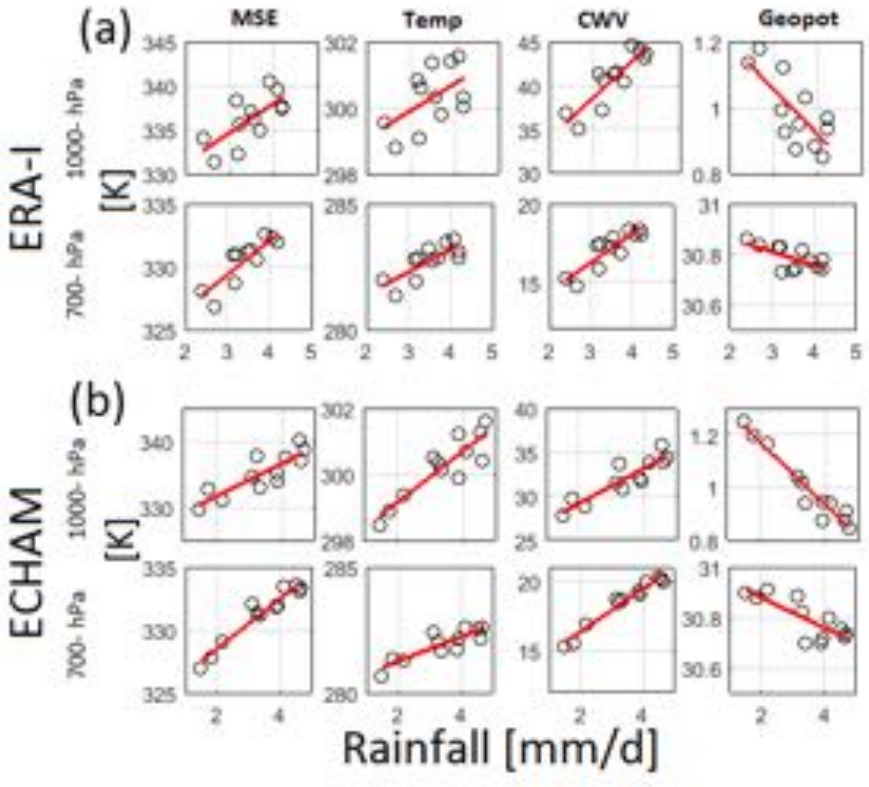

Fig. 2.9. (a) Linear regression between seasonal cycle of the central Africa rainfall from the mean of both GPCP (Huffman et al. 2009) and CMAP datasets (Xie and Arkin 1997) and moist static energy, temperature, precipitable water (CWV), and geopotential height at (top) near surface and (bottom) at 700- hPa. (b) ECHAM5.3 correlation between seasonal cycle of central Africa rainfall and moist static energy, temperature, precipitable water, and geopotential height at (top) near surface and (bottom) at 700- hPa. In all panels, red solid line is the linear trend.

These physical processes over Central Africa are sustained by strong positive correlation between the annual cycle of Central Africa rainfall and moist static energy (h/c_p), internal energy (T) and column water vapour (CWV), while the correlation is negative for surface potential energy (ϕ/c_p) (Fig. 2.9a). Precipitable water or column water vapour (CWV) is calculated as mass-weighted vertically integration of specific humidity (q) from surface to midlevel (700- hPa). At midlevel (700-hPa), the above relationships are characterized by the same features (Fig. 2.9b). At 700-hPa, I used specific humidity instead of column water vapour. After studying the major role played by near-surface water vapour latent heat and dry static energy in the seasonal variation of the thermodynamic energy budget, we further investigate the vertical profile of moist static energy and saturated moist static energy over central Africa in ERA-Interim and ECHAM5.3 (Fig. 2.10). High

dry static energy occurs mainly in the upper troposphere, while higher latent heat ($L_v q/c_p$) occur in the lower troposphere (Fig. 2.10a-h). The moist static energy does not increase uniformly throughout all the troposphere. Moreover, Fig. 2.10 shows that, in the boundary layer (from surface up to 800- hPa), the vertical gradient of moist static energy ($\partial_p h$) is small and somewhat positive ($\partial_p h \sim 0$), suggestive of atmospheric neutral conditions year-round. Hence, over central Africa, high temperature warms moist air, which is likely to rise as its density is less than the surrounding environment. This leads to low pressure conditions in the boundary layer. From 800- to 600- hPa, the moist static energy decreases, while $\partial_p h < 0$, indicative of deep convection. In MAM, an air parcel lifts from near surface and may saturate at ~750- hPa, at which the cloud base is formed and deep convection initiated (Fig. 2.10a). This convective cloud might extend up to 300- hPa (cloud top). This supports the occurrence of strong convective rainfall over central Africa. Aloft (up of 600- hPa), $\partial_p h$ increases significantly regardless of the seasons (Fig. 2.10a-d). The vertical gradient of saturated moist static energy ($\partial_p h^*$) is negative from surface to ~600- hPa and it increases aloft (Fig. 2.10a-d). This suggests that atmospheric temperature decreases from surface to 600- hPa and increases from 600- hPa. In JJA, slight increase of dry static energy (Fig. 2.10b;d) owes particularly to the strengthening of potential energy (ϕ/c_p). This indicates that increased subsidence occurs over central Africa. Moreover, the subsidence limits the atmospheric moisture (Fig. 2.10f;h), while it is accompanied by weakened internal energy (T). This indicates the suppression of convection, leading to less rainfall over central Africa. Indeed, a relatively colder air parcel should either lift higher at ~600 hPa to saturate or does not saturate at all due to a combination of slightly drier conditions in the boundary layer and subsidence (Fig. 2.10). For the next seasons (SON and DJF), the atmospheric water vapour is enhanced, while the subsidence is weakened (Fig. 2.10, top and middle). These atmospheric conditions similar to the MAM season do allow the warm moist air parcel to saturate around 750- and 600- hPa (Figs. 2.10, top and middle). Hence, increased atmospheric water vapour ($L_v q/c_p$) leads to much instability in the lower troposphere and to strong convective activity (Biasutti et al. 2004). Conversely, decreased water vapour ($L_v q/c_p$), in the low levels, associated with higher potential energy (ϕ/c_p) leads either to suppressed convection or to shallow convection over central Africa.

Moreover, year-round, positive biases of moist static energy (h) and latent heat ($L_v q/c_p$) occur between near-surface and 800- hPa (boundary layer), while the negative biases happened aloft (800- to 100- hPa) (Fig. 2.10 bottom). As for the saturated moist static energy (h^*) and saturated latent heat ($L_v q^*/c_p$), positive biases occurred throughout whole the troposphere, except in SON, in the boundary layer where they are negative (Fig. 2.10, bottom). Overall, this suggests that warm air saturates at higher pressure level in ECHAM5.3 than in ERA-Interim, except in SON. Meanwhile, warm biases in dry static energy occurred in all seasons in ECHAM, except in SON in the boundary layer (Fig. 2.12i-l). This indicates that the air is colder in ECHAM5.3 than in ERA-

Interim, except in SON. In the mid-level, the air is getting warmer in ECHAM5.3 before increasing further at upper-level (Fig. 2.10, bottom).

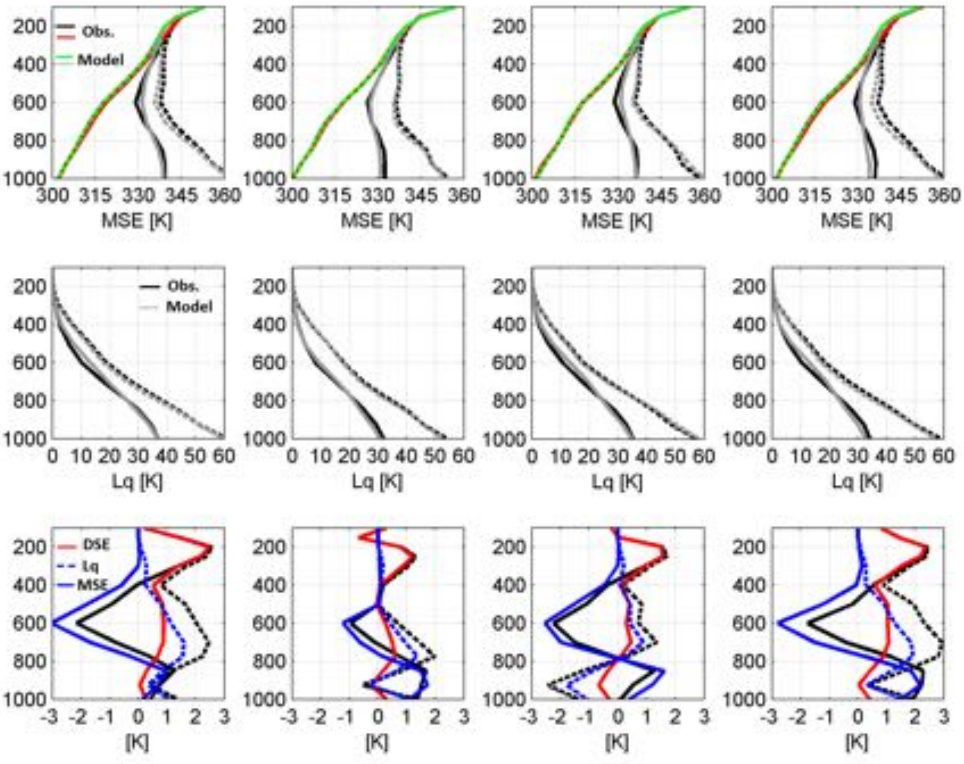

Fig. 2.10. ERA-Interim vertical profile of (first row) moist static energy, (middle row) latent heat ($L_v q/c_p$) and (bottom row) bias over central Africa (a,e,i) MAM; (b,f,j) JJA; (c,g,k) SON and (d,h,l) DJF

2.6. Atmospheric dynamics over central Africa and its links to rainfall intensity

In this section, we try to address the following questions: (i) how do the vertical profiles of dry static energy (DSE/c_p) and latent heat ($L_v q/c_p$) differ seasonally with rainfall intensity over central Africa? (ii) What is the seasonally vertical structure of the atmospheric dynamics properties associated with the zonal circulation with respect to rainfall intensity? To do so, we make a composite of the vertical profile of dry static energy (DSE/c_p), latent heat ($L_v q/c_p$), zonal wind (u) and atmospheric wind divergence ($\nabla\vec{u}$) at largest percentage of occurrence of central Africa rainfall intensity i.e. at the maximum value of PDF for each season (cfr. Fig. 2.3). Thus, we average dry static energy, latent heat, zonal wind and atmospheric divergence over Central Africa and each season (DJF, MAM, JJA, SON). For ERA-Interim (ECHAM5.3), the largest value of PDF for central Africa rainfall is 3.78 (4.49) mm/d in MAM, 2.71 (1.58) mm/d in JJA, 3.82 (4.29) mm/d in SON and 3.31 (3.77) mm/d in DJF respectively. Note that for a given season, when rainfall amount is larger or less than the maximum value of PDF, it will be referred as deep convective or shallow convective rainfall. Limitation to this interpretation could be made for JJA season when subsidence is likely to

suppress convection over central Africa (Figs. 2.8d-e; 2.9d-e). Rainfall is binned at 0.001 mm/d interval. Figures 11, 12 and 13 show the vertical profile of dry static energy (DSE/c_p) and latent heat ($L_v q/c_p$) for the difference between the deep convective rainfall and the shallow convective rainfall in ERA-Interim and ECHAM5.3 respectively.

In SON, latent heat ($L_v q/c_p$) and dry static energy (DSE/c_p) have opposite value during deep and shallow convective rainfall. More atmospheric water vapour (Fig. 2.11c) is accompanied by reduced temperature (Fig. 2.11c) in central Africa surface boundary layer (surface to 850- hPa) during deep convective rainfall, except over Atlantic offshore region (5^oE-15^oE). Indeed, the land-ocean contrast over the Atlantic offshore region controls the limited anomalous eastward moisture flux (Figs. 2.13c; 2.12c) and so leads to relatively strong anomalous temperature advection from Atlantic Ocean (Fig. 2.11c) during deep convective rainfall (Biasutti et al. 2004). The resulting east-west anomalous dry static energy gradient over central Africa is likely to induce strong anomalous westerly wind at low-levels (Fig. 2.13c). The upward motion of air leading to deep convective rainfall is likely to trigger wind convergence build up at low-levels (Fig. 2.13c). However, due to low temperature over Rift valley highlands (between 25^oE-35^oE), the ascending air does not uplift further than over the Atlantic coastal (between 7^oE-15^oE) region (Fig. 2.11c), consistent with moist convective stability (Fig. 2.10). This situation favours the moisture enhancement over central Africa, with higher water vapour over Rift valley highlands (Fig. 2.12c). Additional atmospheric water vapour could be owed to convective heating (Ueda et al. 2003). Additionally, the zonal thermal contrast, due to dry static gradient at low-levels over central Africa subcontinent, is likely to drive the anomalous AEJ at midlevels (i.e. between 750- and 600- hPa), consistent with Nicholson and Grist (2003). However, the core of AEJ seems to be confined over Atlantic offshore region and it is associated with wind convergence (Fig. 2.13c). On the other hand, over central to east Africa, the anomalous westerly wind is associated with anomalous wind divergence (Fig. 2.13c). At upper levels, strong anomalous moisture (Figs. 2.12c), due probably to the convective heating, is associated with strong easterly (Fig. 2.13c). However, Atlantic coastal region shows strong anomalous divergence, while central and east Africa is associated with wind convergence (Fig. 2.13c). Notably, ECHAM5.3 does capture the zonal thermal contrast between Rift Valley highlands and Atlantic coastal region, but with weaker magnitudes, particularly over Atlantic coastal region (Figs. 2.11g).

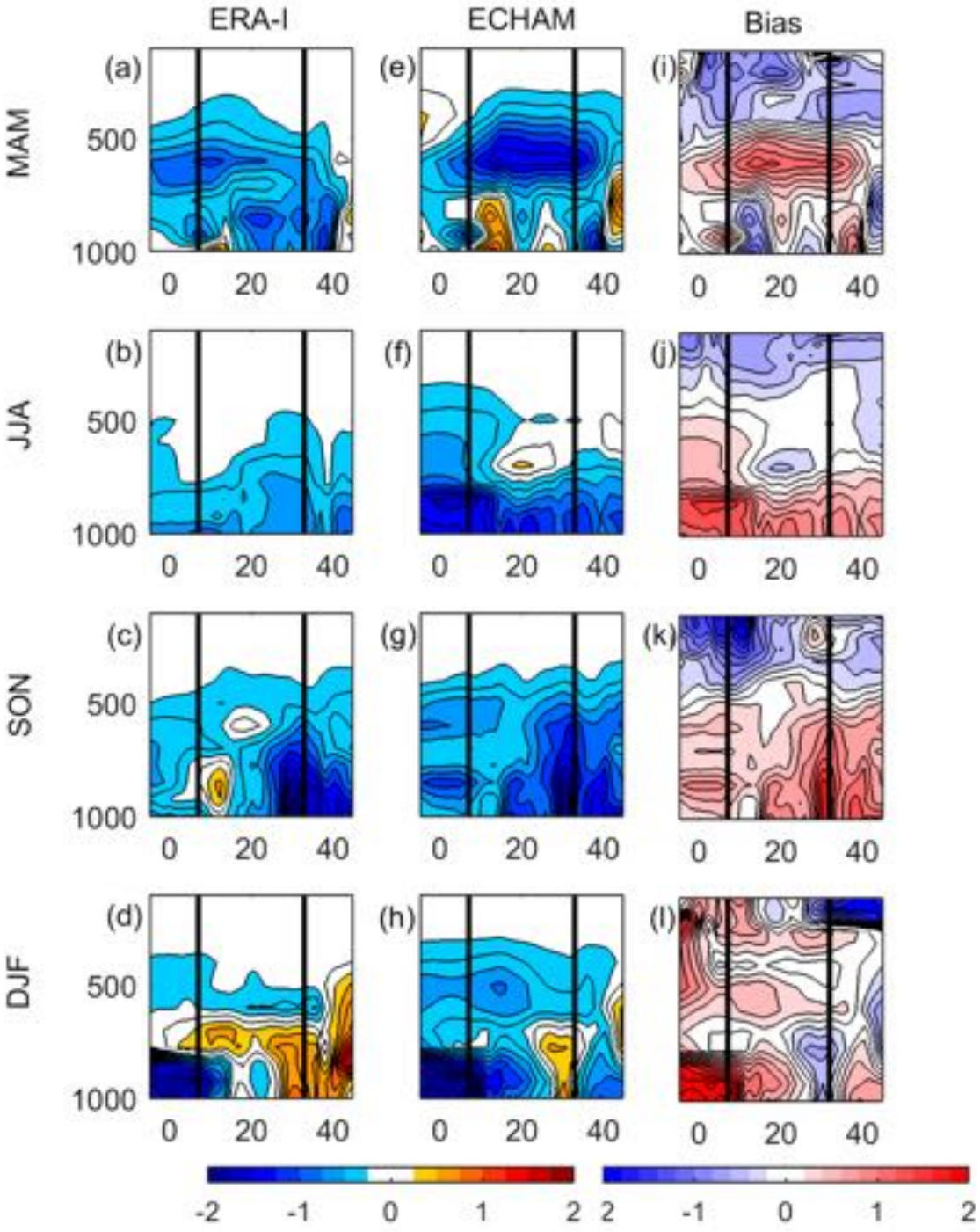

Fig. 2.11. Vertical profile difference of dry static energy (DSE/c_p, K) between deep convective and shallow convective rainfall from the mean of both GPCP (Huffman et al. 2009) and CMAP datasets (Xie and Arkin 1997) over central Africa. ERA-Interim (left column); ECHAM5.3 (middle column), and bias (ERA-Interim minus ECHAM, right column). (a, e, i) MAM; (b, f, j) JJA; (c, g, k) SON and (d, h, l) DJF. The contour interval is 0.5 K for dry static energy.

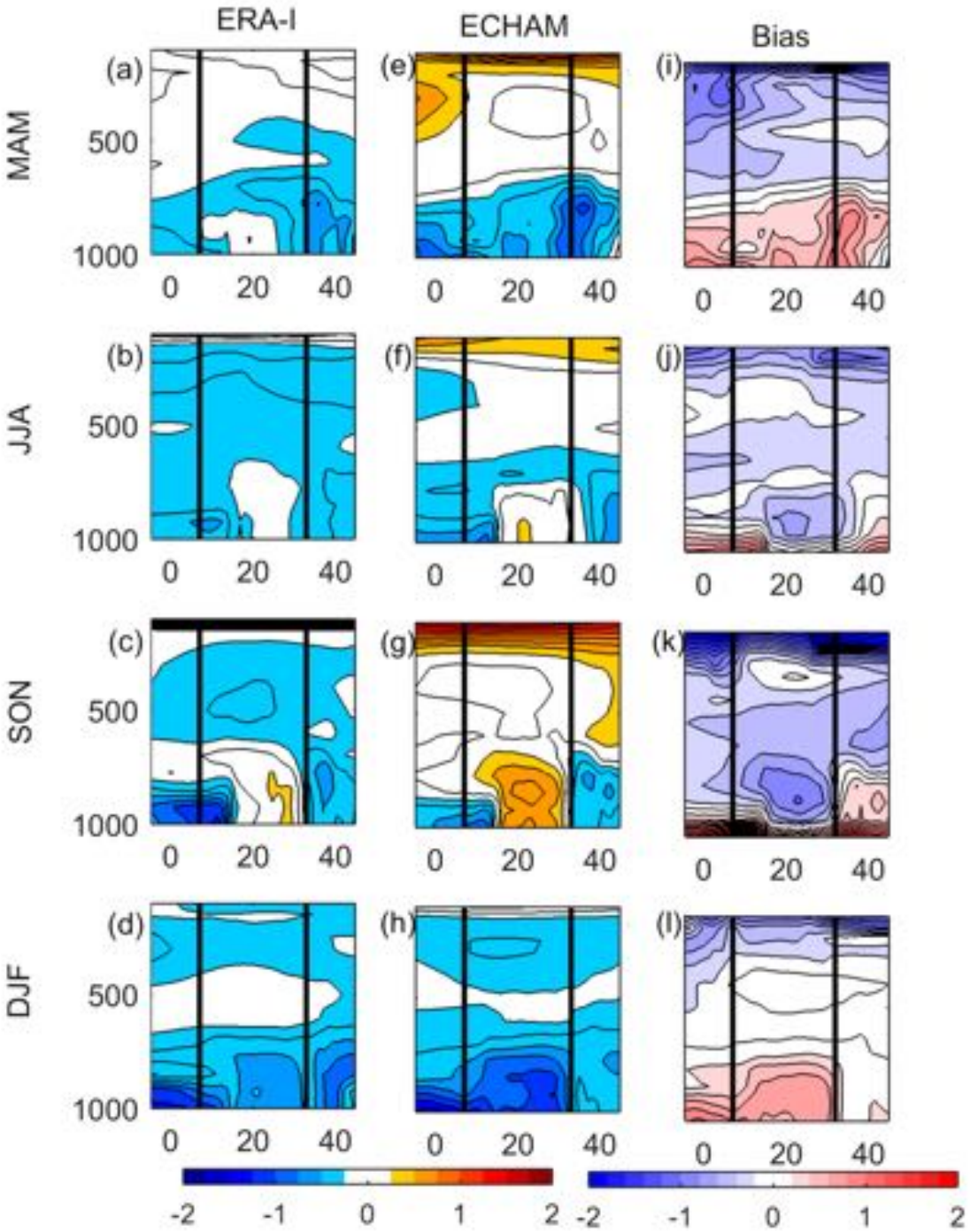

Fig. 2.12. Vertical profile difference of latent heat ($L_v q/c_{p,}$ K) between deep convective and shallow convective rainfall from the mean of both GPCP (Huffman et al. 2009) and CMAP datasets (Xie and Arkin 1997) over central Africa. ERA-Interim (left column); ECHAM5.3 (middle column), and bias (ERA-Interim minus ECHAM, right column). (a, e, i) MAM; (b, f, j) JJA; (c, g, k) SON and (d, h, l) DJF. The contour interval is 0.5 K for latent heat.

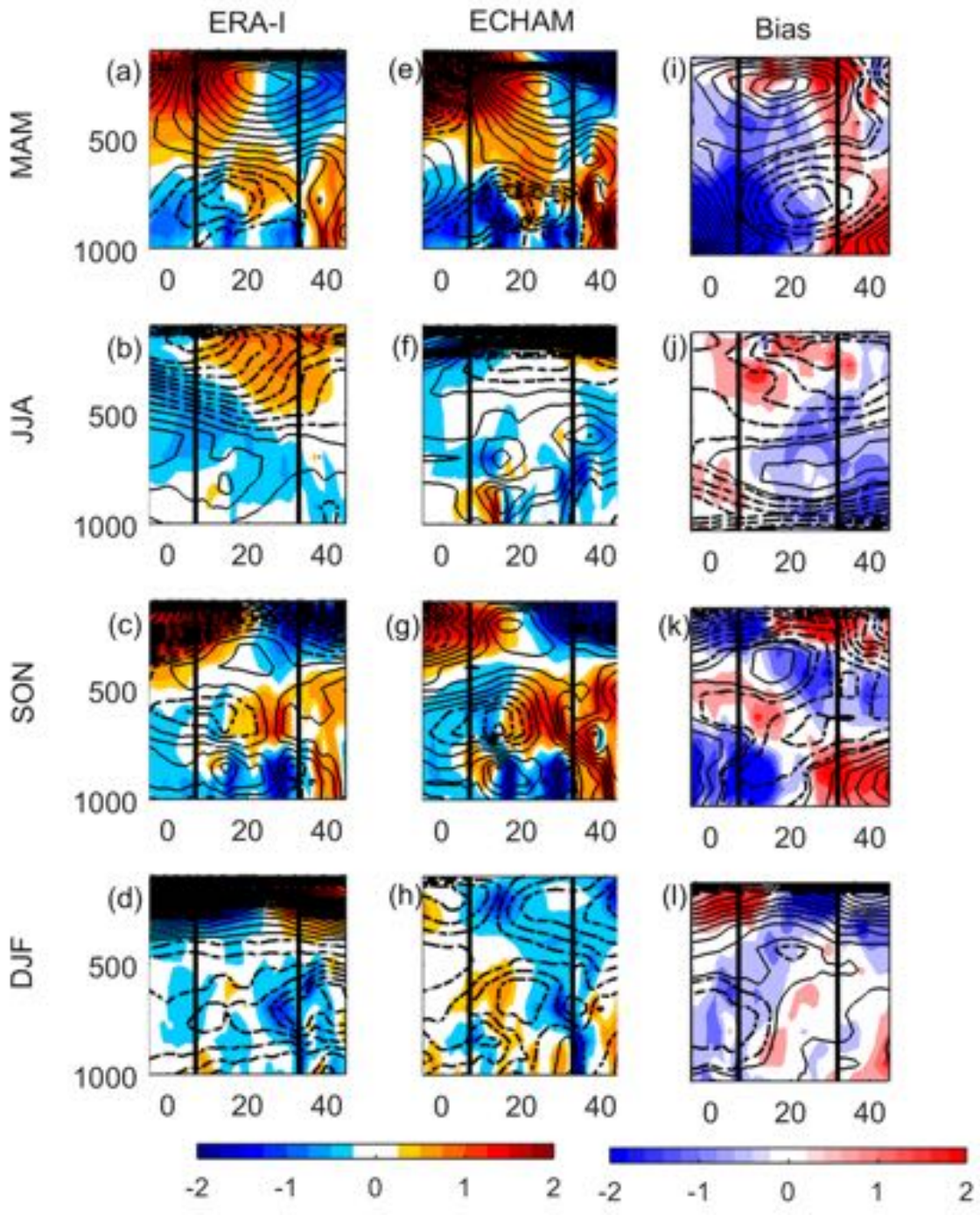

Fig. 2.13. Vertical profile difference of divergence (shading, s^{-1}) and zonal wind (contours, m) during deep convective and shallow convective rainfall from the mean of both GPCP (Huffman et al. 2009) and CMAP datasets (Xie and Arkin 1997) over central Africa. ERA-Interim (left column); ECHAM5.3 (middle column), and bias (right column). (a, e, i) MAM; (b, f, j) JJA; (c, g, k) SON and (d, h, l) DJF. The contour interval is 0.5 m/s for zonal wind and $0.5x10^{-5}s^{-1}$ wind divergence respectively.

The dry static energy bias of difference during deep and shallow convective rainfall indicates that the low-level troposphere over central Africa is warmer, while it is colder at upper-levels (Fig. 2.11l). Further, ECHAM5.3 overestimates the atmospheric water vapour over central Africa, particularly at low-levels (Figs. 2.12g). Thus, reduced atmospheric moisture bias occurs throughout all the troposphere, except over east Africa and Atlantic boundary layers (Fig. 2.12l). Moreover, ECHAM5.3 reproduces quite well the atmospheric circulation, particularly the induced African easterly jet and its associated wind convergence, but with higher amplitudes (Figs. 2.13g). The wind convergence bias occurs over Atlantic offshore region (Fig. 2.13l) but it is separated, at midlevels, by wind divergence bias. Over central and east Africa, wind divergence bias is separated by wind convergence bias at midlevels (Fig. 2.13l). However, dominant easterly bias occurs at low levels, while westerly bias is visible at upper levels (Fig. Fig. 2.13l).

In DJF, the vertical profile difference of latent heat ($L_v q/c_p$) between deep and shallow convective rainfall features significant anomalous reduction of moisture at low-levels over central Africa and its adjacent oceans (Fig. 2.12d). While the dry static energy and zonal wind show a longitudinal contrast – anomalous low temperature at low-levels (from surface to 750- hPa) over eastern Atlantic (from 10^{o}W to 5^{o}E) and Atlantic coastal region (Fig. 2.12d) is associated with anomalous wind convergence at upper levels (400- to 100- hPa) (Fig. 2.13d). While over central and east Africa (from 20^{o}E to 45^{o}E), the anomalous high temperature at low-levels are associated with anomalous wind divergence at upper levels (Fig. 2.13d). The resulted zonal thermal contrast is stronger than that in the previous season (SON), with opposite sign. This strong anomalous thermal contrast strengthens the induced anomalous easterly flow (from surface to 400- hPa) over central Africa blowing from warm east Africa to cold eastern Atlantic (Fig. 2.13a). Noted that the core of this anomalous easterly wind has shifted eastward, at around 30^{o}E (over Rift valley highlands), between 750- and 600- hPa, (Fig. 2.13d). Midlevel westward advection of positive dry static energy (Fig. 2.11d) is accompanied by wind convergence build up over central Africa and its adjoining Oceans (Fig. 2.12a). The difference between deep and shallow convective rainfall could be attributed to the enhanced transport of larger dry static energy at midlevels by a stronger African easterly jet (AEJ) over central Africa (Figs. 2.11d & 2.13d). At around 500- hPa, dry static energy further weakens and changes sign (Fig. 2.12d). In addition, a westerly flow occurs at upper levels (Fig. 2.13d). ECHAM5.3 does not well reproduce the zonal thermal contrast (Figs. 2.11h) at low-levels over central Africa subcontinent as well as its induced midlevel westward advection of larger dry static energy (Fig. 2.12h). This leads to the misrepresentation of African easterly jet in ECHAM5.3, which shifts westward with its core centered over central Africa. Meanwhile the associated wind divergence shows opposite values: anomalous wind divergence over Atlantic offshores regions and anomalous wind convergence over central and east Africa (Fig. 2.13h). Note that throughout all the troposphere over central Africa and its adjoining oceans, easterlies are predominant. And at upper levels particularly, anomalous easterlies are associated with wind

convergence build up (Fig. 2.13h). Interestingly, the dry static energy bias highlights the low-level thermal contrast over central Africa, with warm bias over Atlantic offshore region and cold bias over central Africa landmass (Fig. 2.11l). This means that in ECHAM5.3, temperature is warmer over Central Africa landmass and colder over Atlantic coastal regions than in ERA-Interim at low-levels. This low-level thermal contrast bias is associated with positive moisture bias over central Africa (Fig. 2.12l). Atmospheric circulation bias show mid-lower easterly bias over Atlantic and mid-lower westerly over east Africa (Fig. 2.13l). At upper levels, negative moisture bias is associated with dominant westerly bias. However, central Africa appears at upper-level to be separated in two parts – wind divergence bias over Atlantic region and wind convergence bias over east Africa (Fig. 2.13l).

In MAM, the vertical profile of the difference in atmospheric circulation between deep and shallow rainfall illustrates the strengthening of two kind of wind regimes over central Africa, in comparison to DJF season – mid-lower anomalous easterly and mid-upper anomalous westerly (Figs. 2.13a; 2.11a). The lower branch (from near surface to 750- hPa) of the anomalous easterly is associated with anomalous wind convergence, while its upper branch (between 750- and 600- hPa) is accompanied by anomalous wind divergence over central and east Africa (20^{o}–45^{o}E) and anomalous wind convergence over Atlantic offshore region (Fig. 2.13a) respectively. Conversely, the mid-upper anomalous westerly is associated with wind divergence over Atlantic offshore region and anomalous wind convergence over east Africa (Fig. 2.13a). The reinforcement of the induced mid-lower anomalous easterly is related to the weakening of low-level thermal contrast over central Africa (Fig. 2.11a), consistent with Nicholson and Grist (2003). In fact, during deep convective rainfall, dry static energy is smaller than during shallow convective rainfall (Fig. 2.11a). The resulted reduced temperature at low-levels is attributed mainly to the reduction of insolation by the cloud cover, owed by deep convection. Further, no significant change of atmospheric moisture occurs over central Africa, but some large moisture change is visible over east Africa boundary layer, where the anomalous westerly is dominant (Fig. 2.12a). ECHAM5.3 simulates quite well the vertical profile difference of dry static energy, latent heat and zonal atmospheric circulation. However, the ECHAM5.3 model enhances the low-level thermal contrast (Fig. 2.11e) and overestimates the midlevel westward transport of dry static energy (Figs. 2.12e; 2.13e). Moreover, the low-level thermal contrast bias (Fig. 2.11i) is associated with positive latent heat bias (Fig. 2.12i). While at upper levels, negative anomalous dry static energy bias (Fig. 2.11i) is associated with negative anomalous latent heat bias (Fig. 2.12i), strong anomalous westerly bias and wind divergence bias (Fig. 2.13i). The positive anomalous westward transport of dry static energy bias (Fig. 2.13i) is found at midlevels and is associated with strong anomalous mid-lower easterly bias (Fig. 2.13i). Anomalous wind convergence bias is found over Atlantic and central Africa, while anomalous wind divergence occurred over east Africa (Fig. 2.13i).

Finally, in JJA, the anomalous zonal circulation turns westerly at mid-lower levels and easterly at mid-upper levels (Fig. 2.13b) over central Africa and its surroundings regions. Contrary to other seasons, this zonal circulation suggests that the zonal wind is stronger at low-levels and weaker at mid-upper levels respectively during shallow convective rainfall than during deep convective rainfall. The mid-lower anomalous westerly is associated with anomalous wind convergence (Fig. 2.13b), while the mid-upper anomalous easterly is associated with anomalous wind divergence (Fig. 2.13b). The latent heat difference during deep and shallow convective rainfall suggests that weakening of zonal wind, at mid-lower levels, during deep convective rainfall does not influence significantly the water vapour flux over central Africa (Fig. 2.12b). Moreover, the reduction of dry static energy during deep convective rainfall, at low-levels (Fig. 2.11b), indicates the stability of low troposphere over central Africa. In other words, during shallow convective rainfall, at low-levels, relative warm air is associated with strong mid-lower westerlies and high pressure over central Africa, consistent with to Fig. 2.6. The resulted anomalous subsidence associated with anomalous atmospheric stability over the lower atmosphere is likely to generate the anomalous weak convergence build up. This is likely to lead to less rainfall, characteristic of shallow convection. ECHAM5.3 reproduce the negative dry static energy (Fig. 2.11f), with larger magnitude than in ERA-Interim, indicative of higher temperature and pressure during shallow convective rainfall than during deep convective rainfall. In addition, higher latent heat occurred during shallow convective rainfall than during deep convective rainfall, while anomalous reduced latent heat is visible over surrounding oceans (Fig. 2.12f). At midlevel, a limited anomalous eastward advection of dry static energy is confined over central Africa (Figs. 2.11f; 2.13f). However, strong anomalous westerly flow encompassed the mid-lower levels, while weaker anomalous easterly is confined only at upper levels (Fig. 2.13f). Nevertheless, positive anomalous dry static energy bias occurred at low-levels, while negative anomalous dry static energy bias occurred at upper levels. At midlevels, negative anomalous moist static energy bias is occurred as suggested by small anomalous dry static (Fig. 2.11f) and moisture (Fig. 2.12f) transport biases at this pressure level. Notably, easterly bias dominates the low-levels, while the westerly bias associated with wind convergence bias occurred at mid-lower levels (Fig. 2.13f). The anomalous westerly bias associated with the anomalous wind divergence dominated at upper levels (Fig. 2.13f).

2.7. Summary and discussion

To further understand central Africa rainfall variability, I try firstly to evaluate available rainfall datasets. It emerges that the scarce distribution of rainfall stations affects the quality of station-based data leading to difference in spatial rainfall patterns within the only rain-gauged datasets. Meanwhile the merged satellite-gauge datasets represent well the spatial distribution and intensity. However, TAMSAT seems to underestimate central Africa rainfall. The SST-forced model, ECHAM5.3 captures the seasonal and the northward and westward marches of central Africa

ITCZ, but it fails to well represent the rainfall intensity. The study of the westward migration of the meridional mean rainfall annual cycle over central Africa lead to the following results:

a) The seasonal cycle of Central Africa rainfall is primarily dominated in the change of atmospheric pressure system (and its associated circulation) and water vapour (latent heat), rather than the local temperature;
b) The seasonal transition between high and low rainy seasons is due mainly to subsidence over Central Africa, which limits the atmospheric water vapour at near surface. Further, the subsidence is associated with the reversal of the meridional wind shear and the weakening of the easterly wind shear. The opposite leads to the transition between low to high rainy seasons;
c) The boundary layer (between 1000- to 800- hPa) in Central Africa is convectively neutral. However, during high rainy season, the atmospheric water vapour is likely to destabilize the low-level troposphere and hence, lead the warm moist air to rise and saturate at ~750-hPa (cloud base) and so lead to unstable atmospheric condition along the season. The convective cloud may extend up to 300- hPa (cloud top);
d) The weakening of the midlevel easterly, in MJJAS seems to generate the “lung-like” zonal pattern of Central Africa rainfall annual cycle and its associated moist static stability; however, year-round, the near-surface westerly is confined at the west of the moist static energy maximum position;
e) Central Africa rainfall maximum (ITCZ) is mostly controlled by moist static stability than by rainfall.

Considering the seasonal evolution of atmospheric conditions related to the largest percentage of occurrence of central Africa rainfall intensity, we notice that to the difference between deep and shallow convective could to be attributed to the low-level zonal thermal contrast that controls the midlevel anomalous easterly from September to May. This induced anomalous AEJ is important for the transport of dry static energy and moisture over central Africa. In addition, this anomalous midlevel easterly is associated with the anomalous wind convergence build up, which could trigger deep convection over central Africa. Conversely in June to August (JJA), the absence of anomalous easterly over central Africa, at midlevel, is related to the lack of low-level zonal thermal contrast. At low-levels, due to high subsidence in this season (JJA), the anomalous westerly and reduced temperature is indicative of stronger zonal wind and higher temperature during shallow convective rainfall than during deep convective rainfall.

Taking account all these above physical processes, we do assume that high rainfall does not primarily occur where strong atmospheric instability occurred, but rainfall intensity seems to be better related to the midlevel anomalous easterly jet associated with anomalous wind convergence

at mid-lower levels over central Africa. Consistent with the aforementioned physical processes, the central Africa rainfall is also driven by sea surface temperature. Further, the difference between deep and shallow convective rainfall highlights two regions of opposite zonal circulation regimes: westerly flow over the Atlantic coastal regions and the easterly flow over Central Africa and beyond (East Africa).

Chap 3

On the structure of the regional–scale circulation of the central Africa rainfall system

3.1. Introduction

The seasonal cycle of Central Africa rainfall is primarily dominated by the change in atmospheric pressure and its associated circulation, water vapour and latent heat, rather than the local temperature. Hence, wind plays crucial role in redistributing the energy and moisture, which in turn, influence temperature and precipitation patterns worldwide. But little is known about the large-scale circulation over central Africa. McCollum et al. (2000) reported that the westerly low-level jet over Atlantic supplied moisture into central Africa landmass and Vigaud et al. (2007) outlined the importance role of this low-level westerly jet for deep convection occurring during summer. Nicholson and Grist (2003) found the existence of African easterly jet (AEJ) and tropical easterly jet (TEJ) in mid- (i.e. ~600- hPa) and upper (200- hPa) troposphere over Central Africa respectively. Another point of view is to consider this low-level transport of moisture as the lower branch of the Walker–type cell over central Africa. But to the best of our knowledge, the large–scale atmospheric dynamics over Central Africa rainfall system has been studies little and is not consistent yet. And hitherto, no consensus has been made on the Walker–type circulation over central Africa. Some papers (Flohn, 1971; Webster, 1983; Yu and Zwiers, 2010; Yu et al. 2012; Thorsten and Richter, 2014) suggested the existence of a Walker–type cell over central Africa. Flohn (1971, cfr his Fig. 12) depicted a dominant asymmetric overturning circulation over Central Africa, with low-level westerlies suppling water vapour fluxes from eastern Atlantic as lower branch.

Over the Rift Valley highlands, warm air uplifts (rising branch), while at upper levels, dominant easterlies form the returning branch. Finally, over the eastern Atlantic, the air subsides, constituting the closing branch. On the other hand, Webster (1983) and recently Thorsten and Richter (2014, cfr their Fig. 13) found a symmetrical overturning cells, with convergent branches, at low-levels, flowing moist air from surrounding Oceans into central Africa. Ascending branch of warm air is located over Central Africa landmass. At upper levels, the upward motion diverges and is considered as the return branches, before sinking over eastern Atlantic and western Indian Oceans respectively, closing the circulation. In addition, Pokam et al. (2014) found at low-level troposphere, a Walker–type overturning circulation driven by divergent circulation over equatorial central Africa (15 – 45^{o}E of longitude and equator – 10^{o}N of latitude), with strong westerlies between 10–15^{o}E. Also, they added that this overturning circulation over Central Africa is due to the differential adiabatic heating between Central Africa and eastern Atlantic Ocean, which is stronger during rainy seasons in September to Novermber (SON) and March to May (MAM) (Pokam et al. 2014). More recently, Kerry and Vizy (2015) and Neupane (2016) outlined an overturning zonal circulation over Congo basin (15–25^{o}E of longitude and 3^{o}S – 3^{o}N of latitude) centered at ~700- hPa, from June to October. This zonal overturning over Central Africa forms when the Atlantic cold tongue SST matures to set up favourable atmospheric conditions for its development. However, this zonal overturning circulation over Central Africa is timing out of phase with central Africa rainfall, but it does play crucial role in regulating precipitation over Sahel and western Africa (Kerry and Vizy, 2015; Neupane, 2016). In this chapter, we try to provides a comprehensive insight of the seasonal cycle of the meridional-mean zonal large-scale dynamics over central Africa and its associated moisture transport as well as its connexion with rainfall and zonal ITCZ position. So, the scope of this study is to answer the following questions:

1. What is the structure of the central Africa zonal large-scale circulation?
2. How does the central Africa zonal overturning cell form and what are its drivers?
3. What is the relation between the central Africa zonal overturning cell and the local rainfall?

Solving those questions help us to understand the dynamics of the central Africa rainfall system.

3.2. Data and methods

To investigate the large-scale circulation over Central Africa, I choose to use the widespread global climate reanalysis data. Moreover, observational datasets are not reliable over central Africa – no radiosondes are performed and climate data are scarce, so that in many studies, reanalysis datasets are used (Balas et a. 2007; Dezfuli and Nicholson 2012; Nicholson and Dezfuli. 2012; etc). The atmospheric variables employed in this study have been taken mainly from the European Centre for Medium-Range Weather Forecasts (ECMWF) Re-Analysis (ERA-Interim) (Dee et al., 2011). But for consistency and robustness of our results, we also used the National Center for

Environmental Prediction (NCEP)–National Center for Atmospheric Research (NCAR) reanalysis (NCEP1) (Kalnay et al., 1996) and the NCEP–Department of Energy (DOE) Atmospheric Model Intercomparison Project (AMIP)-II Reanalysis (NCEP-2) data (Kanamitsu et al., 2002). The ERA-Interim has 37 vertical levels, while the NCEP1 and NCEP2 have 17 vertical levels. The air surface temperature (at 2 m) and the mean sea level pressure are also considered. The ERA-Interim has a 0.75°– horizontal resolutions; and NCEP-1 and NCEP-2 have 2.5° × 2.5° horizontal resolutions. The ERA-Interim and NCEP2 cover the period of 1979 to present and the NCEP1 covers the period of 1948 to present. For rainfall, we used the ensemble of Climate Prediction Center Merged Analysis of Precipitation dataset (CMAP, Xie and Arkin 1997) and the Global Precipitation Climatology Project monthly precipitation dataset (GPCP, Huffman et al. 2009), available at monthly temporal resolution (1979 to present) at 2.5×2.5 degrees. CMAP and GPCP datasets are compiled from merged satellite precipitation data and bias-corrected over land through continental rain-gauge observations (Bolvin et al. 2009). To further understand the key-role of sea surface temperature on central Africa large-scale circulation, we use the European Centre Hamburg Model (ECHAM) version v5.3, which is an atmospheric general circulation model forced by observed sea surface temperature (Roeckner et al. 2003; Gleixner et al. 2016) spanning from 1870 to 2009. All reanalysis datasets are regridded at 0.75°× 0.75°– resolution for better comparison.

To further our understanding of the meridional-mean large-scale zonal circulation over Central Africa, I compute the mass–weighted streamfunctions as they are commonly used for its counterpart Hadley circulation (Oort and Yienger1996; Stachnik and Schumacher 2011; Donohoe et al. 2014; etc) instead of using vertical velocity at specific pressure level (Hua et al. 2016; Dezfuli et al. 2015) or zonal component of divergent wind (Pokam et al. 2012; Yu and Zwiers, 2010; Yu et al. 2012; Cook and Vizy, 2015). The primarily reason is that the mass-weighted streamfunctions will help us to diagnose objectively variations of large-scale circulation over central Africa in terms of strength and width on various time scale.

Following Cook (2003), the conservation of mass, in vertical coordinates, must satisfy the equation:

$$\frac{1}{R\cos\theta}\frac{\partial u}{\partial \varphi} + \frac{1}{R\cos\theta}\frac{\partial(v\cos\theta)}{\partial\theta} + \frac{\partial\omega}{\partial p} = 0 \qquad (3.1)$$

Where u is the zonal wind; v the meridional wind; ω, the vertical velocity; R, the earth radius, ϕ the longitude, θ the latitude.

Whether the equation (3.1) is averaged over latitude, the second term on the left-hand side of the equation is zero. So, that the equation (3.1) could be written, with square brackets denoting the meridional average as follow:

$$\frac{1}{R\cos\theta}\frac{\partial[u]}{\partial\varphi}+\frac{\partial[\omega]}{\partial p}=0 \qquad (3.2)$$

From the equation (3.2), one could state that if one component ($[u]$ or $[\omega]$) is known, the other can be identified. Clearly one variable can be used to fully determine the two-dimensional flow. The continuity and hydrostatic equations allow us to express the combined circulation $[u]$ and $[\omega]$ in terms of mass-weighted (or Stokes) streamfunctions ψ, which define the total eastward mass-flux above a given pressure level and longitude:

$$[u]=\frac{g}{2\pi R}\frac{\partial\psi}{\partial p} \qquad (3.3)$$

$$[\omega]=-\frac{g}{2\pi R^2}\frac{\partial\psi}{\partial p} \qquad (3.4)$$

with g = 9.8 m/s, the gravitational constant.

By solving for ψ, I found the following solution:

$$\psi(p,\phi)=2\pi R<[u]> \qquad (3.5)$$

With the angle brackets denoting the mass-weighted vertical integration from surface to 100hPa:

$$<A>=\frac{1}{g}\int_{100-hPa}^{surface}A\,dp \qquad (3.6)$$

The zonal mass-weighted streamfunction is applied here to characterize the Walker-type circulation over Central Africa. Considering this following convention, whether the mass-weighted streamfunction is positive, it corresponds to clockwise circulation, whereas the counterclockwise circulation corresponds to negative mass-weighted streamfunction. The unit of the mass-weighted streamfunction is Sverdrup (Sv) = 10^9 kgs^{-1}. This definition is also equivalent to 10^6 m^3s^{-1}, which corresponds to the mass flux produced by a 1 Sv flow of water of 10^3 kgm^{-3} of density. Zonal wind is averaged meridionally between 5°N and 5°S, before computing the mass-weighted streamfunctions. However, when computed over entire central Africa latitudes i.e. between 10°N and 15°S, the zonal overturning cell is still visible at low-levels, but with smaller extension, while the strength remains almost of the same range. To better provide an overview of the evolution of the central Africa zonal circulation structure, I focus on the annual cycle. Noted that all metrics defined in our analyses emphasizes the seasonal cycle of the meridional-mean. However, over East Africa, the interpretation of regional circulation at low-levels (1000- to 925- hPa) should be cautious as it could be either artefacts in ERA-Interim or ECHAM5.3 or below the surface.

3.3. Zonal atmospheric circulation over central Africa: seasonal cycle, mean–state, trend and role of sea surface temperture

3.3.1. Structure of the central Africa zonal circulation

All year-round, the zonal atmospheric large-scale circulation over central Africa consists mostly of a predominant clockwise circulation associated with strong rising motion, indicative of deep convection (Fig.3.1a). This dominant easterly circulation is thermally direct, with an ascending branch located over the warm Rift valley highlands (33^{o}E) and the subsiding branch located over cold eastern Atlantic (west of 0^{o}E) (cfr. Fig. 2.8b). At upper levels (~200- hPa), strong tropical easterly jets (Nicholson and Grist, 2003) constitute the return branch. But, at low levels, there is not a closing branch to complete the overturning circulation over Central Africa (Fig. 3.1a), as at west of 0^{o}E, the low-level easterlies are likely driven by the South Atlantic Anticyclone. Thus, contrary to Flohn (1971) and Yu and Zwiers (2010) and Yu et al. (2012), the asymmetric Walker-type cell has no closing branch over Central Africa, and thereafter, it will be referred as a Central Africa "pseudo" zonal overturning cell. In addition, at low-levels, a shallow counterclockwise asymmetric zonal overturning circulation occurs with an ascending branch located at around 24^{o}E and a sinking branch at around 2^{o}E, over eastern Atlantic Ocean (Fig. 3.1). Aloft (between 800- and 750- hPa), the mass-weighted streamfunctions move westward, indicative of strong midlevel easterly jet in Central Africa, before gradually subside over eastern Atlantic Ocean (return branch). The lower branch consists of the low-level jet (between near-surface and 850- hPa) flowing from Atlantic Ocean towards central Africa, completing the overturning cell. This shallow Central Africa zonal overturning cell is also thermally direct, with air warmer in the ascending branch than in the descending branch, where the air is relatively cold and dry (Figs. 3.1a; 3.2a). The surface warming of the central Africa landmass is likely to generate a local quasi-permanent low-surface pressure rather than the adjoining oceans, except during May and June (Fig. 3.2b), when Central Africa experiences a relative small increase of surface pressure, indicative of a subsidence as the low surface pressure shifted towards Indian ocean. However, despite the presence of the land-ocean near-surface thermal contrasts between Central Africa landmass and its surrounding tropical Oceans, it is only the near-surface land-ocean thermal contrast between Central Africa landmass and eastern tropical Atlantic ocean (ΔT_{ATL}) is likely to induce a zonal surface pressure gradient (ΔP_{ATL}), with low-surface pressure over central Africa landmass and relatively high surface pressure over eastern Atlantic (Fig. 3.2b), as suggested by the correlation between land-ocean thermal contrast and sea level pressure (Table 3.1).

For the physical robustness of the Congo Basin Cell feature, I also compute the mass-weighted streamfunctions using NCEP-1 and NCEP-2 datasets (Fig. 3.1b-c). The dominant large-scale circulation feature is still the Central Africa "pseudo" zonal overturning cell, with subsiding motion, easily found over Oceans, west of 2^{o}E, in eastern Atlantic and beyond 40^{o}E, over western Indian and rising motion over Rift valley (Fig. 3.1).

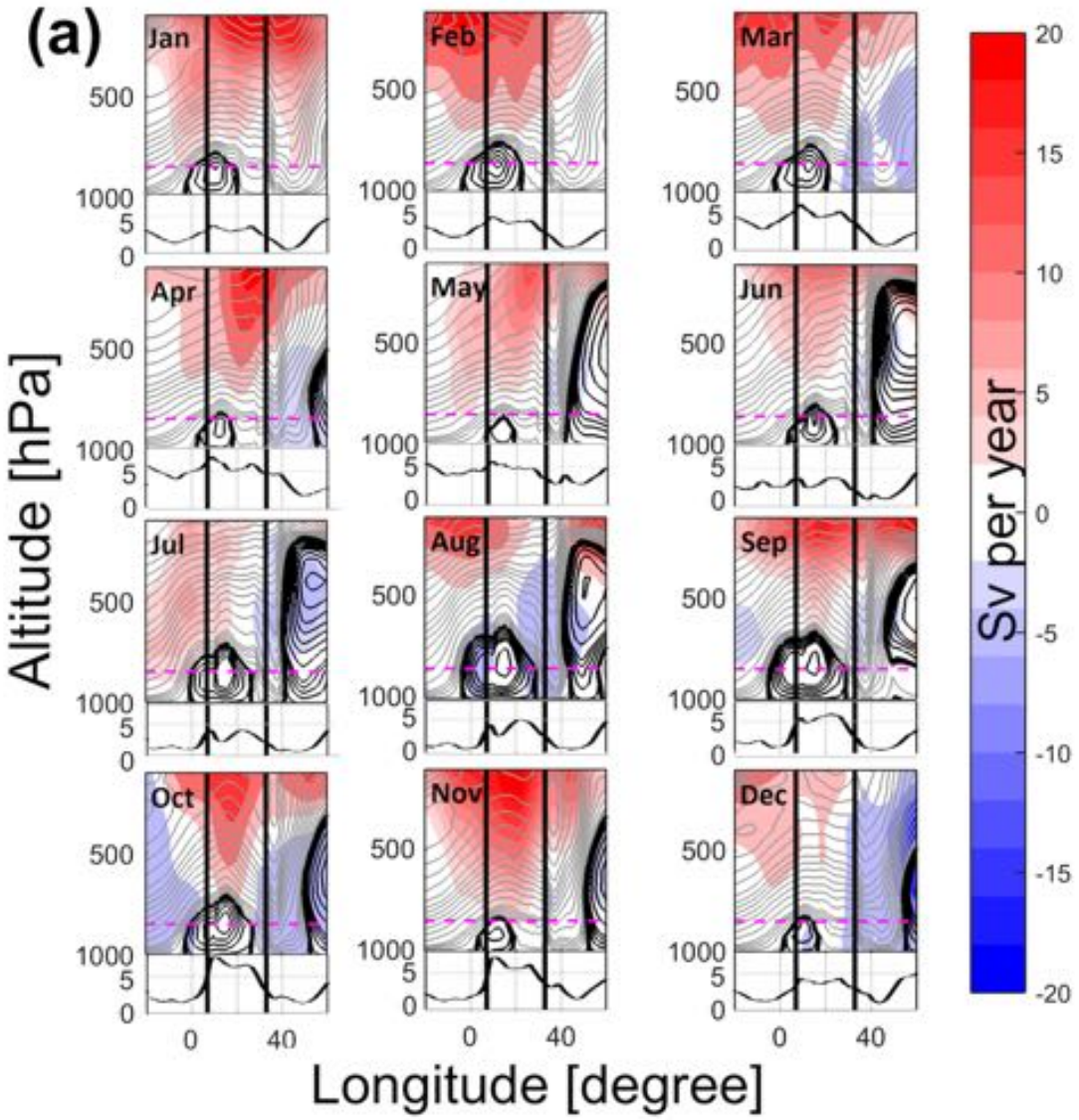

Fig. 3.1. (a) Zonal-mean circulation (contours, Sv) and its trend (shaded, Sv per year) in ERA-Interim and zonal variation pf rainfall (mm/d) over central Africa in both CMAP and GPCP. Gray and black contours represent positive and negative values of mass-weighted streamfunctions. Contours intervals are 20 Sv between 5 and 100Sv; 75 Sv between 150 and 600 Sv and 150 Sv between 700 and 1500Sv. Vertical bars represent central Africa.

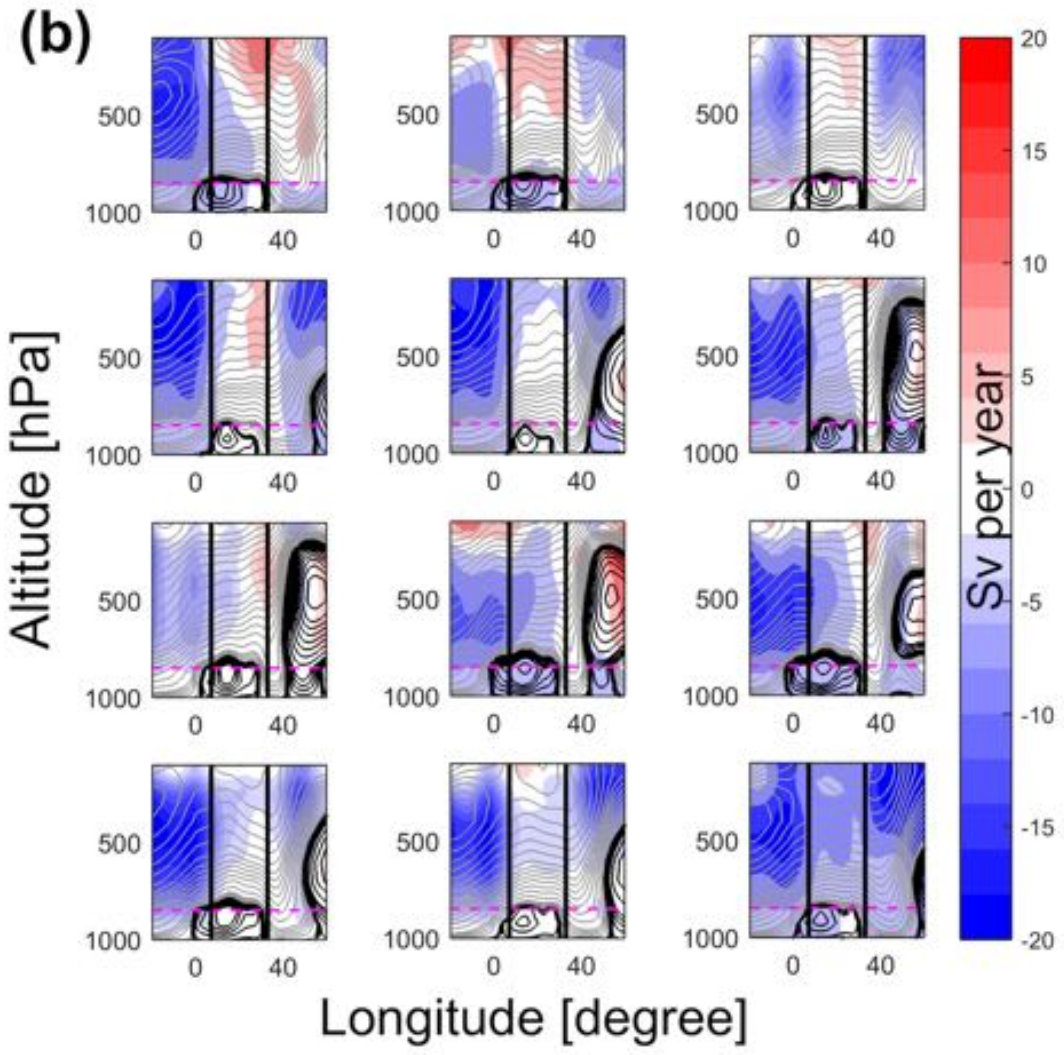

Fig. 3.1 (b) as (a) but for NCEP-1

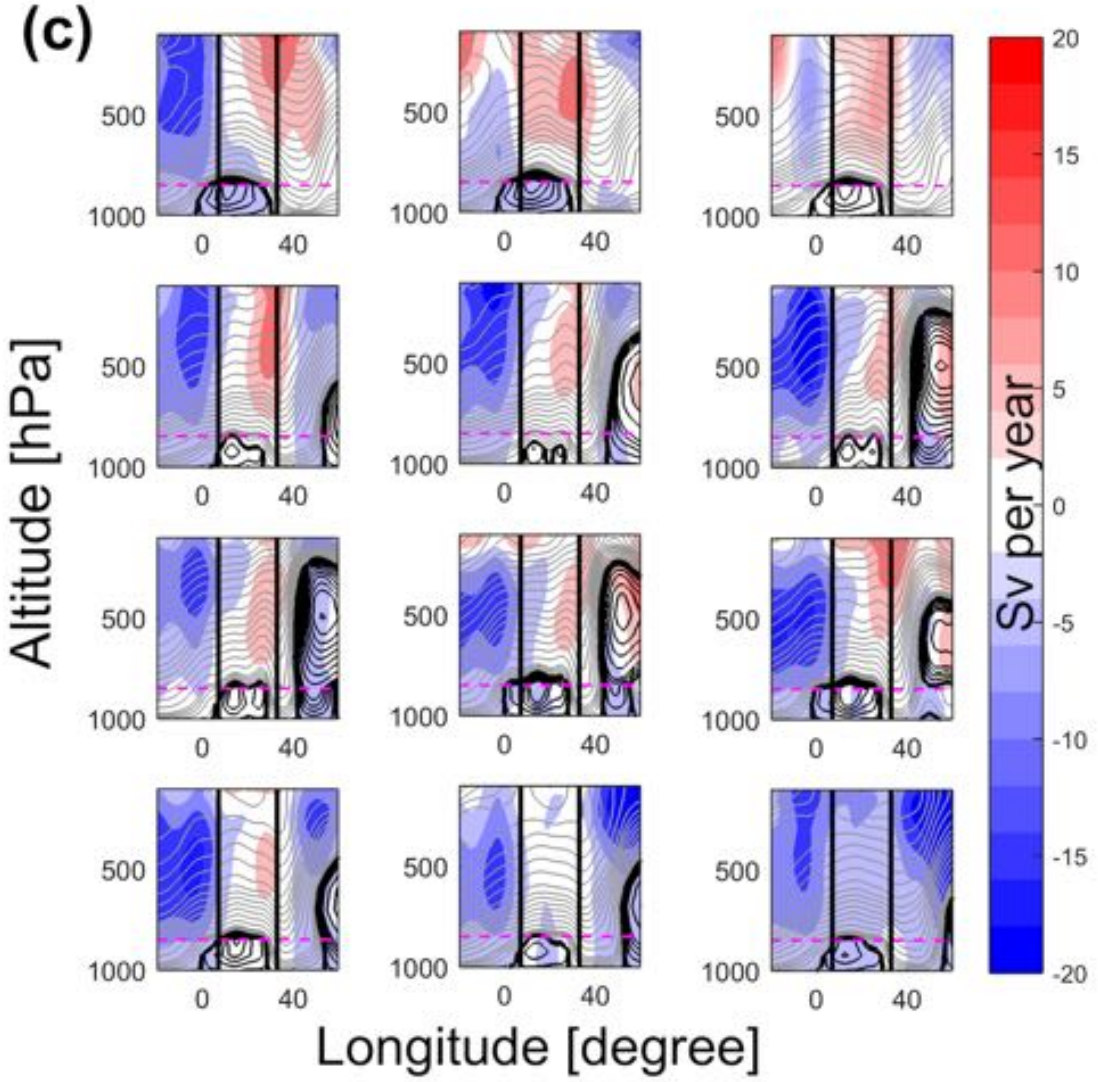

Fig. 3.1 (c) as (a) but for NCEP-2

This surface pressure gradient triggers monsoon-like circulations, at low-levels, from surrounding Oceans (Fig. 3.1). These low-levels jets are so important for the supply of water vapour to the central Africa landmass (Vigaud et al., 2008; Pokam et al. 2012; etc.). Hereafter, this shallow

Central Africa zonal overturning cell will be referred as Congo Basin Cell. Nevertheless, the Central Africa "pseudo" cell transports water vapour from Indian to Atlantic oceans, while crossing Central Africa (Figs. 3.1). At low levels, the shallow Congo Basin Cell emerges as a key feature of large-scale circulation in this region (Figs. 3.1b-c).

Table 3.1. Correlation coefficients of the annual cycle of land-ocean temperature contrast and the annual cycle of the surface pressure gradient between central Africa landmass and its surroundings Oceans in ERA-Interim.

	Atlantic (ΔT_{ATL})	**Indian** (ΔT_{IND})
Atlantic (ΔP_{ATL})	-0.96	-0.64
Indian (ΔP_{IND})	0.12	0.08

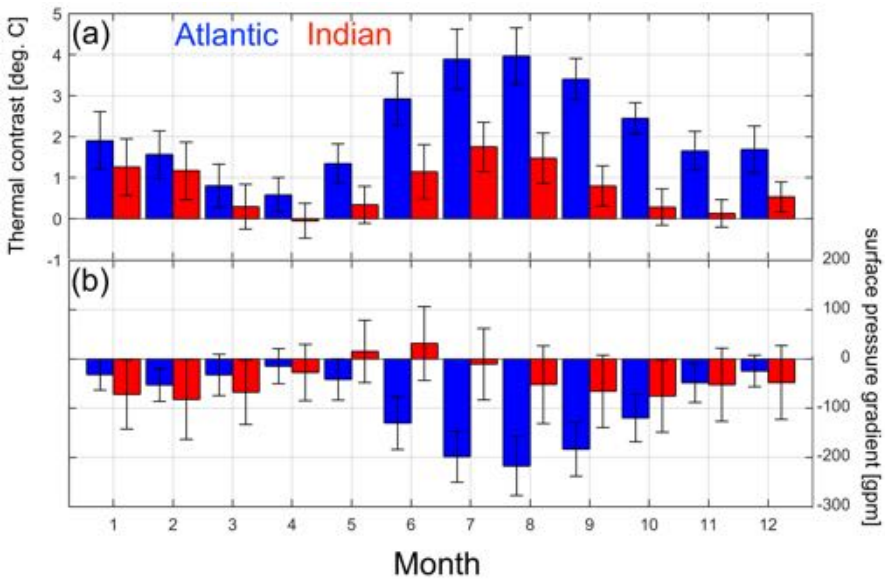

Fig. 3.2. Seasonal cycle of the near-surface thermal contrast (°C) and surface pressure gradient (gpm) between central Africa landmass (15°-30°E; 5°N-5°S, ΔT_{ATL} and ΔP_{ATL}) and eastern Atlantic (5°W-5°E; 5°N-5°S) and western Indian (40°-50°E; 5°N-5°S, ΔT_{IND} and ΔP_{IND}) oceans in ERA-Interim.

All three reanalyses produce similar spatial patterns of annual cycle of zonal mass-weighted streamfunctions (Figs. 3.1-3). Over western tropical Indian, when the Indian monsoon begins to intensify, the atmospheric zonal circulation is characterized by a strong counterclockwise

overturning cell, from May to December, with a maximum air mass circulation at around 500- hPa. Notably, when the Walker cell (meaning zonal overturning cell over Indian ocean) weakens and shrinks, the Congo Basin Cell strengthens and widens from April to October, and vice versa (Figs. 3.1-3). Whereas over eastern Atlantic (around ~20^{o}W), the Atlantic cell (Wang, 2002) is visible, with a maximum air mass circulation at ~400- hPa, except from May to September when it seems to shift westward (Figs. 3.1-3). The Atlantic cell is better established in NCEP1 than in ERA-Interim and NCEP-2, highlighting that there is no clear a priori for why one reanalysis data could be better than others. Actually, one can notice that the widening and strengthening of the central Africa zonal overturning cell are associated with the increase of the near-surface land-ocean thermal contrast (Figs 3.2).

3.3.2. Strength (intensity) of the Congo Basin Cell

To better describe the temporal and spatial evolution of Congo Basin Cell, we calculated the strength and its associated longitude, as the maximum mass-weighted streamfunction (Oort and Yienger, 1996; Donohoe et al. 2014) at 850- hPa (ψ_{850}) and its corresponding zonal location (ϕ_S) respectively. This is somewhat a measure of the Congo Basin Cell intensity and its position respectively. The choice of 850- hPa is made because throughout the lower troposphere, the mass-weighted streamfunction points out its maximum (minimum, as the mass-weighted streamfunction is negative) at this pressure level. The seasonal evolution of Congo Basin Cell indicates that in November, the zonal overturning cell develops and peaks slightly in February and then decreases a month later to reach in May, a minimum value of -26.01$\pm$ 20.19 Sv, -24.80$\pm$ 17.83 Sv and -19.60$\pm$ 17.29 Sv for NCEP1, ERA-Interim and NCEP2 respectively (Figs. 3.3), consistent with the land-ocean thermal contrast (Fig. 3.2a). From July to October, the zonal overturning cell widens and strengthens before peaking in August with a maximum value of -196.92±32.89 Sv for ERA-Interim and in September, for NCEP-1 and NCEP-2, with -199.81±42.39 Sv and -147.56±33.51 Sv respectively (Fig. 3.3). This is then followed by a sudden decrease of Congo basin cell strength until November (Fig. 3.3). This seasonal cycle of Congo Basin Cell seems to be ahead of around two months with respect of what Pokam et al. (2014) argued, with the zonal overturning cell over Central Africa being stronger in MAM and SON. The annual mean strength of the central Africa zonal overturning circulation and its location are -130.07±75.60 Sv at 14.90±4.05^{o}E for NCEP-1, -99.52±62.33 Sv at 13.59±2.26^{o}E for ERA-Interim and -86.08±51.79 Sv at 14.65±4.71^{o}E for NCEP-2 respectively.

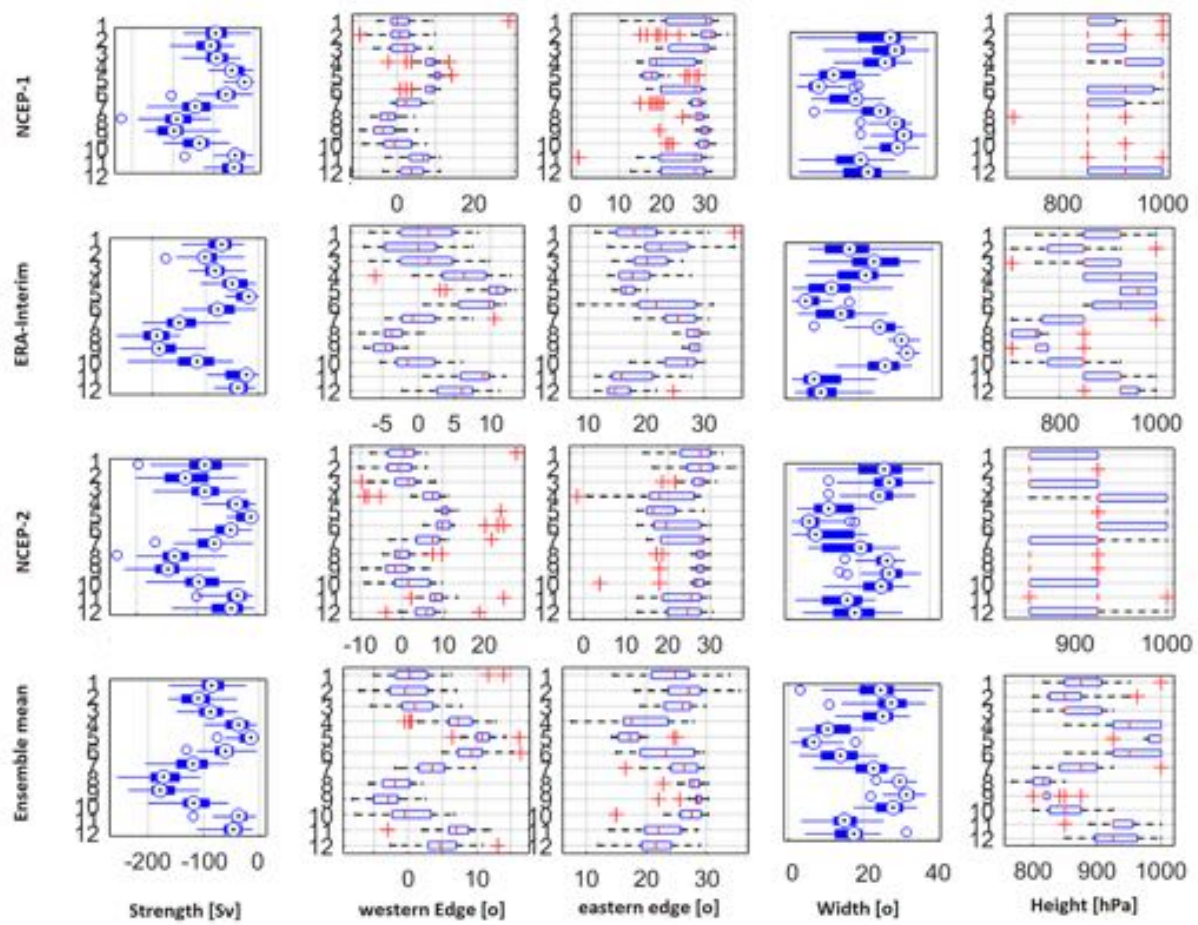

Fig. 3.3. Seasonal cycle of (1st column) strength, (2nd column) western and (3rd column) eastern edges, (4th column) width and (5th column) height of mean-state zonal mass-weighted streamfunction for (1st row) NCEP-1, (2nd row) ERA-Interim, (3rd row) NCEP-2 and (4th row) ensemble mean. In all figures, Y-axis represents all calendar months.

3.3.3. Width and height of the Congo Basin Cell

To diagnose the Congo basin cell width and height, we determine, following Davis and Rosenlof (2012), the longitude and pressure level at which meridional-mean zonal mass streamfunction changes sign i.e. the longitude and the pressure-level where ψ = 0. So, before to diagnose the zonal cross section of central Africa zonal overturning cell and to avoid spurious trends linked to the choice of a single and arbitrary pressure level, we vertically averaged the mass-weighted streamfunctions in pressure level between 1000- and 850- hPa before estimating the western and eastern edge longitudes respectively. Finally, the difference between the two edge longitudes indicates the width of the Congo basin cell. The western edge-longitude give us the location from where the water vapour transport originates from and the eastern edge- longitude, how far the water vapour transport can be transported. Actually, the eastern edge longitude could also be seen as the Congo Air Boundary, meaning the zone (position) where the low-level jet originated from eastern Atlantic and crossing Central Africa meets with the Indian monsoon system (Nicholson, 1996; Tierney et al. 2011). As readily seen in the previous subsection, in all three reanalyses, the

seasonal structure of the Congo Basin Cell is confined between 02°W and 30°E (as shown by the horizontal profile of ψ = 0, Figs. 3.1a). Examining the seasonal cycle of the edge longitudes, we find out that the two edges longitudes vary out of phase with each other, with larger annual cycle amplitude in the western than in eastern edge longitude (Fig. 3.3). This provides some insight on the difference of amplitude of the Congo Basin Cell width – the maximum in the width is mainly due to the strong westward excursion of the western edge longitude particularly during January–February–March (JFM) and August–September–October (ASO) when the eastern edge longitude is almost stuck at ~30^{o}E (Fig. 3.3; 3.1). This finding indicates that further the water vapour originated from, farther the water vapour will be transported into Central Africa landmass. This excursion is larger in NCEP-1 and NCEP-2 than in ERA-Interim. However, the annual cycle of the edges longitudes, is more pronounced in ERA-Interim than in NCEP-1 and NCEP-2 (Fig 3.3). But the most basic feature of the width and the edges longitudes is their 6-month period (bimodal annual signal) with two maxima in JFM and ASO and two minima in AMJ and ND. Indeed, the westward extension of the western edge in JFM and ASO, following by an eastward stretch in AMJ and SOND respectively, while the eastern edge moves in opposite direction than its western counterpart edge longitude (Fig. 3.3). Significant relationship is found between the Congo basin cell and land-ocean thermal contrast, computed as difference between central Africa landmass and its surroundings – Atlantic (ΔT_{ATL}) and Indian (ΔT_{IND}) Oceans (Table 3.2) respectively. These relationships suggest that much of the Congo Basin Cell strength, width and its related edges longitude variances are governed by the land-ocean surface thermal contrast. This means that increased thermal contrast leads to strengthened and widened the Congo Basin Cell, while decreased thermal contrast leads to the opposite. This suggests that the opposition in the relationship between the land-ocean thermal contrasts and both the edges longitudes (Table 3.2) is likely to explain the difference in the behaviour of both the western and the eastern edges longitudes of Congo Basin Cell. While the larger amplitude of annual cycle of the western edge longitude is related to the zonal surface pressure gradient (ΔP_{ATL}) variation owed by the land ocean thermal contrast (ΔT_{ATL}) (Table 3.1).

Table 3.2. Correlation coefficients of the annual cycle of the Congo Basin Cell width and strength with annual cycle of the surface thermal contrast between central Africa landmass and its surrounding Oceans – Atlantic (ΔT_{ATL}) and Indian (ΔT_{IND}) in ERA-Interim. Correlation significant at p < 0.05 are in bold.

	Strength	**Western edge**	**Eastern edge**	**Width ($\Delta\phi$)**	**Height**	**Zonal ITCZ**
ΔT_{ATL}	**-0.82**	**-0.51**	**0.80**	**0.68**	**-0.66**	**-0.40**
ΔT_{IND}	**-0.60**	**-0.46**	**0.54**	**0.53**	**-0.46**	-0.13

The seasonal progression of monthly-mean Congo Basin Cell width and strength indicates that both metrics have a linear relationship throughout the seasonal cycle, with a regression coefficient of about -0.15 Sv per ^{o}E of longitude for ERA-Interim. The regression coefficient is -0.12 Sv and -0.16 Sv per ^{o}E of longitude for NCEP-1 and NCEP-2 respectively. This means that for any strength of -100Sv, the Congo Basin Cell width will vary of about 12^{o}E of longitude. Notable difference is found when examining the height of the Congo basin cell. Maximum height is reached at 750- hPa in August and the minimum at 950- hPa in May for ERA-Interim, consistent with the seasonal variation of the thermal contrast (Fig. 3.3; Table 3.2). In NCEP-1 and NCEP-2, the central Africa zonal overturning cell height is confined underneath between 850- and 925- hPa respectively (Figs. 3.1). But greater Congo basin cell height variability is observed particularly in ERA-Interim (Fig. 3.3). Expansion or shrinking of the Congo Basin Cell width is timing out of phase with high or low rainy seasons in JFMAM and SOND, with rainy/dry season lagging shrinking/expansion of Congo Basin Cell by one or two months, while comparing Figs. 2.2 and 3.3. As a result, more rainfall (> 5 mm/d) occurs when the Congo Basin Cell width is relatively weak and less rainfall happened when it is relatively wide (Fig. 3.1). This indicates an indirect mechanism linking the Congo basin cell to central Africa rainfall via regulation of ITCZ by the land-ocean thermal contrast.

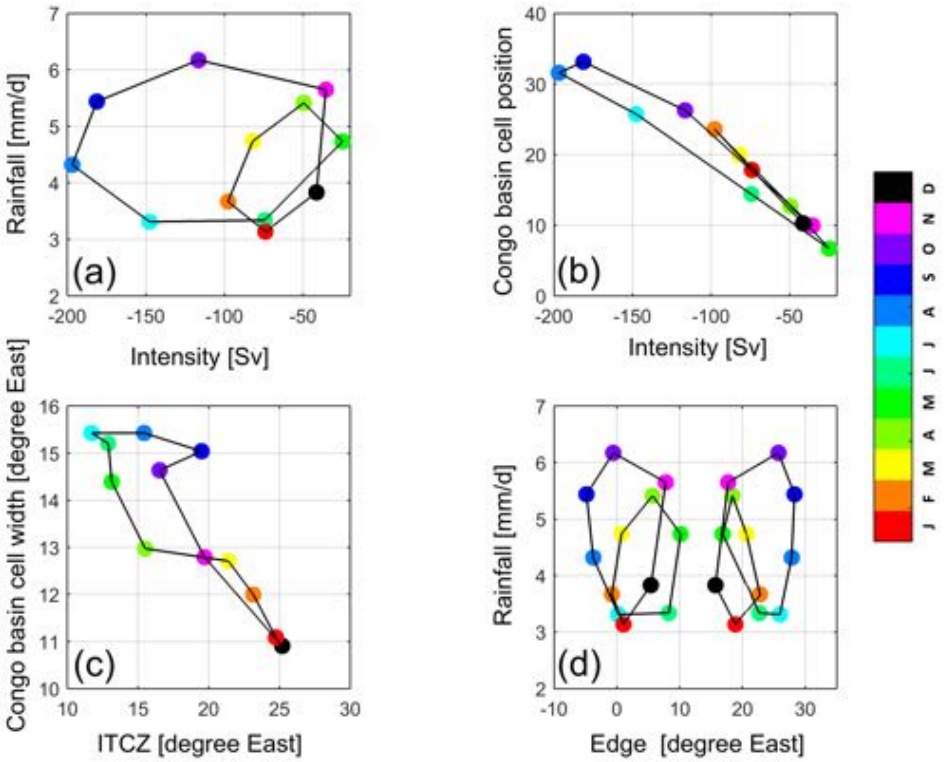

Fig. 3.4. Seasonal cycle of Congo basin cell intensity (Sv) vs (a) local rainfall; (b) Congo basin cell position. (c) Congo basin cell width vs zonal ITCZ position and (d) Edge position vs Central Africa rainfall in ERA-Interim.

To confirm this hypothesis, I look at the monthly evolution of both quantities to find out any relationship that could support this mechanism. So, I plot in Fig. 3.4 (top left and bottom right) the annual cycle evolution of the Congo Basin Cell and rainfall. Thus, no significant link is found between Central Africa rainfall and Congo Basin Cell strength and width. However, the seasonal position of zonal ITCZ seems to be regulated by the Congo Basin Cell position (Fig. 3.4, bottom left), which in turn, is controlled by the land-ocean thermal contrast. This means that enhanced thermal contrast does displace the ITCZ towards Atlantic offshore region, while reduced thermal contrast moves the ITCZ eastward towards Rift valley highlands, consistent with Fig. 2.2. In addition, the longitudinal variation of rainfall shows double maxima over central Africa, with high rainfall associated with eastward and westward motions of the Congo basin cell (Fig. 3.1). Notably, a slight drying is found at around 14^{o}E, where the strength of Congo basin low is maximum, (Fig. 3.1a).

3.3.4. Interannual variability and long term trend of the Congo Basin Cell

Overall, all the three reanalysis datasets behave in the same manner despite minor differences. Fig. 3.5 illustrates the interannual variability of the central Africa overturning cell in terms of its strength, width, height and edges longitude of the three-reanalysis data from 1979 to 2015.

There is a good degree of consistency in the variability of the Congo Basin Cell strength within datasets (ERA-Interim, NCEP-1, NCEP-2), with a slight tendency to find either maximum or minimum in the same year. But pronounced shortcomings between the three reanalyses do appear when analysing the linear trends. In middle and upper troposphere, overturning circulations are intensifying due to positive trend in ERA-Interim and NCEP-1, particularly over central Africa and eastern Atlantic (Fig. 3.1). For NCEP-2, intensification of mass-weighted streamfunctions occur over central Africa (Fig. 3.1c). In contrast, the mass-weighted streamfunctions are slowing down over all the atmospheric column over Oceans (Fig. 3.1). For the Congo Basin Cell, no consistent linear trends in strength, width and height among reanalyses is worth to be mentioned – NCEP-1 intensifies by about -4.28 Sv par decade, while for ERA-Interim slows down of about 11.12 Sv par decade and for NCEP-2, there is no evident trend (-0.07 Sv per decade) during the period 1979–2015 (Fig. 3.5a). The Congo basin cell width trend varies with value ranging from 1.29^{o} and 1.59^{o} E longitude per decade in NCEP-1 and NCEP-2 respectively to nearly -1.16 ^{o}E longitude per decade in ERA-Interim over 1979-2015 period. The extension of the central Africa overturning cell could be justified more by the westward excursion of the western edge longitude (-1.72 and -1.69 ^{o}E longitude per decade) than by a tendency of shrinking of the eastern edge longitude (-0.41 and -0.09 ^{o}E longitude per decade) in NCEP-1 and NCEP-2 respectively.

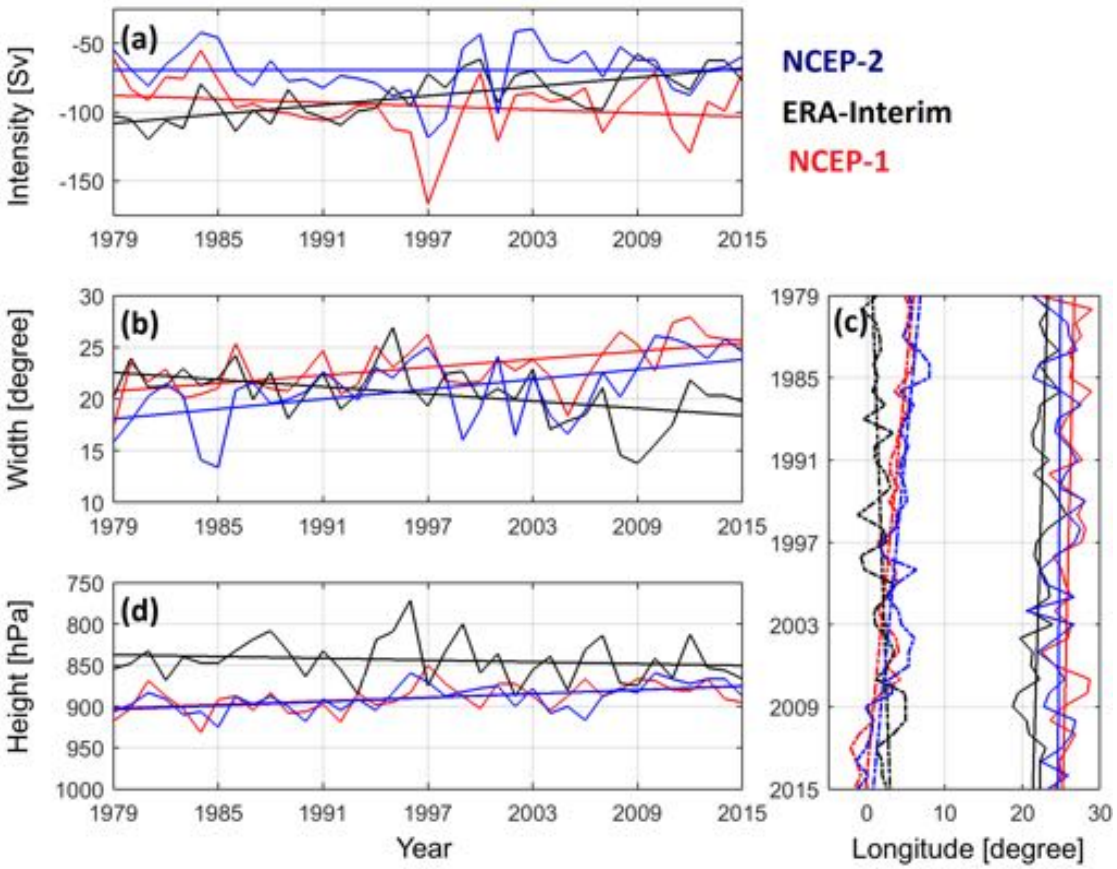

Fig. 3.5. Time series of the strength (Sv), width (^{o}E), western edge longitude (^{o}E) and eastern edge longitude (^{o}E) and height (hPa) of mean-state zonal mass-weighted streamfunction for NCEP-1, ERA-Interim and NCEP-2. In each panel, the straight line indicates the linear trend.

Whereas in ERA-Interim, both western and eastern edge longitude tends to migrate in opposite directions with 0.63 and -0.53 ^{o}E longitude per decade respectively. Finally, the Congo Basin Cell height tends to shorten in NCEP-1 and NCEP-2, with a trend of -7.34 hPa and -7.95 hPa per decade, while it extends in ERA-Interim, with a trend of 3.64 hPa per decade respectively.

3.3.5. Role of sea surface temperature on Central Africa large-scale circulation

To support the results presented above in previous sections and examine any key role played by sea surface temperature (SST) on the Congo basin cell, we made the use of ECHAM5.3 experiments, which are forced with the observed global SSTs. The capability of ECHAM5.3 to capture the seasonality of the Congo Basin Cell in isobaric coordinates is shown in Fig. 3.7. In ECHAM5.3, the Congo Basin Cell is stronger, wider and taller than in ERA-Interim (Figs. 3.7 & 3.1), but with the trend of the mass-weighted streamfunctions almost 50% lower than in ERA-Interim (Figs.3.7 & 3.1). However, the Walker Cell over the Indian Ocean has shrunk and weakened (Fig. 3.7).

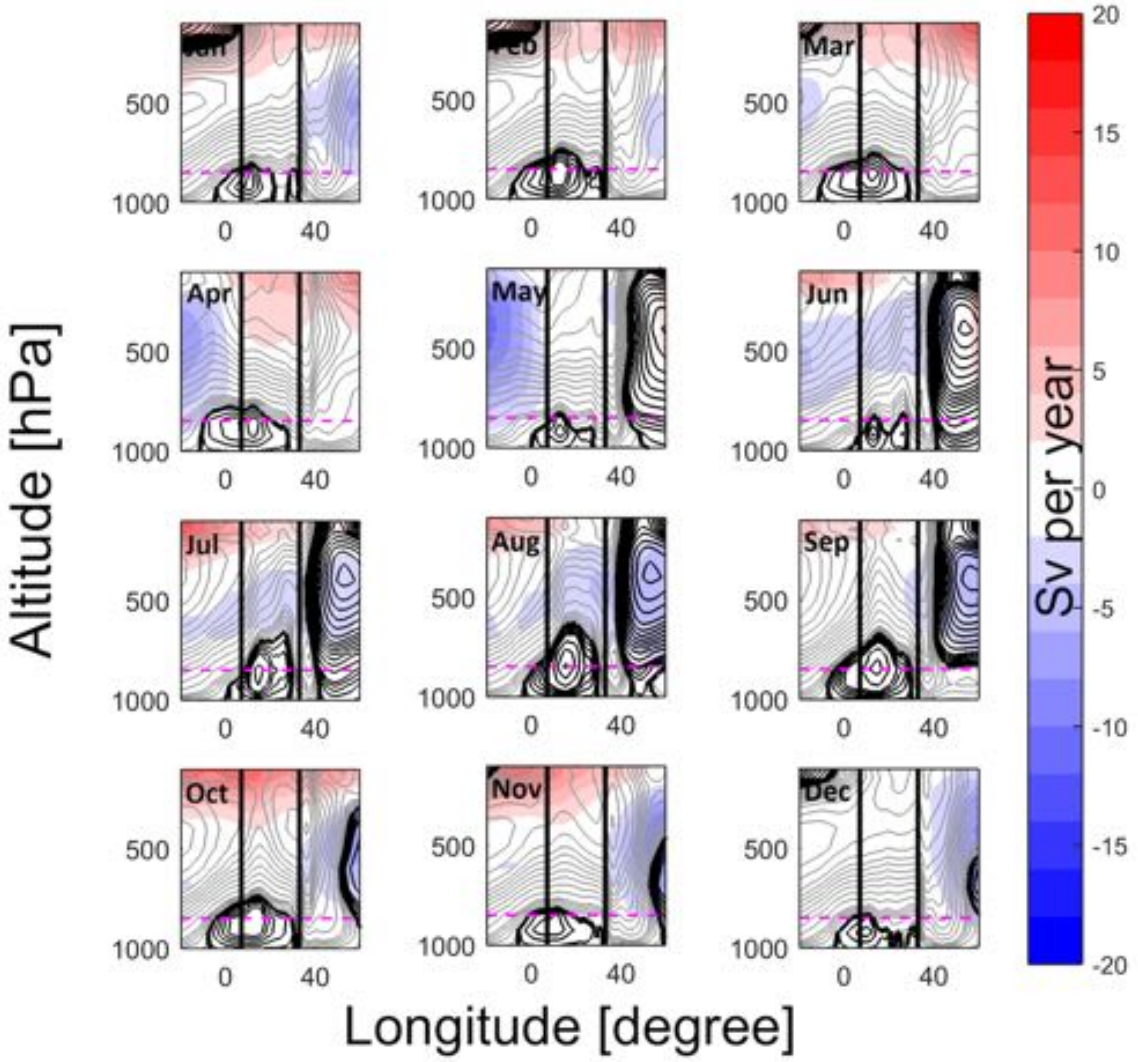

Fig. 3.7. As in Fig. 3.1 but for ECHAM5.3

The near-surface land-sea surface thermal contrast associated with the low surface pressure is also well represented in ECHAM5.3, but the amplitude is two times stronger than in ERA-Interim (Fig. 3.8). All these features of the regional-scale circulation over Central Africa substantiate the key role played by the SST, through the land-ocean thermal contrast in driving the Congo Basin Cell, a shallow thermally direct overturning cell (Schneider and Lindzen, 1977).

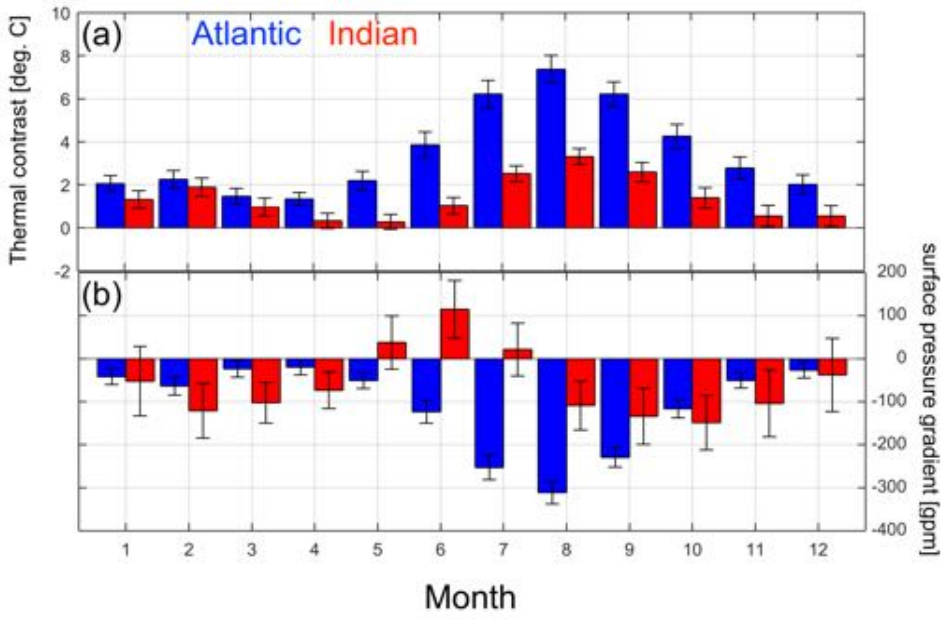

Fig. 3.8. Seasonal cycle of the near surface thermal contrast (°C) and surface pressure gradient (gpm) between central Africa subcontinent (15°-30°E; 5°N-5°S, ΔT_{ATL} and ΔP_{ATL}) and eastern Atlantic (5°W-5°E; 5°N-5°S) and western Indian (40°-50°E; 5°N-5°S, ΔT_{IND} and ΔP_{IND}) oceans in ECHAM5.3.

3.4. Overview of the meridional circulation over central Africa

The zonal land-ocean surface temperature contrast is likely to induce a meridional circulation via the thermal wind relation (Peixoto and Oort, 1992). To better understand this mechanism, we compute meridional mass-weighted streamfunctions for ERA-Interim and show them in Fig. 3.9a. Strong symmetric overturning (Hadley) cells are found over central Africa, with the ascending branch migrating from 15°S in January to 20°N in July and sinking branch at mid-latitudes (Fig. 3.9a). From June to September, a strong anticlockwise Hadley cell encompass the entire Central Africa (Fig. 3.9a). However, from August to December, the Hadley cells are moving backwards (Fig. 3.9a). At upper levels, the circulation is poleward. Owed by the zonal surface land-ocean contrast, the induced vertical meridional wind shear – characteristic of baroclinic flows – occurs at low-levels, depicting a shallow meridional overturning circulation (Fig. 3.9a). And because Hadley cells are thermally direct circulations, the most striking feature is that the Central Africa rainfall maximum (Fig. 3.9a, bottom panels) is more determined by the ascending branch at the midlevels than at the surface where the temperature is higher year-round than aloft. Indeed, at near surface, water vapor transported across the equator warms up while reaching the Sahel (between 10°N and 20°N), where the surface temperature is the warmest. The atmospheric (convective) instability $(\partial h/\partial z)$ over Central Africa is associated with the southward import of higher moist static energy (h), through the strong negative Hadley cell. Between 750- and 600- hPa, the air saturates and initiates a deep convection (Fig. 3.9a, right panels). It is this deep convection at midlevel that determine the position of rainfall maximum over Central Africa (Fig. 3.9a). The seasonal trend of

mass-weighted streamfunctions shows intensification of rising motion for the northern Hadley cell associated with high rainfall. While for the southern Hadley cell, positive trend is associated with weakening of vertical motion, leading to less rainfall (Fig. 3.9a).

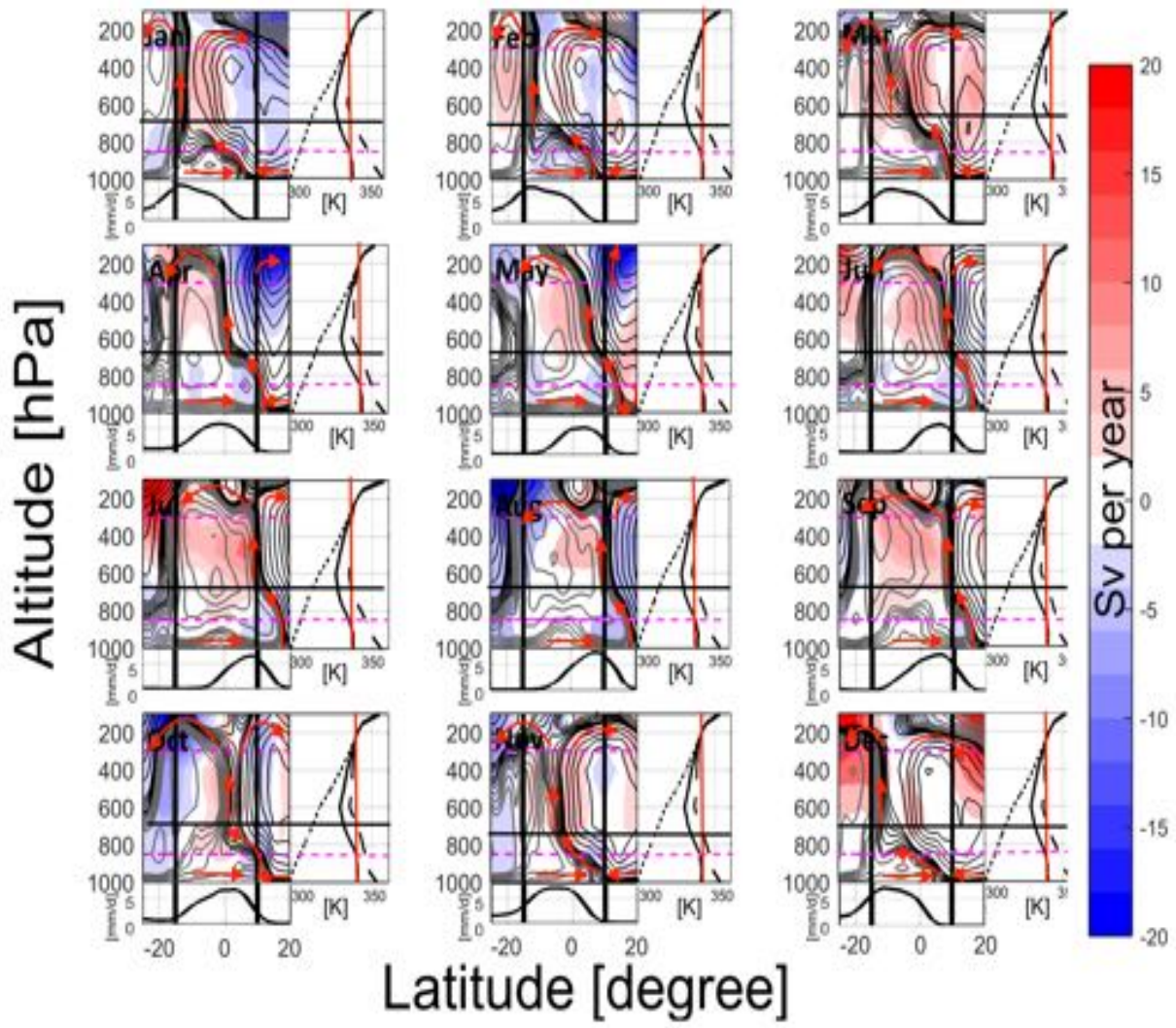

Fig. 3.9a. Meridional-mean circulation (contours, Sv) and its trend (shaded, Sv per year) and rainfall (mm/d) over central Africa. Gray and black contours represent positive and negative values of mass-weighted streamfunctions. Contours intervals are 20 Sv between 5 and 100Sv; 75 Sv between 150 and 600 Sv and 150 Sv between 700 and 1500Sv. Vertical bars represent central Africa. All variables are from ERA-Interim.

As for ECHAM5.3, the annual cycle of Walker Cells over Central Africa is well reproduced in Fig. 3.9b. But at the mid-level, the ascending branch has weakened (Fig. 3.8). Nevertheless, the induced shallow meridional overturning circulation illustrated by a baroclinicity of the meridional circulation at low-levels and owed by the land-ocean surface thermal contrast is also well

reproduced (Fig. 3.9b). These findings confirmed that the SST do play a major role in the formation and maintenance of the Hadley cells over Central Africa.

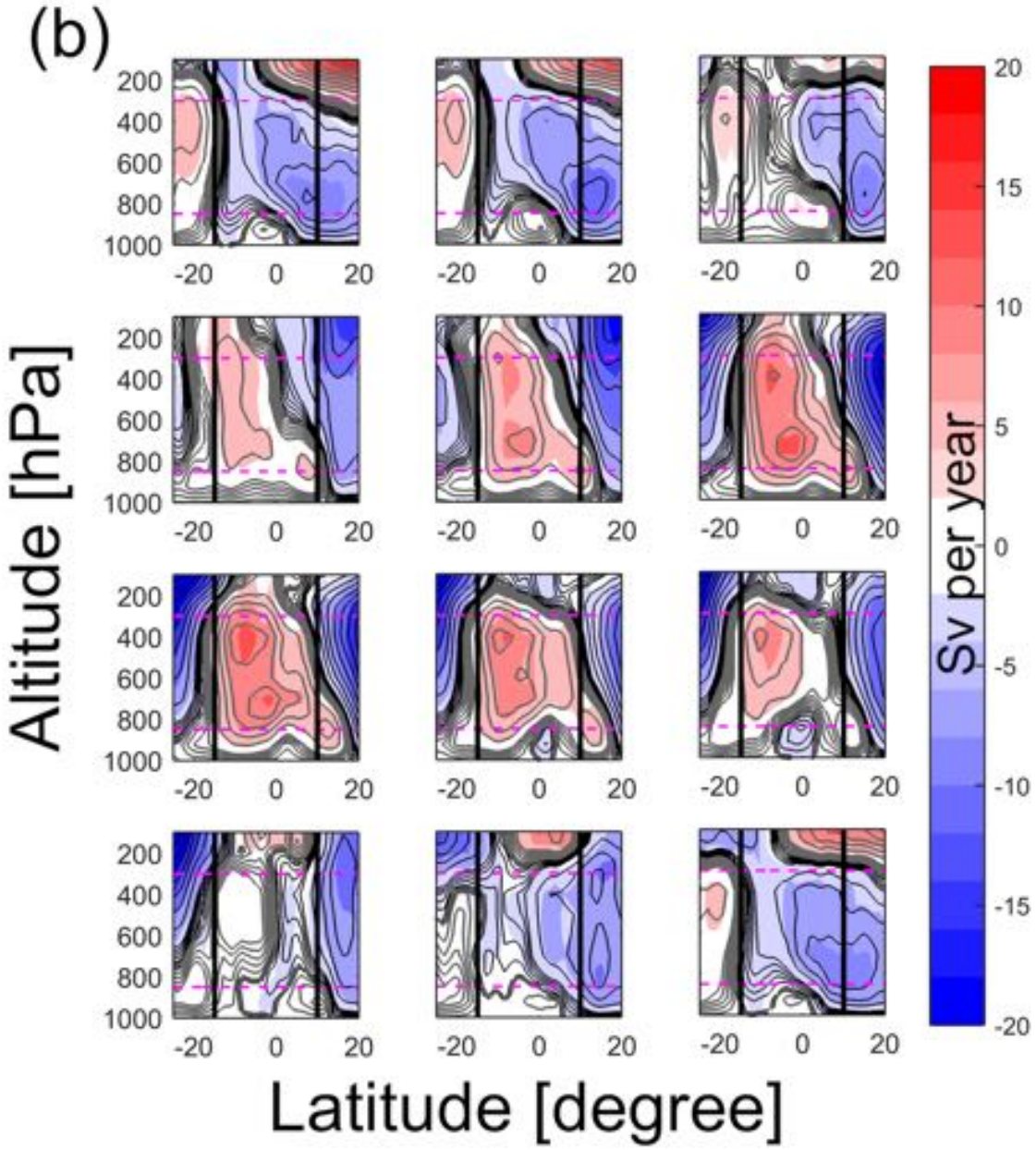

Fig.3.9b. As in Fig. 3.9a but for ECHAM5.3. In this figure, the vertical profile of saturated moist static energy, dry and moist static energies and the longitudinal variation of rainfall are not represented.

3.5. The proposed thermodynamical mechanism controlling the formation of Congo Basin Cell

Firstly, we want to assess the sensibility of the Congo Basin Cell variation to the land-ocean thermal contrast at interannual time scale in ERA-Interim and evaluate how this response is simulated in ECHAM5.3. Then, we would like to find out how the thermodynamical mechanism is involved in the formation of Congo Basin Cell. To do so, we plot the relationship between the ΔT_{ATL}

and Congo Basin Cell strength (intensity) and width in Fig 3.10. To objectively characterize this relationship, we compute the joint distribution of the above variables. The joint distribution is calculated as joint probability density functions (pdf) derived from two-dimensional Gaussian Kernel estimator (Marshall and Molteni 1993, Botev et al. 2010). The ΔT_{ATL} and Congo Basin Cell intensity and width are effectively split into bins into which the probabilities are estimated. Strong and significant relations are found between the near-surface land-ocean thermal contrast and Congo Basin Cell at interannual time scale in ERA-Interim and ECHAM5.3 respectively (Fig. 3.10).

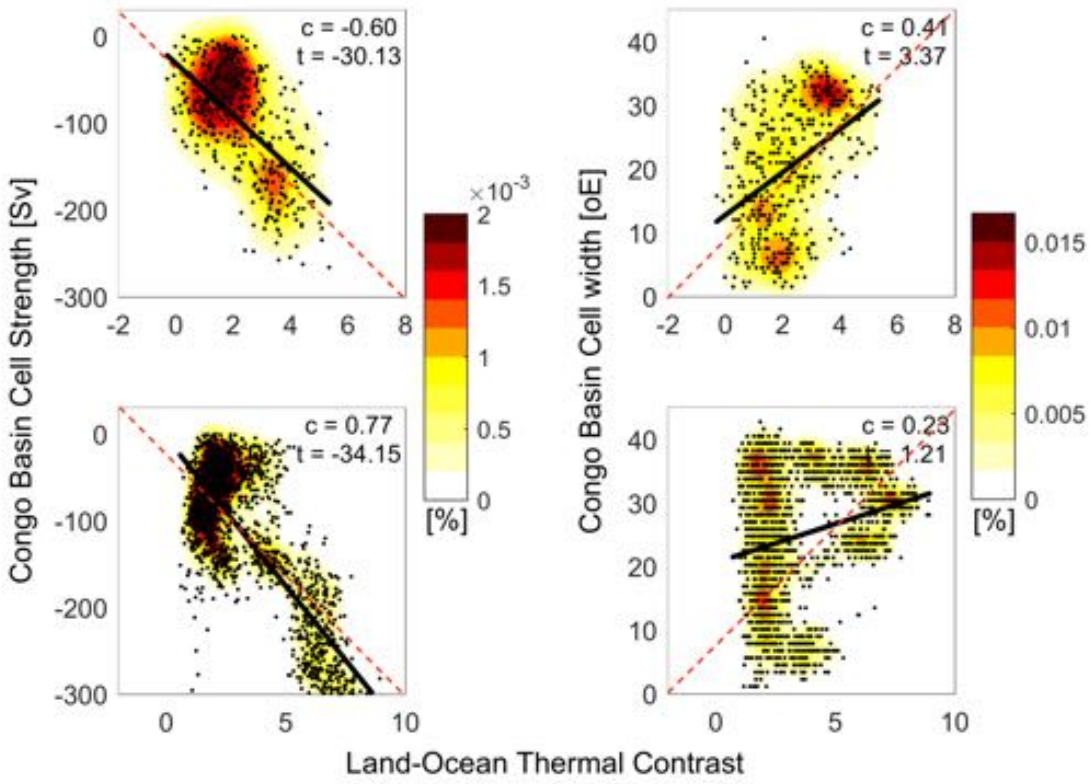

Fig. 3.10. Scatterplot (black dots) and joint distribution (shaded, %) of (X-axis) the near-surface land-ocean thermal contrast (^{o}C) between central Africa landmass (15^{o}-30^{o}E; 5^{o}N-5^{o}S) and eastern Atlantic Ocean (5^{o}W-5^{o}E; 5^{o}N-5^{o}S) and (Y-axis) Congo Basin Cell (left) strength (Sv) and (right) width. (Top) ERA-Interim and (Bottom) ECHAM5.3. In each panel correlation coefficient correlation (c) and slope (t) are shown. The black bold and red dashed straight lines represent the slope and the diagonal of slope 1:1 respectively. All variables are from ERA-Interim.

This suggests that the variability of the Congo Basin Cell strength and width are more modulated by land-ocean thermal contrast than by other physical mechanisms, but with strong impacts on Congo Basin Cell strength than on Congo Basin Cell width. Also, the joint distribution of Congo Basin Cell strength and land-ocean thermal contrast is characterized by a first maximum (measured at the highest probability) located at lower land-ocean thermal contrast of around 1^{o}C in ERA-Interim compared to ~2^{o}C in ECHAM5.3 for a maximum strength of around -80 Sv (Fig.

3.10, left panels). A pronounced second maximum of Congo Basin Cell strength occurs at around ~180 Sv for a thermal contrast of around 4^{o}C (Fig. 3.10, left panels). On the other hand, the Congo Basin Cell width displays a first maximum at the width of 30^{o}E for the thermal contrast of around 4^{o}C (Fig. 3.10, right panels). This indicates that strengthening and widening of Congo Basin Cell is associated with high land-ocean thermal contrast, as outlined by their slope (Fig. 3.10). It is important to note that the ECHAM5.3 experiments simulate quite well the response of Congo Basin Cell to the land-ocean thermal contrast (Fig. 3.10, bottom panels).

To determine the thermodynamic mechanism responsible of the formation of the Congo Basin Cell, we conduct a closer inspection of Figs. 3.1, 3.6 and 3.10 and Table 3.1. The schematic diagram of the proposed mechanism is summarized in Fig. 3.11.

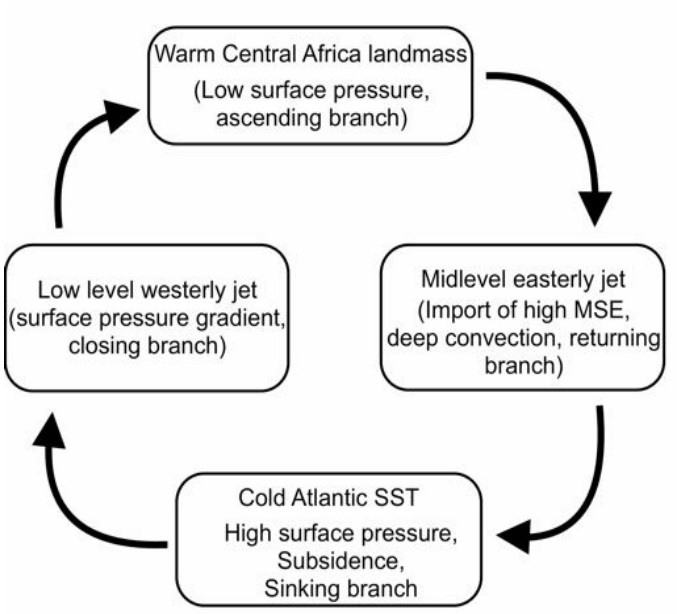

Fig. 3.11. Schematic diagram of the mechanism driving the Congo basin Cell

Throughout the year, the Central Africa landmass is warming more than its surrounding oceans and it is associated with positive atmospheric convective stability $(\partial h/\partial z > 0)$ in the boundary layer (Fig. 3.6). For convection to occur over Central Africa, the atmospheric convective instability should be associated with the import of higher moist energy content air from the Sahel (Fig. 3.6). At around 24^{o}E, while the warm air is moving up adiabatically (Figs. 3.1; 3.6), the land-ocean temperature difference between Central Africa landmass and Atlantic Ocean generates a surface pressure gradient, with lower surface pressure system over Central Africa landmass than over adjoining Oceans. At ~750- hPa, associated with the midlevel easterly jet over Central Africa, the induced southward warm moist air mass cools adiabatically and saturates (red line, cloud base, Fig. 3.6), and releases latent heat (condensation) and increase of temperature, indicative of deep convection. This finding is consistent with Nicholson and Grist (2003), who assumed any potential

influence of midlevel easterly jet to trigger convection over Central Africa. Aloft 750- hPa, the air mass ascends moist adiabatically to reach stability at ~200- hPa (top of cloud, Fig. 3.6). This atmospheric conditions lead to strong convective rainfall over central Africa. Nevertheless, saturated air mass subsides over a cold eastern Atlantic, leading to limited column water vapour, evaporation and rainfall.

3.7. Conclusion and discussion

In this chapter, we used a combination of commonly used reanalysis datasets to further understand the zonal large-scale atmospheric dynamics over central Africa and its adjoining Oceans. To do so, we computed the zonal mass-weighted streamfunctions as it is commonly employed in its Hadley circulation studies to objectively define indices that help to describe variations of large-scale circulation structure in terms of width and intensity over central Africa. In all datasets used, we identify, at low-levels, the existence of a shallow zonal overturning circulation thermally direct, namely the Congo Basin Cell, which persists throughout the year, with a maximum strength and width in August and minimum strength and width in May. However, the Congo Basin Cell strength and width are controlled by the near-surface thermal contrast between warm Central Africa landmass and cold eastern tropical Atlantic Ocean rather than the divergent component of the tropical atmospheric circulation as proposed by Pokam et al. (2014). Meanwhile, the Central Africa "pseudo" Walker-like Cell is likely to be driven by the thermally divergent wind component of the tropical atmospheric flow, as suggested by Yu and Zwiers, 2010 and Yu et al. 2012. Interestingly, the ECHAM5.3 captures quite well the response of the Congo Basin Cell on the land-ocean thermal contrast. No consistent trends in Congo Basin Cell intensity and width among datasets since 1979 are significant. In contrast, the eastern edge longitude of the Congo Basin Cell has a shrinking tendency in all datasets. On the other hand, no direct relationship between the Congo Basin Cell and local rainfall at annual and monthly time scale is noted. But the Congo Basin Cell is likely to determine the position of the zonal rainfall maximum (ITCZ). Notably, the surrounding oceans are not only the main suppliers of water vapour air mass to central Africa. Essentially, the Atlantic Ocean might play a crucial role, via the land-ocean surface thermal contrast by either invigorating deep convection by inducing southward import of high moist static energy or by regulating the westward/eastward displacement of the Congo Basin Cell. Aloft 750- hPa, the strong easterly large-scale circulation is barotropic. However, the meridional large-scale circulation is baroclinic, consistent with Biasutti et al. (2003). These findings modify substantially our representation of zonal large-scale circulation over Central Africa and its surrounding Oceans. To summarize this, we propose, in Fig. 3.10, a schematic diagram of large-scale circulation over Central Africa. This regional circulation is dominated by a "pseudo" Walker-like Cell, which crosses Central Africa landmass, from western tropical Indian Ocean to eastern Atlantic Ocean. However, the structure of this regional circulation is reminiscent of the Central Africa overturning cell as proposed by Flohn

(1971), but with at low-levels, a shallow zonal overturning cell, namely Congo Basin Cell (Fig. 3.10).

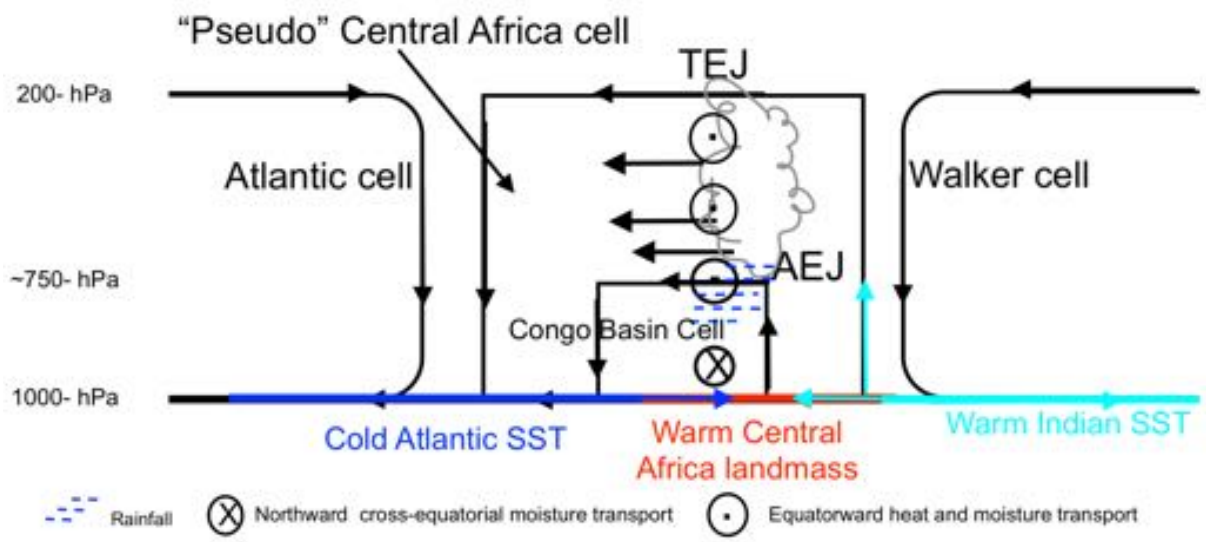

Fig. 3.12. Schematic diagram of the zonal large-scale circulation over central Africa and its surrounding Oceans as proposed in this study.

Furthermore, accordingly, to aforementioned thermodynamic mechanisms leading to Congo Basin Cell, we propose that rainfall over central Africa occurs in three phases. Firstly, the solar heating warms more central Africa landmass than its adjacent Ocean. The unsaturated air uplifts dry adiabatically at ~24^{o}E (ascending branch). The resulted land-ocean temperature contrast between central Africa landmass and Atlantic Ocean generates a quasi-permanent low surface pressure over central Africa, which can trigger a monsoon-like circulation at low-levels, particularly over eastern Atlantic (lower branch), with lower energy content over eastern Atlantic and higher energy content over western Indian. This initiates a thermally direct circulation controlled by the land-ocean thermal contrast over central Africa (initiation). Secondly, favoured by the midlevel easterly (returning branch, between 800- and 750- hPa), the equatorward warm moist air saturates and lead to convection, before gradually subside over Atlantic Ocean (sinking branch). By a feedback mechanism, the released water vapour (condensation) associated with strong midlevel easterly jet leads to a strong moisture flux convergence, which can increase the local latent heat over central Africa. Moreover, the vertical recirculation associated with the Congo basin cell sustains the atmospheric water vapour recycling so that from September to April, it is raining out over central Africa (development). Finally, from May to August, the land-ocean thermal contrast enhanced, which deepen further the low surface pressure gradient, indicative of subsidence of central Africa. This intensifies and widens the Congo basin cell so that it prevents more low-level moisture flux from Indian Ocean to reach the central Africa landmass. This situation is likely to lead to less central Africa rainfall due to less atmospheric water vapour advection by low-level jets (Decay). The ECHAM5.3 simulation provides a support to this mechanism.

Chap. 4

On the Central Africa Low: Identification, evolution, variability and its influence on regional climate

4.1. Introduction

The land-ocean thermal contrast, with warmer Central Africa landmass than its surrounding oceans, is likely to generate a local quasi-permanent low surface pressure system over central Africa (chapter 3). Moreover, the annual cycle of Central Africa rainfall is negatively correlated to the underlying low pressure system at surface and 700- hPa respectively (chapter 2). However, few papers (Dezfuli et al. 2015 and Dezfuli 2017) highlighted some characteristics of a low-pressure system over equatorial region of Central Africa from December to March. Thus, the main motivation of this chapter is limited to assess these threefold issues:

(a) How to characterize the Central Africa low-pressure? What is its seasonal evolution, location and intensity?
(b) To diagnose how does the Central Africa Low modulate rainfall, adjoining SST and their associated moisture transports
(c) To examine what are the relationships between Central Africa Low and large–scale circulation over central Africa as well as the ITCZ.

4.2. Data

We used atmospheric variables from the European Centre for Medium-Range Weather Forecasts (ECMWF) ERA-Interim reanalysis (0.75^{o} grid, Dee et al., 2011) spanning the 37-year period from 1979 to 2015 to characterize the Congo basin low. The geopotential height, air temperature, specific humidity, vertical velocity, zonal and meridional wind components at 13 pressure levels (1000, 925, 850, 775, 700, 750, 700, 600, 500, 400, 300, 200, 100) at monthly time steps have been selected. For rainfall, we use the average of satellite/rain-gauge estimates of the Global Precipitation Climatology Project (GPCP) monthly precipitation data set (Adler et al., 2003) and Climate Prediction Center Merged Analysis of Precipitation (CMAP, Xie and Arkin, 1997). We interpolate the satellite data sets to 1 × 1° grids from 1979 to 2015. Both data sets are reliably reproducing the spatial patterns of precipitation over central Africa (Negro Juarez et al. 2009; Dezfuli and Nicholdon, 2012). Finally, all these variables are used to compute the moist static energy (Neelin and Held, 1987) and mass-weighted streamfunctions (chapter 3) respectively. For the sea surface temperature (SST), the global monthly of the NOAA optimum interpolated (OI) SST version 2.2 (Reynolds et al., 2002) and Extended Reconstructed Sea Surface Temperature versin 3b (ERSST, Smith et al. 2008) were used.

4.3. Identifying the Central Africa Low

To highlight the formation and development of the Central Africa Low, we first analyse the seasonal evolution of the vertically mean (between 1000- and 500- hPa) of the geopotential height (mid-lower geopotential thickness) area-averaged over the large Central Africa domain (20˚W – 60˚E; 25˚S – 20˚N). The low-pressure system over Central Africa that is less than 1.5% of the mid-lower (geopotential) thickness Gaussian distribution (Fig. 4.1), i.e. below the 2580- (geopotential) thickness (gpm) value will be referred as Central Africa Low.

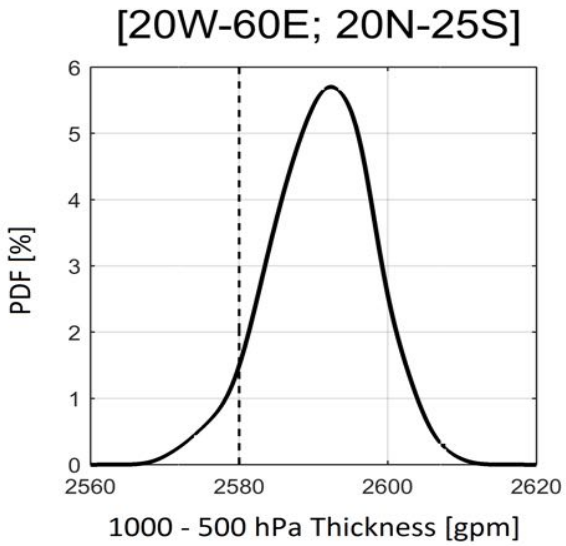

Fig. 4.1. Gaussian distribution (Probability density functions, %) of 1000-500- hPa geopotential thickness (gpm) over large Central Africa domain (20^{o}W-60^{o}E; 20^{o}N-25^{o}S) in ERA-Interim.

To further identify the Central Africa Low, we illustrate the trajectory of the annual cycle of the mid-lower thickness over central Africa domain in Figs 4.2-3. The Central Africa Low 2580- gpm isoline (red contour) encompasses the entire central Africa region from October to April (ONDJFMA) and defines a prominent cyclonic system over Central Africa (Fig. 4.2). The rainfall associated with this low-pressure system represents around 70% of total rainfall (Fig. 4.2). From October to April, the Central Africa Low 2580- gpm isoline is surrounded by regions that experience relatively high tropospheric pressure (Figs. 4.2-3). This means that the wind, over central Africa troposphere, will be essentially north-easterly in the northern Hemisphere and south-easterly in southern Hemisphere (Figs. 4.2-3), indicative of barotropic circulation. At low-levels, the Central Africa Low is associated with weak wind (Fig. 3.2). At the same time, the Central Africa Low is accompanied by strengthened mid-lower wind, originated essentially from the northern Hemisphere (Fig. 4.3).

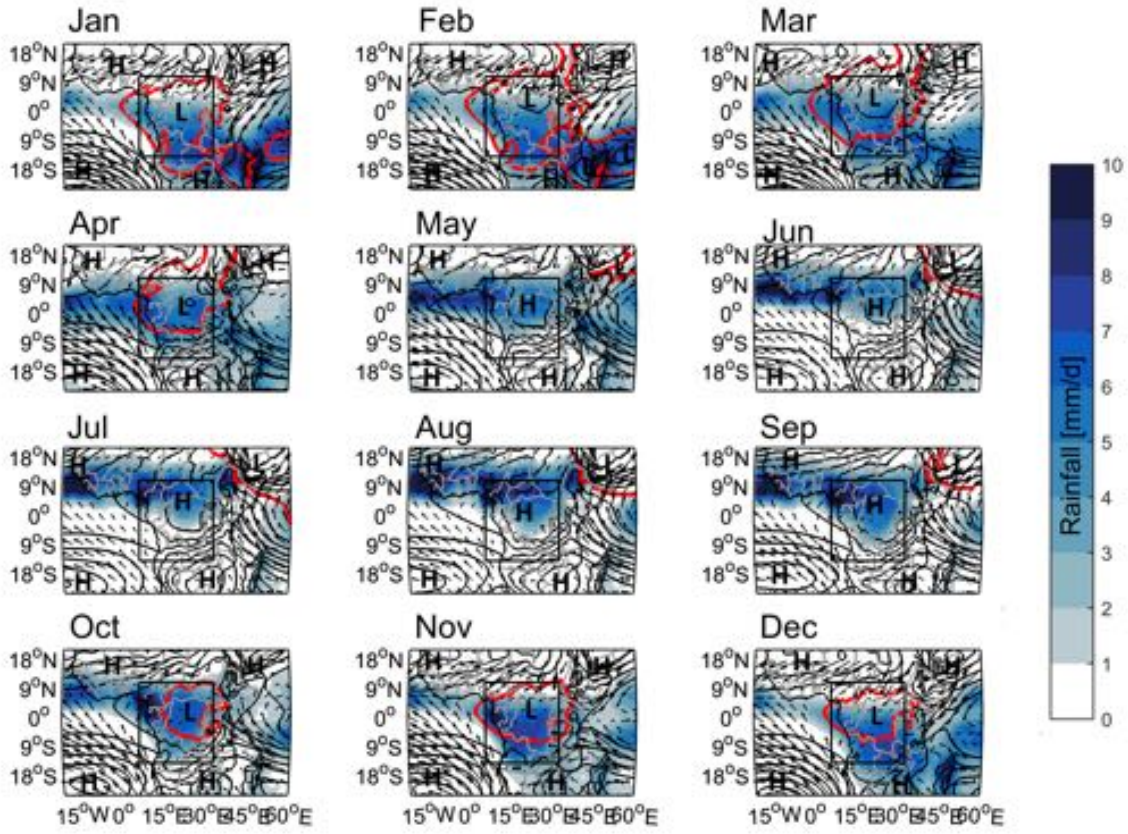

Fig 4.2. Annual cycle of the mid-lower thickness (geopotential height vertically averaged between 1000- to 500- hPa, contours, gpm), horizontal wind at low-levels (vertically average between 1000 and 850- hPa, arrows, m/s) and rainfall (shading, mm/d). Wind speed with less than 1m/s is not represented. The red contour indicates the 2580- gpm isoline, indicative of Central Africa Low. H and L represent the High and Low pressure systems respectively. All variables are from ERA-Interim. More details in the text.

Notably, the presence of low-pressure system over Central Africa landmass and the relative high pressure over surrounding Oceans, which is related to the high-pressure system prevailing over tropical Atlantic and Indian Oceans. This situation highlights a land-ocean pressure gradient over Central Africa that is related to the underlying land-ocean thermal contrast (chapter 3).

In May to September (MJJAS), the Central Africa Low 2580- gpm isoline jumps further to the northeast and emerges over the Arabia sea (Figs. 4.2-3). This leads to the surge of high geopotential thickness over central Africa, suggestive of a relative higher pressure or subsidence, than during the previous season (from October to April) namely Central Africa subsidence (Fig. 4.2). This northern displacement of the 2580-gpm isoline is associated with the meridional displacement of rainfall and the reversal of the circulation at lower and middle troposphere over East Africa and the Horn of Africa (Figs. 4.2-3). The relative high pressure system over Central Africa in MJJAS is associated with less rainfall over the region (Figs. 4.2-3). This suggests a subsidence over Central Africa due to the weakening of Central Africa Low, which in turn, is likely to suppress local convection. However, this subsidence over Central Africa landmass shows relatively lower pressure system than over surrounding tropical Indian Ocean, west Africa and Sahel (Figs. 4.2-3). In addition, the subsidence over Central Africa is associated with weaker low-levels wind (Fig. 4.2), while it reinforces mid-lower wind in the southern Hemisphere (Fig. 4.3). Throughout the year, in the southern Hemisphere, the regional atmospheric circulation features two dominant anticyclones – one over Botswana (namely, Botswana High, Driver and Reason, 2015) and another one in the southern Atlantic (namely, South Atlantic High) (Figs. 4.2-3). Hence, the south-easterly is dominant over southern Hemisphere, with the south Atlantic anticyclone as the main driver of the low-level circulation. Indeed, low-level easterlies are stronger over Atlantic than the mid-lower easterlies (Figs. 4.2-3).

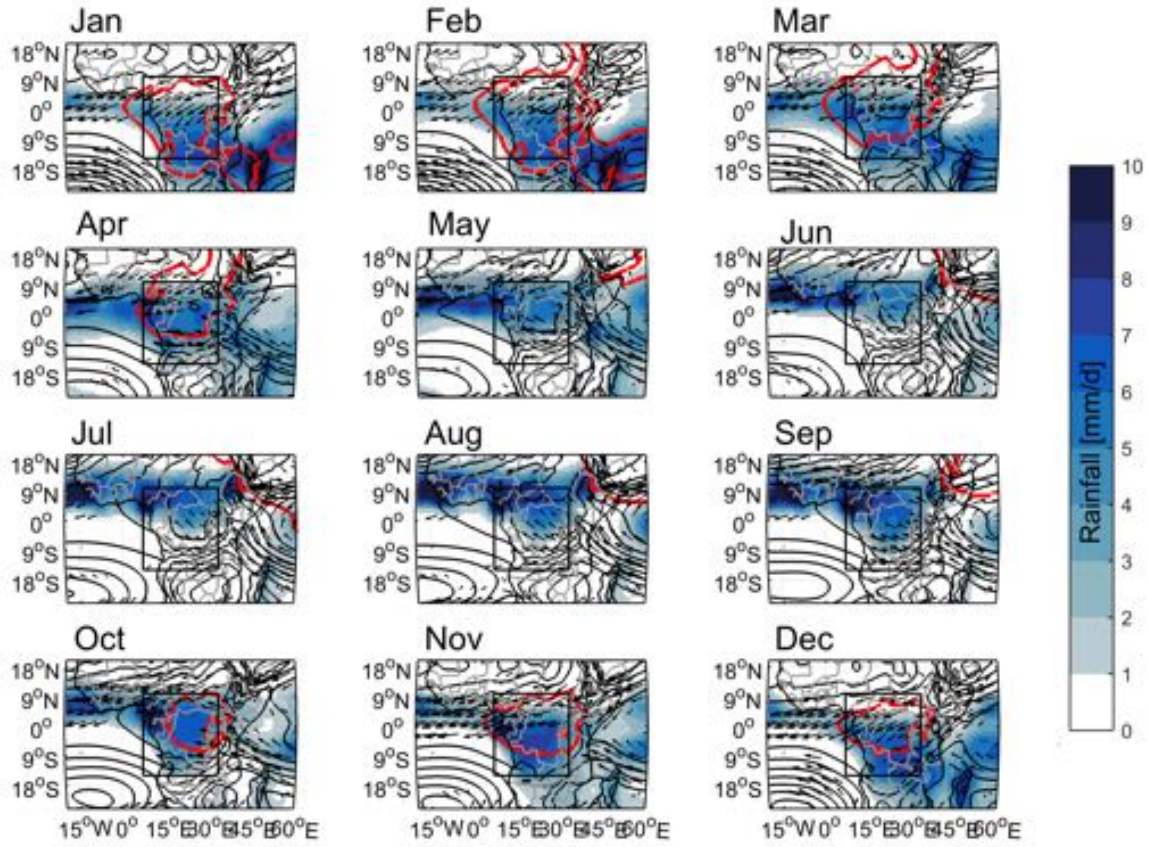

Fig 4.3. as in **Fig. 4.2.** but with horizontal wind (vertically average between 850 and 500- hPa, arrows, m/s). More details in the text.

4.4. Seasonal evolution of Central Africa Low

To further understand the evolution of the Central Africa Low, we focus on the October to April season, when the Central Africa Low 2580- gpm isoline is located mainly over Central Africa. The seasonal evolution of the central Africa cyclonic system is shown in Fig. 4.4. We also plot in Fig. 4.5, the seasonal evolution of the vertical structure (longitude–height) of the temperature (contours) and specific humidity (shading) across the Central Africa Low (i.e. averaged between 5°N and 5°S) as well as the vertical profile of vertical velocity over Central Africa and its neighbouring regions (Eastern Atlantic and East Africa, Fig. 4.5, right panels). Where maximum vertical velocity is found at upper levels, this vertical structure is referred as top-heavy structure and it is associated with deep convection (Back and Bretherton, 2006, Sobel et al. 2007). Conversely, bottom-heavy structure is referred for any vertical velocity with maximum at low-levels. This bottom-heavy structure is associated with shallow convection (Back and Bretherton, 2006, Sobel et al. 2007). Moreover, the structure of the rising motion determines the sign of vertical moist static energy, with the top-heavy structure associated with more sensible heat export that stabilize the local atmosphere (Back and Bretherton, 2006; Chou and Chen, 2010). The bottom-heavy structure is associated with import of column moist static energy, which destabilize the local atmosphere via moistening (Back and Bretherton, 2006; Chou and Chen, 2010).

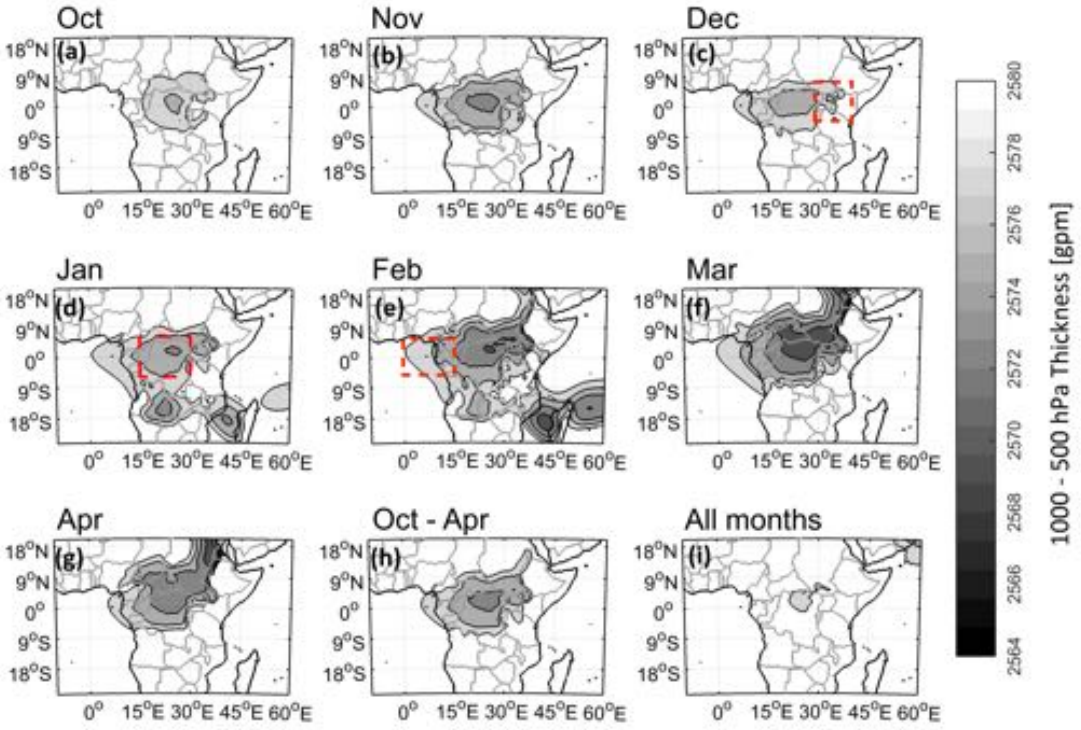

Fig. 4.4. Seasonal evolution of Central Africa Low in ERA-Interim: (a) October; (b) November; (c) December; (d) January; (e) February; (f) March; (g) April; (h) October to April season (ONDJFMA) and (i) Annual. (Unit: gpm). Red dashed boxes in (c), (d) and (e) delineate East Africa, Congo basin and Eastern Atlantic respectively.

In October, an oval-shaped low-pressure system develops and bestrides above Central Africa landmass in the east–west direction (Fig. 4.4a), with a core centred at around 5°N–5°S; 15°–30°E (Fig. 4.4d, dashed red box). Stronger Central Africa Low (minimum of the mid-lower thickness, green line) is positioned in the midst of Congo basin rainforest at 26°E and at west in the vicinity of area with intense surface heating (Rift valley highlands, red line) (Fig. 4.5a). This maximum of surface temperature over central Africa is located closely to the minimum of precipitable water at 33°E (Rift Valley highlands, Fig. 4.5a). The precipitable water or column water vapour is calculated as mass-weighted vertically integrated of the specific humidity from surface to 500- hPa. Over East Africa (30°–40°E; 5°S–5°N), a distinct and small trough (dashed red box in Fig. 4.4c) similarly develops in October and matures in December, when the short rainy season occurs in this region (Cook and Vizy, 2013; Wang et al. 2014). We note that the Central Africa Low forms in a region of higher moist static energy (below 600- hPa, Figs. 4.4; 4.1) associated with top-heavy structure, with the boundary layer (below 800- hPa) relatively stable ($\omega = 0$, solid black line, Fig. 4.5a, right panel), suggestive of deep convection. This convection leads to a high rainfall in October representing more than 11.45% of Central Africa annual total rainfall.

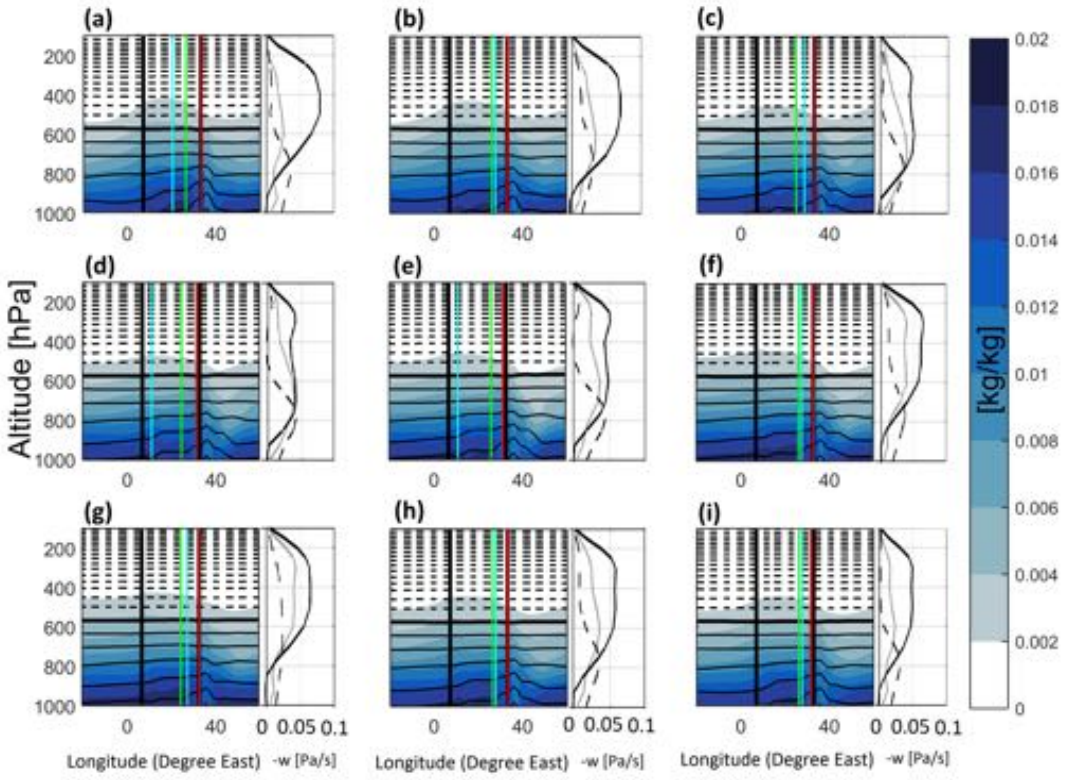

Fig. 4.5. Longitude-height seasonal evolution of specific humidity (shaded), temperature (contours, positive solid and negative, dashed) and vertical profile of vertical velocity: (a) October; (b) November; (c) December; (d) January; (e) February; (f) March; (g) April; (h) October to April season (ONDJFMA) and (i) Annual. Contour interval for temperature is 5^{o}C, with 0^{o}C as bold black contour. In each panel, solid cyan, green and red lines represent the position of the maximum precipitable water, the minimum geopotential thickness and the maximum surface warming over Central Africa respectively. Bold black vertical lines limit Central Africa. All variables are from ERA-Interim.

However, while the Central Africa Low matures, the water vapour column maximum is moving eastward from 20^{o}E in October to 30^{o}E in December (Figs. 4.5a-c). Meanwhile, the East Africa low is associated with high surface warming, which is collocated with precipitable water minimum, as suggested by low latent heat (specific humidity) values between 30°-40°E (Fig 4.5a). In addition, East Africa is characterized by a bottom-heavy structure, indicative of shallow convection. This shallow convection associated with the short rainy season leads to less local rainfall, amounting to two times less rainfall than that over central Africa. In January, even though the Central Africa Low matures and merges with the East Africa low, its local vertical velocity weakens and shows two large amplitudes at 300- and 750- hPa respectively (Fig. 4.5d), indicative of suppression of

deep convection. Due to this slight modification of vertical velocity structure over Central Africa, the rainfall is reduced by about 50% with relative to the rainfall rate in October. This reduced rainfall is associated with an eastward jump of high water vapour column towards Atlantic offshore regions (Fig. 4.5d). Over southern Africa, one can readily see two distinct dominant low-pressure systems: one over the landmass situated at 15°–30°E; 9°–20°S, reminiscent of Angola low (Fauchereau et al. 2009; Hart et al. 2010) and another one over the Mozambique channel at 35°–45°E; 15–25°S (Figs. 4.4d-e). In February, in response to intense surface warming, the Central Africa low intensifies and widens as indicated by deepened convection over Central Africa (Figs. 4.4e, 4.5e), that lead to high rainfall over Central Africa. In the same time, the Angola low weakens and the Mozambique channel low strengthens (Fig. 4.4e). In March, the central Africa low deepens further and continues its poleward displacement, when the Angola and Mozambique channel lows abruptly decline (Fig. 4.4f). This northward displacement of the central Africa low, spanning towards the Arabian sea, is tightly associated with northward moving surface warming (Fig. 4.4f), consistent with Biasutti et al. (2003). This poleward displacement surface warming is associated with westward moving of higher water vapour column (Fig. 4.5f). In April, the persistence of central Africa low is associated with amplified local top-heavy vertical structure (Figs. 4.4g; 4.5g), which favour strong local convective rainfall (~5.41 $mmday^{-1}$). At the same time, over East Africa, precipitable water increases so that the shallow convection provides moisture and moist static energy aloft (Figs 4.5g); which, in turn, support deep convection (Sobel and Neelin, 2006 and Back and Bretherton, 2009). This is indicative of top-heavy structure over East Africa (Fig. 4.5g). This vertical motion favours strong convective rainfall, representing ~15.5% of total local yearly rainfall in this region. Furthermore, the vertical pressure velocity over eastern Atlantic (0°–15°E; 5°N–5°S) depicts a seasonally varying vertical velocity structure, with top-heavy shape from October to January – behaving similarly to central Africa (gray solid line, Fig. 4.3). While, from February to April, the vertical velocity structure turns to a bottom-heavy shape.

Notably, the seasonal evolution of Central Africa Low is quasi-stationary equatorward, as indicated by little movement of the minimum of geopotential thickness (located at 26 ^{o}E) over Central Africa for around seven months (Fig. 4.5a-g, green line). In addition, the proximity of this core of Central Africa Low and higher precipitable water (Fig. 4.5h-i) suggests less rainfall variability, indicative of a blocking system. Indeed, the rainfall variance at the core of the Central Africa Low, around Congo basin rainforest (15^{o}E-30^{o}E; 5^{o}N-5^{o}N) is 0.27. This rainfall variance is lower than the rainfall variance occurring over its neighbouring regions over the same latitude. Over eastern Atlantic Ocean (5^{o}W-5^{o}E), the rainfall variance is 0.28, while over East Africa (33^{o}-40^{o}E), it is 0.40 and over western Indian Ocean (40^{o}-60^{o}E) it is 0.43.

4.5. Central Africa Low interannual variability: influence on regional climate and trend

4.5.1. Rainfall and sea surface temperature

In this section, we use the normalized mid-lower (vertically average between 1000- and 500- hPa) thickness index as a metric to describe the intensity of the interannual variability associated with the Central Africa Low to examine the change on regional climate associated with the Central Africa low. To do so, we consider rainfall and SST variables as the main representative of climate. The anomaly is calculated by subtracting the climatological mean value of 1979-2015 October–April (7-month) season of the vertically mean mid-lower thickness from the yearly October–April at each grid point for each of the 37 years. Then, normalized anomaly is obtained by dividing, at each grid point, by the respective standard deviation of 1979-2015 October–April period. Finally, the Central Africa Low index is extracted at the core of Central Africa Low (15^{o}-30^{o}E; 5^{o}N-5^{o}S, red box in Fig. 4.4d) and detrended as we are only interested by the interannual variability. Fig. 4.6a depicts the normalized Central Africa Low index. We selected all years with a value greater than 0.5 standard deviation or less than -0.5 standard deviation. The Central Africa Low is positive (CAL > 0.5) during 13 years (1983, 1987, 1988, 1990, 1991, 1992, 1995, 1998, 2002, 2003, 2007, 2010 and 2015) and Central Africa Low experienced negative phase (CAL < -0.5) for 12 years (1982, 1984, 1985, 1986, 1989, 1996, 2000, 2006, 2008, 2009, 2011 and 2012).

The composite of Central Africa Low as identified by the 2580- gpm isoline during the positive and the negative phases is shown in Fig. 4.7c. During the negative phase (CAL < -0.5), the Central Africa Low 2580-gpm isoline (blue contour) is well developed over all the tropical Africa area and its adjoining Oceans, indicative of deep convection (Fig. 4.6c). Meanwhile, the Central Africa Low climatology (black contour) indicates that strong convection is mainly located over Central Africa landmass. By comparison, the area of strong convection during negative phase of Central Africa Low is almost three time larger than its climatological mean structure. Noted that, in this negative phase, the Central Africa Low encloses the Angola Low (Figs. 4.7c; 4.4d-e). On the other hand, during positive phase, the Central Africa Low 2580- gpm isoline shrinks further (red contour) so that deep convection is essentially confined at its core, which is almost five time smaller than the climatological (mean structure) of the Central Africa Low 2580- gpm isoline (Fig. 4.7c). During positive phase, the position of the Central Africa Low is suggestive of a strong local influence. Hereafter, the positive and negative years will be referred as passive phase and active phase of the Central Africa Low respectively. The composite difference of rainfall during active and passive phases of Central Africa Low is shown in Fig. 4.6b. There is no substantial change of rainfall over central Africa during these two phases, suggesting that despite high rainfall-mean over central Africa, the Central Africa Low is likely to limit the interannual variability of local rainfall. Nevertheless, above normal rainfall is found over southern Africa and the Atlantic offshore region, while below normal rainfall occurred in East Africa and western Indian Ocean (Fig. 4.7b),

reminiscent of the impacts of El Nino southern Oscillation (ENSO) on these specific regions (McHughes, 2006).

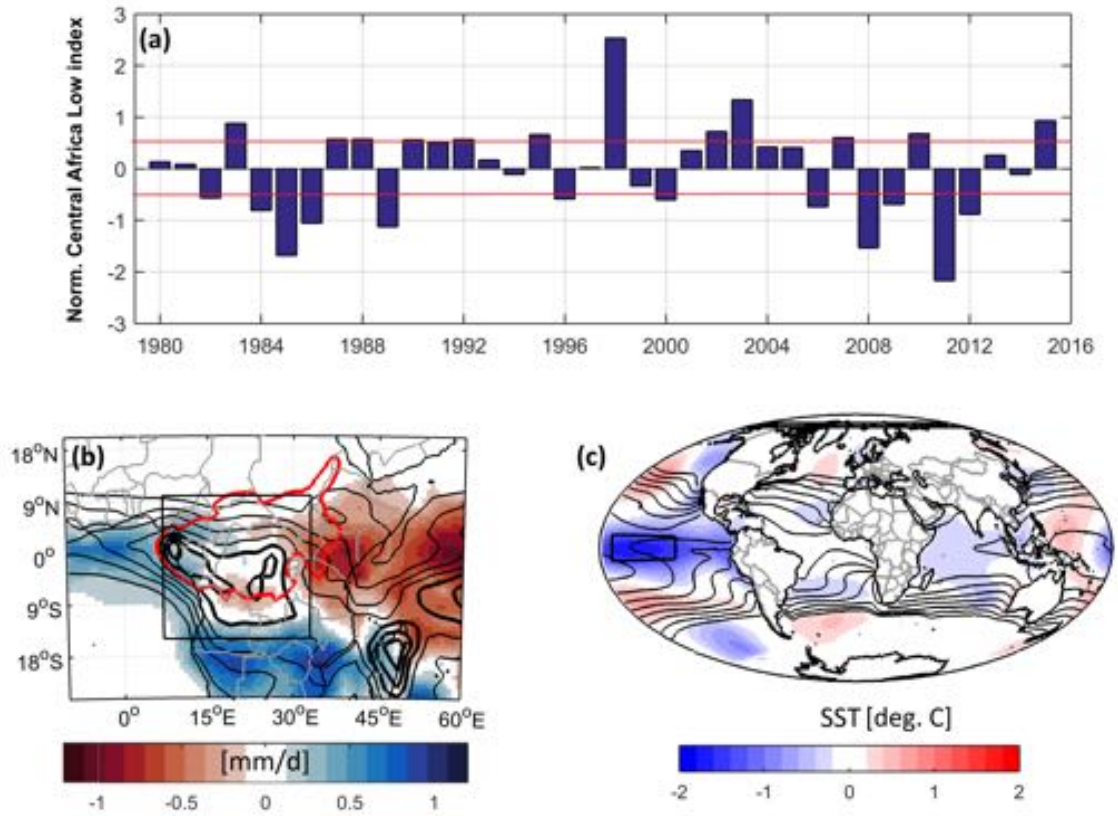

Fig. 4.6. (a) Normalized Central Africa Low index (gpm). Difference composite during negative and positive phase of (a) rainfall (shaded, mm/d) from both CMAP (Xie and Arkin, 1997) and GPCP (Adler et al., 2003) and (b) SST (shaded, ^{o}C) from ERSST3b (Smith et al. 2008). Contours are seasonal mean-state of rainfall and SST respectively. Contour interval are 1 mm/d in (a) and 1^{o}C in (b) respectively.

This finding appears to disprove the idea that enhanced rainfall is caused by intense low-pressure (chapter 2). To shed more light on their connection, I plot the scatter plot of Central Africa Low index and local rainfall (Fig. 4.8h). I find out that less variance of central Africa rainfall is driven by Central Africa Low as indicated by the weakness of the correlation between Central Africa rainfall and Central Africa Low index ($r \sim -0.17$, Fig. 4.8h, black dots). This finding may explain little change in the likelihood of central Africa rainfall during both active and negative phase of Central Africa Low (Fig. 4.6b). But while we consider the annual mean (all months, gray dots) of central Africa rainfall and Central Africa Low, a strong correlation appears ($r \sim -0.4$, $p < 0.005$, Fig. 4.8h), with

more rainfall occurring when low-pressure system dominates central Africa, consistent with our findings in chapter 2.

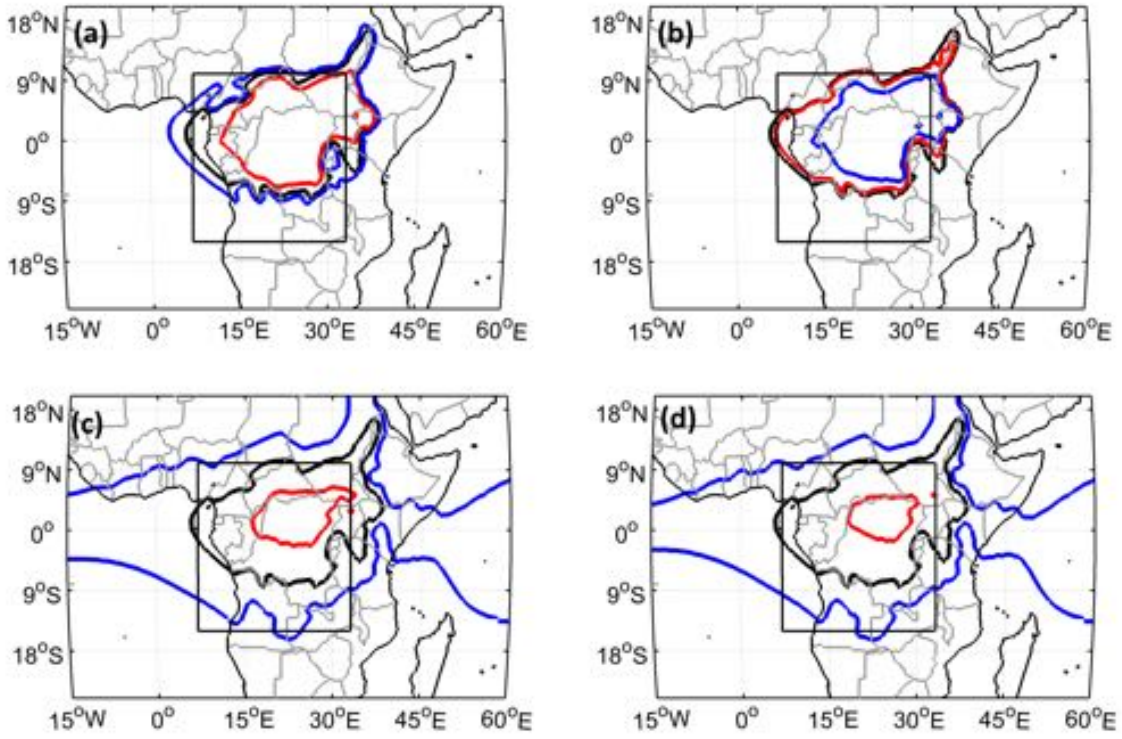

Fig. 4.7. Central Africa Low, as described by its 2580-gpm isoline, for land-ocean thermal contrast (a) at surface during positive years (red contour) and negative years (blue contour); (b) as in (a) but for the mid-lower troposphere (1000- to 500- hPa). (c) as in (a) but for Central Africa low phases; (d) as on (a) but for El Nino phases. In all panels, the black contour represents climatological mean structure of the 2580-gpm associated with Central Africa Low;

This link between central Africa rainfall and Central Africa Low is emphasized by the slope of the regression line, in Fig. 4.8h, indicating that for any decrease of 10 m geopotential thickness there is an increase of about 0.16 mm day^{-1} of rainfall, which is much larger than the 0.09 mmday^{-1} for the October-April season when the Central Africa Low dominates (Fig. 4.4h). Nevertheless, it appears that the Central Africa Low is likely to act as a blocking system over central Africa, limiting the local interannual rainfall variability. This provides a first insight on why the impacts of Central Africa Low are very limited over central Africa, but rather they occur over margin regions of Central Africa Low 2580- gpm isoline, i.e. over Atlantic offshore region and beyond the Rift valley highlands (East Africa).

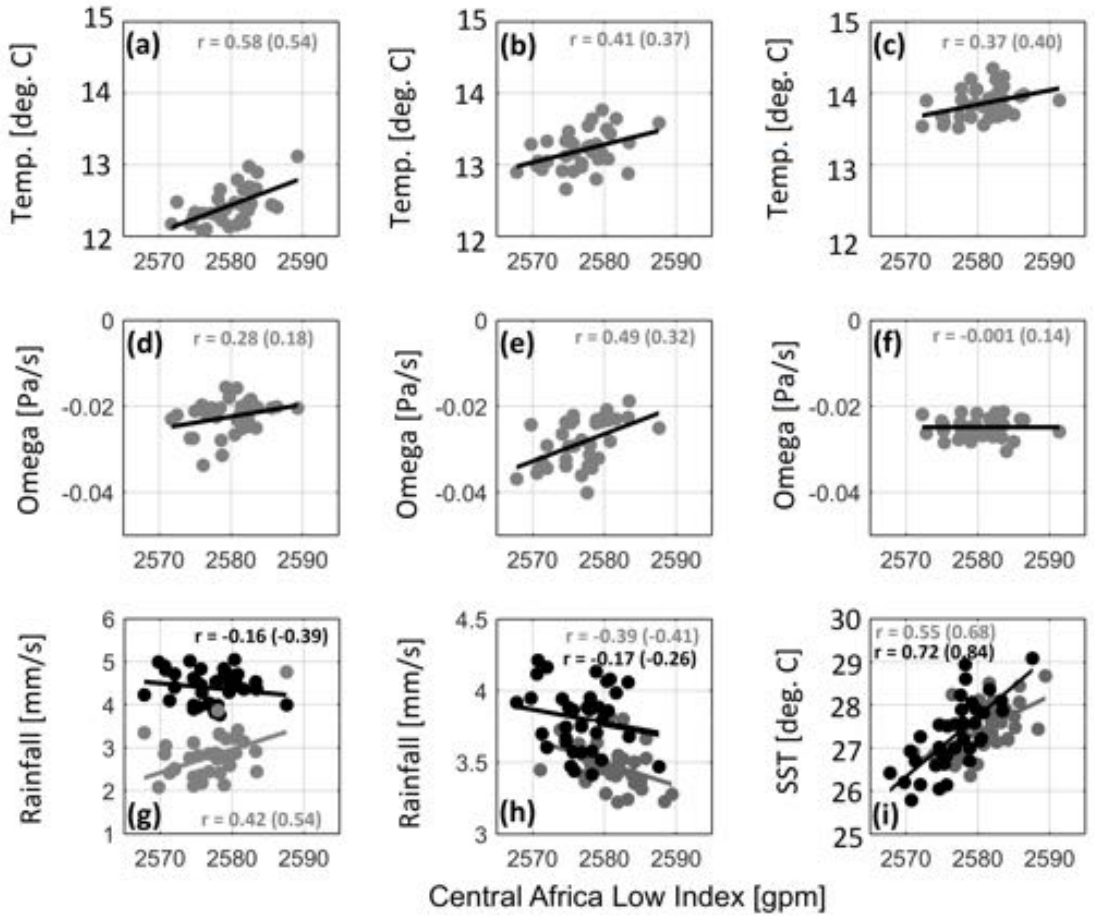

Fig. 4.8. Scatterplot of Central Africa Low index (gpm) vs (a-c) mid-lower tropospheric temperature (^{o}C); (d-f) vertical velocity (Pa/s); (g) eastern Atlantic rainfall (mm/d); (h) central Africa rainfall (mm/d); (i) SST over equatorial central Pacific. In (g), black and gray dots represent Eastern Atlantic and East Africa during October-April season, whereas in (h) and (i) they represent October-April season and annual (all months) – means respectively. The black or gray lines represent the linear trend. For more details see text.

For SST, composite difference between active and passive phases of Central Africa Low denotes a strong La Niña-like condition, with cold SST over tropical Pacific during active phase of Central Africa Low (Fig. 4.6c). Strong correlation is found between ENSO and Central Africa Low indices (r ~ 0.72), suggesting that Central Africa Low variance is primarily controlled by ENSO (Fig. 4.8i). The correlation between Central Africa Low and ENSO is improved to 0.84 while considering detrended normalized anomalies. This finding outlines the similarity of the spatial structure of the Central Africa Low 2580- gpm isoline during both Central Africa Low and ENSO phases (Fig. 4.7d). Except that during El Niño-like conditions over central Pacific, the pattern of the 2580-gpm isoline is relatively smaller than during passive phase of Central Africa Low (Fig. 4.7d). This confirms that the Central Africa Low interannual variability is actually driven by ENSO.

4.5.2. Vertical structure of the vertical velocity, moist static energy and Central Africa Low

Biasutti et al. (2003) suggested that solar heating may be the main driver of Central Africa climate. This indicates the baroclinic nature of the atmosphere over Central Africa. Thus, one can assume that the Central Africa Low is likely to behave more as thermal low than as a tropical low. To test this hypothesis, I merely plot the scatterplot of mid-lower thickness and mid-lower temperature in Fig. 4.8 for Central Africa and its neighbouring regions. Central Africa low is modulated by the mid-lower tropospheric temperature, with some spatial difference – as suggested by their significant correlation ($p<0.005$, Figs. 4.8a-c).

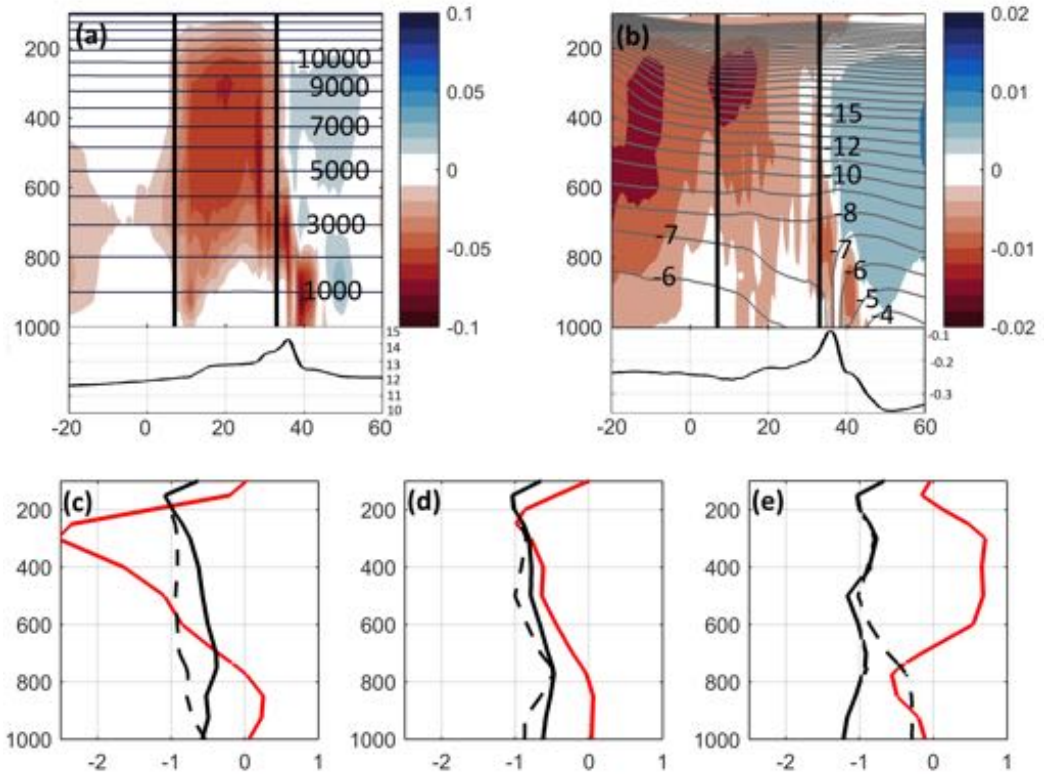

Fig. 4.9. (a) Longitude-height cross section of October – April mean of vertical velocity (shaded, unit: Pa/s) and geopotential height (unit: gpm). (b) Longitude-height cross section of vertical velocity (shaded, unit: Pa/s) and geopotential height anomaly (contours, gpm). Variables are averaged over 5^{o}N-5^{o}S. (c-e) Vertical profile of moist static energy (black solid line, K), saturated moist static energy (dashed solid line, unit: K) and vertical velocity (red solid line, Pa/s) over (c) eastern Atlantic, (b) central Africa and (d) east Africa respectively. The contour interval for the geopotential height is 1000- gpm in (a) and 1- gpm in (b).

But much of Central Africa low variance remains non-explained. In addition, the warm ascent air within the East Africa low is capped by a mid-tropospheric subsidence at ~700- hPa (Figs. 4.9a),

suggestive of thermal low formation (Johnson, 2003). East Africa high rainfall occurs during high value of Congo basin low index (gray dots), while over eastern Atlantic, high rainfall occurs at low values of the Congo basin low (black dots, Fig. 4.8g). In other words, rainfall over East Africa is probably due to moisture advection from surrounding regions than to convection, which is supposed to be suppressed by the subsidence. This is confirmed by the lack of elation between the East Africa low index and the vertical velocity (Fig. 4.8f). Whereas over eastern Atlantic, due to the weakness of the ~~relation~~ correlation (0.28), the influence of the Central Africa Low on eastern Atlantic convection is limited (Fig. 4.8d). On the other hand, the Central Africa low is modulated by both local vertical velocity ($r = 0.49$, $p < 0.001$; Fig. 4.8e) and mid-lower tropospheric temperature ($r=0.41$, $p < 0.001$; Fig. 4.8b). This leads to infer that the Central Africa low could be considered as a combination of tropical and thermal low. However, the Central Africa low is likely a tropical low above 800-hPa, while at low-levels, it behaves as a thermal low (Fig. 4.9a), consistent with Johnson (2003). It is primarily this thermal low nature of the Central Africa low, at low levels, that is conducive to the development of a shallow Congo basin cell.

To understand the thermodynamic processes leading to the rainfall difference over central Africa during active and passive phases of the Central Africa Low, we examine the vertical structure of the atmosphere over Central Africa and its surrounding regions. The moist static energy is used to analyse atmospheric heating and moisture content as it related to the energy content of the atmosphere (Neelin and Held, 1987). The vertical velocity is used as a proxy for ascending motion, indicative of convection. The composite difference in Fig. 4.9 shows that the instability of the atmosphere is favoured by mid-lower warming and low-level water vapour (latent heat). This means that during the active phase, the Central Africa Low is associated with less atmospheric water vapour and lower tropospheric temperature than during the passive phase of the Central Africa Low. This is due to reduced solar insolation due to the cloud bands associated with the strong convection that occurs in the mid-upper levels (Figs. 4.9c-d). The strong convection is more pronounced over east Atlantic (Fig. 4.9c) than over Central Africa (Fig. 4.9d), indicative of rainfall surplus (Fig. 4.7b). Thus, the difference in atmospheric stability condition between eastern Atlantic and Central Africa highlights the crucial role play by land-ocean thermal contrast. Whereas, over East Africa, the anomalous high warming in the boundary layer is associated with unsaturated air, which is likely to uplift (Fig. 4.9e). At mid-upper levels, a strong anomalous subsidence capped the ascending air, preventing it to saturate (Fig. 4.9e). This atmospheric condition leads to anomalous drought conditions over east Africa (Fig. 4.7b). This mechanism outlines the Central Africa Low as one of the key features of central Africa atmospheric circulation.

Finally, it is also crucial to find out how the land-ocean thermal contrast between Central Africa landmass and surrounding Oceans could influence the Central Africa Low. Using the same methodology as in the previous subsection 4.5.1, we compute the normalized surface land-ocean

temperature contrast (ΔT_S) and mid-lower (ΔT) land-ocean thermal contrast. The land-ocean thermal contrast index at surface and at mid-lower troposphere is obtained by subtracting temperature time series of the two selected regions: Central Africa landmass (15°E-30°E; 5°N-5°N) and eastern Atlantic Ocean (5°W-5°E5°N-5°N). I selected years when the detrended land-ocean thermal contrast is greater than 0.5 standard deviation or less than -0.5 standard deviation. Surface land-ocean temperature contrast is positive for 12 years (1980, 1981, 1983, 1987, 1992, 1997, 2005, 2007, 2012, 2013, 2014 and 2015) and is negative for 12 years (1985, 1986, 1994, 1995, 1996, 1998, 1999, 2000, 2001, 2003, 2004, 2008). While the mid-lower land-ocean temperature contrast has 7 positive years (1980, 1982, 1983, 1992, 2012, 2014 and 2015) and 8 negative years (1995, 1996, 1998, 1999, 2000, 2001, 2003 and 2004.

The composite of Central Africa Low 2580- gpm isoline for land-ocean thermal contrast is plotted in Fig. 4.7(a-b). For the surface land-ocean temperature contrast (ΔT_S), the Central Africa Low 2580- gpm isoline envelope extends slightly westward towards Atlantic Ocean during negative phase of ΔT_S and shrinks eastward over Central Africa landmass during positive phase of ΔT_S (Fig. 4.7a). Whereas for the mid-lower land-ocean temperature contrast (ΔT), the Central Africa Low 2580-gpm isoline shrinks eastward toward landmass during negative phase of ΔT, while it remains relatively unchanged during positive phase of ΔT with respect to the climatological mean structure (black contour, Fig. 4.7b). It important to note that the influence of surface land-ocean thermal contrast (Fig. 4.7a) is likely to be opposite to that of the mid-lower land-ocean thermal contrast (Fig. 4.7b). These results suggest that the influence of the land-ocean thermal contrast on Central Africa Low is very sensitive to the vertical profile of temperature over Central Africa landmass and its surroundings Oceans.

4.5.3. Weakening of Central Africa Low

It could be interesting whether, we could address the intensity of the year-to-year change of Central Africa low in the recent decades (1979 to 2015). In the present climate, the Central Africa Low presents a consistent slow weakening, with an average of 1.5 meter of geopotential thickness per decade, with the shape of the positive Central Africa Low trend orientated in a southeast-northwest direction over Central Africa landmass (Fig. 4.11). This weakening of Central Africa Low may be due to the global warming the Central Africa landmass experienced during these recent decades. Also, consistent with the role of the Central Africa Low on regional climate, its weakening is likely to prevent intense rainfall to occur over Central Africa as subsidence is expected to prevail via regulation of latent heat and moisture transport from adjacent Oceans. On the other hand, the weakening of Central Africa Low is likely to enhance rainfall over Sahel and southern Africa and reduce rainfall over East Africa.

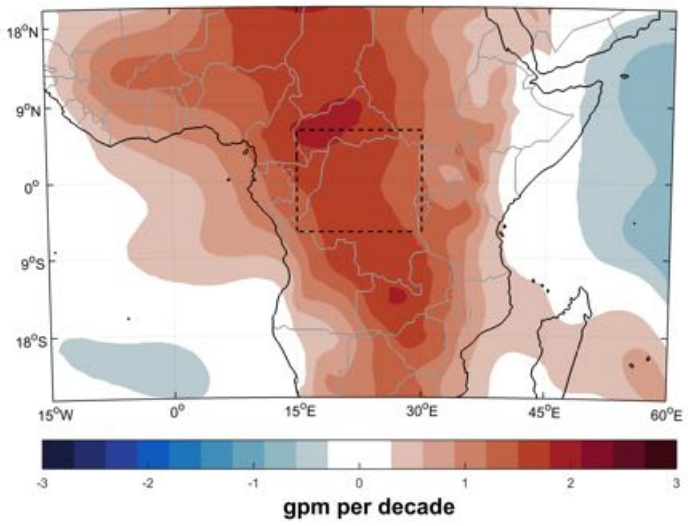

Fig. 4.10. Trend of Central Africa low (gpm per decade). Dashed box delineates the core of Central Africa Low (Congo basin area).

4.6. How does Central Africa Low link to Congo Basin Cell and its associated water vapour transport?

The third objective of this chapter is to determine what is the relationship between the Central Africa low and the Congo Basin Cell, in terms of edges longitudes, width, strength and position. An insight of the behaviour of the water vapour transport over Central Africa is given by the longitudinal position of the edge associated with the Congo Basin Cell. We find that the Central Africa Low regulates the Congo Basin Cell and increased Indian Ocean water vapour transport into Central Africa, with a crucial contribution of ENSO (Fig. 4.10). Indeed, one can readily see that active phase of Central Africa Low is associated with La Niña events (indicated by the colour of data points), while the passive phase of central Africa Low often corresponds to El Niño conditions (Fig. 4.10). As identified earlier, the Central Africa Low is correlated with ENSO. The ENSO index is computed as the 7-month (October–April) mean values of SST for each grid point over the Niño-3.4 region located in the central Pacific (5^{o}S–5^{o}N, 120^{o}–170^{o}W, Fig. 4.6c, black box). All anomalies have been calculated by subtracting the climatological mean value of 1979-2015 October–April from the yearly October–April for each of the 37 years. And finally, we normalize the anomalies by dividing by their respective standard deviation of 1979-2015 October–April period. The Niño-3.4 region is ideally located to capture SST variation associated with Central Africa low events because the amplitude is largest there (Fig. 4.6c).

It is worthy to note that there is a distinct positive asymmetry between the two phases of Central Africa Low, as illustrated by the relationship obtained through the robust fit regression showing a slope and a correlation using samples during both phases (Fig. 4.10). The Congo Basin Cell shrinks and weakens during active phase of Central Africa Low and widens and intensifies during passive phase, with a feedback sensitivity of 0.56° and -0.19° east of longitudes per meter of geopotential thickness respectively (Fig. 4.10c).

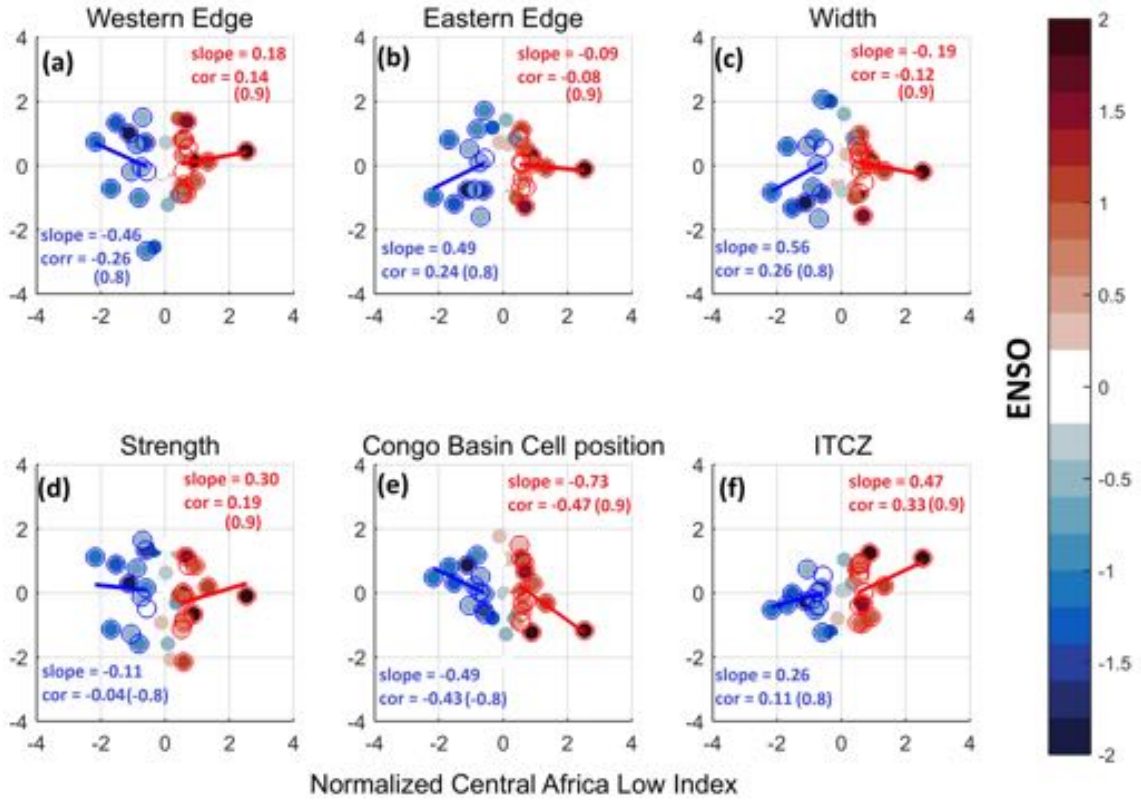

Fig. 4.11. Scatter plot of Central Africa Low index vs. (a) western edge longitude; (b) eastern edge longitudes; (c) width; (d) strength and (e) its related position for the Congo basin cell and (d) zonal ITCZ position. The shading of the dots corresponds to ENSO. All times series have been detrended.

The strengthening of the Congo Basin Cell is around of 0.11Sv per meter of geopotential thickness, and the weakening of ~0.30 Sv per meter of geopotential thickness (Fig. 4.10d). The shrinking of the Congo Basin Cell width is primarily due to the enhanced low-level easterly jet, originating from the Indian Ocean (Fig. 3.10b). In the same time, reduced low-level westerly is confined over the Atlantic offshore regions (Fig. 3.10b), consistent with Pokam et al. (2014). This means that at low-levels, the Indian Ocean is the main supplier of atmospheric water vapour over central Africa landmass during active phase of Central Africa Low. In addition, for any change of 1 meter of

geopotential thickness of the Central Africa Low during its passive phase, the zonal ITCZ and Congo Basin Cell positions will move further east of around 0.47° and -0.73° of longitude than during its active phase respectively (Figs. 4.10e-f). The asymmetry of the impacts of Central Africa Low on Congo Basin Cell and its associated water vapour transport suggests that the Central Africa Low cycle (defined as succession of active and passive phases) as an entity is conducive for large-scale circulation over central Africa, by regulating low-level water vapour transport through the Congo Basin Cell, with ENSO playing an indirect substantial role.

4.7. Summary

The results presented in this chapter highlight the existence of a dominant low-pressure system in the mid-lower (1000-to 500- hPa) troposphere of Central Africa, namely the Central Africa Low, that drives primarily the atmospheric circulation over central Africa. The Central Africa Low is a cyclonic pattern and an atmospheric blocking feature over central Africa. It is well established from October to April. The Central Africa Low is classified as a tropical low, with some thermal low characteristics at low-levels, where the shallow Congo basin cell develops. However, the Central Africa Low is very sensitive to the vertical profile of temperature over Central Africa landmass and its surrounding Oceans so that different impacts are found at the surface and at mid-lower level of the troposphere. In addition, a small distinct heat low is observed over East Africa, while over southern Africa, the Angola Low and Mozambique channel Low are also dominant in December and January. The Central Africa Low is correlated with the El Nino Southern Oscillation (ENSO). However, the Central low variability, it is weakly connected to local rainfall variability. This seems to disprove the idea that enhanced central Africa rainfall is caused by more intense low-pressure system. This contradiction is due primarily to the blocking nature of the Central Africa low, which weakens further any advection of water vapour and reduces the interannual rainfall variability at its core. This results to no substantial year-to-year change of rainfall over Central Africa, despite high rainfall rate in this region. In other words, the Central Africa low is characterized by strong convective activity due to unstable atmosphere over Central Africa, which lead to high rainfall representing around 70% of total rainfall over central Africa, while associated with less rainfall interannual variability. Furthermore, Central Africa Low has a differential impact on local regional rainfall, with rainfall surplus over West Africa, Sahel and Southern Africa and rainfall deficit over East Africa. This influence of the Central Africa Low is owed through the regulation of mid-lower tropospheric heating and atmospheric water vapour transport. In addition, the Central Africa Low might play a crucial role to govern the Congo basin cell intensity and extension, and so to influence the low-level moisture transport. In recent decades, the Central Africa Low is found to weaken, which favoured enhanced rainfall over eastern Atlantic and southern Africa and reduced rainfall over East Africa. This suggests that the Central Africa Low is a key feature of tropical atmospheric system.

Chap. 5

Role of African Easterly Jet on water budget over Central Africa

5.1. Introduction

Nicholson and Grist (2003) showed the existence of AEJ and TEJ in mid- (i.e. ~600- hPa) and upper (200- hPa) troposphere over central Africa respectively. In addition, the seasonal cycle AEJ over central Africa is dominated either by the northern component of AEJ (AEJ-N) and/or by the southern component (AEJ-S) (Nicholson and Grist, 2003). They also speculated that the AEJ forms due to the meridional reversal of surface temperature gradient. Pokam et al. (2014) argued that AEJs over Central Africa drive the seasonal spatial pattern of moisture flux over central Africa. Rather than to provide a survey of the mean conditions of AEJs over central Africa, we study the physical mechanisms leading to understand the atmospheric phenomena explaining water vapour transport variability over central Africa. Using ERA-Interim reanalysis data, the primary objectives of this chapter are (i) to give an overview of the structure and seasonality of the AEJ over central Africa and what do maintain it; (ii) to document water vapour transport over central Africa and finally, (iii) to provide information on what do control the water budget variation over central Africa.

5.2. Datasets

We obtained winds, geopotential height, temperature, vertical velocity and specific humidity from the European Centre for Medium-Range Weather Forecasts (ECMWF) ERA-Interim reanalysis (Dee et al., 2011), used here for 1979-2015 period and taken at 13 pressure levels (1000, 925,

850, 775, 700, 750, 700, 600, 500, 400, 300, 200, 100) at monthly mean resolution. Rainfall is an average of the satellite/rain-gauge estimates of the Global Precipitation Climatology Project (GPCP) monthly precipitation data set (Adler et al., 2003) and Climate Prediction Center Merged Analysis of Precipitation (CMAP, Xie and Arkin, 1997). We interpolate the satellite data sets to 0.75 × 0.75° grids from 1979 to 2015. Finally, all these variables were used to compute the moist static energy (Neelin and Held, 1987). For the sea surface temperature (SST) the global monthly the NOAA optimum interpolated (OI) SST version 2.2 (Reynolds et al., 2002) and Extended Reconstructed Sea Surface Temperature (ERSST, Smith et al. 2008) are used.

5.3. Annual cycle and maintenance of the AEJs over Central Africa

5.3.1. Annual cycle of AEJs over Central Africa

The overview of the annual cycle of vertical profile of zonal and meridional wind components, specific humidity, vertical velocity (ω) and moist static energy area-averaged over Central Africa, eastern Atlantic and East Africa respectively is shown in Fig. 5.1. To highlight the seasonality of all atmospheric variables, the annual cycle is repeated twice. For additional characteristics of the zonal wind component over Central Africa and its surrounding regions, we also plot the annual cycle of wind at 850-, 750-, 700- and 600- hPa respectively.

Over eastern Atlantic and central Africa, the low-level south-westerly air is moister and higher in energy content than aloft (Fig. 5.1). This south-westerly flow is associated with a more stable atmosphere in boundary layer (below 850- hPa), as suggested by $\omega \approx 0$, with relatively weaker speed (< 2 ms^{-1}) throughout the year (Fig. 5.1). But in the south-eastern part of Central Africa (i.e. over Katanga and Zambia), the zonal wind component may surge, from April to November, and could reach a maximum of ~ -10m/s in September (Fig. 5.2a). At the same time, aloft at around 750- hPa, over West Africa and Sahel, a strong easterly wind (> -10 m/s) is observed year around, with an extended tail over Central Africa in October to December (Fig. 5.2b). Notably, from April to November, when the core of this easterly wind over West Africa is confined far away of Central Africa, one can notice a relative strong easterly wind, with a maximum of ~ -6 m/s, located at the south of the equator, between 5°S and 10°S (Fig. 5.2c). This southern branch of this relative strong easterly (AEJ-S) matures in September-October-November (SON, Fig. 5.2b). At 700- and 600-hPa pressure levels, the atmospheric circulation over tropical Africa is barotropic with the core of the northern branch of the easterly wind located over Central Africa (between 5°N and 10°N) from October to April when the Central Africa Low is dominant, with a maximum greater or equal than -10 m/s (Fig. 5.2c-d). This northern branch of AEJ (AEJ-N) spans from the eastern Atlantic to the east boundary of Central Africa (Figs. 5.2c-d). In addition, weakened south-easterly over Central Africa in mid-lower troposphere is associated with strong ascending motion, indicative of deep convection (5.1k). This leads to high rainfall over the southern Hemisphere (Fig. 5.2e).

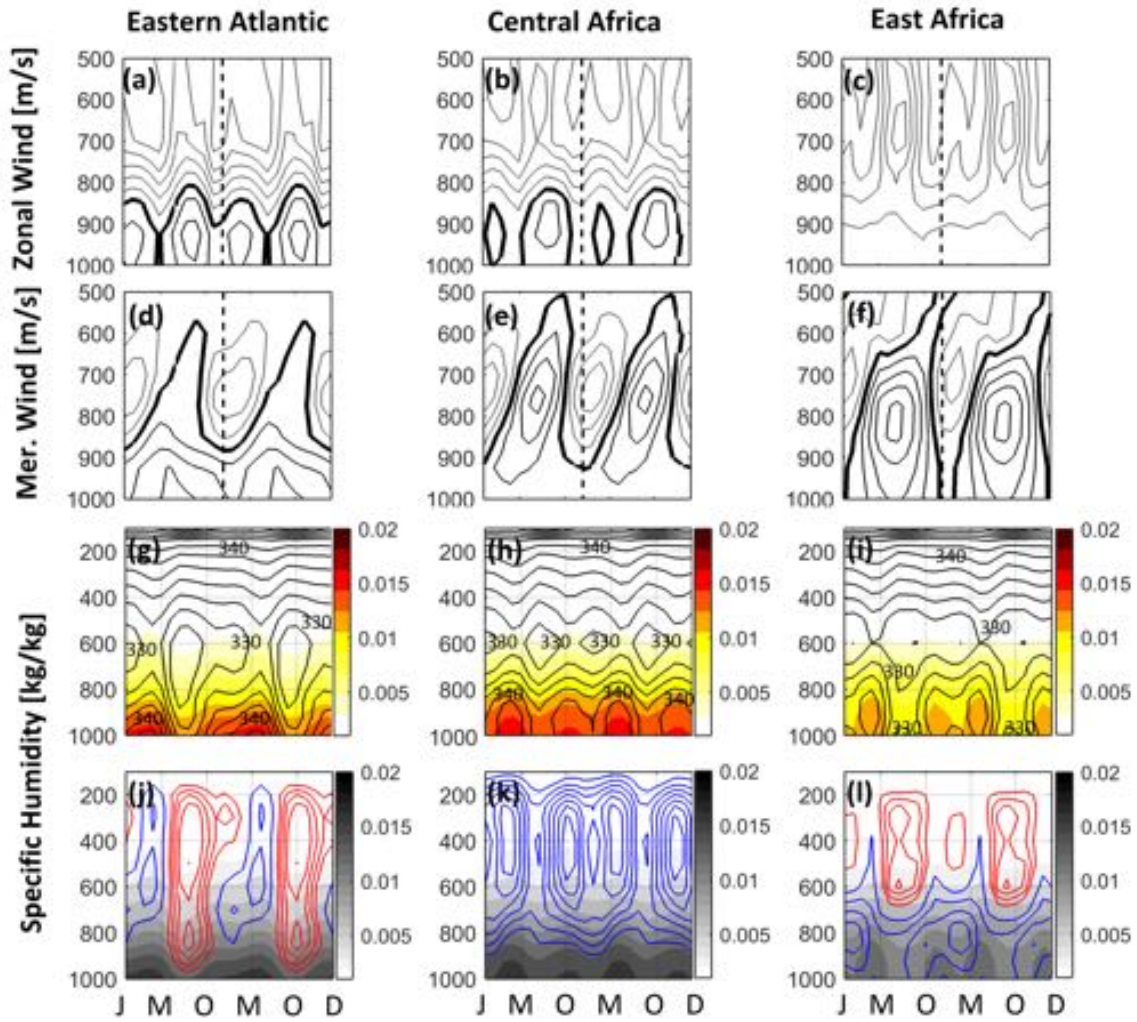

Fig. 5.1. Annual cycle of the vertical profile of zonal wind (a-c, m/s), meridional wind (d-f, m/s); specific humidity (g-l, shading, kg/kg), moist static energy (g-l, contours, K) and vertical velocity (j-l, blue and red contours indicate negative and positive values respectively, Pa/s) averaged between 5^{o}S and 5^{o}N over central Africa (15^{o}–30^{o}E) and its adjacent regions: eastern Atlantic (0^{o}–15^{o}E) and East Africa (30^{o}–40^{o}E). The annual cycle is repeated twice to highlight the seasonality of all the atmospheric variables. Dashed vertical black line defined January month and bold black line in represent the 0 m/s, with the contour interval of 1m/s, with black and gray lines represent positive and negative value. For moist static energy, the contour interval is 2.5K (bottom panel). All variables are from ERA-Interim.

The change of direction of the meridional wind component is consistent with the annual cycle of Central Africa Low (see Figs. 5.2c-e). From May to September (MJJAS), the surge of subsidence over Central Africa is associated with the jump of the Central Africa Low 2580-gpm isoline from Central Africa landmass to Arabia sea (red contour, Fig. 5.2e). This atmospheric condition reverses the meridional circulation at mid-lower troposphere over Central Africa and reinforces the AEJ-S, which in turn, is associated with less rainfall in the southern Hemisphere (Fig. 5.2e). At the same time, the northward retreat of the core of AEJ-N out of Central Africa widens and strengthens over West Africa and Sahel, with a maximum of more than -15 m/s (Figs. 5.2c-d). It is during this season (MJJAS) that the AEJ-N is widely studied by many authors (Cook, 1998; Thorncroft, 2011) to understand its influence over West Africa and Sahel climate. More interesting, at 700- hPa, while the AEJ-N is moving out of Central Africa, the AEJ-S is reinforced from April to October, with a maximum of -6 m/s (Fig. 5.2c), while at 600- hPa, the AEJ-S is only observed in August to December (Fig. 5.2d). But between 1000- and 500- hPa, the maximum of the easterly jet over central Africa coincides with the minimum of the moist static energy at ~600- hPa (Figs. 5.1h & 5.2d), while the meridional component has its maximum between 750- and 700- hPa (Fig. 5.1e). However, the AEJ-S shows a strong seasonal variability in intensity and structure.

Different from central Africa, where deep convection occurred all year around (Fig. 5.1k), the Eastern Atlantic is characterized by the change of meridional wind component, which is associated with strong subsidence (Fig. 5.1j). Whereas East Africa is characterized by south-easterly wind in the mid-lower troposphere, year-round, except from January to March, when the wind is predominantly north-easterly between 800- and 600- hPa (Figs. 5.1c;f). Convection occurs in the mid-lower atmosphere and its capped by subsidence at ~600- hPa, indicative of thermal low (Johnson, 2003, chapter 4). Throughout all the tropospheric column over East Africa, the easterly flow is predominant year-round (Fig. 5.1c). In addition, the energy content of air over East Africa is higher than over eastern Atlantic and Central Africa due to strong tropospheric heating and less latent heat (Fig. 5.1h). Above 600- hPa, the wind flow is south-easterly all the year around over East Africa (Fig. 5.1i). The meridional wind component does change direction particularly in December to February, with its maximum migrating between 750- hPa in June and 600- hPa in February respectively (Fig. 5.1f), while the zonal wind component does not change direction (Fig. 5.1c). Over eastern Atlantic and Central Africa, it appears that at the midlevel (750- and 600- hPa), where the speed is maximum, the principal contributor to the jet is the zonal component of wind (Fig. 5.1). While over East Africa, the meridional wind component is identified as the leading contributor (Fig. 5.1). We also represent the time series of the cores of both AEJ branches in Fig. 5.3. We found out that both AEJ branches show strong seasonality and variability, with large speed difference at different pressure levels, suggesting a relatively strong wind shear (Fig. 5.2a-d).

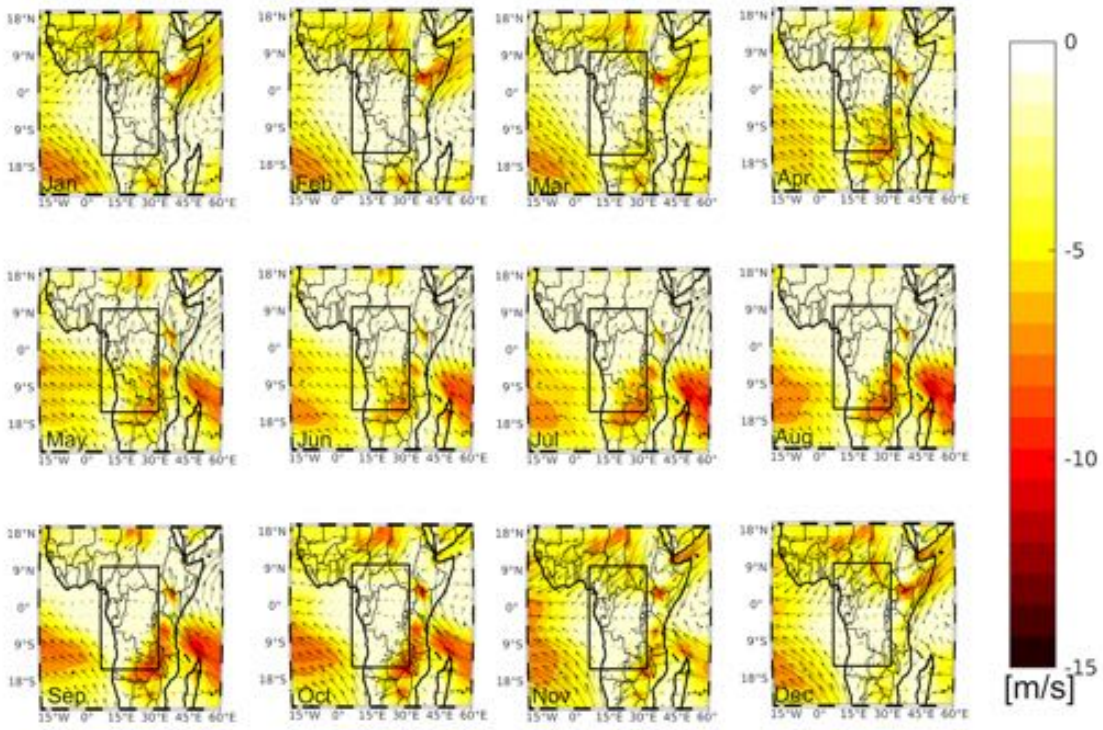

Fig 5.2a. Annual cycle of the horizontal wind (arrows) over Central Africa at 850- hPa in ERA-Interim. To outline the strength of the easterly jet, the zonal component of the horizontal wind is shaded [m/s].

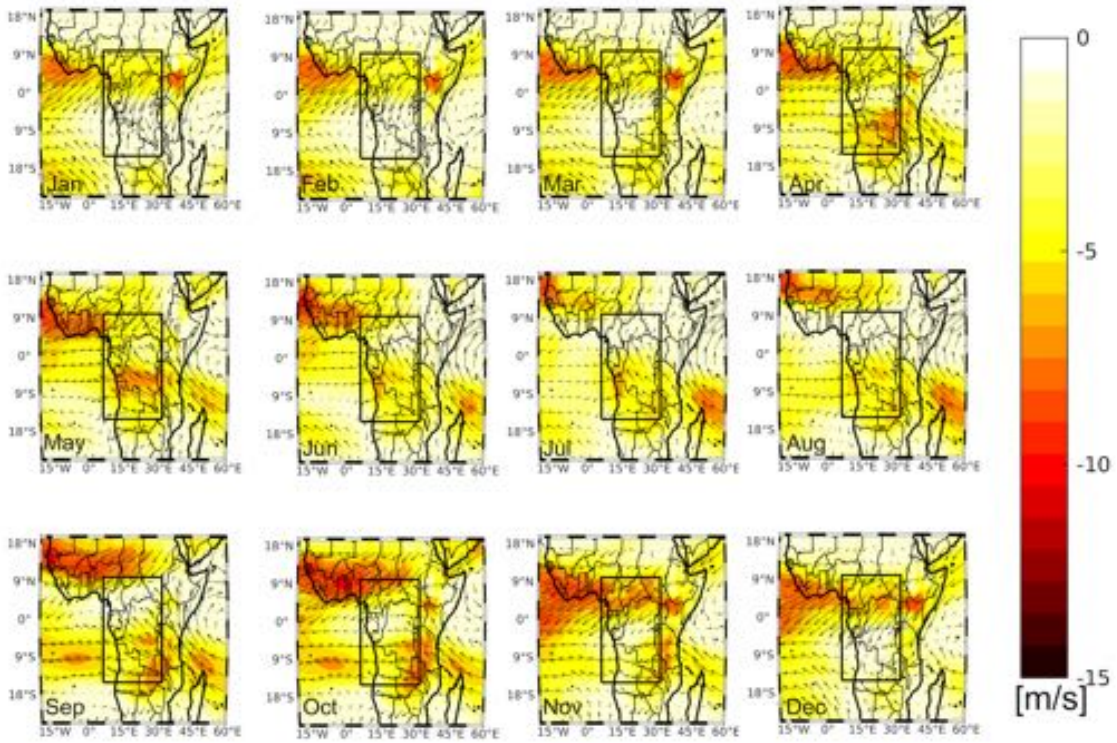

Fig 5.2b. As for (a) but at 750- hPa

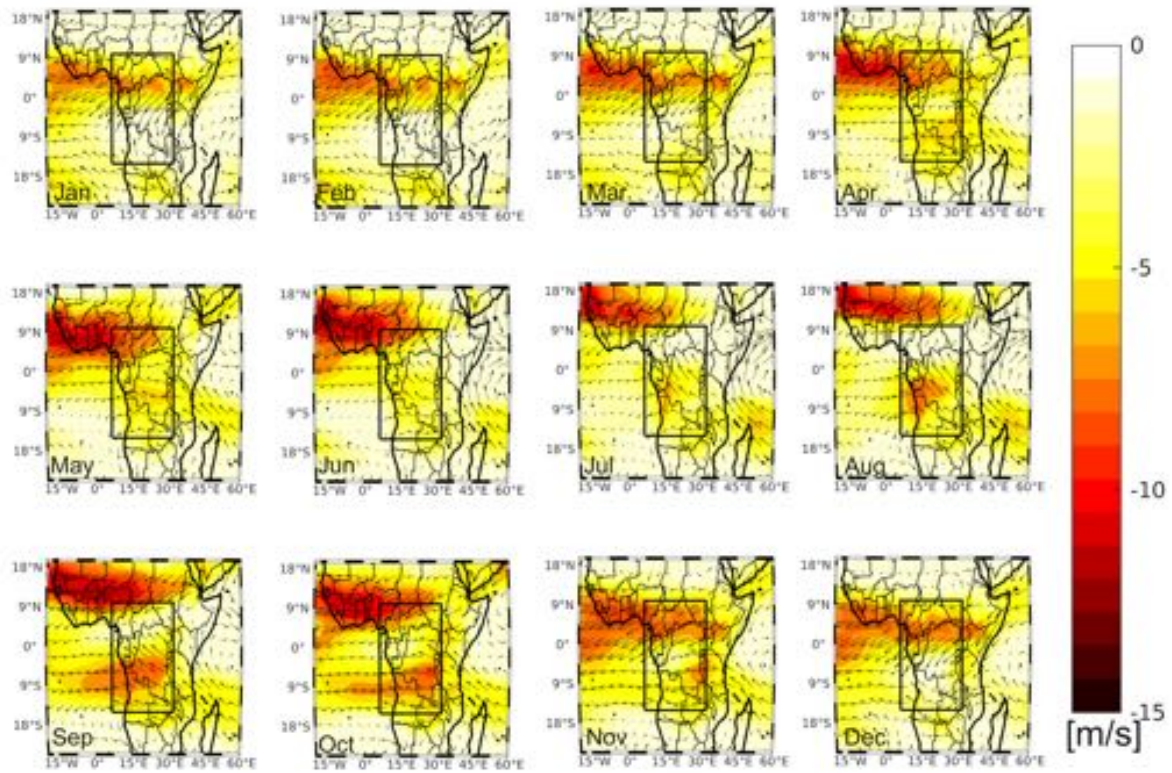

Fig 5.2c. As for (a) but at 700- hPa

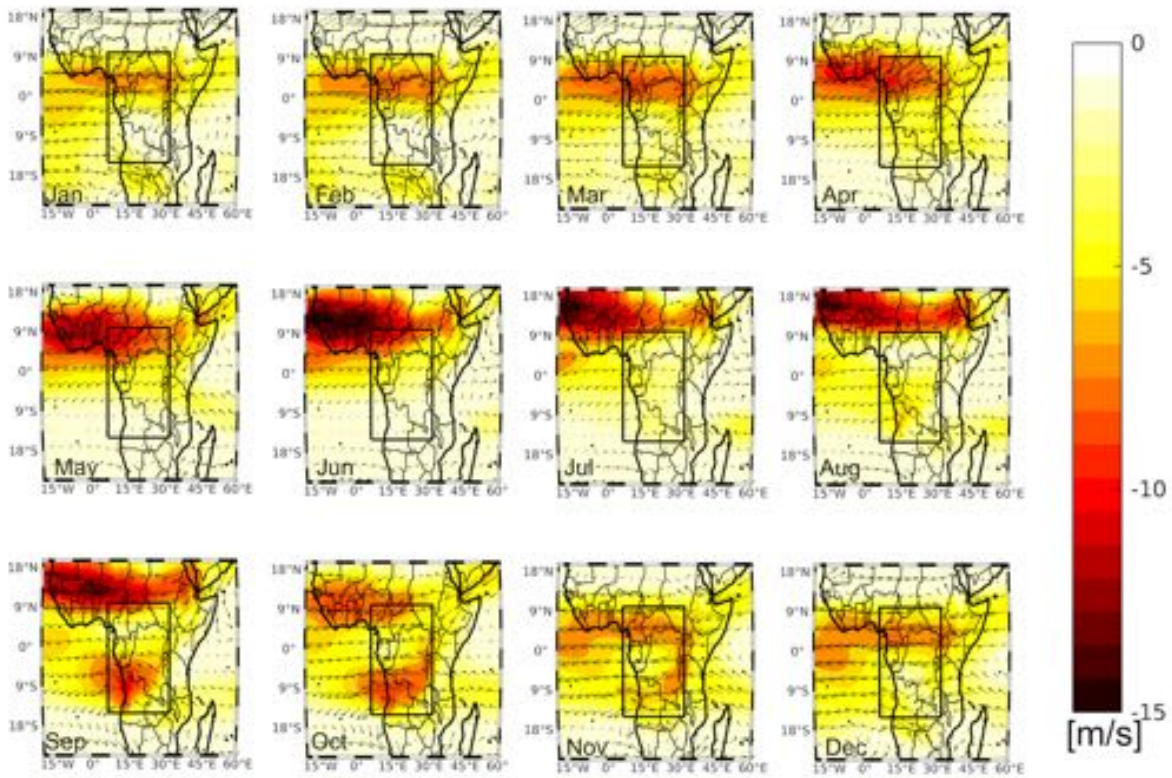

Fig 5.2d. As for (a) but at 600- hPa

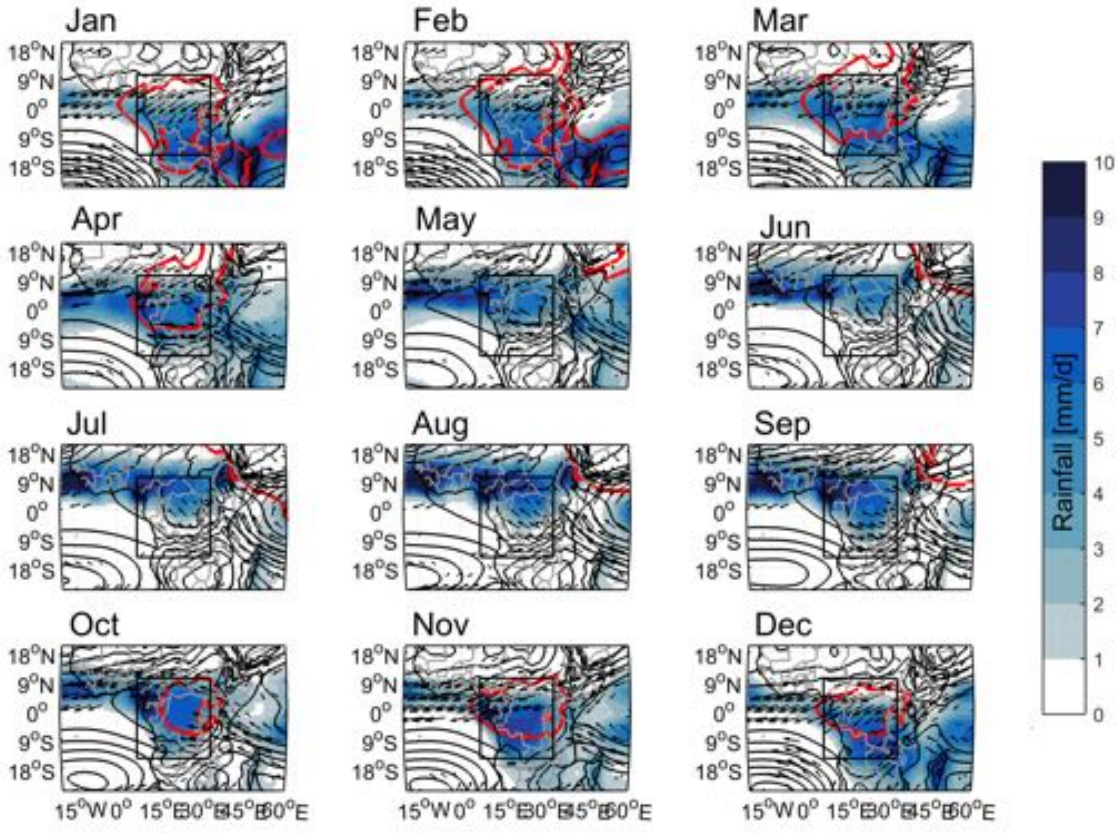

Fig 5.2e. As for (a), but for the Central Africa Low, horizontal wind at mid-lower (vertically average between 850 and 600- hPa, arrows, m/s) and rainfall (shading, mm/d). The wind speed that is less than 1m/s is not represented. The red contour indicates the 2580gpm isoline. All variables are from ERA-Interim.

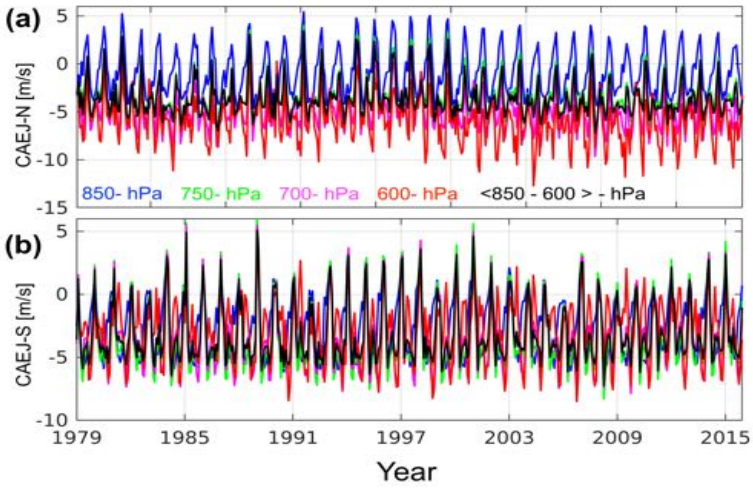

Fig. 5.3. Times series of both (a) AEJ-N and (b) AEJ-S in ERA-Interim.

The seasonal cycle of AEJ over Central Africa reveals two branches, with their strength being influence alternatively by Central Africa Low and/or its subsidence (Figs. 5.2a-e). These findings

indicate that the Central Africa Low is the primarily driver of AEJ over Central Africa, which in turn, could affect Central Africa rainfall. Indeed, over Central Africa, the AEJ-N may trigger deep convection through an upward motion in the mid-lower troposphere (from 900- to 500- hPa, Fig. 5.1e) and to more rainfall over West Africa, Sahel and in the northern Hemisphere (Figs. 5.1k, 5.2a-e, Cook, 1998; Nicholson and Grist, 2003; Thorncroft et al. 2011) and less rainfall in the southern Hemisphere (Fig. 2e). Meanwhile the reinforcement of AEJ-S could lead to the opposite (Figs. 2a-e). Nevertheless, the quasi-permanent position of both cores of AEJ over Central Africa is consistent with Nicholson and Grist (2003) and as such could be easily referred as "Central" African easterly jet (CAEJ).

5.3.2. Maintenance of AEJ over Central Africa

In this section, we would like to unravel how and why the momentum balance does change seasonally over Central Africa. The important question to answer could also be, what do regional forces cause simultaneously opposite behaviour of the northern and southern branches of the AEJs over Central Africa, suggesting that when the northern branch of AEJ enhances, the southern branch of AEJ should weaken or vice versa.

The *u*- and *v*- momentum equations are as followed:

$$\frac{du}{dx} = +fv - \partial_x \Phi + F_x \qquad (5.1)$$

$$\frac{dv}{dx} = -fu - \partial_y \Phi + F_y \qquad (5.2)$$

with *u*, *v*, the mid-lower zonal and meridional wind components; *f*, the Coriolis force; Φ, the mid-lower thickness and F_x and F_y represent the fictional terms. To consider any vertical migration of Central Africa easterly jet, the zonal and meridional wind have been averaged between 850- and 500- hPa, while the geopotential height is vertically averaged between 1000 and 500- hPa.

During both seasons (October – April and May – September), the primary balance over Central Africa occurs between wind tendency (Figs. 5.4a,e) and frictional term (Figs. 5.4d,h). While over East Africa and Horn of Africa, the balance occurred between the geopotential thickness gradient term ($\partial\Phi$, Figs. 5.4c,g) and frictional term (F). The Coriolis term is much weaker and so, could be neglected (Figs. 5.4b,f). The wind tendency is mainly positive, with zonal extension in both seasons (Figs. 5.5a-b), suggesting deceleration of each branch of the central African easterly jet due primarily to the frictional term (Figs. 5.4d,h). This frictional term is conducive to strong vertical wind shear, which is longitudinal elongated in each season. Nevertheless, the maximum of deceleration

is meridionally symmetrical to the equator accordingly to the season, and so, highlighting the northern and southern branches of central Africa easterly jets.

The seasonal transition (difference between these seasons) of wind tendency features an opposite spatial pattern, which underscores two zonal streams areas of opposite acceleration (Fig. 5.4i). The slowing down of the northern branch of AEJ, confined between the equator and 10°N, and extended along west Africa from 20°W to 30°E (Fig. 5.4i), is associated with a maximum acceleration of ~0.5 ms^{-2} at 15°-20°E; 5°-10°N. This leads to more rainfall north of the equator. On the other hand, the acceleration of the southern branch of AEJ, spanning from western Indian to eastern Atlantic, with a maximum of about 1 ms^{-2} located at 20°-30°E; 5°-12°S (Fig. 5.4i), is associated with rainfall deficit.

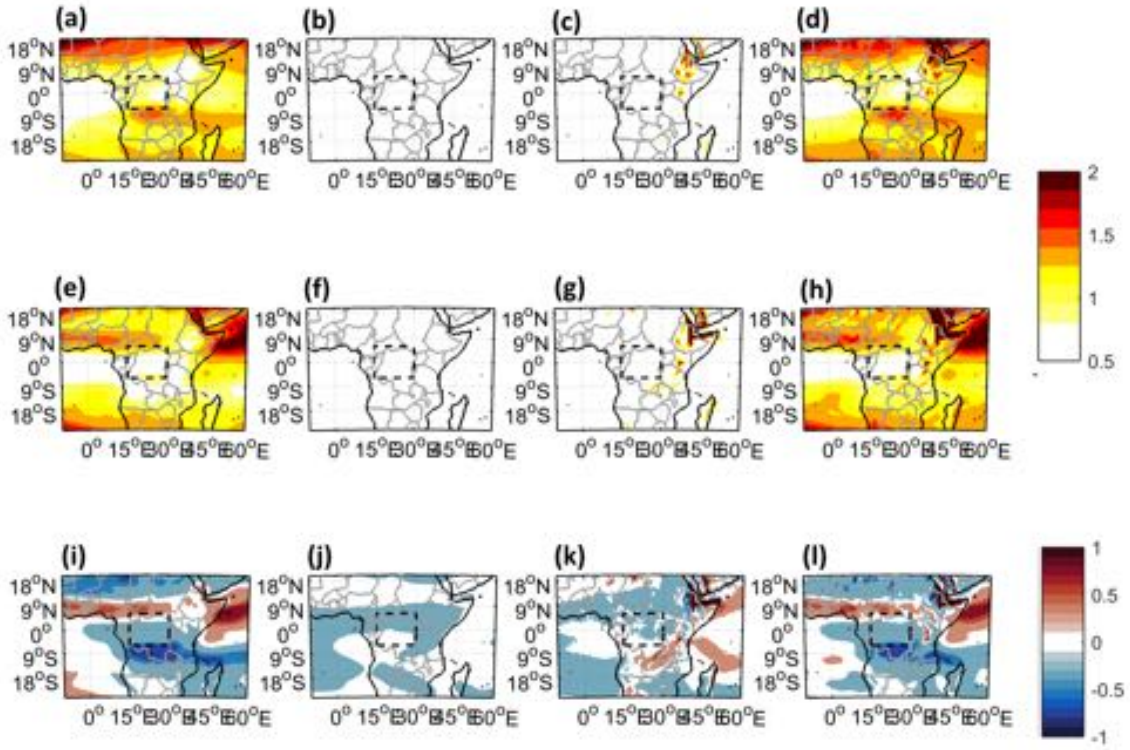

Fig. 5.4. (a,e,i) wind tendency (m/s^2); (b,f,j) Coriolis term (m/s^2); (c,g,k) thickness gradient ($\partial\Phi$,m/s^2)) and (d,h,l) Friction term (m/s^2) respectively. (top) October-April season, (middle) May-September (bottom) May-September minus October-April. Dashed black box highlights the Congo basin area (15°-30°E; 5°S-5°N). All variables are from ERA-Interim.

These results outline the key role of vertical wind shear to enhance local rainfall by invigorating convection through the reduction of intensity of the southern or northern branch of central African

easterly jets. Finally, the mid-lower geopotential thickness gradient term ($\partial\Phi$) shows a meridional extension orientated in the direction south-west (centered in Katanga region, DRC) and north-east (centered at Arabia sea) (Fig. 5.4c,g). This is suggestive of orographic influence not only to drive and maintain the African easterly jet over east Africa, but also to favour convective rainfall over Ethiopia (Fig 5.3e).

5.4. Water vapour transports over Central Africa

5.4.1. Vertical profile of water vapour transport into Central Africa

Before assessing water vapour transports intensity and preferential channels into Central Africa, it is necessary to break down the specific humidity flux into two parts, i.e, the mean state (i.e. climatology) and the induced Central Africa low perturbation (anomalies) to explore their respective contribution (Peixoto and Oort, 1992):

$$\overline{qu} = \overline{q}\,\overline{u} + \overline{q'}\,\overline{u'} \qquad (5.3)$$

with *u,* the zonal component of the horizontal wind; *q* the specific humidity. The overbar represents the climatological mean state of the variable, and the prime represents Central Africa low anomaly to the mean state (i.e., the perturbation).

We would like to focus on the vertical profile of the zonal moisture transport to find out at which pressure level, the water vapour is transported into or out Central Africa (and its neighbouring regions). It is readily seen in Fig. 5.5. that the greatest contribution in the zonal specific humidity transport into Central Africa and its neighbouring regions comes from $\overline{q}\,\overline{u}$, suggestive of dominant climatological moisture advection by climatological wind. The specific humidity transport is higher in October – April season than in May – September season, with maximum at midlevels (i.e. between 800- and 600- hPa), where mid-lower easterly jets are dominant in both seasons. However, at low-levels, the eastward specific humidity transport appears over Central Africa only in May to September, meaning that the weakening of Central Africa low is likely to strengthen the low-level westerlies.

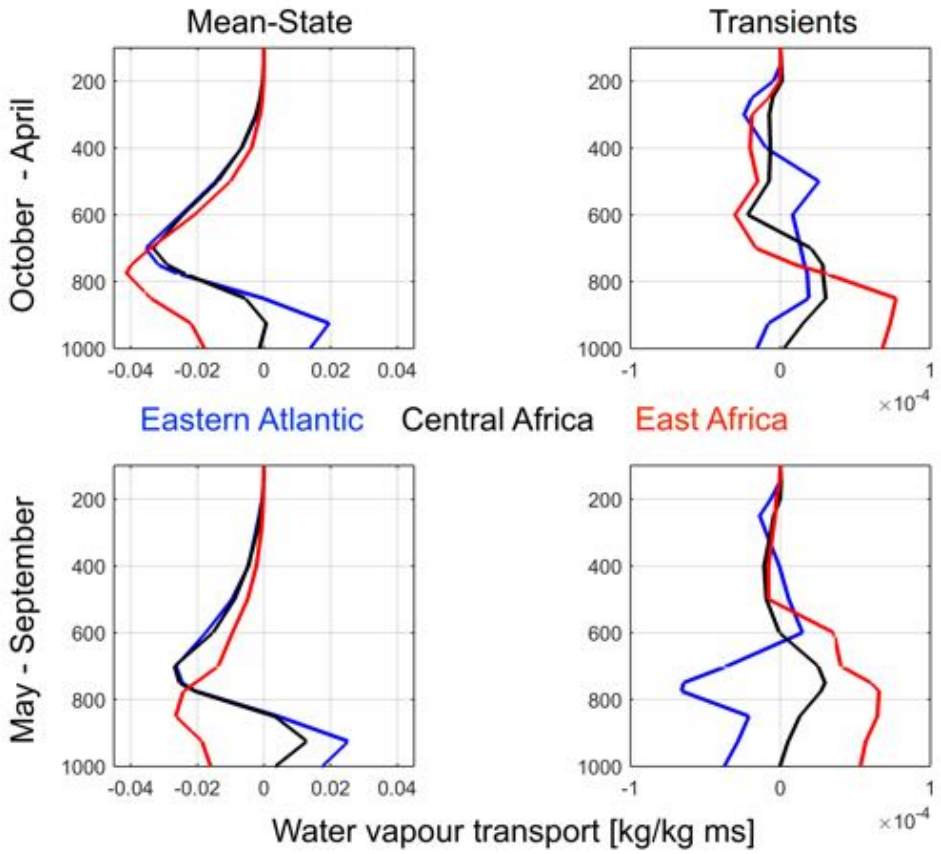

Fig. 5.5. ERA-Interim vertical structure of the two-specific humidity transport perturbation terms (kg/kg ms) from Eq. (5.3) (top) October to April and (bottom) May to September seasons. (left) the $\bar{q}\,\bar{u}$ term (climatological moisture advected by climatological wind); (right) the$q'u'$ term (anomalous moisture advected by the anomalous wind) over eastern Atlantic (5°-15°E; 5°S-5°N, blue line); Central Africa (15°-30°E; 5°S-5°N, black line) and East Africa (30°-40°E; 5°S-5°N, red line).

5.4.2. Water vapour transports channels and their intensities over central Africa

To find out what are the main channels of moisture transport over Central Africa (black box, in Fig. 5.6), the vertically integrated water vapour transport, throughout all the tropospheric column (surface to 100- hPa) and at low-levels (surface to 850- hPa) is shown in Fig. 5.6. To understand any potential role the Central African low might play to influence the progression of water vapour transport, an insight of the inflows and outflows of water vapour over Congo basin (red box, in Fig. 5.5) are also plotted. The vertically integrated moisture transport (flux, *Q*) is computed as in Trenberth et al. (2005):

$$Q_u = - < qu > \qquad (5.4)$$

$$Q_v = - < qv > \qquad (5.5)$$

with *u* and *v*, the zonal and meridional component of the horizontal wind; *q* the specific humidity; and the angle bracket < > is the mass-weighted vertically integration.

In October to April, owed by the presence of Central Africa low, the spatial pattern of water vapour transport into Central Africa is carried by the AEJs (Fig. 5.6g). The visual analysis of water vapour transports over central Africa lead us to determine three incoming channels: the southern, eastern and northern boundaries and one export channel: the western boundary (Fig. 5.6g). The characteristic of moisture transports over central Africa demonstrates two dominant channels at the eastern (4003.5±391.0 kg m^{-1} s^{-1}) and northern (3018.0±368.1 kg m^{-1} s^{-1}) boundaries, and a weaker incoming channel (112.7±16.2 kg m^{-1} s^{-1}) at the southern boundary (Fig. 5.6j).

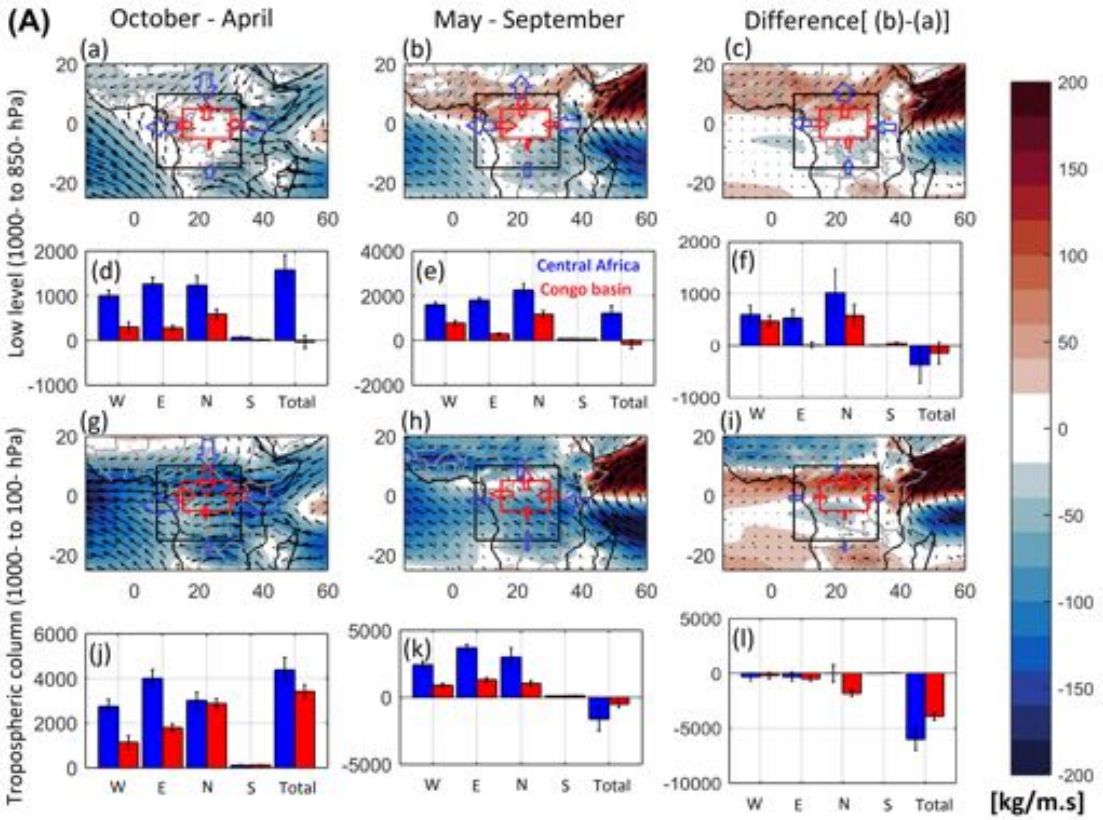

Fig 5.6. (A) ERA-Interim vertically integrated water vapour transport throughout all the tropospheric column (surface to 100- hPa, arrows, (a-c) and the intensities of each moisture transport channel at each boundary of Central Africa and Congo basin (d-f, blue and red bars)) and at low-levels (surface to 850- hPa, arrows (g-i) and the intensities of each moisture transport channel at each boundary of Central Africa and Congo basin bars (j-l, blue bars)). In each panel, the zonal water vapour transport is overlaid (shading, kg/ms).

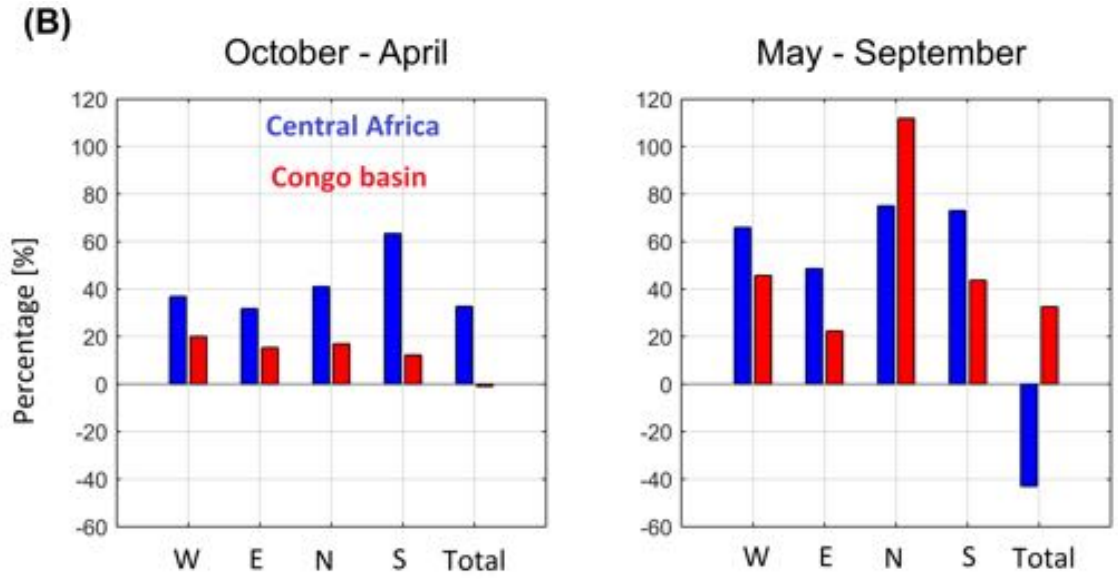

Fig. 5.6. (B) Contribution of the low-level water vapour transport to the total (tropospheric) water vapour transport for each channel for Central Africa (blue bars) and Congo basin (red bars) for (left panel) October to April and (right panel) May to September seasons.

The export channel, with moisture flux intensity of 2745.9±316.6 kg m^{-1} s^{-1}, is of the same range of magnitude as the northern channel (Fig. 5.6j). By comparison, the intensity of the southern water vapour transport channel is much weaker than the three remaining moisture fluxes channels, suggesting its minimal contribution to the moisture flux balance over Central Africa, and it can therefore be neglected (Figs. 5.6d; j). Over Congo basin region (red box), there are two incoming channels at its northern and eastern boundaries and two outcoming channels at its western and southern boundaries. However, while moving to the western boundary of central Africa (7°E), the outcoming moisture flux from Congo basin is strengthened by the south Atlantic anticyclone (Fig. 5.6g). At the same time, the incoming moisture flux in the eastern channel of central Africa decreases while reaching the Congo basin. This reduced moisture flux at the eastern channel of Congo basin is probably due to deep convection associated with Central Africa low, which convert moisture flux into rainfall (Fig. 5.6j). The intensity of the northern channel is almost the same when its reach the Congo basin (Fig. 5.6j).

The water vapour transport has a quasi-barotropic structure, as shown at low-levels (Figs. 5.6a; d). In general, the low-level water vapour transport channels are similar to those outlined above, throughout all the central Africa tropospheric column (Figs. 5.6g; i). The westerly moisture content air advected from the eastern Atlantic seems to be confined over the offshore region of central Africa (between 7° and 15°E), so that the intensity of the incoming moisture flow over Congo basin is 295.1±114.1 kg m^{-1} s^{-1}. Albeit high water vapour associated with Congo basin rainforest, the weakness of this inflow in the western channel of Congo basin region is due to the presence of the Central Africa low, which seems

to reduce further the low-level westerly over Central Africa landmass (Fig. 5.6a). Overall, the Congo basin region has three inflow moisture transport channels and one outgoing moisture transport channel located in its northern boundary. This latter channel is dominant, with an outflow water vapour intensity of about 589.0±107.2 kg m^{-1} s^{-1}, representing the intensity of all incoming water vapour fluxes combined (Fig. 5.5d). The strong northerlies flow crossing the northern boundary of Central Africa at 10^{o}N blocked water vapour to flow out of the Congo basin at 5^{o}N (Fig. 5.6a) and, enhance moisture flux convergence in this region, leading to relatively low rainfall (Fig. 5.2e). A substantial reduction of the intensity of easterly water vapour transport at the eastern channel of Congo basin (30^{o}E, Fig. 5.6a; d) may be attributable to the conversion of moisture flux into rainfall as moist air is lifted up over the Rift valley highlands. The water vapour flux through the southern channel decrease further as it approaches the core of Congo basin low, as suggested by the weakness of low-level wind (Figs. 5.5a; d). However, the magnitude of each of these low-level components of moisture transports are low and their contribution to their respective tropospheric water vapour transport channel ranges between 12.2% for the southern channel to 20% for the western channel for Congo basin region (Fig. 5.6B. left panel, red bars). Whereas over the central Africa region, the contribution of low-level water vapour transport ranges between 31.7% for the eastern to 63.4% for the southern channels (Fig. 5.6B, left panel). This finding suggests a crucial contribution of the mid-lower easterly jet to total (tropospheric) water vapour transport into Central Africa. The total moisture transport (4388.4±556.4 kg m^{-1} s^{-1}) shows that Central Africa is a sink of water vapour, originating predominantly from the Indian Ocean (Figs. 5.6g; j). The reduction in total water vapour flux values of about 22% over Congo basin (Fig. 5.6j) is indicative of increased rainfall over this region (Fig. 5.6d). At low-levels, despite Central Africa being a sinking region of water vapour, the Congo basin seems to be a small source of water vapour due probably to the weakness of the components of horizontal wind over the Congo basin rainforest, owed by the quasi-permanent presence of Central Africa Low. This suggests that the water vapour provides by Congo basin rainforest play a local role via recirculation (Pokam et al. 2012). Overall, this suggest that, in October to April, the main supplier of moisture over central Africa domain appear to be the Indian Ocean, owed by AEJs, particularly, the eastern water vapour transport channel (Figs. 5.5a; Fig. 5.6g).

In May – September, the weakening of Central Africa Low – associated with the jump of the 2580- gpm isoline over Arabia sea – reverses the water vapour flow of the northern water vapour transport channel over Central Africa (Figs. 5.6b; h). Hence, Central Africa has two incoming channels, the eastern channel (3703.8±252.6 kg m^{-1} s^{-1}) and the southern channel (100.6±7.1 kg m^{-1} s^{-1}) and two outgoing channels, the northern (2996±694.2 kg m^{-1} s^{-1}) channel and the western channel (2426.0±287.9 kg m^{-1} s^{-1}) (Fig. 5.6h). The weakening of Central Africa Low, associated with the jump of the 2580 gpm isoline towards Arabia Sea, strengthens the moisture flux from surrounding Oceans at low-levels (Fig. 5.5e). The advected water vapour from Atlantic Ocean penetrates further into Central Africa landmass (Fig. 5.6b). The reversal of the northern water vapour transport channel is associated with northward migration of high rainfall over Central Africa (Fig. 5.2e), with a strong increase of the low-level water

vapour flux at the northern branch of the Congo basin area. Nevertheless, the low-level moisture flux contribution to the total tropospheric moisture flux values over central Africa ranges from ~50% for the eastern water vapour transport channel to 75.1% for the northern water vapour transport channel (Fig. 5.6B, right panel). At the same time, over Congo basin, the low-level moisture transport contributions to the total moisture transport are lower than 45% on all moisture transport channels, except on the northern channel, which reach almost twice the value of the total moisture transport i.e. ~112% of the total moisture flux (Fig. 5.6B, right panel). This can be explained by the fact the total water vapor transport is the sum of all water vapor transport channels at each of the 4 boundaries of Central Africa and Congo basin regions respectively. Indeed, from May to September, when the Central Africa 2580 gpm isoline jumps to the Arabia sea, the reversal of low-level moisture transport increases due to the strengthening of the meridional component of the low-level horizontal wind. Thus, the northern channel of moisture flux, at the Congo basin area, strongly reinforces to reach almost twice the value of total moisture flux (with each water vapor transport cancelling out each other) over Congo basin i.e. almost ~112% of the total moisture flux over the Congo basin region. This substantiate why the outgoing flow turn the Congo basin into a source of moisture transporting it out towards East Africa and Great Horn of Africa. This finding suggests a crucial role play by this low-level moisture transport at the northern channel to modulate the total moisture flux variability and to affect its associated rainfall in this season. Total tropospheric moisture flux over central Africa indicates that Central Africa is a source of moisture (Fig. 5.6k), even though at low-levels, central Africa is a sink of moisture (Fig. 5.6e). This result provides an interesting insight on how the water vapour is likely to be advected out of central Africa (-1618.0±878.3 kg m^{-1} s^{-1}) towards East Africa and Great Horn of Africa, consistent with Anyah and Semazzi (2005). However, the weakness of low-level water vapour inflow from Atlantic Ocean is likely to lead to water vapour being rained out over Central Africa rather than to be transported to Sudan and Ethiopia, inconsistent with Viste et al. (2013). So, we infer that it is the Congo basin rainforest water vapour that is transported out of central Africa. However, Viste et al. (2013), using Lagrangian method, argued that the moisture of the Atlantic Ocean is transported towards Ethiopia and others remote regions. Thus, during this season, both Atlantic and Indians Oceans are the main contributors of water vapour over Central Africa, with Congo basin rainforest as an additional source.

For the seasonal transition between the two seasons, the similarity of spatial pattern between the momentum wind budget (frictional term) and the vertically integrated moisture flux emphasizes that the AEJs over Central Africa are key carriers of water vapour into Central Africa. In addition, accordingly to the season, Central Africa may shift from the source to the sink of water vapour, owed to the northern water vapour transport channel and related to the seasonal variation of Central Africa low (Fig. 5.6f;l). This suggests that indeed that the Congo basin rainforest is the third source of water vapour over central Africa.

5.5. Relationship between AEJ branches and moisture flux channels over Central Africa: an ENSO influence?

The momentum balance of the horizontal wind components over Central Africa shows dipole-like pattern representing two wind regimes of different accelerations: the first regime (AEJ-N) depicting acceleration and the second one (AEJ-S) showing a deceleration. Despite this different behaviour of these two branches of AEJ over Central Africa, we try to find out whether there is any relationship between them in October to April and May to September seasons respectively. So, we summarized, in Table 5.1, the correlation coefficients between AEJ branches and each moisture transport channels. First, we plotted the interannual variability of AEJs anomalies in Fig. 5.8 by area-averaging at the cores of both the northern (15^{o}-20^{o}E; 5^{o}-10^{o}N) and southern (20^{o}-30^{o}E; 5^{o}-12^{o}S) branches for October to April and May to September respectively. Then, a correlation map between these both AEJs indices (CAEJ-N and CAEJ-S) with SST anomalies in both seasons (October to April and May to September) is shown in Fig. 5.9. It emerges that during October- April season, both AEJ branches over Central Africa are significantly correlated, though the correlation seems to be relatively weak ($r = 0.34$, $p < 0.05$), while no trend is noted (Fig. 5.6a). In May-September season, the northern and southern branches of AEJs are strongly anticorrelated ($r = -0.53$, $p < 0.05$), indicating that when the northern branch strengthens, its southern counterpart is reduced and vice-versa (Fig 5.7b). Additionally, the increasing trend rate of the southern branch of AEJ is of about 0.5m/s per decade, while the reduction rate for the northern branch is of 0.4m/s per decade (Fig. 5.7b) for the present climate (1979 to 2015 study period). The strong correlations between AEJs branches and moisture transport channels clearly show that moisture transport variability over central Africa is regulated by AEJs, which in turn is strongly related to ENSO (Table 5.1 and Fig. 5.8, top left). This means that El Nino condition leads to weaken the Central Africa Low and its associated convection, which in turn, strengthen both branches of AEJs over Central Africa and lessen the local total moisture transport and its associated rainfall over central Africa in October – April season. This finding is consistent with the impact of Central Africa Low on Central Africa rainfall (see chapter 4).

Table 5.1. Correlation coefficients between northern and southern AEJs branches over Central Africa (CAEJ-N and CAEJ-S): and moisture transport at each central Africa boundaries in October – April (May – September). Correlation in bold is significant $p < 0.05$. Total moisture flux transport over central Africa is defined as the balance between incoming and outgoing of moisture transport channels in October – April (May – September).

	West	East	North	South	Total
CAEJ-N	**-0.42** (**-0.74**)	-0.14 (-0.08)	**-0.63** (**-0.75**)	-0.19 (-0.13)	**-0.28 (0.82)**
CAEJ-S	**-0.54** (**0.41**)	**-0.61** (**-0.36**)	**-0.29** (**0.33**)	**-0.40** (**-0.45**)	**-0.32 (-0.50)**

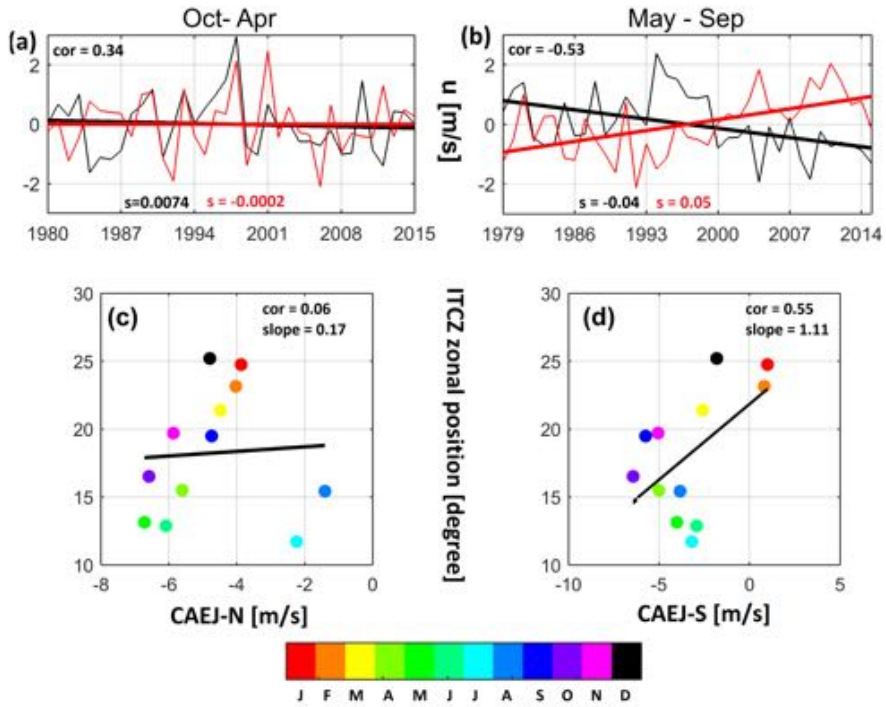

Fig. 5.7. Time series of northern and southern branches of AEJs over Central Africa (a) October to April and (b) May to September. Black and red lines in (a) and (b) indicate the linear trend of the northern and southern braches of Central African easterlies jets. Scatterplot of the seasonal cycle of zonal ITCZ position over central Africa vs (c) northern and (d) southern branches of central African easterly jets. Black line is the linear trend and the colour bar indicates the calendar month.

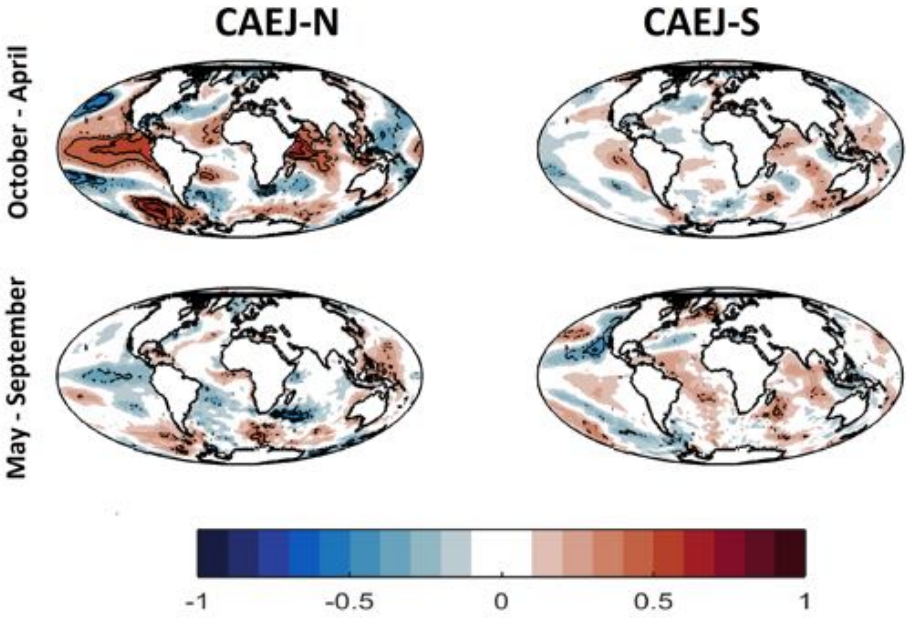

Fig. 5.8. Correlation map between SST from ERSST (Smith et al. 2008) and northern (left column) and southern (right column) branches of AEJs in October to April (top panels) May to September (bottom panels) from ERA-Interim. Only significant correlation at $p < 0.1$ is plotted.

Meanwhile in May – September season, strong branches of AEJs over Central Africa are out of phase with local total moisture transport over central Africa (Table 5.1). In fact, La Nina condition over equatorial Pacific (Fig. 5.8, bottom left) would lead to induce anomalous convection by weakening the subsidence over Central Africa, which in turn, increase the total moisture flux for the northern branch and reduces the total moisture transport of the southern branch (Table 5.1 and Fig. 5.8, bottom panels). Despite stronger magnitude of the leading incoming moisture transport (i.e. at the eastern boundary), no significant relationship is found between western water vapour transport channel and the northern branch of AEJ over Central Africa year-round. Furthermore, in both seasons, the southern branch of AEJ is weakly linked to El Nino condition, which is confined mainly over eastern equatorial Pacific (Nino 2.1 region, Fig. 5.8, right column).

This result corroborates that in October – April, both branches of AEJ over Central Africa are only poles of variability, in terms of their characteristics, interannual variability and relationship with Central Africa hydroclimate. Meanwhile in May – September, the northern and southern branches are dipole of variability of AEJs (Figs. 5.7b). More, the central Africa water vapour transport channels are mostly controlled by the southern branch of AEJ, suggesting that the southern branch of AEJ over Central Africa may regulate the Central Africa rainfall distribution. To assess how do AEJs link to rainfall distribution, ~~I~~we plot the seasonal cycle of both AEJs branches over Central Africa with zonal ITCZ position in Fig. 5.7(c-d). It appears that the southern branch of AEJ (Fig. 5.7b) may play a more important role than its counterpart northern branch (Fig. 5.7a) to determine the zonal ITCZ position, and hence the rainfall distribution over central Africa, consistent with findings of Fansworth et al. (2011).

5.6. Atmospheric water budget over central Africa

Finally, to understand what are the components controlling the water vapour budget variation over central Africa. It is well established that regional rainfall over central Africa is roughly a balance between precipitation, evaporation and remote moisture transport (Vizy and Cook, 2002). Following Peixoto and Oort (1992), the rainfall distribution over Central Africa needs to satisfy the atmospheric moisture budget equation:

$$P - E = -< \partial_t q > + < -\nabla.(\boldsymbol{v}q) > + < -\partial_p(wq) > \qquad (5.6)$$

Where $\boldsymbol{v}$=(u,v) is the horizontal wind, with *u* and *v*, the zonal and meridional component of the horizontal wind; *w*, the vertical velocity; *q* the specific humidity; E, the evaporation; P is rainfall, all given in units of mm d^{-1} and *p*, the pressure level and the angle bracket < > is the mass-weighted vertically integration.

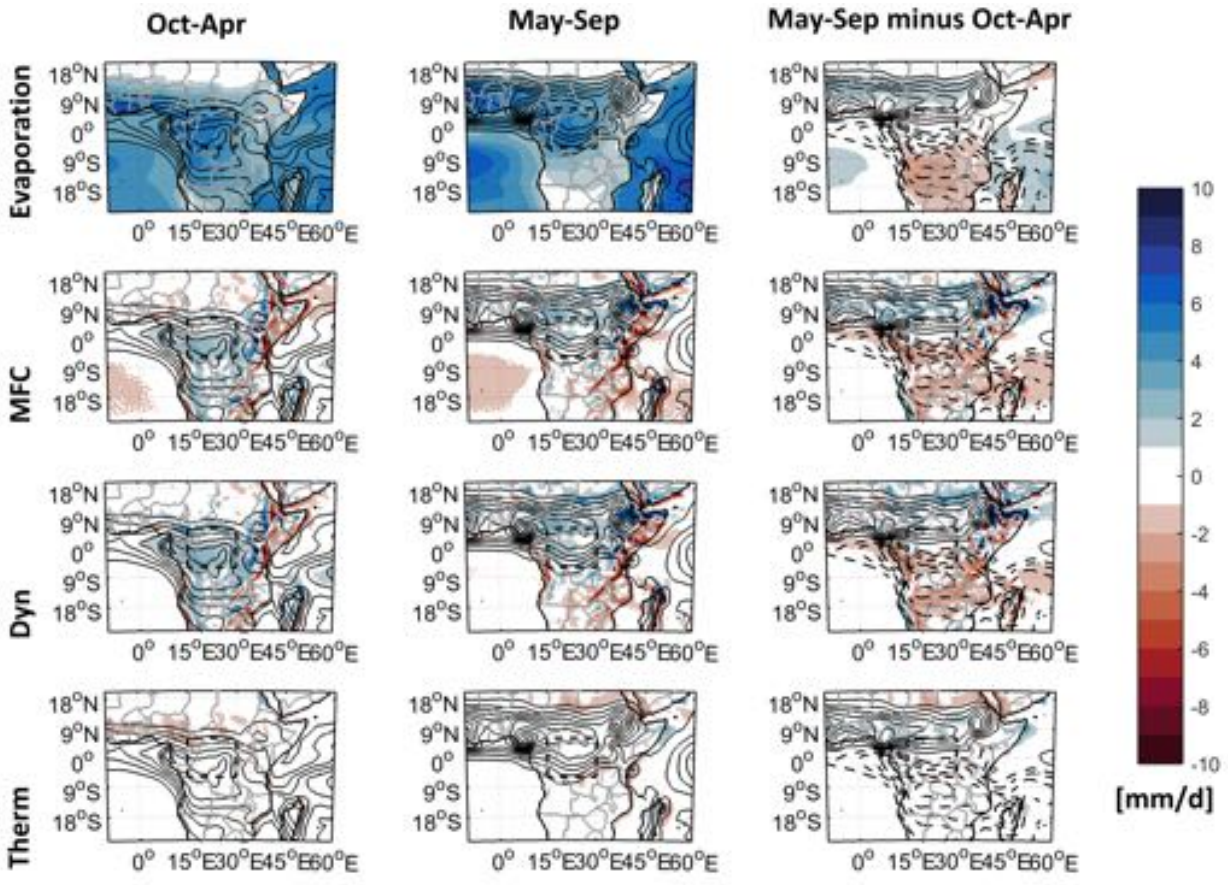

Fig. 5.9. (a-c) Evaporation (shaded), (d-e) moisture flux convergence (<$-\nabla.(vq)$>, shaded) (g-i) dynamic term (<$-q\nabla.(v)$>, shaded) (j-l) thermodynamic term (<$-v\nabla.(q)$>, shaded). In all panels, rainfall (contours) is overlaid. Unit: mm/d. (left) October-April season, (middle) May-September (right) May-September minus October-April. Dashed black box highlights Congo basin area (15°-30°E; 5°S-5°N)

For long-term mean (climatology), the specific humidity tendency term $< \partial_t q >$ is supposed to be negligible, while the vertical moisture gradient term $< \partial_p(wq) >$ is very weak over central Africa despite strong ascending motion. In fact, over central Africa, high water vapour (due to Congo basin rainforest) is associated with stable atmosphere ($\omega \approx 0$) at low-levels (Fig. 5.1k), while strong ascent motion is associated with less moisture ($q \approx 0$, Fig. 5.1k), consistent with Pokam et al. (2012). Further, in agreement with some studies (e.g. Banacos and Schultz, 2005; Held and Soden, 2006), the moisture flux convergence $- < \nabla.(\boldsymbol{v}q) >$ is further decomposed into the product of moisture and wind convergence $- < q\nabla.\boldsymbol{v} >$ (dynamic) and moisture advection $- < \boldsymbol{v}.\nabla q >$ (thermodynamic) components and plotted in Fig. 5.9. The dominant balance averaged over central Africa is between rainfall and surface evaporation (Fig. 5.9a-c), with a substantial contribution from $- < \nabla.(\boldsymbol{v}q) >$ (Figs. 5.9d-f). However, throughout the year, surface evaporation is limited over eastern Atlantic and east Africa (Figs. 5.9a-b). Moreover, high rainbelt over central Africa during October – April and May – September seasons is associated with strong moisture

flux convergence term, $- < \nabla.(\boldsymbol{v}q) >$ (Fig. 5.9d-f), suggesting an important role of the water vapour in the atmospheric column over central Africa, consistent with previous results (Pokam et al. 2012). Further decomposition shows that the dominant term of the moisture flux convergence is the dynamic component term $- < q\nabla.\boldsymbol{v} >$ (Fig. 5.9g-i). The thermodynamic term $- < \boldsymbol{v}.\nabla q >$ becomes more prominent, in October – April season, in west Africa (between 20°W–30°E; 5°–10°N, Fig. 5.9j). Therefore, Central Africa rainfall is strongly dominated by variation of large-scale circulation, rather than by variation in tropospheric column water vapour, inconsistent with Biasutti et al. (2003), who speculated that large-scale circulation does not play any crucial role in regulating rainfall over Central Africa.

5.7. Conclusion

This chapter investigates the dynamics of central Africa mid-tropospheric circulation by outlining the processes that cause the Central African easterly jet to maintain and control the moisture budget variation. I find the following results:

1. The mid-lower easterly jets over Central Africa and its neighbouring regions are driven year-round by the Central Africa Low, with a branch in each Hemisphere. These both branches of Central African easterly jet are referred as poles of variability in terms of their characteristic, interannual variability and relationship to Central Africa rainfall.
2. In October to April, both the Central African easterly jet branches are poles of variability as suggested by their correlation; while in May to September, the southern and northern branches of the Central African easterly jets are a dipole of variability.
3. The water vapour into Central Africa landmass is primarily transported by the mean-state circulation (climatology of the specific humidity and wind) rather than by any perturbations (anomalies). The water vapour transports over Central Africa are also driven by Central Africa Low as well.
4. When the Central Africa Low is dominant over Central Africa during the October – April season, Central Africa is a sink of water vapour, with the Indian Ocean as the main supplier. In May–September, the weakening of Central Africa low lead to the reversal of water vapour flow at the northern boundary channel, leading Central Africa to become a source of moisture, with Congo basin rainforest as an additional source.
5. Central African easterly jets do control the moisture convergence flux over central Africa and its associated rainfall, through the modulation of moisture transport channels, with a substantial role of the southern branch;
6. The maintenance of both northern and southern branches of central African easterly jets is owed by the mid-lower troposphere friction, rather than the geopotential thickness gradient;
7. The central Africa rainfall variability is primarily due to large-scale circulation variation, rather than by atmospheric water vapour variation.

Chap. 6

How does the land–ocean thermal contrast control the Central Africa hydroclimate variability?

6.1. Introduction

It is still unclear what are the specific mechanisms through which the atmospheric circulation above central Africa is forced at the interannual time scale. Indeed, Schneider and Lindzen (1977) argued that a shallow circulation at low-levels, due to the near-surface land-ocean thermal contrast, cannot explain the strong large-scale circulation leading to deep convection and high rainfall over Central Africa. But we found out in ECHAM5.3, a good correlation between the annual cycle of the near-surface land-ocean temperature contrast and the local surface pressure gradient between Central Africa landmass and its surrounding oceans (chapter three). This surface pressure gradient induces a shallow low-level circulation that transports moisture from adjoining oceans, which is important in the modulation of Central Africa rainfall variability (chapter 5). These findings imply a remote forcing mechanism through sea surface temperature (SST) that may play a crucial role to explain the regulation of Central Africa rainfall through the regional scale circulation. Using the ERA-Interim reanalysis, the purposes of this chapter are to (i) further the work of Vigaud et al. (2007, 2009) and Nicholson and Girst (2003) by testing the hypothesis that the mid-lower land-ocean thermal contrast affect Central Africa hydroclimate by modulating the atmospheric water vapour transport; and (ii) to assess how this mechanism is represented in the ECHAM5.3 datasets.

6.2. Data

To analyse the atmospheric circulations and its associated moisture transports, I use the monthly-mean of horizontal wind, air temperature and geopotential heights at different levels obtained from ERA-Interim reanalysis (Dee et al., 2011). We also use the monthly-mean Global Precipitation Climatology Project (GPCP) version 2.2 (Huffman et al., 2009) and Climate Prediction Center (CPC) Merged Analysis of Precipitation (CMAP; Xie and Arkin, 1997) for rainfall. But because of the limited period covered by NOAA optimum interpolated (OI) SST version 2.2 (Reynolds et al., 2002), Extended Reconstructed Sea Surface Temperature (ERSST, Smith et al. 2008) is also used, unless otherwise stated. All these reanalyses datasets span from January 1979 to December 2015. In addition, we also use the ECHAM version 5.3 (Roeckner et al. 2003, Gleixner et al. 2016) to assess how physical mechanisms are captured. The monthly means are averaged over the season to get the seasonal means. The anomalies are departures from their respective seasonal mean values averaged over the study period for each grid. The normalized anomalies are obtained by dividing by their respective standard deviation for each grid and for each season. Before computing any correlation, the monthly anomaly data are detrended linearly.

6.3. Vertical profile of water vapour transports originated from surrounding Oceans

The vertical cross section of water vapour transports in the core region (15^{o}E-30^{o}E; 5^{o}N-5^{o}S) of Central Africa are shown at its zonal and meridional boundaries in Figs. 6.1-2 for ERA-Interim and ECHAM5.3. The reason for choosing the core region of Central Africa is to highlight the influence of the Central Africa low. Although the spatial pattern of moisture flux is relatively similar than those at the boundaries of Central Africa region (7^{o}E-33^{o}E; 10^{o}N-15^{o}S), the southern branch of the central African easterly jet seems to be weak at 7^{o}E or at any Atlantic offshore position.

Year-round, the moisture flux occurs from the near-surface up to ~400- hPa over central Africa and its neighbouring regions (Figs. 6.1 & 6.2). From October to April, at the eastern boundary (30^{o}E), the moisture flux is predominantly easterly with its core located at around 5^{o}N between 800- and 600- hPa, which is lower in height than the core of the northern central African easterly jet (Fig. 6.1a, bottom left). However, a distinct small core of moisture flux is found in the southern Hemisphere at around 15^{o}S; 800- hPa (Fig. 6.1a, bottom left). The principal source of this moisture is the Indian Ocean. Whereas at the western boundary (15^{o}E), between 800- and 600- hPa, the water vapour transport has the same feature as for the eastern boundary, with the outgoing moisture flux originates from Indian Ocean still conveyed by African easterly jet. This westward water vapour transport seems to cross the central Africa in the east-west direction (Fig. 6.1a, top left). At low-levels (below 800- hPa), the monsoon-like moisture flux is entering into Central Africa towards its core between the 10^{o}S and 5^{o}N (Fig. 6.1a, top left).

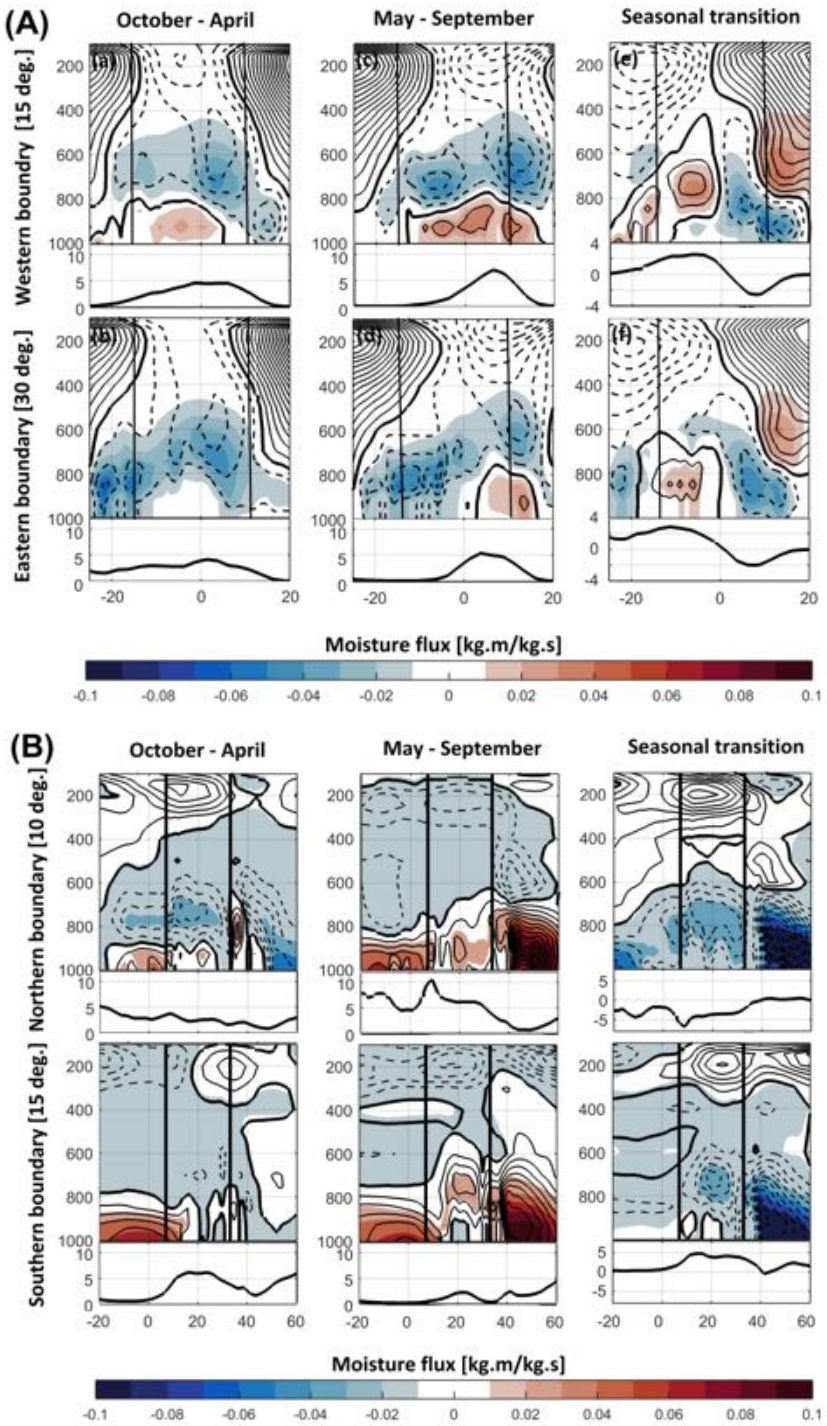

Fig. 6.1. Vertical cross section (A) (Latitude – height) of the zonal water vapour transport (in kgm/kgs) and associated rainfall (in mm, black line in the bottom panel). Rain rate is averaged between 5°N-5°S at the western (15°E) and eastern (30°E) boundaries and (B) (Longitude – height) of the meridional water vapour transports and its associated rainfall averaged between 15°E-30°E at the northern (5°N) and southern (5°S) boundaries of Central Africa for ERA-Interim. The black vertical bars represent in (A) the meridional and in (B) the zonal limit of Central Africa respectively. In all panels, the zero-line (0 m/s) is delineated by the black bold line.

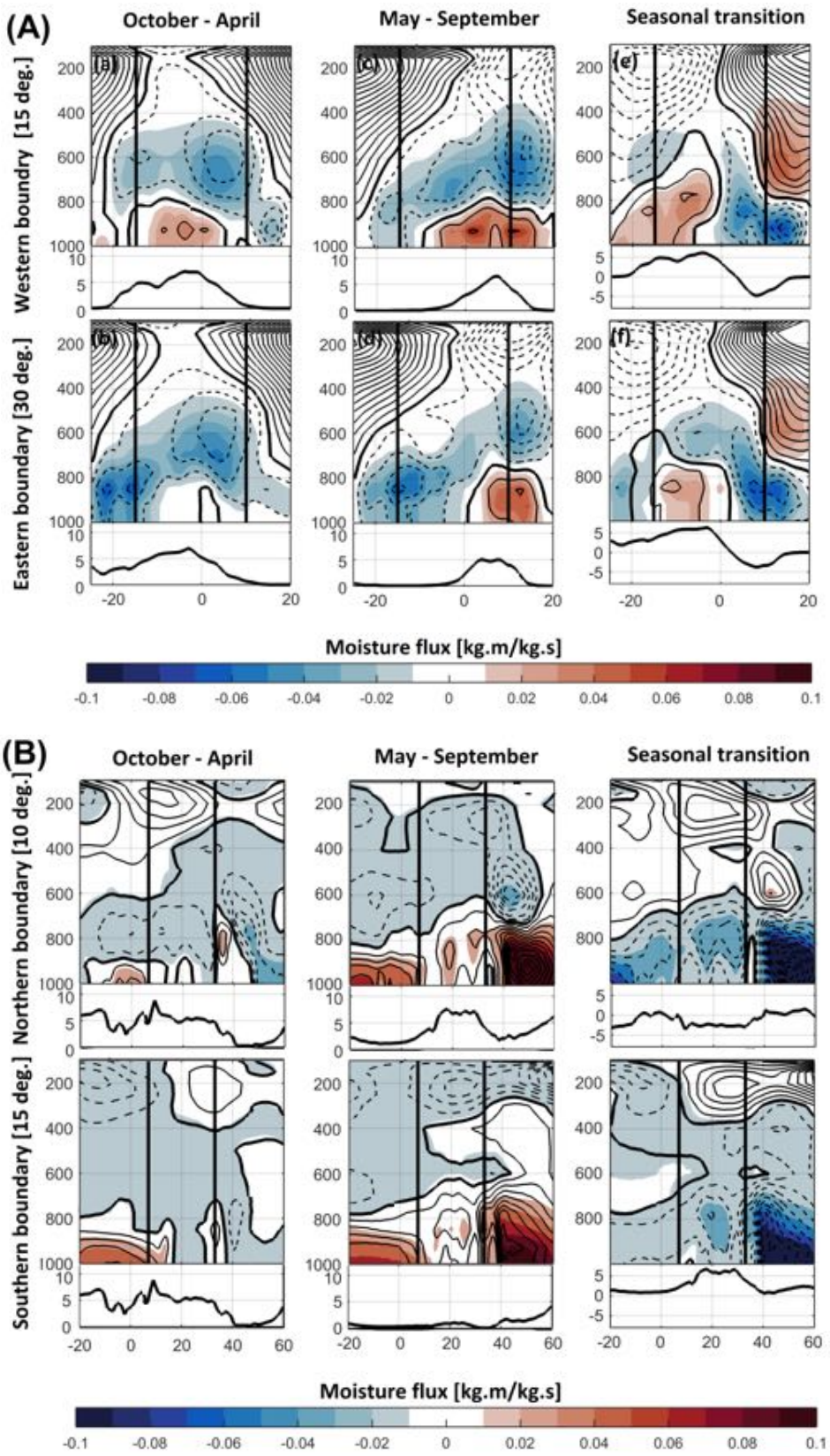

Fig. 6.2. As Fig. 6.1. but for ECHAM5.3

This water vapour has presumably its origin over eastern Atlantic, where the low-level westerly is dominant (Fig. 6.1a, top left). The position of high rainfall (~5 mm/d) seems to be determined by the position of the core of the northern branch of the central African easterly jet (Figs. 6.1a, left). At the northern boundary (5^{o}N), the water vapour is conveyed mostly by the midlevel northerly (800- to 600- hPa) into Central Africa, with the Congo basin rainforest as the main source of water vapour; while the water vapour originating from Atlantic Ocean is transported into west Africa and the Atlantic offshore region by low-level southerly (Fig. 6.1b, left). These findings at the northern and western boundaries of Central Africa confirm that water vapour originating from Central Africa landmass (Congo basin rainforest) is transported to West Africa monsoon region, as shown by Fontaine et al. (2003). Over the Indian Ocean, a strong southward water vapour is dominant in the boundary layer (Fig. 6.3b). The longitudinal variation of rainfall shows a gradual decrease of rainfall, with high rainfall over Atlantic and low rainfall over the Indian Ocean (Fig. 6.1b, top left). At upper levels, a strong southerly flow dominates Central Africa (Fig. 6.1b, top left). At the southern boundary (5^{o}S), the strong southerly flow in the boundary layer over the Atlantic Ocean is associated with higher northward water vapour transport than at its northern counterpart boundary (Fig. 6.1b bottom left). The mid-level circulation has significantly weakened with respect to that at the northern boundary, so that its associated moisture flux is very limited (Fig. 6.1b, bottom left). However, the strong northward water vapour transport over Atlantic is associated with high rainfall over central Africa, while it seems to lead to low rainfall over Atlantic Ocean (Fig. 6.1b, bottom left). High rainfall occurs over Indian Ocean despite a very weak southward moisture flux (Fig. 6.3b). This suggests that high rainfall is not associated with the water vapour transport.

From May to September, the water vapour transport has a relatively similar pattern than for October to April period. There is a substantial increase of moisture flux associated with a strengthened easterly jet that has shifted northwards (Fig. 6.1a, top middle). The northwards shift of central African easterly jets is due to the weakening of Central Africa low. These enhanced moisture fluxes leading to high rainfall (~8 mm/d) between the equator and 10^{o}N, which is almost two time more rainfall than in the previous season, particularly for the western boundary (Fig. 6.1a, top middle). Note that the core of the northern branch of the African easterly jet is located over the Sahel, i.e. between 10^{o}N and 20^{o}N. The southern branch of central African easterly jet is lower than its counterpart northern branch (Fig. 6.1a, top middle). The low-level westerlies strengthen. The westward water vapour transport outflow over East Africa between the equator and 20^{o}N (Fig. 6.1 top middle). At both boundaries, the position of high rainfall seems to be associated more with low-level westward water vapour transport (Fig. 6.1 top middle), consistent with Fig. 5.5 (see chapter five) than by the position of strengthened moisture fluxes associated with both branches of the central African easterly jets. The meridional boundaries show two distinct atmospheric circulation regimes over Central Africa: southerlies flow at low-levels (1000- to 750- hPa) and northerly flow in the mid-upper (750- to 100- hPa) levels (Fig. 6.1b middle). At the northern

boundary, the reversal of the meridional wind component at mid-lower levels, particularly over central Africa and western Indian Ocean is accompanied by its strengthening. However, the longitudinal variation of rainfall seems to be determined by the low-level northward water vapour transport over central Africa, with rainforest as a main source of moisture. Over the Indian Ocean, a strong water vapour transport is associated with low rainfall (Fig. 6.1b middle). The southern boundary has a similar structure of water vapour transport than its northern counterpart, but with a relatively strong midlevel southward moisture transport (Fig. 6.1b, middle). At this southern boundary, high rainfall over central Africa seems to be determined by the weak southward moisture flux (Fig. 6.1b middle bottom).

The seasonal transition (difference between October to April and May to September seasons) outlines similar patterns of the atmospheric circulation and its associated water vapour transport at both zonal and meridional boundaries (Figs. 6.1a-b, right). For the zonal boundaries, these patterns feature two opposite sign of water vapour transports at mid-lower (800- to 600- hPa) troposphere and in each hemisphere as well as their associated rainfall (Fig. 6.1a, right panels). Indeed, over Central Africa, the mid-lower westerly circulation and its related water vapour transport is associated with high rainfall, while the mid-lower easterly flow and its related water vapour flux is associated with low rainfall (Fig. 6.1a, right panels). This highlights the strengthening or the weakening of each branch of Central African easterly jet and its association with rainfall accordingly to the season (Fig. 6.1a, right panels). As for the meridional boundaries, the southward water vapour transport is dominant over Central Africa and its neighbouring region, with higher water vapour transport over the Indian Ocean and Central Africa landmass than over Atlantic Ocean (Fig. 6.1b, right panels). However, the water vapour transport is larger over Indian Ocean than over central Africa landmass (Fig. 6.1b, right panels). The midlevel southward water vapour transport over Central Africa landmass is associated with lower rainfall than over its surrounding oceans at the northern boundary, while at the southern boundary, it is associated with higher rainfall than over its surrounding oceans (Fig. 6.1b, right panels).

ECHAM5.3 reproduces quite well those water vapour transport patterns and their associated rainfall at all boundaries, with some positive biases compared with ERA-Interim (Fig. 6.2). However, ECHAM5.3 fails to capture the strengthening of the southern branch of the central African easterly jet from May to September (Fig. 6.2a, middle panels). Also, ECHAM5.3 misrepresents the strengthened southerly flow and its associated water vapour transport from October to April (Fig. 6.2b, left), as shown with comparison with ERA-Interim. For the rainfall, from October to April, the zonal maximum in ECHAM5.3 occurs in the southern Hemisphere, at around 5^{o}S and at the equator (Fig. 6.2a), while in observations, it occurs in the northern Hemisphere (Fig. 6.2a). The rainfall maximum seems to be determined by the low-level westerly moisture flux in ECHAM5.3 (Figs. 6.2a-b).

6.4. Interannual variability of moisture transports from surrounding Oceans

To further understand what is the year-to-year interannual variation of moisture transport from surrounding oceans and how they influence the Central Africa hydroclimate, we describe the interannual variability of the zonal water vapour transport originating from surrounding oceans by using empirical orthogonal functions (EOF) analysis. The analysis is performed on zonal water vapour transport at the eastern and western boundaries for the 1979 -2015 period for October to April and May to September respectively. As a first step, we calculate the seasonal anomalies of the zonal moisture transport with respect to the long-term mean of each season at each grid box. Next, we detrend the zonal moisture flux anomalies as we are only interested in the interannual variability. We retain two first distinct dominant modes of variability, which together can account for 67.5 % to 71.2% of total variance for the October to April period and the May to September period respectively. In ECHAM5.3, they account for between 76.4% to 83.0% of total variance. Over Central Africa, the patterns associated with each of the two first leading modes of zonal water vapour transport have a similar structure at both boundaries in ERA-Interim and ECHAM5.3.

The first leading mode (EOF1) consists of a dipole of anomalous water vapour transport associated with the two branches of AEJ over Central Africa (Fig. 6.3a, top). The southern branch of AEJ is associated with outgoing anomalous water vapour transport over Central Africa, while the northern branch is associated with incoming anomalous water vapour transport over Central Africa (Fig. 6.3a, top). In comparison to the spatial pattern of the seasonal mean-time water vapour transport at the western boundary (Fig. 6.1a, top panels), this first leading mode suggests the intensification of the northern branch and the weakening of the southern branch of AEJ over Central Africa respectively. The anomalous westward water vapour transport is located at lower level at the eastern boundary of Central Africa than at its counterpart western boundary, with weaker magnitude (Fig. 6.3a, top). At midlevels, Southern Africa is associated with an anomalous eastward water vapour transport, while the Sahel is characterized by an anomalous westward water vapour transport (Fig. 6.3a, top). This latter structure of anomalous water vapour flux associated with the northern branch of AEJ over Sahel, which is widely documented by many authors (Thorncroft et al. 2011). In addition, the spatial patterns of the first leading modes, at the two zonal boundaries, are almost similar, with their principal components having a strong correlation of around 0.9 (significant at 99%) (Fig. 6.3a, top). This suggests that any intrusion of water vapour at any zonal boundary of Central Africa is likely to cross the second one, consistent with the closing and the return branches of the Congo Basin Cell at low- and mid-levels respectively (see chapter 3). The spectral analysis of the first leading principal component (Fig. 6.3a, top right) exhibits a highly significant peak at around 12 years (Fig.6.4, top left), indicating that the water vapour transport is associated with a decadal oscillation in this mode of variability.

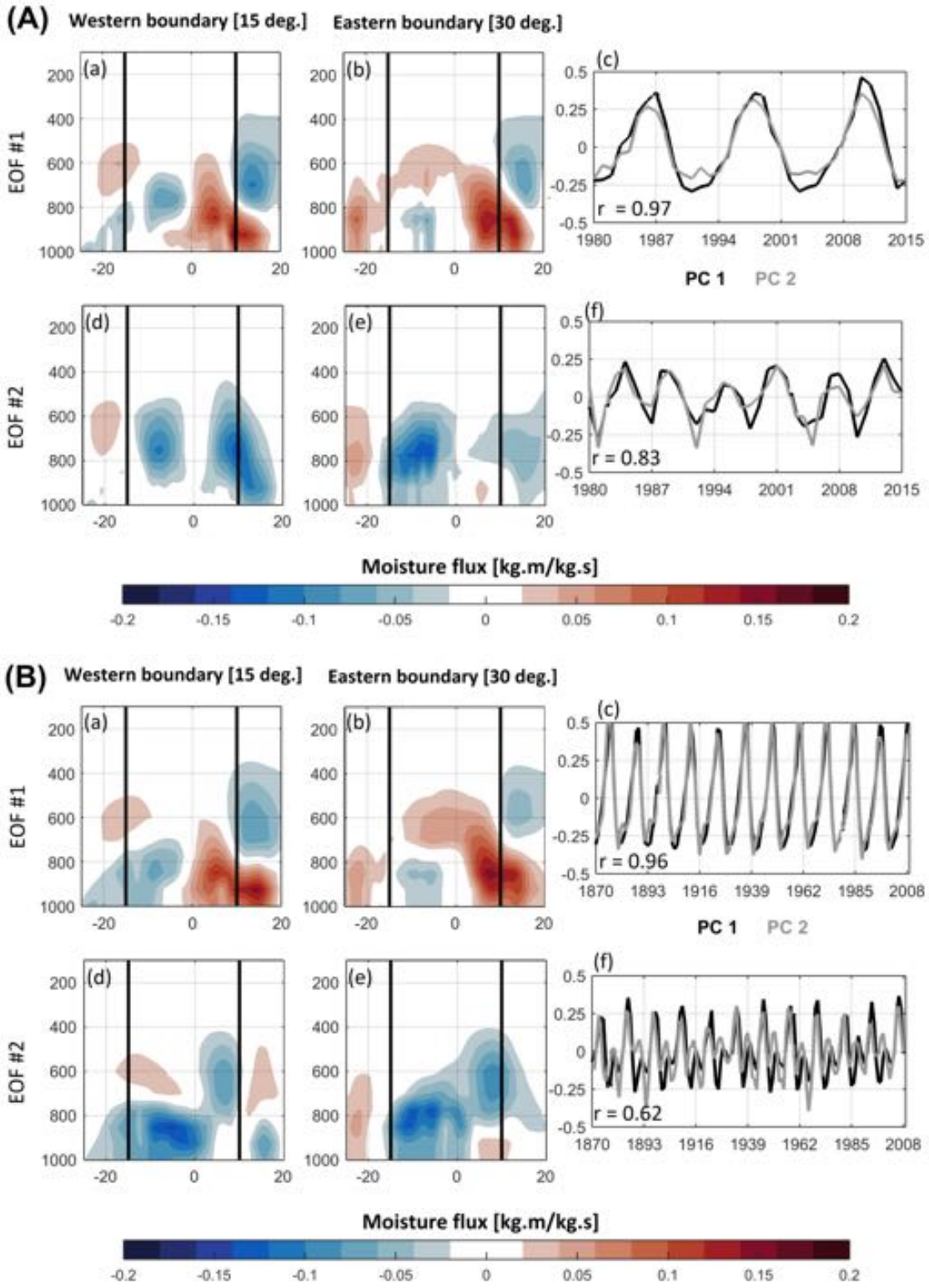

Fig. 6.3. Vertical cross section (Latitude – height) of the two first leading modes of water vapour transports variability and theirs associated principal components (PC) at western (15°E) and eastern (30°E) boundaries of Central Africa for (A) ERA-Interim and (B) ECHAM5.3. The black vertical bars represent the zonal limit of Central Africa.

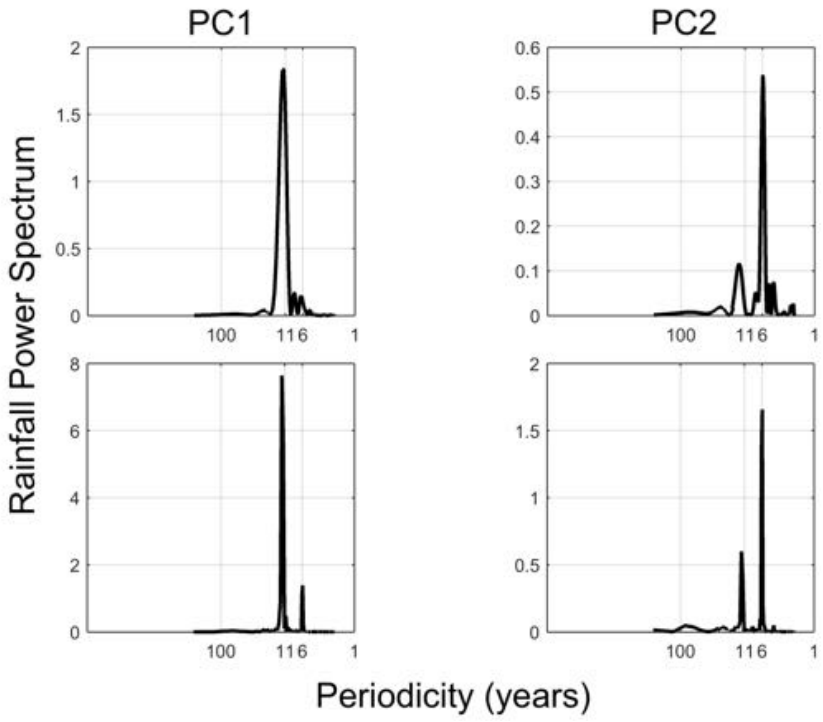

Fig. 6.4. Power spectrum of the two first principal components for water vapour transports at the western boundary (15°E) for (top) ERA-Interim and (bottom) ECHAM5.3. (Right) first and (left) second principal component of the leading mode of water vapour transport. Y-axis, mm^2/d^2 and X-axis, period in years.

This low-frequency variability of the crossing water vapour transport at the western boundary of Central Africa may somewhat be related to the South Atlantic anticyclone variability (Venegas et al. 1997), with some influence of El Nino condition prevailing over the tropical Pacific as suggested by Dieppois et al. (2016).

The 2nd leading mode of the water vapour transport at the western boundary outlines two poles for Central African easterly jet centered at 750- hPa (Figs. 6.3a, bottom). The first pole of Central African easterly jet is located at 6°S, while the second one is positioned at 10°N respectively (Figs. 6.3a, bottom). This spatial structure of the 2nd leading mode is different of the seasonal mean-time of water vapour transport, shown in Fig. 6.1a, in that the interannual variability of the east-west water vapour fluxes are reinforced and more westward (Fig. 6.3a, bottom; Fig. 6.4, top left). This reinforcement of the water vapour transports while crossing Central Africa landmass in the east-west direction may be due to abundant Congo basin rainforest moisture. The spectral analysis of the 2nd principal component shows an interannual variability of a period of ~6 years (Fig.6.4, right), which could be related to ENSO oscillation (Capotondi et al. 2015). The ECHAM5.3 misrepresents the position of the water vapour transport associated with both Central African easterly jet

branches. The northern branch of the westward water vapour transport is located higher, at ~600-hPa, than its counterpart southern branch at ~850- hPa (Fig 6.3b, bottom). The correlation between the principal components of these 2nd leading structure at the both zonal boundaries is ~0.8 in ERA-Interim and ~0.6 in ECHAM5.3 (Fig. 6.3a, right).

From May to September, the two first leading modes of water vapour transport at the western and eastern boundaries of Central Africa bear a strong resemblance to the spatial patterns of the two first leading modes obtained in the previous season (October to April) in ERA-Interim and ECHAM5.3 respectively. Furthermore, I found significant simultaneous correlation of around 0.6, between Central Africa rainfall anomalies and the 2nd principal component of each boundary in October to April. None of the two principal components at the western and eastern boundaries is significantly correlated with surrounding equatorial Oceans: eastern Atlantic SST (5°W-5°E; 5°N-5°S) and western Indian (5°W-5°E; 5°N-5°S). But strong correlation is found between El Nino South Oscillation (ENSO) and the 2nd principal component of water vapour transports at the western ($r = -0.44$, $p < 0.05$) and eastern ($r = -0.33$, $p < 0.1$) boundaries.

6.5. The dependence of surrounding Atlantic and Indian Oceans on AEJ and its associated water vapour transport

To understand the year-to-year variability of the water vapor transport variability at any zonal boundaries of Central Africa and how the higher and/or lower water vapor transport influence on Central Africa rainfall. So, we try to find out what is the mechanism underlying the connection between the 2nd leading mode of the water vapour transport at the western boundary of Central Africa and Central Africa rainfall. We examined in detail the composite of vertically integrated moisture flux and rainfall for events in which the principal component is greater than 0.125 or less than -0.125, corresponding to high and low water vapour transport respectively. We also show the correlation of the 2nd principal component of the water vapour transport with the latent heat (evaporation) and SST anomalies. We showed that the vertically integrated moisture flux is primarily controlled by the central African easterlies jets (chapter five). Due to the strong correlation of water vapour transports at the eastern and western border (chapter 5), I am looking only at the western boundary (over the Atlantic Offshore region) for the rest of this chapter.

The composite during higher water vapour transport phases shows the stronger than normal Central Africa Low (as indicated by the 2580- gpm geopotential thickness isoline) is associated with positive rainfall anomalies (Fig. 6.5a, top left), suggestive of deep convection. The underlying strong easterly circulation conveys more water vapour across Central Africa landmass, with a major contribution from evaporation (Fig. 6.5a, bottom left).

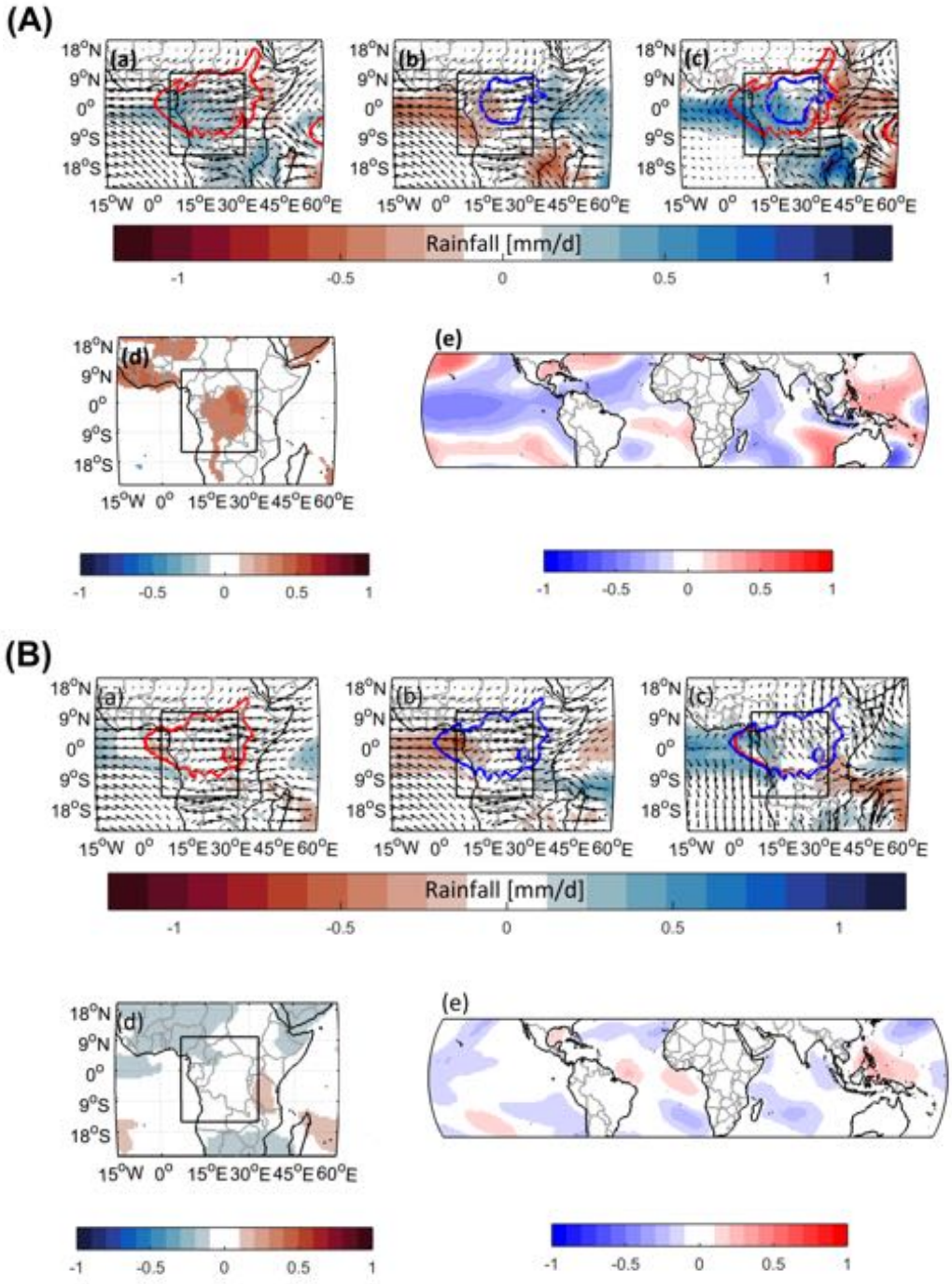

Fig. 6.5. (Top) Composites of rainfall (shaded, mm/day) and vertically integrated moisture flux (vectors, kg/ms) during the higher and lower water vapour transport phases defined as the events (years) in which the 2nd PC of water vapor transport at the western boundary (15^{o}E) of Central Africa is greater than 0.125 standard deviation (left panel) and smaller than -0.125 standard deviation (middle panel) and their difference (composite difference, right panel). (Bottom) Correlation coefficients of the 2nd PC of water vapour transport at the western boundary (15^{o}E) vs evaporation (left panel) and SST anomalies (right panel). For (A) ERA-Interim and (B) ECHAM5.3. The vertical bar represents the zonal limit of Central Africa. Only significant correlation at $p < 0.1$ is plotted.

This indicates that the Congo basin rainforest acts as the main source of water vapour, which leads to the strengthening of the westward water vapour transport associated with both branches of Central African easterly jets, identified in the second EOF pattern (Fig. 6.3a, bottom). At the same time, at the east of the Central Africa Low 2580- gpm isoline, East Africa experiences a rainfall deficit (Fig. 6.5a, top left). This rainfall deficit over East Africa is associated with negative SST anomalies over the Indian Ocean (Figs. 6.5a, bottom right). Whereas over the equatorial Atlantic, the negative SST anomalies are associated with positive rainfall anomalies (Figs. 6.5a, top left). This leads me to assume that mechanisms affecting linking rainfall and the atmospheric circulation over Central Africa landmass and its surroundings oceans could be different. Indeed, over Central Africa landmass, rainfall is related to atmospheric circulation via both large-scale and small-scale process (associated with evaporation over Congo basin rainforest). While over surrounding oceans, rainfall seems to be associated with only large-scale processes. Over, the Atlantic and Indian Oceans, the atmosphere seems to force the Ocean through the mid-lower easterly jets, which in turn, are governed by the mean surface level pressure as suggested by Venegas et al. (1997). In fact, if the atmosphere was driven by the ocean, the circulation would strengthen and transport more water vapour associated with warmer SST anomalies, and this would result in above normal rainfall conditions over adjoining (Atlantic and Indian) Oceans, which is opposite for this positive phase (years) (Fig. 6.5a, top left and bottom panels).

The composite during lower water vapour transport phases shows a weaker than normal Central Africa Low (as suggested by the shrinking of the 2580- gpm geopotential thickness isoline). This is associated with shallow convection and reduced evaporation over central Africa (Fig. 6.5a, top middle). A weaker Central Africa Low enhances the rainfall contrast over Central Africa, with negative rainfall anomalies over Atlantic Offshore region associated with positive Atlantic SST anomalies and positive rainfall anomalies over East Africa (starting from around 30^{o}E at the Rift Valley highlands) associated with positive Indian SST anomalies. This indicates that over the Indian Ocean, the warmer SST anomalies, associated with strong overlying mid-lower easterly jets, induce higher than normal water vapour transport, which lead to positive rainfall anomalies over East Africa. This suggests that the mid-lower easterly jets act as the leading atmospheric forcing of the Atlantic SST anomalies, consistent with Venegas et al. (1997).

The composite difference between high and low water vapour transport phases is characterized by an anomalous rainfall contrast over central Africa region owed by the Central Africa Low area change, with positive rainfall anomalies over Atlantic offshore region and Southern Africa and negative rainfall anomalies over East Africa (Fig. 6.5a, top right). More, over Atlantic, the rainfall surplus is associated with an anomalous small cyclonic circulation, which lead to anomalous moisture flux convergence, conducive to high rainfall. The anomalous westerly circulation over

East Africa is indicative of less landwards advection of water vapour from the Indian Ocean (Fig. 6.5a, top right). This indicates that the strength of the water vapour transport into Central Africa from the Atlantic Ocean is related to the intensity of the Central Africa Low (see chapter four), which is outlined by Central Africa Low area change. It is important to note that Central Africa Low not only drives the water vapour transport from surrounding oceans, but also highlights the atmospheric pressure gradient between Central Africa landmass and the oceans. Therefore, the resulting anomalous rainfall contrast over Central Africa emphasizes the substantial role of the Central Africa Low area change on regional rainfall (see chapter four, Fig. 4.6b). Overall, the strong connection between the water vapour transport at Central Africa zonal boundaries and equatorial central Pacific negative SST anomalies suggests that La Nina enhances the east-west water vapour transport through the impact of the Central Africa Low (see chapter four).

In ECHAM5.3, rainfall and water vapour transport patterns are quite well represented (Figs. 6.5b, top). But ECHAM5.3 fails to capture the influence of the Central Africa Low, particularly during the period of low water vapour transport years, as there is a weaker connection with equatorial central Pacific (Fig. 6.5b, top). This suggests that the land-ocean thermal contrast driving the mid-lower water vapour transport through the zonal pressure gradient between Central Africa landmass and its adjacent oceans is not well represented. In addition, during this period of low water vapour transport, there is a misrepresentation of the contribution of local evaporation to Central Africa rainfall (Fig. 6.5b, bottom left). The shortcomings in the ECHAM5.3 to represent the influence of the mid-lower water vapour transport on Central Africa rainfall at interannual time scale is consistent with Zhou et al. (2009), who argued that the SST-forced AGCM is better suited to examine the atmospheric response at the surface than at middle or upper atmospheric levels.

6.6. The impact of land-ocean thermal contrast on Central Africa rainfall

The near-surface land-ocean thermal contrast is strongly associated with its overlying zonal surface pressure gradient (chapter three), which drives the low-level circulation over Central Africa (chapters three, four and five). But the strong easterly circulation crossing the Central Africa landmass cannot be explained by the near-surface land-ocean thermal contrast, which is likely to drive a shallow circulation (Schneider and Lindzen, 1977; chapters three and five). So, I define the mid-lower layer thickness ($\Delta\phi$) as the vertical integration of geopotential height between 1000- and 500- hPa. This mid-lower layer thickness is considered as a better approximation of the heat content of that atmospheric layer than the mid-lower mean layer temperature (T) over central Africa and its adjoining Oceans (Turrent and Cavazos, 2009).

Thus, the atmospheric layer thickness is related to the mean-layer temperature as follow (Dai et al. 2013):

$$\Delta\phi = \frac{RT}{g}\left[\ln\left(\frac{p_o}{p_1}\right)\right] \qquad (6.1)$$

with R, the gas constant; g the Earth acceleration; p_o and p_1 are the pressure levels.

The difference between the mid-lower layer thickness $\Delta\phi$ and the mean layer temperature T is the factor $[\ln(p_o/p_1)]$. Therefore, whether the temperature is taken at low-levels, between 1000- and 850- hPa, the factor is [ln(1000/850)] = 0.16252; while between 1000- and 500- hPa, the factor will be [ln(1000/500)] = 0.69315. This means that for the same temperature gradient, the 1000- 500- hPa tropospheric layer thickness contributes 4.265 times than the low-level layer thickness (1000- 850- hPa) to the zonal wind shear, that drives the central African easterly jet (Nicholson and Grist, 2003). Therefore, it is more important to consider the mid-lower layer thickness to determine both the strength and variation of the induced African easterly jet and its associated moisture transport. So, the land-ocean thermal contrasts between Central Africa landmass and Atlantic ($\Delta\phi_{ATL}$) and Indian ($\Delta\phi_{IND}$) Oceans are computed as follow respectively:

$$\Delta T_{ATL} = \Delta\phi[15^oE - 30^oE;\ 5^oS - 5^oN] - \Delta\phi[5^oW - 5^oW;\ 5^oS - 5^oN] \qquad (6.2)$$

$$\Delta T_{IND} = \Delta\phi[15^oE - 30^oE;\ 5^oS - 5^oN] - \Delta\phi[40^oE - 60^oE;\ 5^oS - 5^oN] \qquad (6.3)$$

No significant correlation is found between the land-ocean thermal contrasts and central Africa rainfall. But when I decompose the water budget according to Seager and Henderson (2009), the rainfall is balanced by the moisture flux convergence as follow:

$$P - E = < -\nabla.(\boldsymbol{v}q) > \qquad (6.4)$$

with P, rainfall, E, latent heat (evaporation) and *vq*, the horizontal moisture flux convergence; *q*, the specific humidity and v = (*u*, *v*), where *u* is the zonal and *v*, the meridional components of the horizontal wind.

A strong relationship emerges between the moisture flux convergence over Central Africa and the land-ocean temperature contrast with correlation of around -0.33 ($p < 0.1$) with $\Delta\phi_{ATL}$ (Atlantic) and -0.43 ($p< 0.05$) with $\Delta\phi_{IND}$ (Indian) Oceans respectively (Fig. 6.6a). In other words, this link indicates that land-ocean thermal contrasts modulate central Africa rainfall variation through moisture flux convergence via a large-scale process. Once more, this finding highlights that the moisture flux convergence variability is dominated by the variation of large-scale circulation, which in turn, drives the central Africa rainfall variability (chapter five). In ECHAM5.3, this large-scale

process is also relatively well captured as shown by the strong and significant correlation (spanning from 1871 to 2009) with only the Indian Ocean (r = -0.44, p < 0.05, Fig. 6.6b).

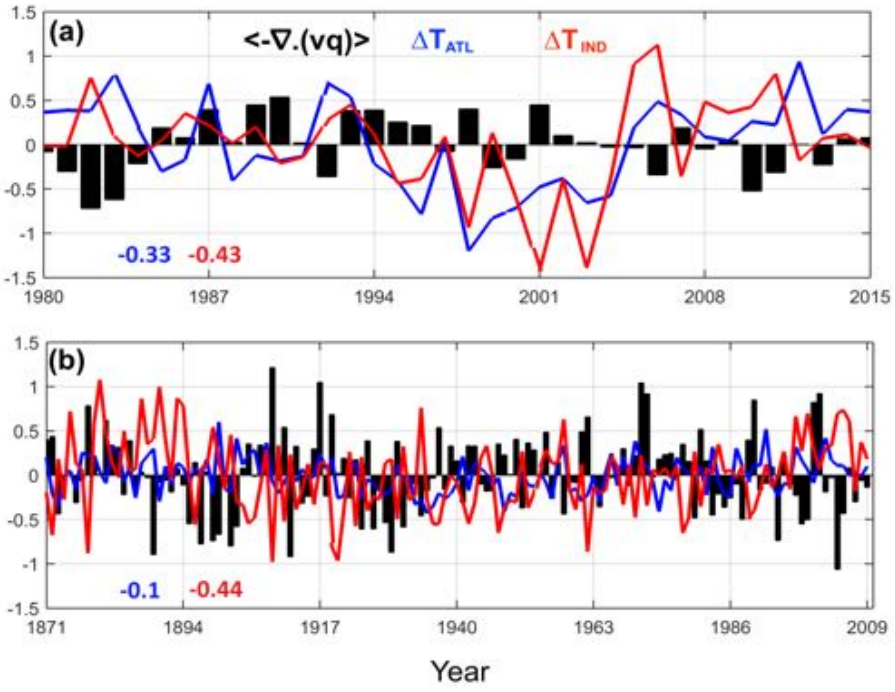

Fig. 6.6. Time series of moisture flux convergence over Central Africa and land-ocean thermal contrast between Central Africa landmass and Atlantic and Indian Oceans For (A) ERA-Interim and (B) ECHAM5.3.

This suggests a possible mechanism relating the combination of strengthened large-scale circulation and mid-lower tropospheric warming to enhance water vapour (latent heat) through Clausius-Clapeyron relation, which in turn, lead to intense central Africa rainfall. To test this hypothesis, I plot, in Figs. 6.7 and 6.8, the correlation coefficients between the mid-lower land-ocean thermal contrast and column water vapour (precipitable water) as well as the mid-lower zonal wind shear ($u_{500} - u_{1000}$) to find out how the land-ocean thermal does control the African easterly jets, and so its associated water vapour transport. In each panel, I also overlaid the composite of Central Africa Low 2580- gpm isoline during positive and negative events of the land-ocean thermal contrast. The event is positive when the normalized land-ocean thermal contrast anomaly is greater or smaller than 0.5 or -0.5 respectively.

For positive events of ΔT_{ATL}, the convection has deepened further than during negative events, as shown by the Central Africa Low 2580-gpm isoline (Fig. 6.7a, top left). The induced anomalous westward wind shear over central Africa – with its cores centered at 5^{o}S; 15^{o}E and at 15^{o}S; 55^{o}E respectively – is associated with anomalous high column water vapour (Figs. 6.7a, bottom left).

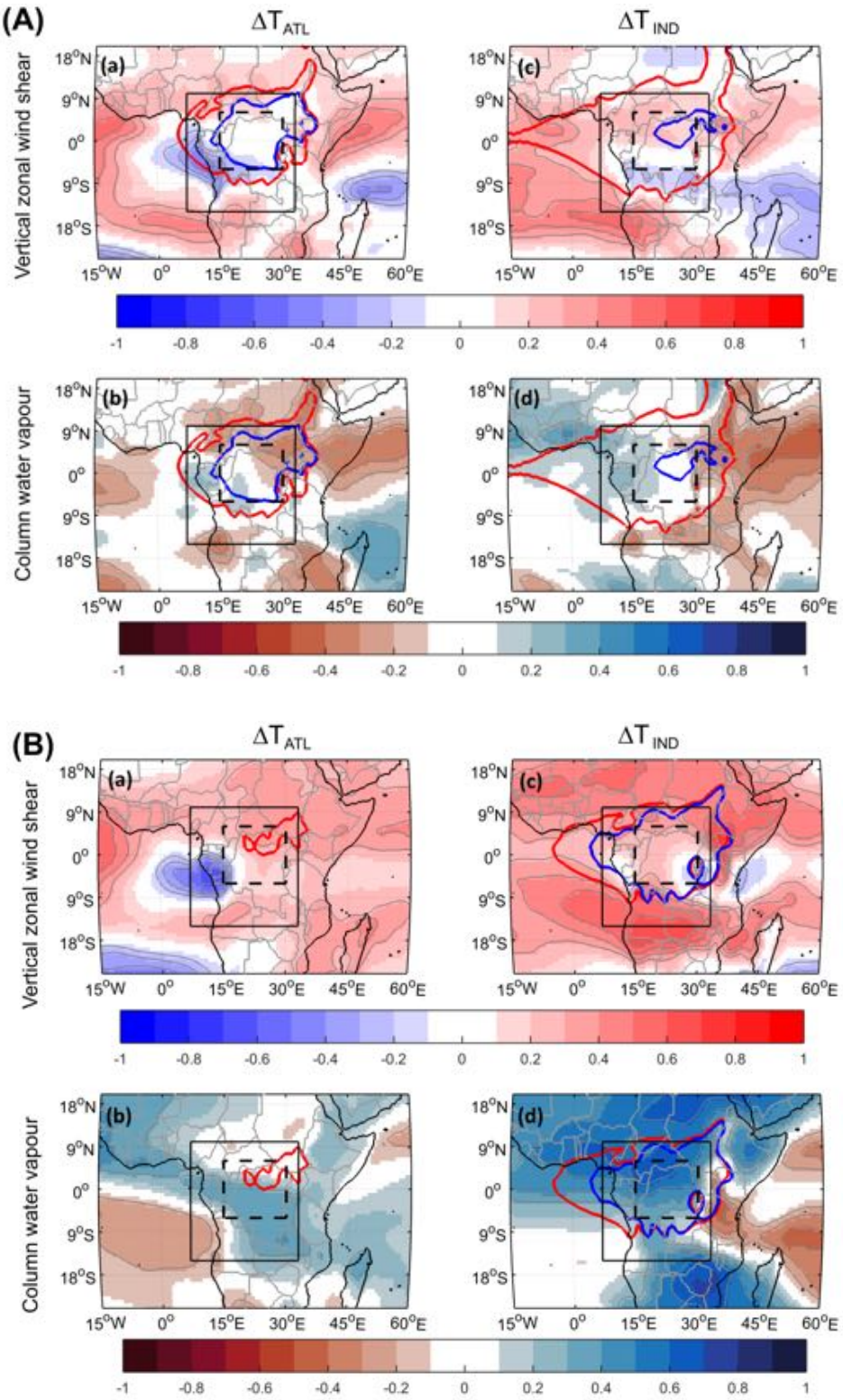

Fig. 6.7. Correlation coefficients between land-ocean thermal contrast and (top) vertical zonal wind shear and (bottom) column water vapour for (A) ERA-Interim and (B) ECHAM5.3. The vertical bar represents the zonal limit of Central Africa. Only significant correlation at $p < 0.1$ is plotted.

This anomalous westward wind shear pattern is consistent with the pattern of the friction term of the momentum balance (in October to April season, see chapter five; Fig. 5.3a). So, it appears that it is mainly the southern branch of the African easterly jet that conveys the Indian ocean water vapour into Central Africa landmass. This confirms that the southern branch of the Central African easterly jet distributes the rainfall over central Africa (see chapter five). Over East Africa, the anomalous eastward wind shear is associated with column water vapour deficit (Figs. 6.7a bottom left). This is due to anomalous mid-lower westerly that prevent the landwards of moisture flux from Indian Ocean. However, at the core of the Central Africa Low, the zonal wind shear and its associated column water vapour are very weak (Fig. 6.7a, left). This finding shows less supply of water vapour at the midst of Central Africa, emphasizing the blocking nature of the Central Africa Low (see chapter 4). Deepened convection occurs over the entire Central Africa region during the positive events of ΔT_{IND} (Indian), while during negative events, it further weakens and confines only over the northern edge of Congo basin region (Fig. 6.7a, top right). The induced anomalous zonal wind shear pattern is similar to that of ΔT_{ATL}, but with lower amplitudes. However, the anomalous mid-lower westerly jet associated with eastward wind shear is likely to bring more water vapour from the Atlantic Ocean, which rain out over Atlantic offshore region, while the reduced African easterly jet does not supply water vapour into Central Africa landmass (Fig. 6.7a, right). Over East Africa, the anomalous mid-lower westerly jet is associated with the anomalous column water vapour deficit (Fig. 6.7a, right), which is quite similar to the teleconnection between anomalous rainfall and the 2nd principal component of water vapour transport at the western boundary (Fig. 6.5, top). Moreover, I show, in Fig. 6.8, the mid-lower temperature distribution during intense and low rainfall years over central Africa. Intense rainfall years are defined as years when the normalized central Africa rainfall anomaly is greater than 0.5. The opposite lead to low rainfall years. The intense rainfall years are characterized by deepened Central Africa Low associated with more mid-lower tropospheric cooling over Central Africa landmass than over its surrounding oceans (Fig. 6.8a), with less atmospheric cooling occurring within the Central Africa Low 2580-gpm isoline (Fig. 6.8a) than over the neighbouring regions. Conversely, during low rainfall years, reduced convection, as suggested by the shrinking of the Central Africa Low 2580-gpm isoline, is associated with mid-lower tropospheric warming (Fig. 6.8b).

This apparent contradiction may be explained by the rainfall–temperature feedback mechanism. Strong surface heating warms up more the air over the vegetated Central Africa landmass than over its surrounding Oceans, resulting in a buoyant convective upward motion of the warm moist air (Hurley and Boos, 2003). Underneath, the rising motion of warm moist air generates a low-pressure system, namely the Central Africa Low (see chapter four). The saturation associated with the adiabatic cooling is conducive to convection. The condensation associated with deep convection increases the cloud cover, which in turn, is likely to block the solar insolation, and hence leads to less temperature over Central Africa landmass than over its adjoining oceans.

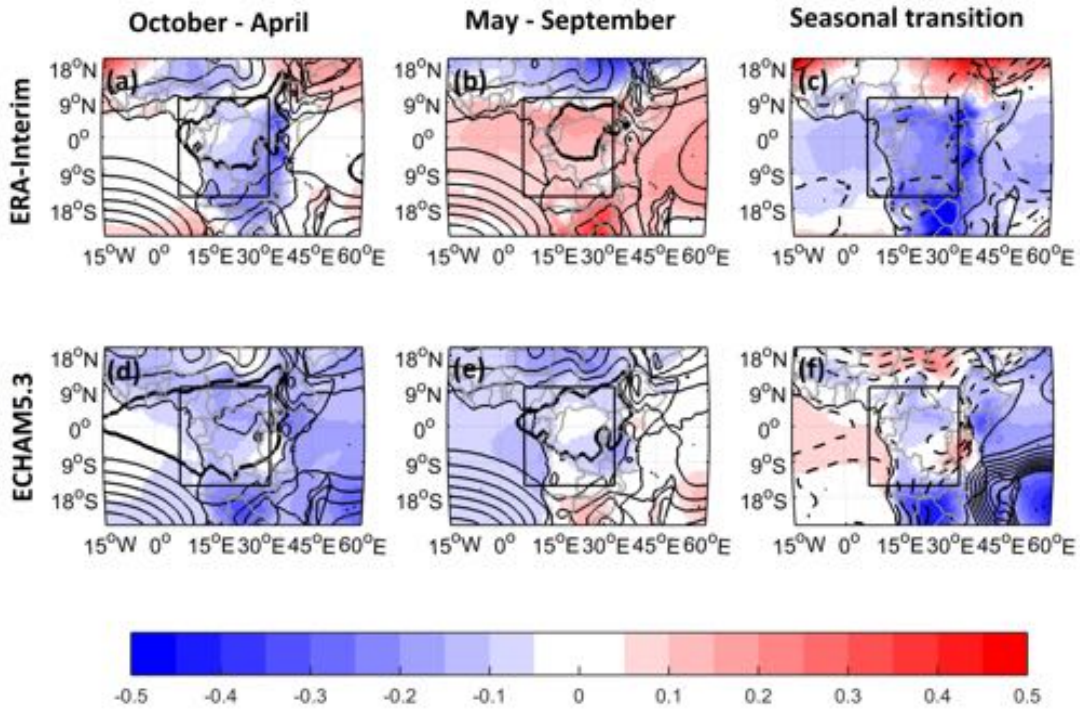

Fig. 6.8. Composite of mid-lower temperature (shaded, °C) and mid-lower geopotential thickness (contours, gpm) during (a) intense and (b) low rainfall years over central Africa for (a) ERA-Interim and (b) ECHAM5.3. Intense rainfall years are defined as years when the normalized central Africa rainfall anomaly is greater than 0.5

ECHAM5.3 does not well represent this mechanism due to the mid-lower land-ocean thermal contrasts to control the African easterly jet and its associated water vapour transport, through the zonal wind shear (Zhou et al. 2009; Fig. 6.7b). But the ECHAM5.3 has relatively well captured the rainfall–temperature feedback mechanism over central Africa. In addition, by comparing Figs. 6.7a and 6.8 (top), I find out that the reduction of the westward wind shear and meridional mid-tropospheric temperature gradient over central Africa is responsible for the strengthening of the northern central Africa easterly jet (Nicholson and Grist, 2003). Likewise, strengthened southern central African easterly jet is induced by intensified westward wind shear generated by high zonal mid-tropospheric temperature gradient (Holton, 2004).

6.7. Conclusion and discussion

To further the works of Vigaud et al. (2007, 2009) and Nicholson and Grist (2003), I first examine the vertical cross section of the atmospheric circulation and its associated water vapour transport from surrounding oceans at the zonal Central Africa boundaries i.e. at 15°E and 30°E respectively. This analysis confirms that strong mid-lower easterly jets convey atmospheric water vapour originating from the Indian Ocean towards the Atlantic Ocean and crossing the Central Africa

landmass. Also, over the Atlantic, a relatively weak low-level westerly jet carried additional water vapour into Central Africa landmass. The baroclinicity of the water vapor transport at the western boundary of Central Africa (15^{o}E) is strongly related to the mechanisms driving the low-level and mid-lower circulations over Central Africa respectively. The relative strong crossing mid-lower easterly moisture transport over Central Africa from the Indian ocean is driven by the Central Africa Low, while the low-level westerly water vapour transport is induced by the surface pressure gradient due to the near surface land-ocean thermal contrast (see chapters three, four and five). At its counterpart, eastern boundary (30^{o}E), the atmospheric water vapour transport is barotropic, with the strength of the water vapour transport strongly related to the atmospheric easterly circulation, which is due mainly to the intensity of the Central Africa Low (chapter four).

By the means of EOF analysis, the first two leading modes of water vapour transport variability showed a strong dependence on the two zonal boundaries of Central Africa region – the western at 15^{o}E and the eastern at 30^{o}E – as suggested by strong simultaneous correlations between their associated principal components. The first leading mode of the water vapour transport shows a dipole structure of mid-lower jet branches: westward for the southern branch and eastward for the northern branch. This leading mode displays a prominent low-frequency variability at the decadal time scale with about a 12 years' period. The second leading mode of variability, at interannual time scale, illustrates two poles of variability for the mid-lower easterly jets, with each pole located in each side of equator at around either 5^{o}S or 5^{o}N. This second mode of variability of water vapour transport at the western boundary (15^{o}E) is strongly connected to Central Africa rainfall anomalies. The composite analysis indicates that the impact of water vapour transport on regional rainfall is reminiscent of the influence of the Central Africa Low on regional rainfall. This is indicative of a positive feedback. Indeed, the Central Africa Low induces an easterly jet over Central Africa at mid-lower levels. These central African easterly jets conveyed more water vapour into Central Africa landmass, conducive to deep convection (Nicholson and Grist, 2003). The related water vapour transport influence strongly convection, as suggested by the Central Africa Low 2580-gpm isoline. And so, the Central Africa Low, in turn, affects the regional rainfall. In addition to this mechanism, the central African easterly jets influence the surrounding oceans SST, consistent with Venegas et al. (1997), with some contributions of ENSO. Finally, the combination of stronger Central African easterly jets and mid-lower tropospheric warming that enhance water vapour (and associated enhanced latent heat release) through Clausius-Clapeyron relation, is likely to lead to intense rainfall over Central Africa landmass. Thus, these results highlight a pronounced land-ocean contrast in the responses of mid-lower tropospheric temperature and hydrological cycle over Central Africa in ERA-Interim, while in the capability to represent this mechanism in ECHAM5.3 is limited.

Chap. 7

Understanding the Central Africa rainfall interannual variability and its relationship with surrounding Oceans

7.1. Introduction

Central Africa rainfall variability is primarily modulated by variation of large-scale circulation, rather than by variation in tropospheric water vapour (see chapters five and six). Controlled by the land-ocean thermal contrasts, the central African easterly jets are impacted by the sea surface temperatures (SST) over the surrounding tropical Atlantic and Indian Oceans (see chapter six). These findings lead to propose that the SST gradient between the two surroundings oceans might play a role to influence the Central Africa rainfall variation and strength. Although the relationship between Central Africa rainfall and its surrounding Oceans SSTs remains complex and seasonally dependent (Balas et al., 2007), the main objectives of this chapter are to: (i) revisit central Africa rainfall interannual variability; (ii) examine what are the nature of the physical mechanisms involved in the relationships between Central Africa rainfall variability and adjacent oceans by mean of an inter-basin SST gradient index; (iii) unravel how large-scale atmospheric circulation over Central Africa respond to this inter-basin SST gradient.

7.2. Datasets and methods

Ground-based datasets over Central Africa are sparse and sporadic (Washington et al., 2013). So,

for this study, we focus on post-satellite era monthly-mean Global Precipitation Climatology Project (GPCP) version 2.2 (Huffman et al., 2009) and Climate Prediction Center (CPC) Merged Analysis of Precipitation (CMAP; Xie and Arkin, 1997) for rainfall. For SST, we use the NOAA optimum interpolated (OI) SST version 2.2 (Reynolds et al., 2002) and Extended Reconstructed Sea Surface Temperature (ERSST, Smith et al. 2008). To analyse the atmospheric circulations that link the inter-basin SST gradient with Central Africa climate variability, we use horizontal wind, vertical velocities as well as the geopotential heights at different levels from ERA-Interim reanalysis (Dee et al., 2011). Stream functions are calculated as in chapter 3 to describe the Walker-type circulation over my area of interest. For the robustness of my results, we also use Hadley Centre's sea ice and SST (HadISST1, Rayner et al. 2003) for SST and CRUTS3.21 (Harris et al. 2013) for rainfall even if I do not include their figures in this study. We focus on 1979 to 2015 period where reanalysis datasets are also more reliable and GPCP and CMAP rain rate available, unless otherwise stated. Monthly anomalies are departures from their respective mean values averaged over the study period. The monthly anomaly data are averaged over the seasonal months to get the seasonal anomalies data and normalized by corresponding seasonal standard deviation for each season. Finally, the normalized anomalies are detrended linearly. All seasons are referred to those of the Southern Hemisphere, unless explicitly noted.

7.3. Revisiting Central Africa rainfall interannual variability

7.3.1. Seasonality of Central Africa rainfall

Central Africa rainfall seasonality is regulated by the Central Africa Low (see chapter four). The annual cycle of zonal-mean rainfall over Central Africa (averaged between 15^{o}-30^{o}E) shows a meridional displacement of rainfall associated with the seesaw of the Central Africa Low, with an increase in rainfall of up to 7 mm/d in JJA between 10^{o}N and equator (Fig 7.1a). This high rainfall corresponds to a monsoonal condition over western Africa and Sahel (Thorncroft et al. 2011), and it is associated with a weakening of the Central Africa Low (see chapter four). While high rain occurs in the northern edge of Central Africa, low rainfall occurs in the southern edge and vice versa (Fig. 7.1a). However, the meridional-mean rainfall over Central Africa (between 10^{o}N-10^{o}S) is controlled by the northward jump of Central Africa Low 2580- gpm isoline over the Arabian Sea (see chapter four). From May to September, decreased rainfall over Central Africa is associated with the weakening of the Central Africa Low (see chapter four; Fig. 7.1b). These four months have a mean rainfall, which is below the 25th percentile of annual rainfall (< 3.14 mm/d) respectively (Fig. 7.1c). Conversely, from September to April, high rainfall occurs over the entire Central Africa with increase (> 5mm/d) in October to December and in April/May, separated by a small decrease in December/January (Fig. 7.1b), while the Central Africa Low prevails. Three months (October, November and March) experience above normal rainfall conditions i.e. excessing 75th percentile (4.00 mm/d) and five months have almost normal conditions (September, December, January, February, April) as their rainfall distribution is between the 25th and 75th percentile (Fig. 7.1c).

Because of the strong influence of the Central Africa Low on Central Africa rainfall (see chapter four), the rainfall seasonality has almost a bimodal characteristic, with a long rainy (from September to April), when approximately more than seventy percent of annual rainfall occur and a short rainy season (May to August), when rainfall is reduced due to the weakening of Central Africa Low, indicative of subsidence. Additionally, there is no significant trend (-0.013 mm per decade) of Central Africa rainfall during the 1979 – 2015 study period, as shown in Fig. 7.1d using the mean rainfall between the GPCP and CMAP datasets. This is consistent with Lau and Wu (2007) who did not find any trend for rainfall over Central Africa from 1979 to 2003, but Yin and Grube (2010) and Diem et al. (2014) identified a strong decline of rainfall only in southern part of Congo basin in recent decades and it is attributed to the decrease of local evaporation and the large-scale ocean-atmospheric dynamics (Nogherotto et al., 2013; Lawrence and Vandecar, 2015) respectively.

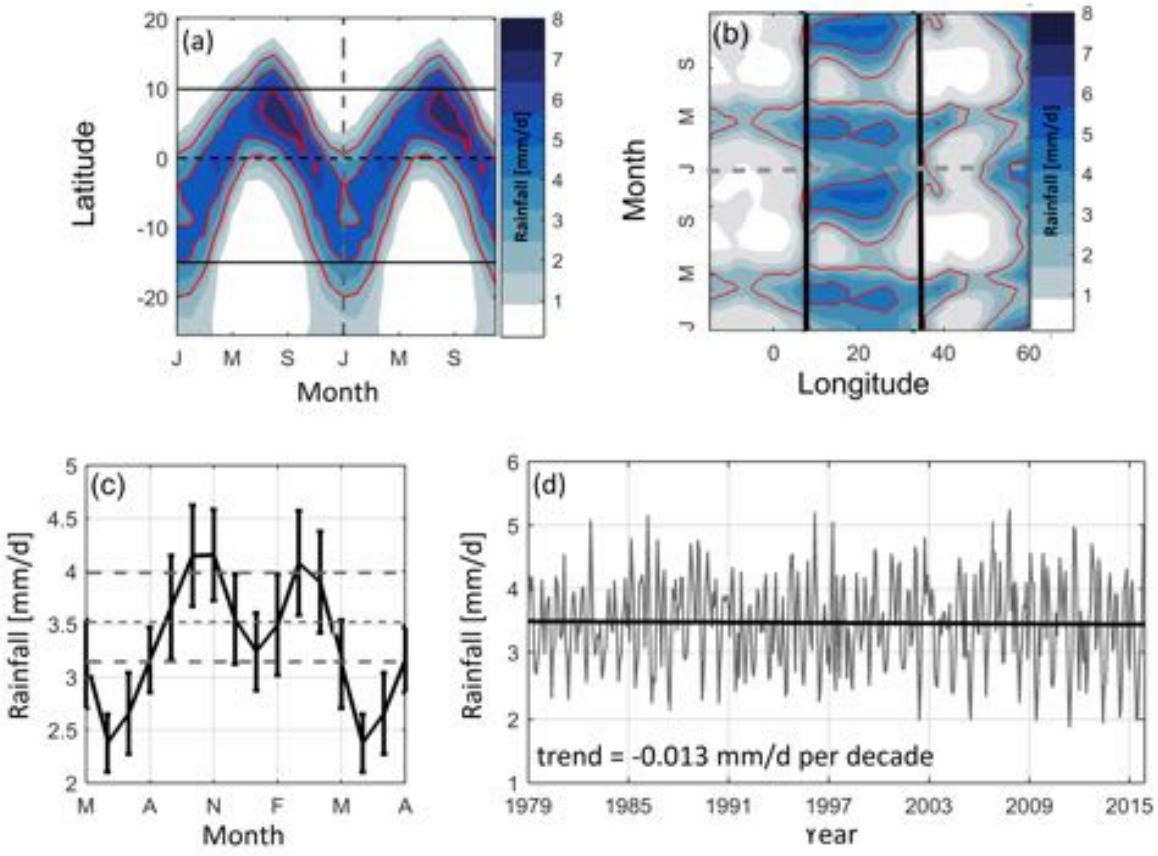

Fig. 7.1. The annual cycle of GPCP central Africa rainfall. Red contours in (a) and (b) represent the 3, 5 and 7 mm/d isoline respectively. In (c) the annual cycle start in May. In (a) to (c), the seasonal cycle is repeated twice. (d) Monthly times series and trend of Central Africa rainfall.

7.3.2. Interannual variability of Central Africa rainfall

Before to further investigate that interannual variability over Central Africa with respect to the seasons retained in the previous section, it is important to point that the persistence of the 8-month

(September to April) rainfall season over Central Africa is in fact strongly related to the quasi-permanent position of Central Africa Low (see chapter four). The seasonal evolution of rainfall over Central Africa does not show any substantial sub-seasonal signal in the spatial pattern and intensity (Fig. 7.1). To capture the essential features of central Africa rainfall variability, I apply the empirical orthogonal functions (EOF) analysis to explore the spatio-temporal variability of rainfall. To ensure the physical robustness of the EOF analysis, we remove the linear trend from the normalized rainfall anomalies at each grid point before applying the EOF analysis. The first two spatial patterns for long and short rainy seasons are shown respectively in Fig. 7.2. The first leading modes (EOF1) for the long rainy season (31.0% of total variance) and the short rainy season (35.0% of total variance) are characterized by a homogeneous pattern over central Africa that consists of above normal rainfall conditions, with strongest values centered either in Democratic Republic of the Congo (DRC) for the long rainy season or Atlantic offshore regions for the short rainy season (Figs. 7.2, left panels).

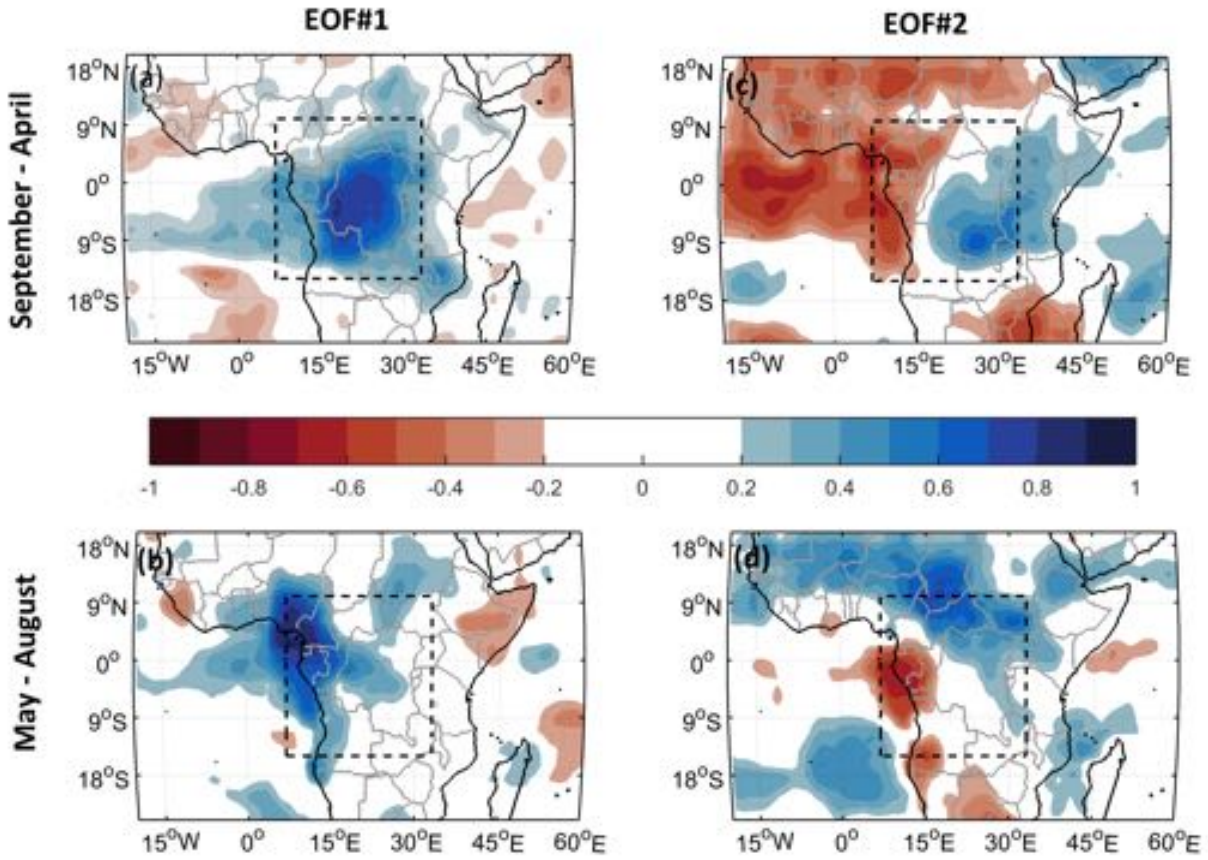

Fig. 7.2. The first two EOF patterns of Central Africa rainfall. The EOF analysis is performed over central Africa (7°E-33°E; 10°N-15°S) for (top) long rainy season (September to April) and (bottom) short rainy season. (left) EOF1 and (right) EOF2. These leading patterns are correlation coefficients between the two first principal components and rainfall anomalies. Only significant correlation at $p < 0.1$ is plotted.

To find out what could be the cause of this leading modes of rainfall variability, we plot in Fig. 7.3 (top panels), the correlation coefficients between the central Africa rainfall index, area-averaged between 10°N-15°S and 7°E and 33°E (dashed black box in Fig. 7.3), and rainfall anomalies during the long and short rainy seasons respectively. The correlation patterns of central Africa rainfall anomalies in both seasons resemble to the first leading modes of variability (EOF1-patterns), which support the existence of this homogeneous pattern over central Africa as its intrinsic mode of variability.

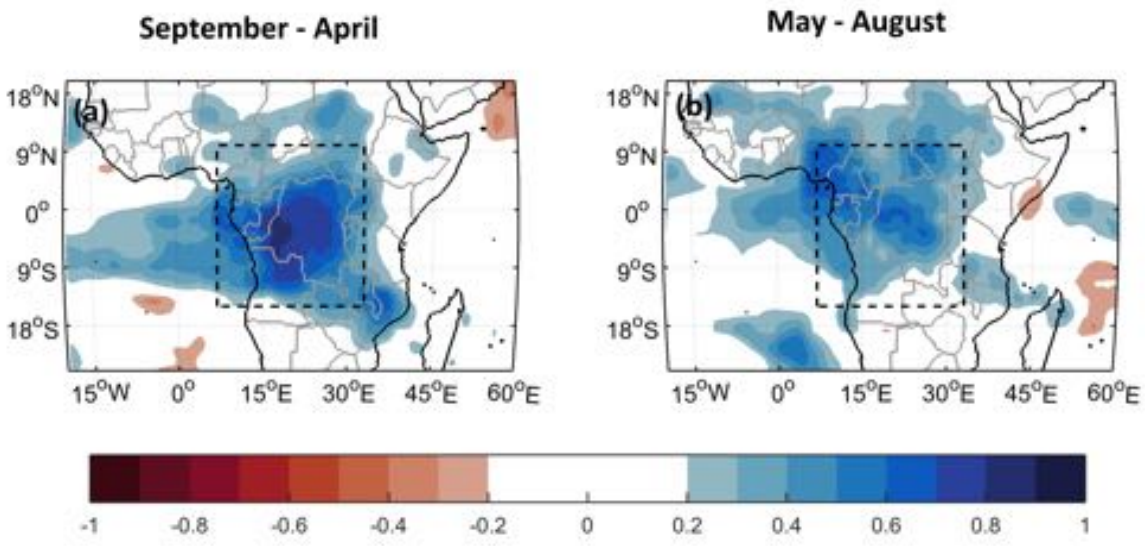

Fig. 7.3. (a) Correlation between Central Africa rainfall index (area-averaged between 7°-33°E; 10°N- 15°S) and rainfall anomalies (a) September – April (long rainy) season and (b) May – August (short rainy). Only significant correlation at $p < 0.1$ is plotted.

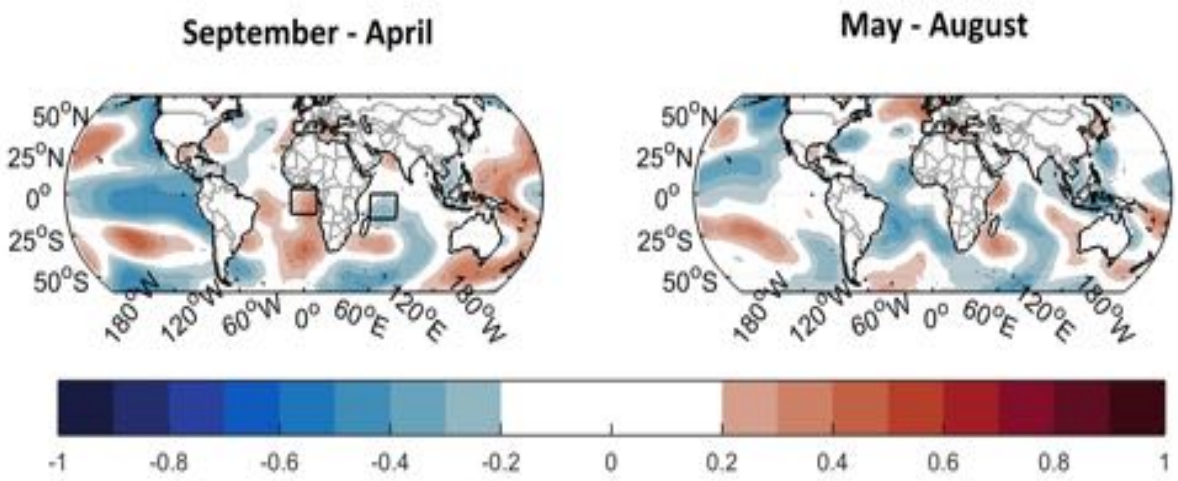

Fig. 7.3 (b). Correlation between Central Africa rainfall index (area-averaged between 7°-33°E; 10°N- 15°S) and sea surface temperature (SST) anomalies (left) September – April (long rainy) season and (right) May – August (short rainy). Only significant correlation at $p < 0.1$ is plotted.

The second mode of central Africa rainfall variability shows a dipole-like pattern that outlines opposite sign rainfall anomalies between Atlantic offshore regions and the eastern part of Central Africa (Fig. 7.2, right panels). During the long rainy season (September to April), the 2nd mode (EOF2, 18.4% of total variance) shows a rainfall deficit over Atlantic offshore regions (7°-15°E; 10°N-15°S) and West Africa and Sahel; and a rainfall surplus, over East Africa (Fig. 7.2c). This 2nd leading mode of Central Africa rainfall variability cannot only be explained by the Central Africa Low, even though the spatial pattern of the EOF-2 is reminiscent of the impact of the Central Africa Low on Central Africa rainfall, with opposite polarity between Atlantic offshore region and East Africa (see chapter four). But the impact of the Central Africa Low appears to extent to the Sahel where it is associated with below normal rainfall (Fig. 7.2c), while over Southern Africa, the rainfall deficit seems to be limited mainly over Mozambique, Zimbabwe and South Africa (northern east region) (Fig. 7.2c). In the short rainy season (May to August), the second leading mode (EOF2, 16.9% of total variance) features an out-of-phase pattern of rainfall anomalies orientated in a northwest–southeast direction, with dry rainfall anomalies along the Atlantic coast and southern Africa and wet rainfall anomalies from the Sahel to Central Africa, with the strongest values at the northern boundary of central Africa (Fig. 7.2d). This type of rainfall variability is not consistent with the weakening of the Central Africa Low, associated with the northward migration of the Central Africa Low 2580- gpm isoline (see chapter four).

What are the causal factors governing the fundamental patterns of central Africa rainfall variability during these two distinct rainy seasons? Explaining the mechanisms behind these rainfall patterns could help not only to understand central Africa rainfall variability, but also to predict its variability. To find which oceans areas are most important for central rainfall variability, we correlate the central Africa rainfall index with global SST anomalies in both seasons. During the long rainy season, the normalized SST anomaly features a distinctive warm basin-wide Atlantic (5°W-7°E; 3°N-10°S) and cold south Indian Ocean (50°-70°E; equator-15°S) (Fig. 7.3c). The highest correlation between central Africa rainfall and global SST anomalies is found over equatorial central Pacific, and amount to around -0.4 ($p < 0.005$, Fig. 7.3c). This suggests that ENSO impacts central Africa rainfall variability (Balas et al., 2007; Dezfuli and Nicholson, 2012; Nicholson and Dezfuli, 2012), even though a large fraction of central Africa rainfall variance remained unexplained. However, throughout regionalisation methods over Central Africa rainfall, some studies (Dezfuli and Nicholson, 2012; Nicholson and Dezfuli, 2012; Balas et al. 2007) found stronger correlations while considering either Atlantic offshore regions or over East central Africa. For the short rainy season, tropical Indian Ocean depicts an IOD pattern (Fig. 7.3d), with warm western tropical Indian (west of 60°E) associated with higher rainfall and cold eastern Indian associated with lower rainfall. These results in both long and short rainy seasons confirm the

existence of a SST anomaly gradient between tropical Atlantic and Indian SSTs that can modulate Central Africa rainfall variability, consistent with Dezfuli and Nicholson 2012) and Balas et al. (2007).

7.4. Definition of the interbasin sea surface temperature between tropical Atlantic and Indian Oceans

Before to test the hypothesis that the SST anomaly gradient between tropical Atlantic and Indian Oceans influences central Africa rainfall variability, we define the inter-basin SST gradient index (hereafter ΔSST) as the difference between the detrended normalized SST anomaly area-averaged over western tropical Atlantic (tropical Atlantic index, 10°W-10°E; 3°N-12°S) and the western tropical Indian index, 50°-70°E, 0°N-15°S). We plot the ΔSST index in long (September to April) and short (May to August) rainy seasons in Fig. 7.4. We note that for the 1979-2015 period, the ΔSST amplitude weakens, with a linear trend of -0.17°C per decade for long rainy season, and -0.15°C per decade for short rainy season (grey line, Figs. 7.4, top panels).

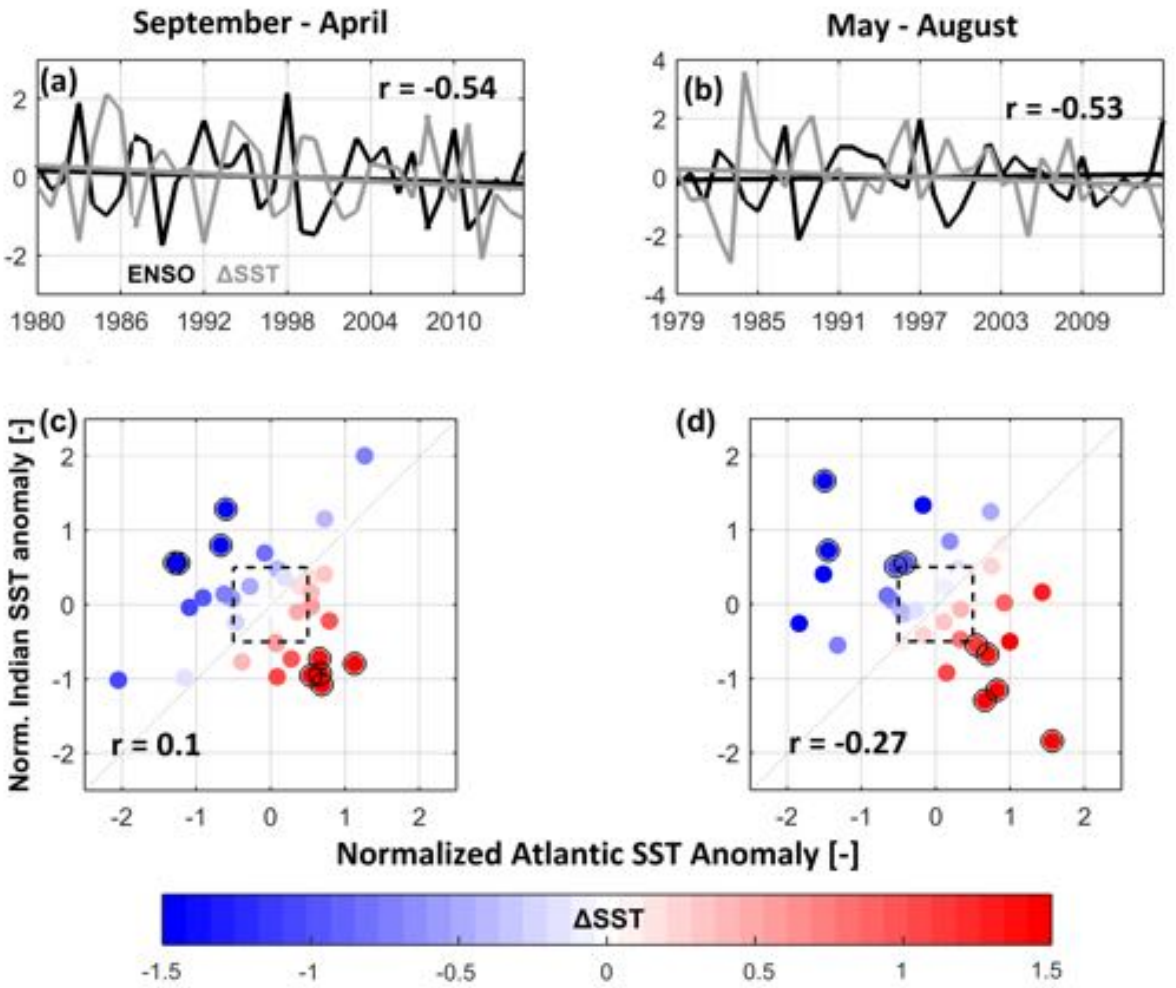

Fig. 7.4. (top) Time series of inter-basin SST anomalies gradient (ΔSST, grey line) and ENSO (black line). (bottom) Scatterplot of normalized Atlantic SST anomaly vs normalized Indian SST anomaly. In

each panel, shading of dots corresponds to ΔSST and back dashed lines are the ± 0.5 standard deviations. (left) long rainy season and (right) short rainy season. The diagonal of slope 1:1 is also visible in the bottom panels.

No significant correlation has been found between Atlantic and Indian Oceans during long rainy (September to April) season. The two oceans are not well correlated (-0.27, p <0.005) during the short rainy (May to August) season, meaning that the Atlantic and Indian oceans SST variability are independent of each other. However, accordingly to ΔSST, the tropical Atlantic Ocean SST anomaly variability is mirroring the tropical Indian Ocean anomaly with respect to the diagonal (of slope of 1:1), but with opposite sign in both seasons (Fig. 7.5, bottom panels). In addition, the ΔSST is strongly anti-correlated with ENSO (r = -0.5, p<0.001), indicating that ENSO partially controls the ΔSST variation (Figs. 7.5, top panels). When the El Niño condition is dominant over equatorial central Pacific, the ΔSST is negative i.e. cooling of tropical Atlantic and warming of Indian Ocean associated with a positive IOD-pattern (Figs. 7.6, top panels). La Nina conditions leads to the warming of tropical Atlantic and cooling of Indian Ocean. Likewise, the ΔSST teleconnection with global SST anomaly shows similar ENSO-like pattern, but with opposite polarity (Figs. 7.6, bottom panels). Also, there is a reminiscent of Atlantic Nino-like pattern over tropical Atlantic (Xie and Carton, 2005; Lübbecke and McPhaden, 2013) and cooler SST anomalies over basin-wide Indian Ocean for both seasons (Figs. 7.6, bottom panels).

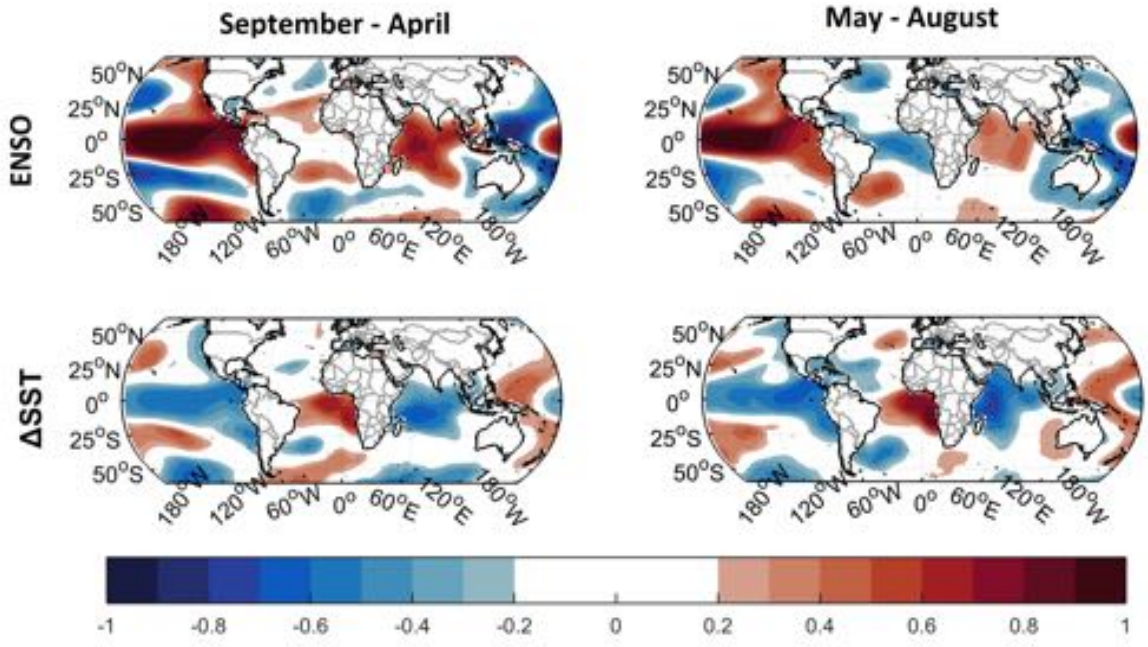

Fig. 7.5. Correlation coefficients between SST anomalies vs (top) ENSO and (bottom) ΔSST. (left) long rainy season and (right) short rainy season. Only significant correlation at p < 0.1 is plotted.

To characterize the inter-annual SST signals associated with ENSO, we use an index similar to the Nino3.4 index, which is calculated by area averaging the SST anomalies over (5°N-5°S, 170°-120°W) over equatorial central Pacific (Trenberth, 1997) and normalized it by dividing with standard deviation. For our study period, the Pacific Ocean cools moderately with a linear trend of -0.1^{o}C per decade (black line, Fig. 7.5, top left), corresponding to a La Niña-like cooling pattern (Huang and Xie, 2015; Bellanger et al. 2014; Christensen et al. 2013). In contrast, in the short rainy season, the Pacific SST increases, with a linear trend of 0.054^{o}C per decade (Fig. 7.5, top right).

7.5. Regional rainfall and atmospheric large-scale circulation associated with ΔSST

7.5.1. Regional rainfall

To explore the mechanisms underlying the influence of ΔSST, I examine in detail the composites of rainfall over central Africa and mid-lower tropospheric (1000- to 500- hPa) layer thickness to highlight the role of Central Africa Low and subsidence for extremes events of the positive and negative phases of ΔSST in Figs. 7.7. The composite difference between these both phases of ΔSST is also plotted. A Positive phase of ΔSST is defined when the detrended normalized ΔSST index that is greater than 1 standard deviation, and in the same time tropical Atlantic and Indian experience simultaneously warm (> 0.5 standard deviation) and cold (< -0.5 standard deviation) SST anomalies (Fig. 7.5, bottom panel) respectively. This indicates an Atlantic warming. The opposite condition leads to the negative phase, indicative of Indian Ocean warming. For the long rainy season, the positive phase of ΔSST corresponds to the 5 following years: 1985, 1986, 1994, 2008 and 2011, while the negative phase of ΔSST occurred during the 4 following years: 1983, 1987, 1992 and 2012. Whereas for short rainy season, years of positive phase of ΔSST are 1984, 1989, 1996, 1999, 2002, and years of negative phases are 1980,1981,1982,1983 (Table 7.1).

Table 7.1. The years corresponding to positive and negative phases of ΔSST in September-April and May-August respectively.

	Positive phase of ΔSST	Negative phase of ΔSST
September – April	1985, 1986, 1994, 2008 and 2011	1983, 1987, 1992 and 2012
May – August	1984, 1989, 1996, 1999 and 2002	1980,1981,1982 and 1983

For the long rainy season, the positive phase of ΔSST (Atlantic warming) is characterized by strong convection, lower than normal Central Africa Low pressure over tropical Africa region, with rainfall surplus over the Atlantic offshore region (07^{o}-15^{o}E; 10^{o}N-15^{o}S) and southern Africa, and rainfall deficit

over Ethiopia (Fig. 7.7a). For the negative phase of ΔSST (Indian warming), the Central Africa Low weakens and shrinks to be confined between 15°E-33°E; 10°N-6°S, conducive to shallow convection (Fig. 7.7b). This weakening of the Central Africa Low is accompanied with reduced rainfall from the equatorial Atlantic regions to southern Africa, and with enhanced rainfall anomalies from the southern edge of central Africa (Katanga, DRC) to south western Indian Ocean (Fig. 7.7b). The core of the Central Africa Low is associated with no substantial change of rainfall (Fig. 7.7a). This means that the influence of ΔSST and major processes are very low there.

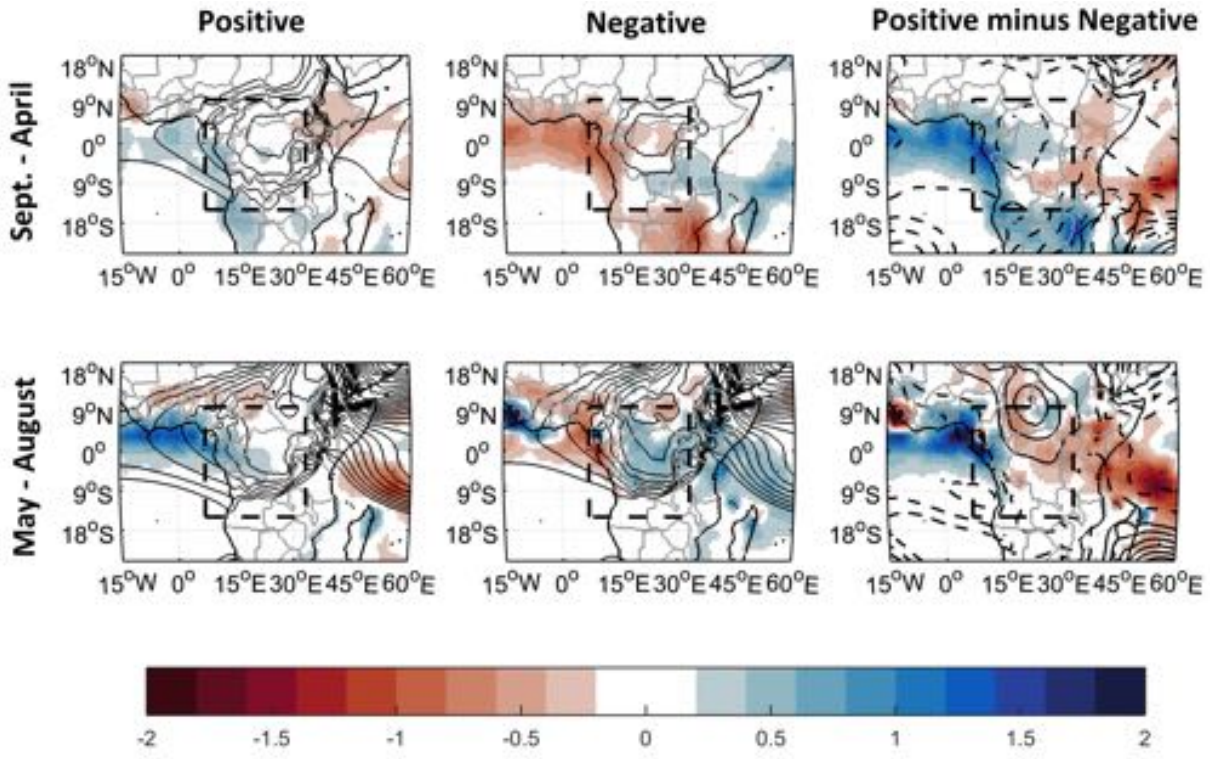

Fig. 7.6. Composite of rainfall anomalies (shaded, mm/d) and mid-lower geopotential thickness (Central Africa Low, contours, gpm) during (left) positive; (middle) negative and (right) positive minus negative phase of ΔSST. The Contour interval for the Central Africa Low is 2 gpm from 2560 to 2580 gpm and from 2580 to 2620 gpm for long and short rainy respectively.

The composite difference (Fig. 7.7c) of rainfall and geopotential thickness anomalies during both ΔSST phases shows Central Africa rainfall contrast, with above normal rainfall over Atlantic Offshore region and below normal rainfall over East Africa (from 30°E to beyond). This substantiates the fact that the core of the Central Africa Low separate two distinct areas of opposite rainfall pattern over central Africa (Fig. 7.7c), referred as poles of rainfall variability by Dezfuli and Nicholson (2012), and associated with a zonal pressure gradient between the Central Africa landmass and adjacent tropical Oceans (eastern Atlantic and western Indian). This mid-lower

tropospheric pressure gradient between central Africa landmass and southern Atlantic and Indian Oceans indicates a crucial role play by the land-ocean thermal contrasts (see chapter six). A similar rainfall contrast pattern over Central Africa was reported in December to March by Dezfuli et al. (2015) over south Equatorial Africa (10^{o}E – 40^{o}E; equator – 12.5^{o}S), called zonal asymmetric pattern, while using daily precipitation data. The zonal asymmetric pattern is driven by a diagonal interhemispheric pressure gradient between the northern Atlantic Ocean and southern western Indian (Dezfuli et al. 2015). Furthermore, this pattern is reminiscent of the impact of Central Africa Low on regional rainfall over central Africa. This result confirms that Central Africa rainfall contrast is primarily controlled by Central Africa Low variability, which, in turn, is modulated by the inter-basin SST gradient, with a major contribution of ENSO (Table 7.2).

Table 7.2. Correlation between Oceanic indices and Central Africa Low in September-April and Central Africa High in May-August. All indices have been detrended before computing the correlation. The correlation in bold is significant at $p < 0.1$.

	Atlantic	Indian	ΔSST	ENSO
Central Africa Low (15-30^{o}E;5^{o}N-5^{o}S)	-0.11	**0.73**	**-0.61**	**0.86**
Central Africa High (15-30^{o}E;5^{o}N-5^{o}S)	**-0.27**	0.18	**-0.29**	**0.49**

For the short rainy season, the Atlantic warming (positive phase of ΔSST) is associated with higher than normal Central Africa High pressure. The geopotential thickness over Central Africa (Central Africa High) highlights an interhemispheric pressure gradient between high pressure over southern Atlantic and Indian Oceans and low pressure over Central Africa landmass (centered at 25^{o}E;10^{o}N). This interhemispheric pressure (geopotential thickness) gradient is associated with above normal rainfall over equatorial Atlantic Offshore regions and below normal rainfall in western Indian (Fig. 7.7d). It is also important to note that the Sahel is associated with rainfall deficit (Fig. 7.7d) at that time. The rainfall pattern associated with the Atlantic warming is reminiscent of the impact of the land-ocean thermal contrast on regional rainfall over Central Africa, even though with opposite polarity of rainfall anomalies (see chapter six). During Indian warming (negative phase of ΔSST), the interhemispheric pressure gradient between southern Oceans and Central Africa landmass intensifies, leading to above normal rainfall over West Africa, Central Africa, East Africa and Indian Ocean regions (Fig. 7.7e). The Sahel and equatorial Atlantic are associated with below normal rainfall (Fig. 7.7e). This finding is consistent with Bader and Latif (2006) who found that both Atlantic and Indian Oceans influence rainfall in Sahel and West Africa. The composite difference between the two phases of ΔSST outlines not only the interhemispheric pressure gradient between southern Atlantic and Indian Oceans and Central Africa landmass, but also the land-ocean pressure contrast between Central Africa landmass and its surroundings Oceans (Fig.

7.7f). This land-ocean pressure contrast, with anomalous subsidence over Central Africa landmass and anomalous low-pressure over surrounding Oceans, is likely to prevent further landwards advection of water vapour originating from surroundings tropical Oceans, leading to rainfall surplus over West Africa and rainfall deficit over Central Africa and East Africa (Fig. 7.7f). The land-ocean pressure contrast is generated by the land-ocean thermal contrast, as suggested by the geopotential thickness which is a better approximation of the heat content of the atmospheric layer (Turrent and Cavazos, 2009). In addition, the Central Africa High may affect the Central Africa hydroclimatic variability by regulating water vapour transport through an atmospheric teleconnection with ENSO (~0.5,.Table 7.2), with a minor contribution from ΔSST, as suggested by the weakness of the connection between the Central Africa High and ΔSST (~ -0.3, Table 7.2).

7.5.2. Large-scale atmospheric circulation

To unravel what the mechanisms are shaping the zonal contrast of central Africa rainfall anomalies patterns associated with ΔSST, we examine the large-scale atmospheric circulation, described by the zonal mass-weighted streamfunctions over central Africa (Fig. 7.9). In addition, to each panel in the Fig. 7.9, the zonal variation of central Africa mean-rainfall is plotted for both ΔSST events and seasons (long and short rainy seasons respectively).

The annual cycle of the zonal large-scale dynamics over Central Africa is characterized by the dominant easterly circulation associated with strong ascending motion over Central Africa landmass and descending branches over its surroundings Oceans (Figs. 7.7d-e). At low-levels, a shallow anticlockwise overturning cell emerges over central Africa landmass, with the rising branch at 24^{o}E and the descending branch at around 0^{o}E (Figs. 7.7d-e). This shallow zonal overturning cell, namely Congo Basin Cell, is generated by the near-surface land-ocean thermal contrast, with higher surface temperature over central Africa landmass than over its surrounding Oceans (see chapters three and six). At surface, the resulted land-ocean pressure gradient triggers the low-level westerly jet from Atlantic Ocean that returns the air mass landwards, where it meets the low-level easterly jet from Indian Ocean, constituting the Congo air boundary (Tierney, 2011). In the meantime, at mid-levels, both the Central Africa Low and tropospheric land-ocean thermal contrast controls the Central African easterly jet (see chapters four, five and six) that closed the Congo basin Cell.

a. Zonal atmospheric dynamics related to different phases of ΔSST

For the short (May to August) rainy season, the Atlantic warming phase (positive phase of ΔSST) is associated with the decreased mid-lower easterly jets, which are associated with strong reduction of subsidence over a warm Atlantic, as suggested by the negative anomalous overturning cell (Fig. 7.7, bottom left). This is conducive to convective rainfall over Atlantic, indicative of a westward shift of vertical motion (Fig. 7.7, bottom left). This suggests that positive Atlantic SST anomalies is likely to destabilize the atmospheric column, which lead to convective

activity and so to relative high rainfall (Fig. 7.7, bottom left). This finding indicates that the Atlantic Ocean is likely to lead the atmosphere (see also chapter five). At the same time, over Central Africa landmass, the mid-lower easterly jet has slightly strengthened, owed by the tropospheric land-ocean pressure gradient between the Central Africa Low pressure and the high-pressure systems over Atlantic and Indian Oceans (Fig. 7.6, bottom left). During Indian Ocean warming (negative phase of ΔSST), the intensification of the tropospheric land-ocean pressure gradient (Fig. 7.6, bottom middle) is associated with reduced vertical motion, which weakens further the African easterly jets over Central Africa (Fig. 7.7, bottom middle), indicative of shallow convective rainfall in this region (Fig. 7.7, bottom middle).

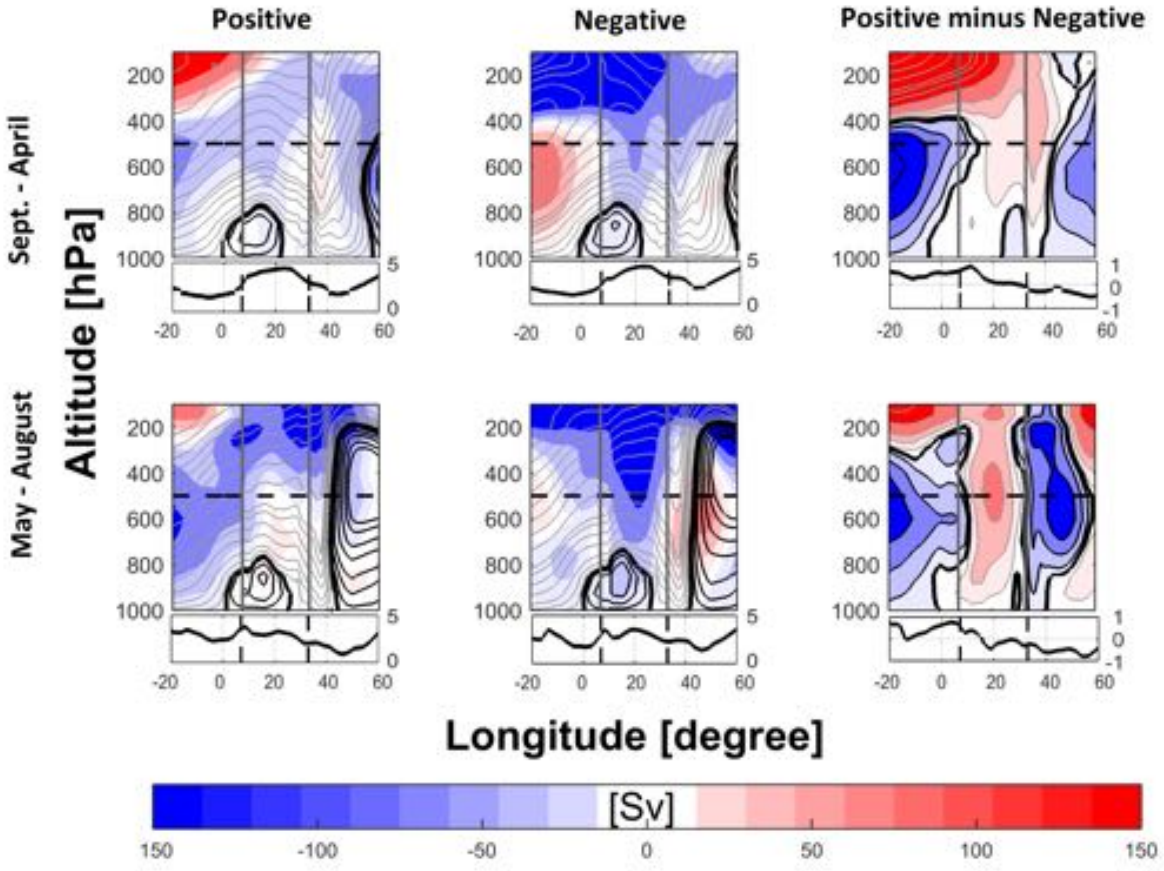

Fig. 7.7. Composite of the mean zonal mass-weighted streamfunctions (contours, Sv) and their associated anomalies (shaded, Sv) during (left) positive; (middle) negative and (right) positive minus negative phase of ΔSST for observations. (Bottom) zonal variation of regional rainfall over central Africa.

In addition, warm Indian Ocean generates a positive anomalous overturning cell that strengthens the subsidence over East Africa (Fig. 7.7, bottom middle panel) and enhances convection over western Indian Ocean (beyond 40^{o}E, Fig. 7.7, bottom middle panel). This indicates an eastward shifting of strong vertical motion towards western Indian Ocean, suggesting that the tropical Indian

Ocean SST anomalies leads the overlying atmospheric circulation (see chapter six). On the other hand, over the relative cold Atlantic SST, the mid-lower easterly jet slightly strengthens (Fig. 7.7, bottom middle panel). The composite difference between the positive and negative phase of ΔSST (Fig. 7.7, bottom right) outlines an opposite atmospheric circulation over central Africa landmass and its surroundings Oceans. Indeed, a shallow anomalous clockwise overturning cell, centered at ~21^{o}E; 500- hPa, encompasses the entire Central Africa, with the ascending branch at its western boundary (~7^{o}E) and descending branch at its eastern boundary (~33^{o}E, Fig. 7.7, bottom right). Over surrounding Oceans, strong anomalous anticlockwise overturning cells are dominant (Fig. 7.7, bottom right). Therefore, it is the presence of the anomalous clockwise overturning circulation over Central Africa that is responsible of the formation of the zonal contrast of rainfall anomalies over Central Africa, with rainfall surplus over Atlantic offshore regions and rainfall over East Africa (Fig. 7.7, bottom right). This finding is quite similar to the zonal asymmetric pattern over the entire southern Central Africa found by Dezfuli et al. (2015) while they examined daily atmospheric data from December to March, although with opposite circulation.

For the long rainy (September to April) season, when the Atlantic warms (positive phase of ΔSST), reduced midlevel Central African easterly jet is associated with a slight decrease of rising motion over Central Africa, but strong enough to sustain deep convection (Fig. 7.7, top left). Over Atlantic, the weakening of the mass-weighted streamfunctions is conducive to relatively strong rising motion associated with the Atlantic warming (positive SST anomalies over Atlantic, Fig. 7.7, top left). Meanwhile, over East Africa and Indian Ocean, the slight increase of the mass-weighted streamfunctions is indicative of strong subsidence, conducive to cold SST (Slawinska et al. 2014, Fig. 7.7, top left). On the other hand, during Indian Ocean warming (negative phase of ΔSST), an anomalous clockwise overturning cell is induced over a colder Atlantic Ocean, suggesting strong subsidence, which suppress convection and lead to less rainfall (Fig. 7.7, top middle). Nevertheless, weaker African easterly jet from western Indian to central Africa is associated with warmer tropical Indian Ocean (Fig. 7.7, top middle). Slowing down of upward motion over central Africa indicates an occurrence of anomalous subsidence. The composite difference, between positive and negative phase of ΔSST, highlights a similar opposite anomalous circulation over Central Africa and its surroundings Oceans, but with weaker amplitudes than during short rainy season, namely zonal asymmetric pattern (Dezfuli et al. 2015) (Fig. 7.7, top right).

b. Meridional dynamics associated with ΔSST events

To understand also the mechanisms leading to the meridional variation of rainfall over Central Africa, it is important to examine the meridional large-scale circulation. Above all, the meridional mass-weighted streamfunctions show the symmetrical overturning Hadley cells over central Africa, one in each Hemisphere, with their rising motion at around 10^{o}N and the downward motion over subtropical latitudes (Fig. 7.8). The Central Africa rainbelt, defined as a region of high rainfall, is driven more by midlevel rising motion, indicative of deep convection (Figs. 7.8) than by the surface

rising motion (see chapter three). Due to the thermally direct nature of the Hadley cells over Central Africa, this inconsistency is explained by the evaporative cooling related to the vegetal surface of Central Africa (see chapter three). Furthermore, at near-surface, the motion is cross-equatorward in the southern Hemisphere and equatorward in northern Hemisphere (Figs. 7.8). At upper levels, the flow is poleward in both hemispheres (Figs. 7.8). However, the northern Hadley cell is much stronger than the southern Hadley cell with respect to their respective intensity (Figs. 7.8).

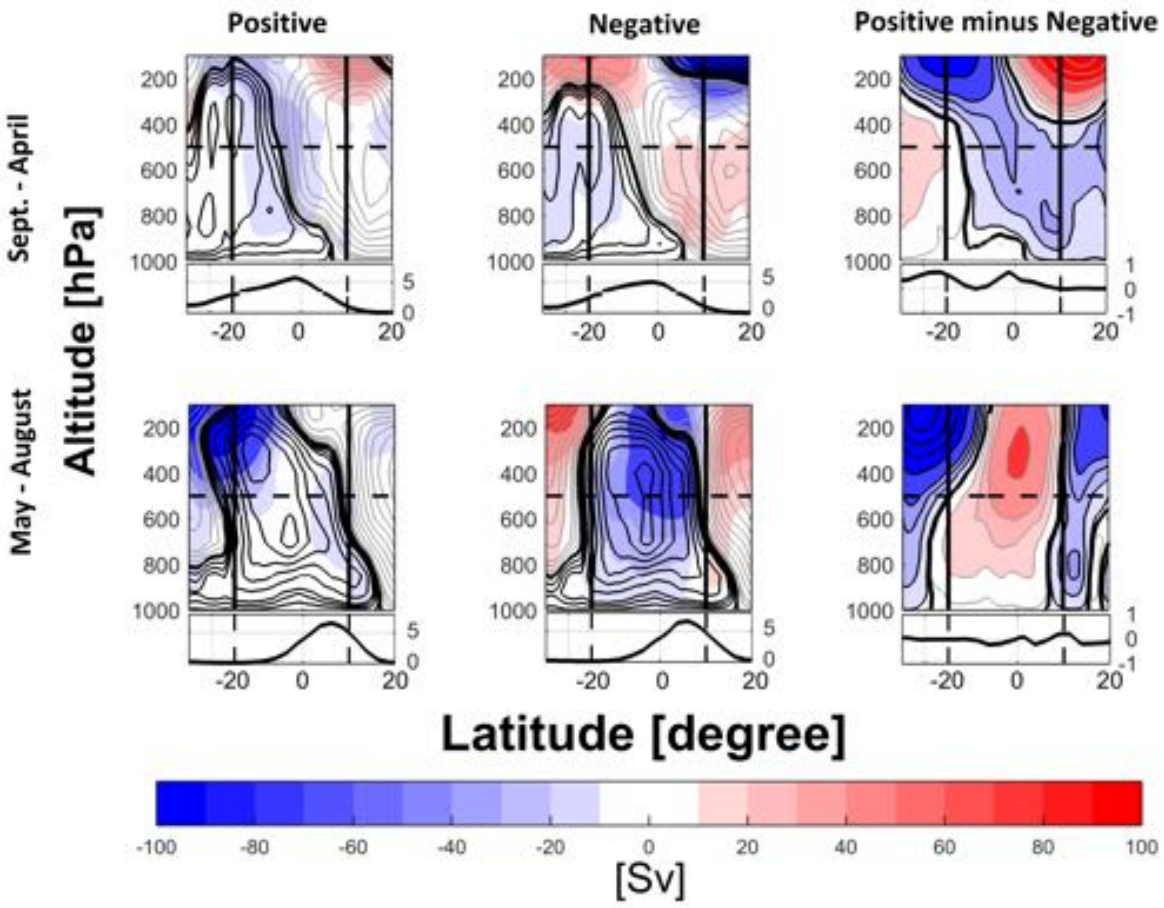

Fig. 7.8. Composite of meridional mass-weighted streamfunctions anomalies (shaded, Sv) and mean (contours, Sv) during (left) positive; (middle) negative and (right) positive minus negative phase of ΔSST for observations. (Bottom) Meridional variation of regional rainfall over central Africa

In the long rainy season, during Atlantic warming (positive phase of ΔSST), deepened Central Africa Low induces an anomalous negative shallow overturning cell, centered at 0^{o}N; 500- hPa (Fig. 7.8, top left). This anomalous overturning cell over central Africa enhances the upward motion around the equator for the Hadley cell in the southern hemisphere, leading to more convective rainfall, while reducing the rising motion in the northern hemisphere, suggestive of subsidence (Fig. 7.8, top left). At upper levels, the ΔSST reinforces the poleward circulation in both hemispheres (Fig. 7.8, top left). Whereas during the Indian Ocean warming (negative phase of

ΔSST), the ΔSST tends to strengthen the mid-lower circulation of both symmetric Hadley cells, while reducing the poleward flow at upper levels in both Hemispheres (Fig. 7.8, top middle). The composite difference of ΔSST positive and negative events suggests that rainfall surplus in southern Africa is due to reduced subsidence at mid-lower levels, while between 5°S-15°S, Central Africa rainfall deficit is due to the anomalous circulation downward motion (Fig. 7.8, top right). Near the equator, the relative rainfall surplus is owed by the anomalous ascending motion in mid-troposphere (Fig. 7.8, top right).

From May to August (short rainy season), a strong anticlockwise Hadley cell encompasses the entire central Africa troposphere, with a rising branch at around 15°N and downward branch at around 15°S (Figs. 7.8, bottom panels). During the short rainy season, the Central Africa Hadley cell has the same thermodynamic properties as during the long (September to April) rainy season. At near surface and upper levels, the flow is poleward (Figs. 7.8, bottom panels). During the Atlantic warming (positive phase of ΔSST), the vertical motion of the Central Africa Hadley cell is slightly reinforced, meaning more convective rainfall in the northern edge of Central Africa and less rainfall due to subsidence in southern Africa (Fig. 7.8, bottom left). The strengthening of the Central Africa Hadley cell (Fig. 7.8, bottom middle) occurs during the warming of the Indian Ocean (negative phase of ΔSST). But a confined weaker circulation occurs at low-levels between 10°N-15°N and at the subsiding branch (beyond 15°S), as suggested by small positive mass-weighted streamfunctions anomalies (Fig. 7.8, bottom middle). The composite difference of ΔSST events shows opposite circulation cells between Central Africa and its surroundings subtropical regions: anomalous positive overturning cell over entire central Africa – centered at 0°N; 300- hPa – associated with less rainfall anomalies due to subsidence (Fig. 7.8, bottom right). Over surrounding subtropical regions, the anomalous negative overturning cell is dominant, with high values at upper levels (Fig. 7.8, bottom right). In addition, above normal rainfall at the northern boundary of Central Africa (10°N) is associated with a shallow overturning cell at low-levels (Fig. 7.8, bottom right). Furthermore, there is no migration of the ITCZ (defined as maximum of rainfall) over Central Africa as highlighted by the difference of ΔSST events (Fig. 7.8, bottom right). This finding is inconsistent with Balas et al. (2007) who speculated a meridional displacement of ITCZ over Central Africa when surrounding Oceans have opposite sign. In addition, the longitudinal variation of Central Africa rainfall shows a gradual reduction of rainfall with longitude, with enhanced rainfall over Atlantic and reduced rainfall over Indian Ocean.

7.6. A proposed mechanism

The inter-basin SST anomalies gradient (ΔSST) between Atlantic and Indian oceans influence the central Africa rainfall anomalies through the modulation of the Central Africa Low and High, which lead to a zonal rainfall contrast over Central Africa. Indeed, the strengthening of the African easterly jets over cold surrounding Oceans SST anomalies suggests a strong influence of land-ocean

atmospheric circulation pressure gradient on tropical Atlantic and Indian Oceans. Indeed, intrinsic modes of the African easterly jet variability imprint themselves on the SST anomalies patterns via the mid-lower zonal wind-shear. Warmer SST anomalies over Atlantic and Indian Oceans are conducive to induce anomalous convection, with upward motion at low-levels capped by subsidence at mid-levels, as indicated by negative mass-weighted streamfunctions anomalies (Fig. 7.9b-c). On the other hand, the weakening of the Central African easterly jets is associated with the weakening of the Central Africa Low. Weakened atmospheric circulation over Central Africa associated with the Central Africa Low area change is likely to induce a shallow anomalous overturning over central Africa, with a rising branch at its western boundary (~7^{o}E) and descending branch at its eastern boundary (~33^{o}E, Fig. 7.9f), which has a structure opposite to the zonal asymmetric pattern proposed by Dezfuli et al. (2015). Thus, it is this induced anomalous midlevel overturning cell over central Africa that shapes the zonal contrast of central Africa rainfall. This mechanism is also evident during the short rainy season, although the Indian Ocean is likely to drive the overlying African easterly jets.

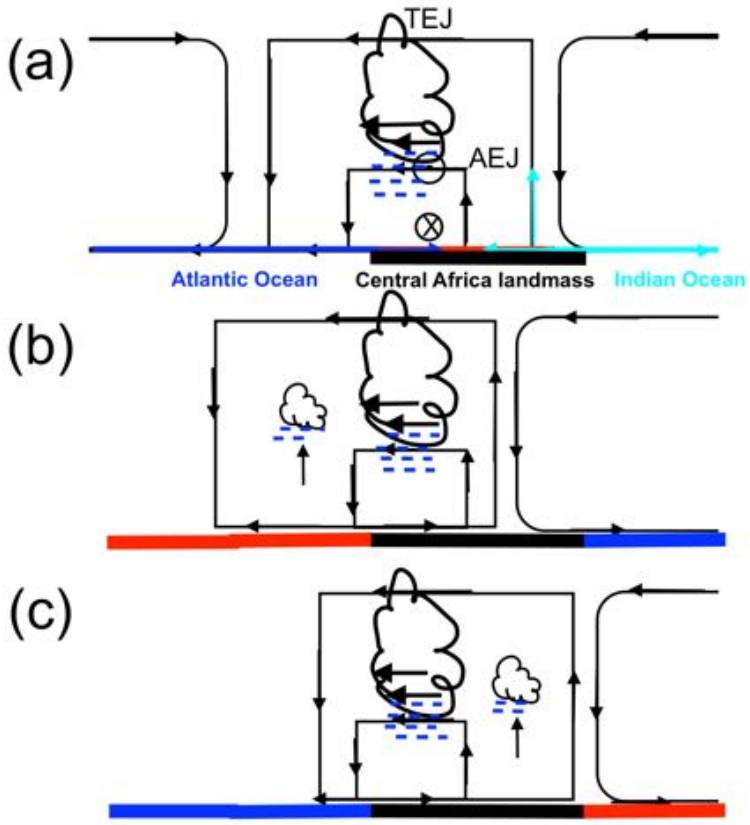

Fig. 7.9. schematic illustration of the zonal large-scale circulation over central Africa associated with ΔSST events (a) normal (b) positive phase and (negative phase) of ΔSST.

7.7. Summary

In this chapter, the objectives were to: (i) revisit central Africa rainfall interannual variability

mechanisms; (ii) examine what are the nature of the physical mechanisms involved in the relationships between central Africa rainfall variability and its adjacent oceans by contributing to an improved definition of the inter-basin SST gradient index; (iii) unravel how large-scale atmospheric circulation over central Africa respond to this inter-basin SST gradient. And the following conclusions are obtained:

1. Accordingly to the seasonality of Central Africa low, two seasons were defined: a long rainy season from September to April (SONDJFMA) associated with the dominant Central Africa low, when approximately more than seventy percent of annual rainfall occurs. A short rainy season from May to August (MJJA), when the Central Africa high is predominant, indicative of subsidence, which suppress convection and limited rainfall.

2. The first leading mode of central Africa rainfall variability illustrates a homogeneous pattern of above normal rainfall anomalies in both seasons (September-April and May-August), which I define as an intrinsic mode of variability. The second leading mode depicts a dipole rainfall anomalies pattern, during the long rainy season, with rainfall deficit over Atlantic offshore regions and southern Africa; and rainfall surplus over East Africa. Whereas during short rainy season, the second mode of central Africa variability shows a north-south dipole, with dry anomalies in the southern hemisphere and wet anomalies over northern Hemisphere of Central Africa. Furthermore, in both seasons, Central Africa rainfall interannual variability is strongly associated with opposite sign of surrounding oceans SST and somehow ENSO.

3. This interbasin SST anomalies gradient (ΔSST) between Atlantic and Indian oceans influences Central Africa rainfall variability through the modulation of the Central Africa Low. The resulting land-ocean pressure gradient between Central Africa landmass and its surrounding Oceans induces an anomalous shallow overturning cell that enhances vertical motion around the equator and strengthens subsidence that suppress convection in subtropics in both hemisphere. This results in a meridional contrast of rainfall anomalies over central Africa. In other hand, the zonal contrast of central Africa rainfall is owed by the land-ocean pressure gradient induced by land-ocean thermal contrast (Turrent and Cavazos, 2009).

4. The ΔSST deepens the land-ocean thermal contrast that generates the land-ocean pressure gradient over Central Africa and its surroundings Oceans. This land-ocean pressure gradient induces an anomalous clockwise zonal overturning cell over central Africa landmass, with ascending branch over Atlantic, indicative of convection that lead to rainfall surplus, and sinking branch over Indian Ocean, indicative of subsistence, which suppress convection and lead to rainfall deficit. The presence of this anomalous clockwise overturning cell over Central Africa landmass confirms the existence of the zonal asymmetric pattern, proposed by Dezfuli et al.

(2015). Moreover, the impact on central Africa rainfall is asymmetrical during positive and negative phases of ΔSST.

5. The mechanism by which the central African easterly jet influences central Africa rainfall is by producing moisture flux convergence or divergence and associated, enhanced or reduced rainfall at the eastern or western sectors of Central Africa landmass. The weakening of central African easterly jets over Atlantic and strengthening of mid-tropospheric wind anomalies over Indian Ocean are associated with subsidence over these regions. They also accompanied a strong mid-tropospheric thermal contrast between central Africa subcontinent and its adjacent Oceans.

6. No migration of the ITCZ occurs over central Africa, inconsistent with Balas et al. (2007) who speculated that the meridional displacement of the ITCZ over central Africa occurs when surrounding ocean's surface temperature anomalies have opposite sign.

7. Despite weak relationship between ENSO and central Africa rainfall, ENSO affects central Africa rainfall directly by controlling the Central Africa Low and High pressure variability, and indirectly perturbing further the Atlantic and Indian Ocean SST, and especially the SST gradient, which in turn, influence the regional large-scale atmospheric dynamics.

Chap. 8

Conclusions

8.1.Conclusions

Central Africa climate studies suffer from the dearth of available data related to lack of sustained meteorological network – with for instance only three stations in Democratic Republic of Congo reporting to global telecommunications system in 2013 (Washington et al. 2013). Firstly, to address the validity of rainfall datasets over Central Africa, we evaluate the annual cycle of rainfall in observations, satellite estimate and reanalysis dataset and a SST-forced Atmospheric General Climate Model – ECHAM5.3. All rainfall datasets capture the rainfall climatology, as well as their seasonality and intensity, except TAMSAT for rainfall distribution. ECHAM5.3 is able to represent the annual cycle of Central Africa rainfall – meridionally and zonally – but it fails to capture realistic seasonal rainfall intensity. Using ERA-Interim data and ECHAM57.3, we found that the lower troposphere over Central Africa is convectively stable throughout the year, with the internal energy representing the bulk of the moist static energy. But, rather than the local temperature, the atmospheric water vapour as well as the low and high pressure systems and their associated circulation play a central role in the Central Africa rainfall seasonality and distribution.

To provide a comprehensive insight of the seasonal cycle of the atmospheric large-scale circulation over central Africa and its associated moisture and atmospheric energy transport; and what physical mechanism does control its structure and formation, we computed the zonal mean mass-weighted streamfunctions (Cook et al. 2003; Nguyen et al. 2013). Central Africa is characterized by dominant easterly circulation associated with strong vertical motion, indicative of deep convection, namely “pseudo” Central Africa zonal overturning cell. At low-levels, there is a shallow zonal anticlockwise

overturning circulation thermally direct, namely the Congo Basin Cell, with a rising branch located at around ~24°E over a warm central Africa landmass and a sinking branch at around ~2°E, over a relatively cooler Atlantic Ocean. Aloft, the strong mid-lower easterly jet, over central Africa, constitutes the returning branch. At near-surface, the Central Africa landmass warming generates a local quasi-permanent low surface pressure. The resulting land-ocean temperature contrast is associated with a zonal surface pressure gradient, which in turn, trigger a monsoon-like low-level westerly jet, flowing from Atlantic Ocean towards central Africa, completing the circulation. Thus, the Congo Basin Cell is a thermally direct circulation, driven by the land-ocean thermal contrast (Scheinder and Lindzen, 1977). This is in contrast with previous studies that suggest either that South Atlantic anticyclone and its associated low-level Benguela jet form the low-level jet over eastern Atlantic Ocean (Fontan et al. 1992; Nicholson and Grist, 2003; Nicholson, 2010) nor the thermally divergent wind component, as suggested by Pokam et al. (2014). The Congo Basin Cell persists throughout the year, with a maximum strength (-196.92±32.89 Sv) and width (30° degree) in August/September and minimum strength (-24.80± 17.83 Sv) and width (~6° degree) in May. This is also inconsistent with Kerry and Cook (2015) who suggested that the overturning circulation over Central Africa occurs only in boreal summer, when the Atlantic cold tongue matures to set up favourable atmospheric conditions for its development. Nonetheless, these findings modify the asymmetric Walker-type circulation schematic over central Africa proposed by Flohn (1971) and confirmed by Yu and Zwiers, 2010 and Yu et al. 2012, with a shallow anticlockwise overturning cell at low-levels and a no closing branch for the "pseudo" central Africa Walker-like cell (Fig. 8.1). This "pseudo" Central Africa Walker-like Cell is driven by the thermally divergent wind component of the tropical atmospheric flow (Yu and Zwiers, 2010 and Yu et al. 2012). However, the Congo Basin Cell does not play any crucial role to modulate central Africa rainfall, but it does control the seasonal zonal ITCZ position.

The surrounding oceans play crucial role via the land-ocean thermal contrast by controlling either the Congo Basin Cell strength or its width through the regulation of its westward and eastward displacement. Moreover, through the thermal wind adjustment, the near-surface land-ocean temperature contrast induces a cross-equatorial southerly that exports water vapour out of Central Africa vegetal surface. The atmospheric convective stability over central Africa is controlled by the southward import of higher moist static energy from the warmer Sahel (between ~10° and 20° N) through the strong anticlockwise Hadley cell. High rainfall is determined by the position of the ascending branch at midlevel, where the moist air saturated year-round. Motivated by the presence of low surface pressure over Central Africa year-round and its link with local rainfall, we used the ERA-Interim reanalysis datasets to analyse and characterize the seasonality as well as the interannual variability of the low-pressure system over Central Africa. Consistently, we found the existence of a dominant lower 1000–500- hPa thickness over central Africa, namely Central Africa Low that drives primarily the atmospheric circulation over central Africa. The Central Africa Low is a

cyclonic pattern and quasi-stationary feature over central Africa, which is well established from October to April.

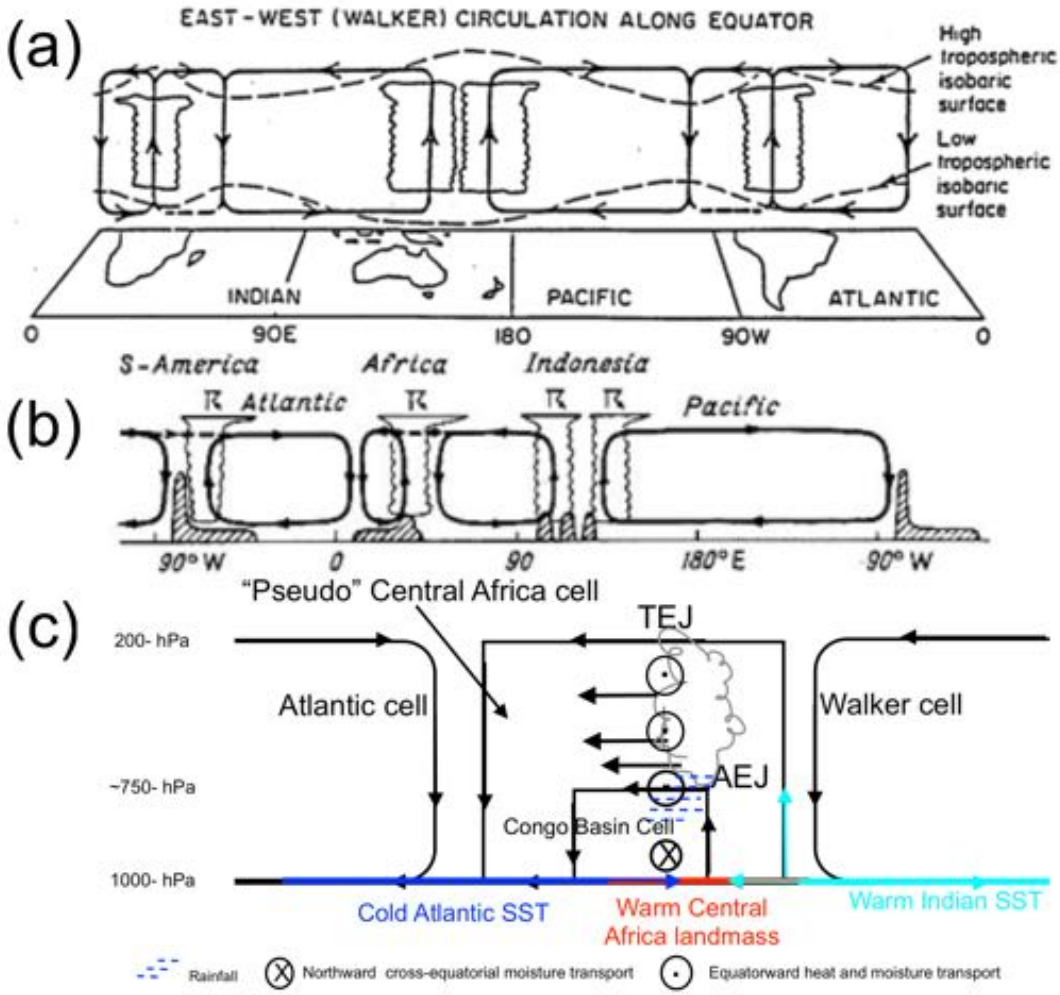

Fig. 8.1. Zonal large-scale circulation along the equator as proposed (a) by Thorsten and Richter (2014) (b) by Flohn, (1971) and Yu and Zwiers, 2010 and Yu et al. 2012; and (c) in this dissertation.

It is characterized by a strong convective activity due to unstable atmosphere over central Africa, which leads to more rainfall representing around 70% of total rainfall over central Africa, while associated with less local rainfall interannual variability. This apparent contradiction of the weak connection between Central Africa low and local rainfall is due primarily to the blocking system nature of the Central Africa Low, that reduces the interannual rainfall variability at its core and weakens further any water vapour transport (Fig. 8.2).

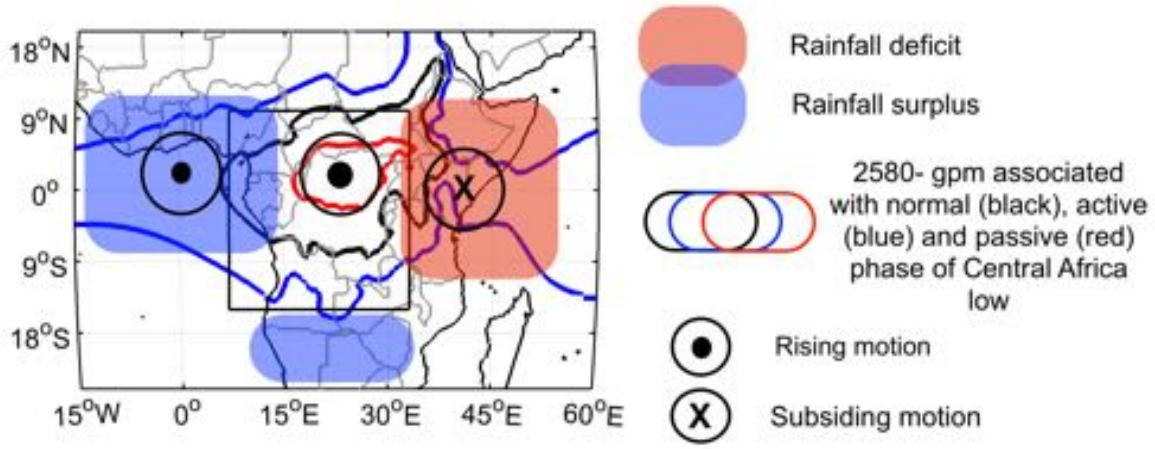

Fig 8.2. Schematic diagram illustrating the impact of the Central Africa Low on regional rainfall and atmospheric circulation.

In addition, the mid-lower land-ocean thermal contrast is likely to induce either relative deep convection over Atlantic Ocean or suppress convection over East Africa (Fig. 8.2). The Central Africa Low is classified as a tropical low, with some thermal low characteristics at low-levels, where the shallow Congo basin cell develops. Central Africa Low is modulated by El Nino Southern Oscillation (ENSO), which can shrink or strengthen the central Africa overturning cell. Moreover, the Central Africa Low triggers a low-level circulation from adjacent oceans to central Africa, which substantiates the crucial role play by these low-level moisture fluxes on central Africa climate, particularly, the ones from the Atlantic (McCollumn et al. 2000; Mpokam et al. 2012). The Central Africa Low also influences rainfall over Sahel, southern Africa and east Africa through the regulation of mid-lower tropospheric heating and atmospheric water vapour transport, owed by a meridional wind shear (Laing et al. 2011).

To further assess the potential role of the midlevel circulation on Central Africa water vapour budget and region climate over Central Africa, the analysis of momentum budget of the mid-lower easterly circulation reveals that the friction term is responsible for the sustainability of both easterly jets, more so than the geopotential thickness is. The northern branch of central African easterly jet intensity is due to the combination of the intensification of the westward wind shear and the meridional mid-tropospheric temperature gradient over central Africa (Nicholson and Grist, 2003), while the southern branch of central African easterly jet is induced by the northward wind shear favoured by the zonal mid-tropospheric temperature gradient. The central Africa rainfall variability is primarily controlled by the variability in large-scale circulation, rather than by variation in tropospheric moisture. Water vapour is transported into Central Africa more by the mean-state circulation associated to the Central African easterly jets than by transient's anomalies. In May to September, additional water vapour from the Atlantic is conveyed into Central Africa by low-level westerlies. The central African easterly jets govern

the moisture convergence flux over central Africa, and control the central Africa rainfall through the modulation of moisture transport channels. Indeed, October – April, when the Central Africa Low is dominant in the region, Central Africa is a sink of water vapour, with the Indian Ocean as the main supplier of water vapour (Fig. 8.3a). This leads to more rainfall over central Africa. In May-September, the weakening of the Central Africa Low over central Africa leads a reversal of the water vapour transport channel at the northern boundary, leading Central Africa to become a source of moisture, with rainforest water vapour likely to be advected mostly out of central Africa (Fig. 8.3b). While at low-levels, the water vapour inflow from Atlantic Ocean is likely to be rained out over central Africa (Fig. 8.3b). During this season, the Atlantic Ocean is the main supplier of moisture over Central Africa (Dezfuli et al. 2013; Pokam et al. 2014), with some additional contribution from Congo basin rainforest. In both seasons, the 2nd leading mode of water vapour transport variability from surrounding Oceans illustrates two poles of actions of the Central African easterly jets, with each pole located in each side of equator at around either 5^{o}S or 5^{o}N. This African easterly jet pattern contributes to establish zonal Central Africa rainfall anomalies contrast, reminiscent of the impact of the Central Africa Low on regional rainfall. Indeed, the mid-lower tropospheric warming over central Africa enhances local water vapour (Fig. 8.3). Owed by the resulted mid-lower land-ocean thermal contrast, strengthened African easterly jets are induced by the vertical zonal wind shear, which in turn, conveys more water vapour over central Africa, conducive to deep convection. These water vapour transports enhance further the convection, as suggested by the 2580-gpm envelope. And so, the Congo basin low impacts the regional rainfall. This positive feedback mechanism shows that land-ocean thermal contrast may affect the Central Africa hydroclimatic, through the regulation of atmospheric water vapour transport. This east-west rainfall dipole over Central Africa highlights the poles of Central Africa rainfall variability (Dezfuli and Nicholson, 2012). In addition, strengthened African easterly jets associated with subsidence are linked to surrounding Oceans SST in October to April (Fig. 8.3a). Conversely, in May to September, despite subsidence, warm Indian Ocean drives the African easterly jet, while over cooler Atlantic Ocean; the African easterly jets are likely to play a crucial role.

To understand what cause the zonal rainfall anomalies contrast over Central Africa, we investigated the mechanism that links Central Africa rainfall variability and its surrounding oceans. In both seasons, the interbasin SST anomalies gradient (ΔSST) affects Central Africa rainfall primarily through modulation of the Central Africa Low, which impinges the zonal water vapour advection from surrounding oceans. In fact, ΔSST modulates the Central Africa Low, so that the Central Africa Low area change, during the both phase of ΔSST, induces the opposite anomalous circulations over central Africa landmass and its surrounding Oceans respectively (Fig. 8.4). Firstly, over Central Africa landmass, the ΔSST–induced anomalous shallow clockwise overturning cell, with ascending branch over Atlantic offshore regions, indicative of deep convection lead to rainfall surplus.

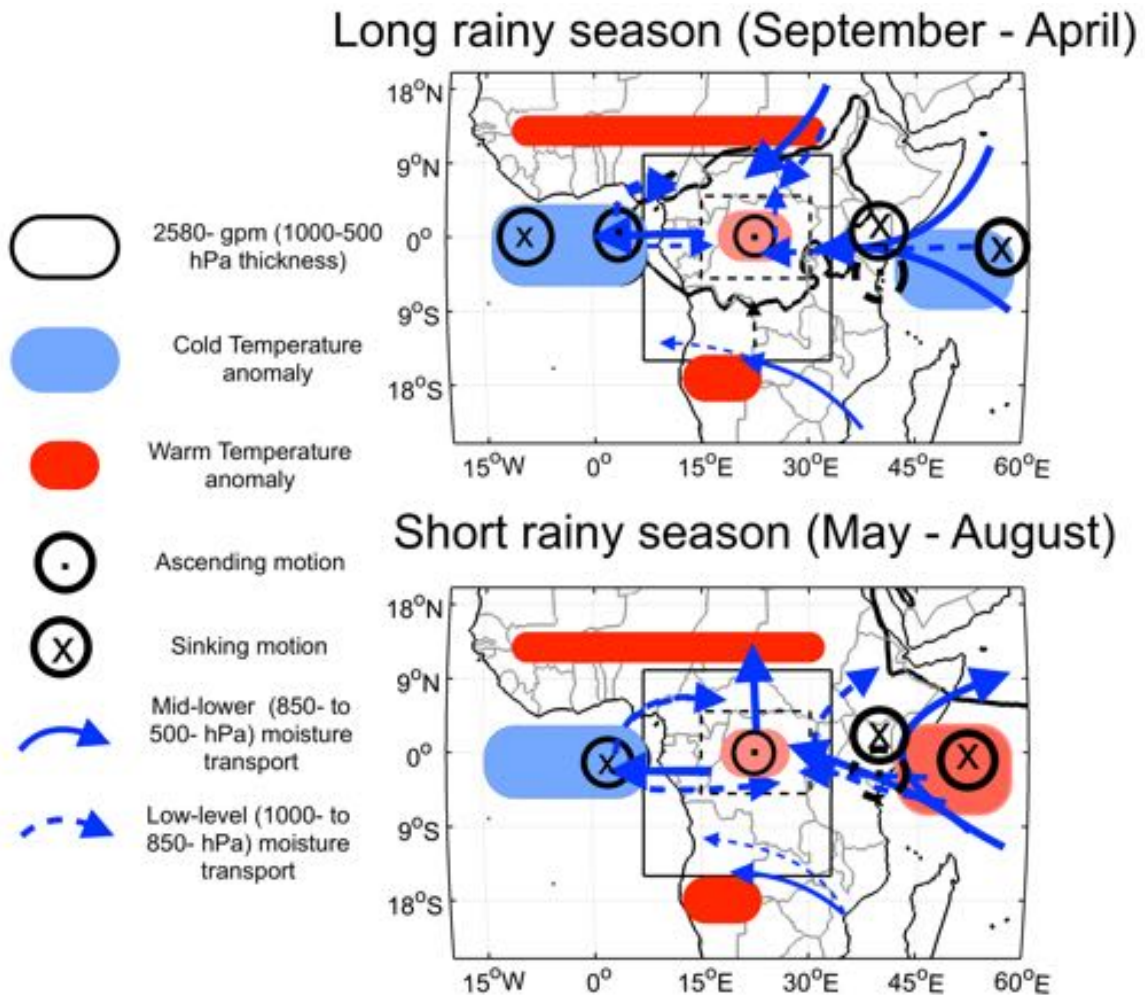

Fig. 8.3. Schematic diagram of mechanisms affecting the water vapour transport over Central Africa and its surroundings regions. Solid and dashed lines represent the circulation at midlevel and low-levels respectively.

Meanwhile the sinking branch of this anomalous shallow clockwise overturning cell occurs over East Africa, indicative of subsistence, which suppresses convection and lead to rainfall deficit over East Africa (Fig. 8.4b). Over tropical Atlantic and Indian oceans, strong anomalous counterclockwise overturning cells over the oceans occur (Fig. 8.4b).

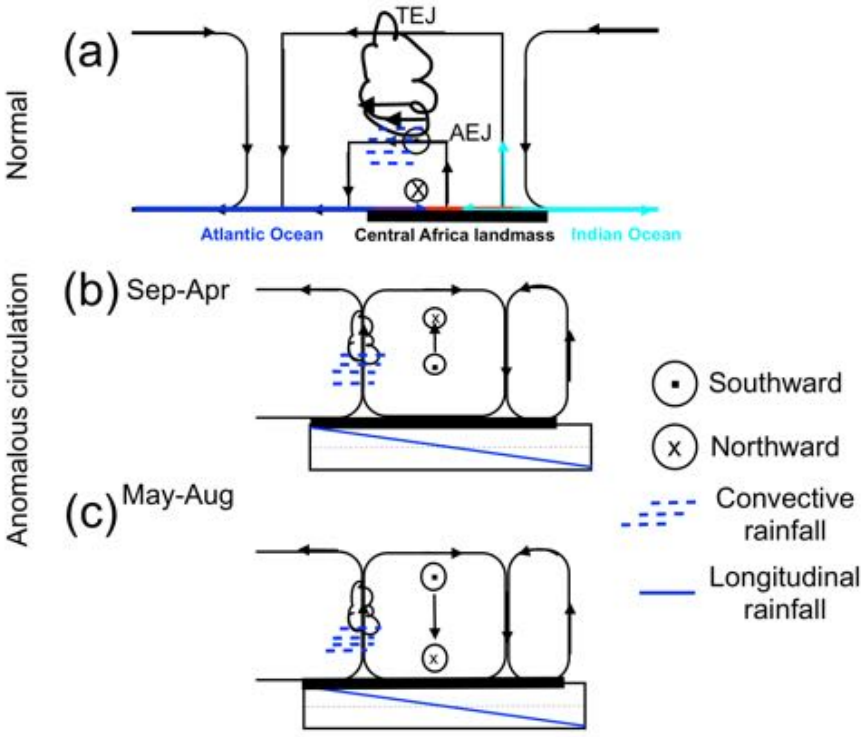

Fig 8.4. Schematic illustration of the anomalous overturning cell associated with positive phase of ΔSST in (a) normal (b) long rainy season and (c) short rainy season.

Moreover, enhanced ΔSST reinforces meridional large-scale circulation through the wind thermal adjustment, which invigorates the midlevel vertical motion around the equator and so contributes to an increase of rainfall over Central Africa landmass (Fig. 8.4b). Conversely, in the short rainy season, enhanced ΔSST weakens the meridional large-scale circulation, which strengthens the subsidence associated with rainfall deficit over Central Africa (Fig. 8.4). These impacts of ΔSST on meridional large-scale circulation are seasonally dependant and consistent with Balas et al. (2007). Despite a weak relationship between ENSO and Central Africa rainfall variability, ENSO may affect central Africa rainfall directly by controlling the Central Africa Low and high pressure system variability, and indirectly by perturbing further the Atlantic and Indian Ocean through ΔSST, which in turn, influence the regional atmospheric large-scale dynamics.

8.2. Future research works

To further our understanding of physcial mechanisms driving the Central Africa rainfall seasonality and variability, we proposed three-fold propositions among many:

(i) *How does global warming influence the water vapour transport over Central Africa?* We showed that the weakening of Central Africa Low that drives the mid-lower easterly winds is related to the continental global warming that occurred in the recent decades over Africa

landmass. It is very interesting to understand how the change of Central Africa Low through global warming is likely to affect the AEJs trends and variability and their associated water vapour transports at low- and at mid-upper levels repectively.

(ii) *What are the responses of the Central Africa hydroclimate to the surface and oceanic forcings?* The Central Africa hydroclimate variability is controlled by the change in the zonal regional-circulation, which in turn, is influenced by forcings from remote and surroundings Oceans. Those oceanic forcings do affect the Central Africa by atmospheric bridges. So, it is very important to find out how those atmospheric bridges are sensitive to the oceanic and surface forcings such as ENSO and/or Central Africa Low and what are the physical mechinaims involve their relationship if any?.

(iii) *Towards better understand of the regional pattern of rainfall extreme over Central Africa? What are the physical mechanims involve in its seasonality and interannual variability of exteme precipitation? How do they change in the context of global warming?* So far, Central Africa is the poorest study region in the world, probably because of the scarcity of in-situ datasets. So, to improve our understanding of physical processes involved in the hydroclimate variability over Central Africa, we do think it is better to advocate for a AMMA-like experience over Central Africa.

References

Adler, R. F., G. J. Huffman, A. Chang, R. Ferraro, P.-P. Xie, J. Janowiak, B. Rudolf, U. Schneider, S. Curtis, D. Bolvin, A. Gruber, J. Susskind, P. Arkin, and E. Nelkin (2003). The Version-2 Global Precipitation Climatology Project (GPCP) Monthly Precipitation Analysis (1979–Present), J. Hydrometeor, 4 (6), 1147–1167, doi:10.1175/1525-7541(2003)004<1147:TVGPCP>2.0.CO;2.

Alexander, M. A., I. Bladé, M. Newman, J. R. Lanzante, N.-C. Lau, and J. D. Scott, 2002: The atmospheric bridge: The influence of ENSO teleconnections on air–sea interaction over the global oceans. J. Climate, 15, 2205–2231, doi:10.1175/ 1520-0442(2002)015,2205:TABTIO.2.0.CO;2.

Anber, U.,Wang S., and Sobel A., (2014). Response of atmospheric convection to vertical wind shear: cloud resolving simulations with parameterized large-scale circulation. Part I: Specified radiative cooling. J. Atmos. Sci., 71, 2976-2993, http://dx.doi.org/10.1175/JAS-D- 13-0320.1

Anyah R O and Semazzi F H M (2006). Climate variability over the Greater Horn of Africa based on NCAR AGCM ensemble Theor. Appl. Climatol. 86 39–62

Asadullah, A, Mcintyre, N, Kigobe, M., (2008). Evaluation of five satellite products for estimation of rainfall over Uganda. Hydrological Sciences Journal, 53 (6), 1137-1150.

Back, L. E, and C. S. Bretherton, (2006). Geographic variability in the export of moist static energy and vertical motion profiles in the Tropical Pacific. Geophys. Res. Lett., 33, L17810, doi:10.1029/2006GL026672.

Bader J, Latif M (2003). The impact of decadal-scale Indian Ocean sea surface temperature anomalies on Sahelian rainfall and the North Atlantic Oscillation. Geophys Res. Lett 30(22):2169. doi: 10.1029/2003GL018426

Balas, N., Nicholson, S.E., Klotter, D., (2007). The relationship of rainfall variability in West Central Africa to sea-surface temperature fluctuations. Int. J. Climatol. 27 (10), 1335–1349

Banacos PC, Schultz DM (2005). The use of moisture flux convergence in forecasting convective initiation: historical and operational perspectives. Weather Forecast 20:351–366

Becker A, Finger P, Meyer-Christoffer A, Rudolf B, Schamm K, Schneider U, Ziese M. (2013). A description of the global land-surface precipitation data products of the global precipitation

climatology centre with sample applications including centennial (trend) analysis from 1901–present

Biasutti M., D.S. Battisti, and E.S. Sarachnik, (2003). The annual cycle over the tropical Atlantic, South America and Africa. J. Climate, 16, 2491–2508

Bolvin, D. T., R. F. Adler, G. J. Huffman, E. J. Nelkin, and J. P. Poutiainen (2009). Comparison of GPCP monthly and daily precipitation estimates with high-latitude gauge observations, J. Appl. Meteorol. Climatol., 48(9), 1843–1857.

Camberlin P, Janicot S, Poccard I. (2001). Seasonality and atmospheric dynamics of the teleconnection between African rainfall and tropical SST. Atlantic vs ENSO. Int. J. of Clim. 21: 973–1005

Capotondi, A., A. T. Wittenberg, M. Newman, E. Di Lorenzo, J.-Y. Yu, P. Braconnot, J. Cole, B. Dewitte, B. Ciese, E. Guilyardi, F.F. Jim, K. Karnauskas, B. Kirtman, T. Lee, N. Schneider, Y. Xue, and S.-W. Yeh, 2015: Understanding ENSO diversity. Bull. Amer. Meteor. Soc., doi:10.1175/BAMS-D-13-00117.1.

Clark, C.A. and Arritt, R.W. (1995) Numerical simulations of the effect of soil moisture and vegetation cover on the development of deep convection. Journal of Applied Meteorology 34, 2029–45.

Chou C and Chen CA (2010). Depth of convection and the weakening of tropical circulation in global warming. J Clim 23:3019–3030

Chou C and Neelin JD. (2004). Mechanisms of global warming impacts on regional tropical precipitation. Journal of Climate 17: 2688–2701.

Chou C, Neelin JD, Chen C and Tu J. (2009). Evaluating the “rich-getricher” mechanism in tropical precipitation change under global warming. Journal of Climate 22: 1982–2005.

Cook, K.H., (2003). Role of Continents in Driving the Hadley Cells. J. Atmos. Sci., 60, 957- 976.

Cook, K. H., (1999): Generation of the African easterly jet and its role in determining West African precipitation. J. Climate, 12, 1165–1184.

Cook, K.H. and Vizy, E. K. (2012). Impact of climate change on midtwenty-first century growing seasons in Africa. Climate Dyn., 39, 2937–2955.

Cook, K. H., and Vizy, E. K. (2015). The Congo Basin Walker circulation: dynamics and connections to precipitation. Climate Dynamics, 47(3), 697–717.

Dai, A., H. Li, Y. Sun, L.-C. Hong, Lin Ho, C. Chou, and T. Zhou (2013). The relative roles of upper and lower tropospheric thermal contrasts and tropical influences in driving Asian summer monsoons, J. Geophys. Res. Atmos., 118, 7024–7045, doi:10.1002/jgrd.50565.

Davis SM, Rosenlof KH (2012). A multidiagnostic Intercomparison of tropical-width time series using reanalyses and satellite observations. J Clim 25:1061–1078. doi:10.1175/JCLID- 11-00127.1

Dee D P et al. (2011). The ERA-Interim reanalysis: configuration and performance of the data assimilation system Q. J. R. Meteorol. Soc. 137 553–97

Dezfuli A K and Nicholson S E (2013). The relationship of rainfall variability in western equatorial Africa to the tropical oceans and atmospheric circulation: II. The boreal autumn J. Clim. 26 66–84

Dezfuli, A. K., Zaitchik, B. F. and Gnanadesikan, A. (2015). Regional atmospheric circulation and rainfall variability in south equatorial Africa. Journal of Climate, 28(2), 809–818.

Diem, J. E., Ryan, S. J., Hartter, J., & Palace, M. W. (2014). Satellite-based rainfall data reveal a recent drying trend in central equatorial Africa. Climatic Change, 126(1–2), 263–272.

Dieppois, B., B. Pohl, M. Rouault, M. New, D. Lawler, and N. Keenlyside (2016). Interannual to interdecadal variability of winter and summer southern African rainfall, and their teleconnections, J. Geophys. Res. Atmos., 121, 6215–6239, doi:10.1002/2015JD024576

Donohoe A, Marshall J, Ferreira D and McGee D (2012). The relationship between ITCZ location and cross equatorial atmospheric heat transport; from the seasonal cycle to the last glacial maximum. J Clim

Donohoe, A., Marshall, J., Ferreira, D., and Mcgee, D. (2013). The relationship between ITCZ location and cross-equatorial atmospheric heat transport: From the seasonal cycle to the Last Glacial Maximum. Journal of Climate, 26(11), 3597–3618

Driver P. and Reason C J (2016), Variability in the Botsana High and its relationships with rainfall and temperature characteristics over Southern Africa, Inter. J. Clim. 37 (S1), doi.org/10.1002/joc.5022

Farnsworth A, White E,Williams C, Black E and Kniveton D R (2011). Understanding the large scale driving mechanisms of rainfall variability over Central Africa African Climate and Climate Change ed C Williams and D Kniveton (New York: Springer) pp 101–22

Fauchereau, N., B. Pohl, C. J. C. Reason, M. Rouault, and Y. Richard, (2009). Recurrent daily OLR patterns in the Southern Africa/Southwest Indian Ocean region, implications for South African rainfall and teleconnections. Climate Dyn., 32, 575–591, doi:10.1007/s00382-008-0426-2

Flohn H. and Fleer H. (1975). Climatic teleconnections with the equatorial pacific and the role of ocean/atmosphere coupling, Atmosphere, 13:3, 96-109
http://dx.doi.org/10.1080/00046973.1975.9648391

Fontaine, B., P. Roucou, and S. Trzaska (2003), Atmospheric water cycle and moisture fluxes in the West African monsoon: mean annual cycles and relationship using NCEP/NCAR reanalyses, Geophys. Res. Lett., 30, doi:10.1029-10.1032.

Giannini, A., M. Biasutti, I. M. Held, and A. H. Sobel, 2008: A global perspective on African climate. Climatic Change, 90, 359–383, doi:10.1007/s10584-008-9396-y.

Giannini, A., (2010). Mechanisms of climate change in the semi-arid African Sahel: the local view. J. Climate, 23, 743-756, doi: 10.1175/2009JCLI3123.1

Gleixner, S., Keenlyside, N.S., Viste, E. and Korecha, D. (2016). The El Nino effect on Ethiopian summer rainfall. Climate Dynamics, 10.1007/s00382-016-3421-z

Harris, I., P. D. Jones, T. J. Osborn, and D. H. Lister (2014). Updated high resolution grids of monthly climatic observations—The CRU TS3.10 dataset, Int. J. Climatol., 34, 623– 642.

Hart, N., C. J. C. Reason, and N. Fauchereau (2010). Tropical-extratropical interactions over Southern Africa: Three cases of heavy summer season rainfall, Mon. Weather Rev. 138 (7). pp. 2608-2623. DOI: 10.1175/2010MWR3070.1.

Held, I. M., and B. J. Soden, (2006). Robust responses of the hydrological cycle to global warming. J. Clim., 19, 5686–5699, doi:10.1175/JCLI3990.1.

Hua W., L. Zhou, H. Chen, S.E Nicholson, A. Raghavendra and Y. Jiang (2016). Possible causes of the Central Equatorial African long-term drought. doi.org/10.1088/1748-9326/11/12/124002

Houze, R. A., Jr. (1993). Cloud Dynamics, Academic, San Diego, Calif.

Huffman, G.J., R.F. Adler, D.T. Bolvin, G. Gu, (2009). Improving the Global Precipitation Record: GPCP Version 2.1. Geophys. Res. Lett., 36(17), L17808, doi:10.1029/2009GL040000.

Hurley, J. V., and W. R. Boos (2014). A global climatology of monsoon low-pressure systems, Q. J. R. Meteorol. Soc., doi:10.1002/qj.2447

IPCC (2007). The Physical Science Basis. Contribution of Working Group I to the Fourth Assessment Report of the Intergovernmental Panel on Climate Change, Cambridge University Press, Cambridge, UK and New York, NY, USA.

Jackson B, Nicholson SE, Klotter D (2009) Mesoscale convective systems over western equatorial Africa and their relationship to large-scale circulation. Mon Weather Rev 137:1272–1294

Kalnay, E., and Coauthors, (1996). The NCEP/NCAR 40-Year Reanalysis Project. Bull. Amer. Meteor. Soc., 77, 437–471.

Kanamitsu, M.; W. Ebisuzaki; J. Woollen; S. –K. Yang; J. J. Hnilo; M. Fiorino; G. L. Potter, (2002). NCEP-DOE AMIP-II Reanalysis (R-2). Bull. Am. Met. Soc., 83, 1631-1643.

Kemball-Cook, S. R. and Weare, B. C. (2001). The Onset of Convection in the Madden-Julian Oscillation. Journal of Climate, 14.

Kucharski, F., Bracco, A., Yoo, J. H., Molteni, F., 2007: 'Low-frequency variability of the Indian Monsoon-ENSO relation and the Tropical Atlantic: The 'weakening' of the '80s and 90s'. J. Climate, 20, pp. 4255-4266, DOI: 10.1175/JCLI4254.1

Kucharski, F., Bracco, A., Yoo, J. H., Molteni, F., 2008: 'Atlantic forced component of the Indian monsoon interannual variability'. Geophys. Res. Lett., 35, L04706, doi:10.1029/2007GL033037

Kucharski, F. Bracco, A., Yoo, J. H., Tompkins, A., Feudale, L., Ruti, P., Dell'Aquila, A., 2009: 'A Gill-Matsun-type mechanism explains the Tropical Atlantic influence on African and Indian Monsoon Rainfall.' Quart. J. R. Met. Soc., 135, 569-579, DOI: 10.1002/qj.406

Lau, K.-M., and H.-T. Wu (2007), Detecting trends in tropical rainfall characteristics, 1979–2003, Int. J. Climatol., 27(8), 979–988, doi:10.1002/ joc.1454.

Lawrence, D., & Vandecar, K. (2015). Effects of tropical deforestation on climate and agriculture. *Nature climate change*, *5*(1), 27–36.

Lutz. K., Jacobeit J., Rathmann J., (2015) Atlantic warm and cold water events and impact on African west coast precipitation, Int. J. of Clim https://doi.org/10.1002/joc.3969

Maidment R I, Allan R P and Black E (2015). Recent observed and simulated changes in precipitation over AfricaGeophys. Res. Lett. 42 8155–64

Malhi Y and Wright J (2004) Spatial patterns and recent trends in the climate of tropical rainforest regions Phil. Trans. R. Soc. B 359 311–29

McCollum, J.R., A. Gruber and M.B. Ba, (1999). Discrepancy between gauges and satellite estimates of rainfall in equatorial Africa. J. Appl. Meteor., 41, 1065-1080.

McGregor, G.R., and Nieuwolt, S., (1998), Tropical climatology: An introduction to the climates of the low latitudes: Chichester, John Wiley & Sons, 311 p.

McHugh MJ. (2006). Impact of South Pacific circulation variability on east African rainfall. Int. J. Climatol. 26: 505–521.

Mohino E, Janicot S, Bader J. (2011). Sahel rainfall and decadal to multi-decadal sea surface temperature variability. Clim. Dyn. 37: 419–440.

Neelin, J. D., (2007). Moist dynamics of tropical convection zones in monsoons, teleconnections, and global warming. The Global Circulation of the Atmosphere, Princeton University Press, 267–301.

Neelin, J. D., C. Chou, and H. Su, (2003). Tropical drought regions in global warming and El Nino˜ teleconnections. Geophys. Res. Lett., 30 (24), 2275, doi:10.1029/2003GL018625.

Neelin, J. D., and I. M. Held, (1987). Modeling Tropical Convergence Based on the Moist Static Energy Budget. Mon. Wea. Rev., 115 (1), 3–12, doi:10.1175/15200493(1987)115h0003:856 MTCBOTi2.0.CO;2.

Neupane, N. (2016). The Congo Basin zonal overturning circulation. Advances in Atmospheric Sciences, 33(6), 767–782.

Nguyen H, Evans A and Lucas C (2013). The Hadley circulation in reanalyses: climatology, variability, and Change. J Clim. 26:3357–3376. doi:10.1175/JCLI-D-12-00224.1

Nicholson, S. E. (1996). A review of climate dynamics and climate variability in Eastern Africa. In T. C. Johnson & E. O. Odada (Eds), The limnology, climatology and paleoclimatology of the East African lakes (pp. 25–56). Amsterdam: Gordon and Breach

Nicholson SE. (2009) A revised picture of the structure of the “monsoon” and land ITCZ over West Africa. Climate Dynamics 32 (7-8):1155-1171.

Nicholson, S. E., & Dezfuli, A. K. (2013). The relationship of rainfall variability in western equatorial Africa to the tropical oceans and atmospheric circulation. Part I: The boreal spring. Journal of Climate, 26(1), 45–65.

Nicholson S E and Grist J P (2003). The seasonal evolution of the atmospheric circulation over West Africa and equatorial Africa J. Clim. 16, 1013–30

Nicholson SE, Kim J (1997) The relationship of the El Niño-Southern Oscillation to African rainfall. Int. J. Clim. 17:117–135

Oort, A. H., and J. J. Yienger (1996). Observed interannual variability inthe Hadley circulation and its connection to ENS O, J. Clim., 9(11),2751 – 2767.

Peixoto, J. P., and A. H. Oort (1992). Physics of Climate, Am. Inst. of Phys., New York.

Pokam WM, Djiotang LAT, Mkankam FK. (2012) Atmospheric water vapor transport and recycling in equatorial Central Africa through NCEP/NCAR reanalysis data. Clim. Dyn.**38**, 1715–1729. (doi:10.1007/s00382-011-1242-7)

Pokam M. W., Bain C. L., Chadwick, R. S., Graham, R., Sonwa D. J., & Kamga, F. M. (2014). Identification of processes driving low-level westerlies in West Equatorial Africa. Journal of Climate, 27(11), 4245–4262.

Reynolds RW, Rayner NA, Smith TM, Stokes DC, Wang W. (2002). An improved in situ and satellite SST analysis for climate. Journal of Climate 15: 1609–1625.

Richter, I., Xie, S.-P., Wittenberg, A.T., Masumoto, Y., (2012). Tropical Atlantic biases and their relation to surface wind stress and terrestrial precipitation. Clim. Dyn. 38, 985–1001.

Roeckner, E., et al. (2003). The atmospheric general circulation model ECHAM5—Part I: Model description, Tech. Rep. 349, Max-PlanckInstitut fur Meteorologie, Hamburg, Germany

Stachnik, J.P., Schumacher, C., (2011). A comparison of the Hadley circulation in modern reanalyses. J. Geophys. Res. 116, D22102.

Schneider U, Becker A, Finger P, Meyer-Christoffer A, Ziese M and Rudolf B (2014). GPCC's new land surface precipitation climatology based on quality-controlled in situ data and its role in quantifying the global water cycle Theor. Appl. Climatol. 115 15–40

Schneider, T., Bischoff, T., and Haug, G. H. (2014). Migrations and dynamics of the intertropical convergence zone. Nature, 513(7516), 45–53.

Schneider EK and Lindzen RS. (1977). Axially symmetric steady-state models of the basic state for instability and climate studies. Part I. Linearized calculations. J. Atmos. Sci. 34:263–79

Seager, R., N. Naik, and G. A. Vecchi (2010). Thermodynamic and dynamic mechanisms for large-scale changes in the hydrological cycle in response to global warming, J. Clim., 23, 4651–4668, doi:10.1175/2010jcli3655.1.

Seth, A., S. A. Rauscher, M. Biasutti, A. Giannini, S. J. Camargo, M. Rojas, (2013). CMIP5 Projected Changes in the Annual Cycle of Precipitation in Monsoon Regions. J. Climate, 26, 7328–7351.

Seth, A., M. Rojas, and S. A. Raucher, (2010). CMIP3 projected changes in the annual cycle of the South American monsoon. Climatic Change, 98, 331-357, doi: 10.1007/s10584-009-9736-6

Siam, M. S., Demory, M.-E., and Eltahir, E. A. B. (2013). Hydrological cycles over the Congo and Upper Blue Nile Basins: Evaluation of general circulation model simulations and reanalysis products, J. Climate, 26, 8881–8894,

Smith, T. M., and R.W. Reynolds, T. C. Peterson, and J. Lawrimore, (2008). Improvements to NOAA's historical merged land–ocean surface temperature analysis (1880–2006). J. Climate, 21, 2283–2296, doi:10.1175/2007JCLI2100.1

Sobel, A. H., G. Bellon, and J. T. Bacmeister (2007). Multiple equilibria in a single-column model of the tropical atmosphere, Geophys. Res. Lett., 34, L22804, doi:10.1029/2007GL031320.

Sperber, K. R., H. Annamalai, I.-S. Kang, A. Kitoh, A. Moise, A. Turner, B. Wang, and T. Zhou. (2013) The Asian summer monsoon: an intercomparison of CMIP5 vs. CMIP3 simulations of the late 20th century. Clim. Dynam., 41, 2711-2744, doi: 10.1007/s00382-012-1607-6.

Sultan B and Janicot S. (2003). The West African monsoon dynamics. PartII: the “preonset” and “onset” of the summer monsoon. Journal of Climate16: 3389 – 3406.

Suzuki, T. (2011). Seasonal variation of the ITCZ and its characteristics over central Africa, Theor. Appl. Climatol., 103,39–60, doi:10.1007/s00704-010-0276-9.

Tanguela, T., V.A. Debertini, Pokam W., Y. Djoumou, A. Haensler, W. Moufouma-Okia, G-N.T. Longandjo, J.-P. Bell, T. Takong (2018), Evaluation of CORDEX Regional Climate Models over Central Africa. Int. J. Clim., submitted”

Tarnavsky, E., D. Grimes, R. I. Maidment, M. Stringer, R. Chadwick, R. P. Allan, E. Black, and F. Kayitakire (2014). Extension of the TAMSATSatellite-based Rainfall Monitoring over Africa and from 1983 to present, J. Appl. Meteorol. Climatol., doi:10.1175/JAMC-D-14-0016.1.

Thorncroft C, Hall N, Kiladis G. (2008). Three dimensional structure and dynamics of African easterly waves. Part III: Genesis. J. Atmos. Sci. 65: 3596–3607.

Thorncroft C D, Nguyen H, Zhang C and Peyrill. P (2011). Annual cycle of the West African monsoon: regional circulations and associated water vapour transport Q. J. R. Meteorol. Soc. 137 129–47

Thorsten, Peters and Richter, Michael (2014). The Atmospheric Circulation. 10.1007/SpringerReference_384448.

Tiedtke, M (1996). An extension of cloud-radiation parameterization in the ECMWF model: The representation of subgrid-scale variations of optical depth, Mon. Weather Rev., 124, 745-75

Tierney, J. E., Russell, J. M., Damst., J. S. S., Huang, Y., & Verschuren, D. (2011). Late Quaternary behavior of the East African monsoon and the importance of the Congo Air Boundary. Quaternary Science Reviews, 30(7), 798–807.

Todd M C and Washington R (2004). Climate variability in central equatorial Africa: influence from the Atlantic sectorGeophys. Res. Lett. 31 L23202

Tokinaga, H., and S.-P. Xie, (2011). Weakening of the equatorial Atlantic cold tongue over the past six decades. Nature Geosci. 4, 222-226, doi:10.1038/ngeo1078.

Trenberth, K, J. Fasullo, and L. Smith, (2005). Trends and variability in column integrated atmospheric water vapor. Climate Dyn., 24, 741–758

Turrent C and Cavazos T. (2009). Role of the land-sea thermal contrast in the interannual modulation of the North American monsoon. Geophysical Research Letters 36: L02808, doi: 10.1029/2008GL036299.

Venegas, S. A., L. A. Mysak, and D. N. Straub, (1997). Atmosphere–ocean coupled variability in the South Atlantic. J. Climate, 10, 2904–2920.

Vigaud, N., Richard, Y., Rouault, M., & Fauchereau, N. (2007). Water vapour transport from the tropical Atlantic and summer rainfall in tropical southern Africa. Climate dynamics, 28(2–3), 113–123.

Vigaud, N., Richard, Y., Rouault, M., and Fauchereau, N. (2009). Moisture transport between the South Atlantic Ocean and southern Africa: relationships with summer rainfall and associated dynamics. Clim. Dyn. 32, 113–123. doi:10.1007/s00382-008-0377-7

Viste, E., D. Korecha, and A. Sorteberg, (2013). Recent drought and precipitation tendencies in Ethiopia. Theor. Appl. Climatol., 112, 535–551, doi:10.1007/s00704-012-0746-3.

Vizy EK, Cook KH (2002). Development and application of a mesoscale climate model for the tropics: influence of sea surface temperature anomalies on the West African monsoon. J. Geophys Res 107(D3):4023. doi:10.1029/2001JD000686

Washington, R., R. James, H. Pearce, W. M. Pokam, and W. Moufouma-Okia (2013). Congo Basin rainfall climatology: Can we believe the climate models?, Philos. Trans. R. Soc. London, Ser. B,368 (1625), doi:10.1098/rstb.2012.0296

Webster, P. J. (1983). Large-scale structure of the tropical atmosphere. In B. J. Hoskins & R. P. Pearce (Eds.), Large-scale dynamical processes in the atmosphere (pp. 235–275). New York: Academic Press.

Xie P, Arkin PA (1997). Global precipitation: a 17-year monthly analysis based on gauge observations, satellite estimates and numerical model outputs. Bull Am Meteorol Soc 78:2539–2558. doi:10.1175/1520-0477(1997)078Ä2539:GPAYMA[2.0.CO;2

Yang, W., R. Seager, M. A. Cane, and B. Lyon (2014). The East African long rains in observations and models, J. Clim.,27(19), 7185–7202, doi:10.1175/JCLI-D-13-00447.1.

Yu Bin, Boer GJ (2002). The roles of radiation and dynamical processes in the El Nino-like response to global warming. Clim. Dyn 19:539–553

Yu Bin, Zwiers F (2010). Changes in equatorial atmospheric zonal circulations in recent decades. Geophys Res Lett 37: L05701. doi:10.1029/2009GL042071

Yu, Bin, W. Zwiers, F, J. Boer, G and Ting, M. (2012). Structure and variances of equatorial zonal circulation in a multi-model ensemble. Climate Dynamics. 39. 10.1007/s00382-012-1372-6.

Zeng N. and J. D. Neelin, 1999: A land–atmosphere interaction theory for the tropical deforestation problem. J. Climate, 12, 857–872.

Zhou T. (2013). The Asian summer monsoon: An Intercomparison of CMIP5 vs. CMIP3 simulations of the late 20th century, Clim. Dyn., 41, 2711–2744, doi:10.1007/s00382-012-1607-6.

Zhou, T., B. Wu, and B. Wang (2009a). How well do Atmospheric General Circulation Models capture the leading modes of the interannual variability of the Asian-Australian Monsoon? J. Clim., 22, 1159–1173.

Zhou, Tianjun, R. Yu, J. Zhang, H. Drange, C. Cassou, C. Deser, D. L. R. Hodson, E. Sanchez-Gomez, J. Li, N. Keenlyside, X. Xin, Y. Okumura (2009b). Why the Western Pacific Subtropical High has Extended Westward since the Late 1970s. Journal of Climate, 22, 2199-2215